# [NiFe] hydrogenases from *Desulfovibrio vulgaris* Miyazaki F and *Aquifex aeolicus* studied by FTIR, IR and electrochemical techniques: Redox intermediates, O$_2$/CO sensitivity and light-induced effects

vorgelegt von
Diplom-Physikerin
Maria-Eirini Pandelia
aus Athen

Von der Fakultät II - Mathematik und Naturwissenschaften
der Technischen Universität Berlin
zur Erlangung des akademischen Grades
Doktor der Naturwissenschaften
Dr.rer.nat.

**genehmigte Dissertation**

Promotionsausschuss:

Vorsitzender: Prof. Dr. Andreas Grohman
Berichter/Gutachter: Prof. Dr. Wolfgang Lubitz
Berichter/Gutachter: Prof. Dr. Peter Hildebrandt

Tag der wissenschaftlichen Aussprache: 28.10.2009

Berlin 2010

D 83

Maria-Eirini Pandelia

# [NiFe] hydrogenases from *Desulfovibrio vulgaris* Miyazaki F and *Aquifex aeolicus* studied by FTIR, EPR and electrochemical techniques: Redox intermediates, O$_2$/CO sensitivity and light-induced effects

[NiFe]-Hydrogenasen sind Enzyme, die die reversible Oxidation von molekularem Wasserstoff katalysieren. Das Verständnis ihres Mechanismus ist notwendig für die Synthese biomimetischer katalytischer Systeme und für ein zukünftige "grüne" Biotechnologie. In dieser Arbeit wurden [NiFe]-Hydrogenasen aus zwei unterschiedlichen Organismen untersucht, eine aus dem streng anaeroben Bakterium *Desulfovibrio vulgaris* Miyazaki F und eine aus dem mikro-aerophilen hyperthermophilen Bakterium *Aquifex aeolicus*.

Der erste Teil der Arbeit konzentriert sich auf die Untersuchung der [NiFe] Hydrogenase aus *D. vulgaris*; hier wurden die Intermediate des Reaktionszyklus durch verschiedene Infrarot-Techniken im Detail untersucht. Durch Einsatz der SEIRA-Spektroskopie, bei der das Enzym an die Oberfläche einer Elektrode gebunden ist, konnte dieselbe katalytische Aktivität wie auch durch FTIR-Spektroelektrochemie in Lösung erhalten werden. Ferner wurde gezeigt, dass der EPR-inaktive Zustand (Ni-SI$_r$)$_I$ lichtempfindlich ist und in einen neuen Zustand, Ni-SL, übergeht. Wellenlängenabhängige und kinetische Messungen zeigten, dass die Lichtempfindlichkeit des (Ni-SI$_r$)$_I$ Zustands auf eine Verschiebung des an das aktive Zentrum gebundenen Hydroxyl-Liganden zurückzuführen ist. Für den Übergang von dem lichtinduzierten Ni-L in den Ni-C Zustand wurde ein (H/D) kinetischer Isotopeneffekt beobachtet. Dies zeigt, dass der geschwindigkeitsbestimmende Schritt dieses Übergangs die Bindung eines Protons an das aktive Zentrum beinhaltet. Mittels FTIR-Spektroelektrochemie und EPR wurde die Inhibierung des Enzyms durch Kohlenmonoxid untersucht und die Bildung von zwei CO-inhibierten Zuständen gezeigt. Zusätzlich wurde die Aktivierungsenergie für die Bindung des CO an das aktive Zentrum mittels zeitaufgelöster FTIR Studien bestimmt.

Der zweite Teil dieser Arbeit befasst sich mit der Untersuchung der Hydrogenase I aus *Aquifex aeolicus*. Chronoamperometrische elektrochemische Messungen belegten die Sauerstofftoleranz dieser Hydrogenase. Durch FTIR-Spektroelektrochemie in Lösung konnten vier Redox-Intermediate detektiert werden, die ein signifikant höheres Redoxpotential aufweisen als die [NiFe]-Hydrogenasen aus anderen Organismen. Die Bindung von Kohlenmonoxid an das aktive Zentrum der Hydrogenase I aus *A. aeolicus* ist deutlich schwächer als diejenige an die Hydrogenase aus *D. vulgaris*. Durch EPR-detektierte Redox-Titrationen konnten verschiedene Typen von Eisen-Schwefel Zentren und alle dazu gehörigen Redoxpotentiale bestimmt werden. Basierend auf diesen Ergebnissen wurde ein Modell für die Sauerstofftoleranz der Hydrogenase I vorgeschlagen. Abschließend wurde die Wechselwirkung des aktiven Zentrums des katalytisch aktiven Ni-C Zustands mit Wasserstoff in *A. aeolicus* mittels moderner EPR-Techniken untersucht, wobei ein schwach gebundenes Hydrid detektiert werden konnte.

*Abstract in English*

Maria-Eirini Pandelia

[NiFe] hydrogenases from *Desulfovibrio vulgaris* Miyazaki F and *Aquifex aeolicus* studied by FTIR, EPR and electrochemical techniqes: Redox intermediates, O$_2$/CO sensitivity and light-induced effects

[NiFe] hydrogenases are important metalloenzymes that carry out the reversible oxidation of dihydrogen. Understanding their mechanism is crucial for the synthesis of biomimetic catalytic systems and future 'green' biotechnology. The present work is focused on the study of two distinct types of enzymes; a [NiFe] hydrogenase from the strictly anaerobic sulphate reducing bacterium *Desulfovibrio vulgaris* Miyazaki F and a [NiFe] hydrogenase from the micro-aerophilic hyperthermophilic bacterium *Aquifex aeolicus.*

The first part is centred on the study of the [NiFe] enzyme from *D. vulgaris,* for which the intermediates of the reaction cycle were studied in detail by infrared techniqes. Using SEIRA spectroscopy the catalytic activity of this enzyme adsorbed on an electrode was monitored, yielding essentially the same results as FTIR spectroelectrochemistry in solution. The EPR silent inactive state (Ni-SI$_r$)$_I$ was shown to be light sensitive and a new state Ni-SL could be detected. Wavelength dependence and time resolved kinetics showed that the light sensitivity corresponds to the dislocation of the hydroxyl ligand present in the active site of (Ni-SI$_r$)$_I$. For the transition from the light-induced Ni-L state to Ni-C a large (H/D) kinetic isotope effect was obtained, showing that the rate limiting step is the binding of a hydron at the active site. Using FTIR spectroelectrochemistry and EPR, the inhibition of the enzyme by carbon monoxide was studied and formation of two CO-adducts demonstrated. Time resolved FTIR studies at low temperatures used the reversible photolysis of the external CO ligand to estimate the activation barrier for its rebinding at the active site.

The second part of this study comprises an in-depth investigation of the Hydrogenase I from *Aquifex aeolicus*. Chronoamperometric electrochemical measurements provided evidence for the oxygen tolerance of this hydrogenase. FTIR electrochemistry in solution detected only four redox intermediate states with significantly more positive midpoint potentials than those measured for standard hydrogenases. Carbon monoxide was shown to bind to the active site of Hydrogenase I much weaker than to that of *D. vulgaris*. By an EPR redox titration the types and midpoint potentials of all iron-sulphur centres were determined. Based on these results a model for the oxygen tolerance of Hydrogenase I is proposed The study is concluded by examining the interaction of the active site with the substrate in the catalytically active Ni-C state, in which a weakly bound hydride was found.

# Acknowledgements

For a journey to begin, one needs two things; an origin and a destination.

Above all, I would like to thank my father Iosif, my mother Kaiti and my brother George for being my origin and the 'safe' port all these years. They have always encouraged me to discover the possibilities of life and taught me not to be afraid to try.

I would like to thank Professor Dr. Wolfgang Lubitz for giving me a destination and making this journey possible. He has been an invaluable supervisor and has been continuously supporting my research on hydrogenase. Lengthy discussions, critical comments and his broad scientific background have significantly influenced the present work.

Dr. Hideaki Ogata and Dr. Marco Flores are gratefully acknowledged for helping me build and visualise my project. Their continuous support has been invaluable.

Dr. Pascale Tron-Infossi and Dr. Marie-Thérèse Giudici-Orticoni are specially acknowledged for giving me the opportunity to study the hydrogenase from *Aquifex aeolicus* and for an excellent collaboration.

Dr. Wolfgang Nitschke is specially thanked for spending countless hours with me performing the EPR redox titrations and his invaluable insight that helped me understand electron transfer processes in proteins.

My companions in this journey are all my coworkers in the Max-Planck Institute. Each one of them contributed to a small or to a larger degree to the completion of this study. Special thanks to Dr. Alexey Silakov, Dr. Jens Niklas, Dr. Shipra Prakash, Brian Wenk, Dr. Christina Kamp, Dr. Alexander Marchanka, Dr. Petra Kellers, Dr. Daniele Biglino and Dr. Özlen Erdem.

Dr. Aruna Goenka-Agrawal and Dr. Maurice van Gastel are thankfully acknowledged for sharing with me their previous observations and experience on the hydrogenase field.

Dr. Eckhard Bill is gratefully thanked for helpful discussions on magnetic/electronic properties of complexes and for critically reading part of the present work.

Dr. Misha Antonkin is gratefully thanked for critically reading part of the thesis and for fruitful discussions concerning iron-sulphur proteins.

*Something…*

*Ερχεται καποια στιγμη στη ζωη, που δεν μας μενει αλλο παρα να διαλεξουμε το δρομο μας.*
*Ερχεται καποια στιγμη που*
*πρεπει να ζωντανεψουμε*
*τα ονειρα μας και να*
*υπερασπιστουμε αυτο που πιστευουμε*

*There comes a time in our life when we do not have any other choice*
*than to choose our own path.*
*There comes a time*
*when we have to awaken our dreams*
*and fight for all the things we believe in.*

*To my Dad, to my Mom and to my Brother*

# Table of Contents

*Table of Contents*

*Table of Contents*

*Table of Contents*

9

# Pȓeface
# Hydrogen from Hydrogenases

Motivation for this work

The use of hydrogen as an energy source is widespread among a variety of microorganisms that, depending on their biotope environment, use different electron acceptors. The reaction catalysed by hydrogenases is deceptively simple:

$$H_2 \rightleftharpoons 2H^+ + 2e^-$$

and it does not reflect the complexity or diversity of the molecular machinery involved in the energy metabolism of each microorganism.

The constantly growing interest in the usage of alternative sources of energy has brought hydrogenases into the spotlight of future applications such as biohydrogen production and biofuel cells. The limiting factor towards this direction is the strict requirement for anaerobicity in order to maintain functionality of these enzymes. The discovery of hydrogen-oxidising microorganisms that utilize molecular oxygen as a final electron acceptor has been pivotal, as it is most likely associated with a molecular modification for their adaptation in oxic environments.

On this basis and in order to gain information that would provide insight into the functional characteristics of these enzymes, the present study comprises an examination of two hydrogenases from distinct species. The first hydrogenase is a membrane attached [NiFe] enzyme from the mesophilic, anaerobic sulphate reducing bacterium *Desulfovibrio vulgaris* Miyazaki F. The second is a membrane bound hydrogenase associated with the respiration metabolic pathway of the hyperthermophilic, microaerophilic bacterium *Aquifex aeolicus*.
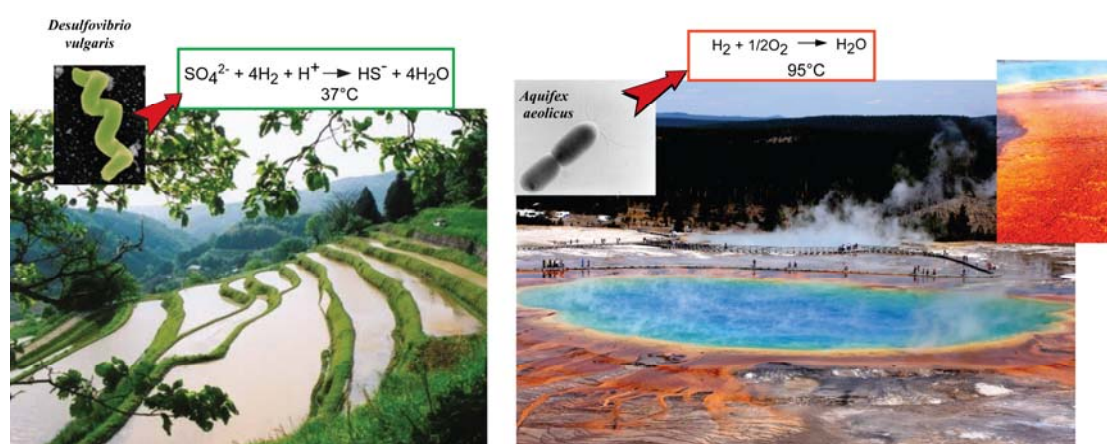


**Figure:** The biotopes of *Desulfovibrio vulgaris* and *Aquifex aeolicus* as well as their primary hydrogen oxidising metabolic processes.

*Preface*

The [NiFe] hydrogenase from *Desulfovibrio vulgaris* Miyazaki has been structurally well characterised. However, there are still important mechanistic aspects to be identified, reflecting the composite nature of the catalytic function of these enzymes and their behaviour towards inhibitors. The study of *Desulfovibrio vulgaris* hydrogenase has a two-fold objective; to disambiguate and advance the existing information on the function of such enzymes and to use the obtained knowledge as a basis for an in-depth understanding of the deficiently characterized hyperthermophilic hydrogenases, e.g. *Aquifex aeolicus*. In view of the enhanced oxygen tolerance and thermostability of the latter, their characterisation is crucial for understanding the reasons underlying these properties. For this purpose a series of spectroscopic and electrochemical studies in the presence of substrate and potential inhibitors were carried out so as to improve our knowledge on the reactivity of this enzyme and determine the redox processes involved.

Chapters 1 and 2 provide a short introduction to hydrogenases and to the experimental techniques employed. The following chapters are arranged into two parts. The first part of the present study focuses on the [NiFe] hydrogenase from *D. vulgaris* Miyazaki F and consists of Chapters 3 to 6. In Chapter 3 electrochemical measurements on this enzyme adsorbed on an electrode monitored by SEIRA are compared to those in solution. In addition, the unready states Ni-A/Ni-SU have been re-examined. Chapter 4 presents a study on the inhibition mechanisms of this hydrogenase with carbon monoxide studied by FTIR electrochemistry. Further low temperature photolytic experiments allow the estimation of the activation barrier for the back conversion processes. Chapter 5 describes the structural changes associated with the light sensitivity observed for the EPR-silent ready state Ni-SI$_r$, a study that contributes significantly to its so far insufficient characterisation. In Chapter 6, isotope labelling and the light sensitivity of the Ni-C state are used in order to identify the rate limiting step in the back conversion reaction from the light-induced state (Ni-L).

The second part comprises Chapters 7 to 10 and is focused on the characterisation of the [NiFe] hydrogenase I from *Aquifex aeolicus*. In Chapter 7 FTIR electrochemistry is employed to identify the redox intermediates involved in the mechanism of this hydrogenase. In addition, protein film voltammetry experiments were carried out to examine the oxygen tolerance of this enzyme. Chapter 8 deals with

the carbon monoxide inhibition and the findings are compared to those from *D. vulgaris* described in Chapter 4. Having determined the redox chemistry of the [NiFe] site, Chapter 9 focuses on the characterisation and redox properties of the iron-sulphur cofactors. A pH dependent EPR potentiometric titration was carried out to identify the type of the electron relay centres in Hydrogenase I from *A. aeolicus* and compare their properties to oxygen-sensitive hydrogenases such as *D. vulgaris*. In Chapter 10 an ENDOR/HYSCORE study of the (H/D) exchangeable hydride ligated to the active site of known [NiFe] hydrogenases is presented. It is shown that this ligand is present in the Hase I from *A. aeolicus* and its photolytic and electronic properties are examined. In Chapter 11 the results from both [NiFe] hydrogenases are combined and the most important conclusions are given. This 'integrating' approach on hydrogenases derived from two different organisms will help to illustrate the properties of each enzyme and understand the mechanistic aspects of their function.

# Chapter 1

## Hydrogenases

The production or utilisation of hydrogen gas plays an important role in the metabolism of many microorganisms[1,2]. Production of dihydrogen is mostly a feature of fermentative anaerobes that utilize protons as terminal electron acceptors. Hydrogen can be also used as a reductant by catalysing its oxidation; the electrons produced can be utilised to generate energy and are ultimately employed to catalyse the reduction of a variety of inorganic species (i.e. $CO_2$, $Fe^{3+}$, $N_2$, $NO_3^-$, $SO_4^{2-}$)[1]. Although most organisms involved in hydrogen metabolism are anaerobic prokaryotes, examples are known from eukaryotes and (micro)aerobes that can derive energy from the reaction of $H_2$ with $O_2$ to form water[1]. The redox chemistry of $H_2$ is catalysed by the enzyme hydrogenase, most likely one of the most ancient enzymes in biology, according to the reaction:

$$H_2 \rightleftharpoons 2H^+ + 2e^- \qquad (E_0 = -414 \text{ mV}),$$

which is the reversible conversion of molecular hydrogen to two electrons and two protons[3]. Hydrogen isotope exchange experiments indicate that the $H_2$ cleavage reaction is heterolytic; thus, a hydride and a proton are generated in the first step[4]. In the second step, the two electrons of the hydride are extracted, and a second proton is formed. The vectorial use of such enzymes (e.g. across a membrane) may represent a primitive mechanism for generating and maintaining proton gradients. All hydrogenases are metalloproteins consisting either of Ni and /or Fe metal cofactors and typically consist of multiple subunits[5]. The use of metals in the catalytic centres of hydrogenases increases the acidity, electrophilicity and/or nucleophilicity of reaction species and thus the ability to donate or receive electrons, while the primary and secondary metal coordination sphere is chosen so as to optimise its reactivity.

Phylogenetically, they can be classified into three distinct groups according to the metal content of their active site[5]; (a) [NiFe] hydrogenases with a hetero-nuclear nickel-iron bimetallic site[6], (b) [FeFe] hydrogenases with a di-iron site linked to a $Fe_4S_4$ cluster[7] and (c) iron-sulphur cluster-free (Hmd) hydrogenases with a mononuclear iron centre[8]. The present study is focused on the characterization of [NiFe] hydrogenases on the basis of their electronic and catalytic properties. It was carried out on enzymes from two extreme families; mesophilic, strictly anaerobic

(*Desulfovibrio vulgaris* Miyazaki F)[9] and hyperthermophilic, microaerobic (*Aquifex aeolicus*)[10] microorganisms, in an attempt to exemplify similarities or differences and gain a better understanding of their functionality as well as their response to inhibitors.

**1.1 Molecular Structure of [NiFe] hydrogenases**

The first crystal structure of a [NiFe] hydrogenase was reported in 1995 for the sulphate reducing bacterium *Desulfovibrio gigas* at a resolution of 2.85 Å[6]. Only two years later, the crystal structure from another sulphate reducer *Desulfovibrio vulgaris* Miyazaki F was published in 1997 at 1.8 Å[11]. Since then, several crystal structures for [NiFe] hydrogenases have been resolved. These crystallographic studies revealed a heterodimeric enzyme, consisting of a large and a small subunit (Figure 1).
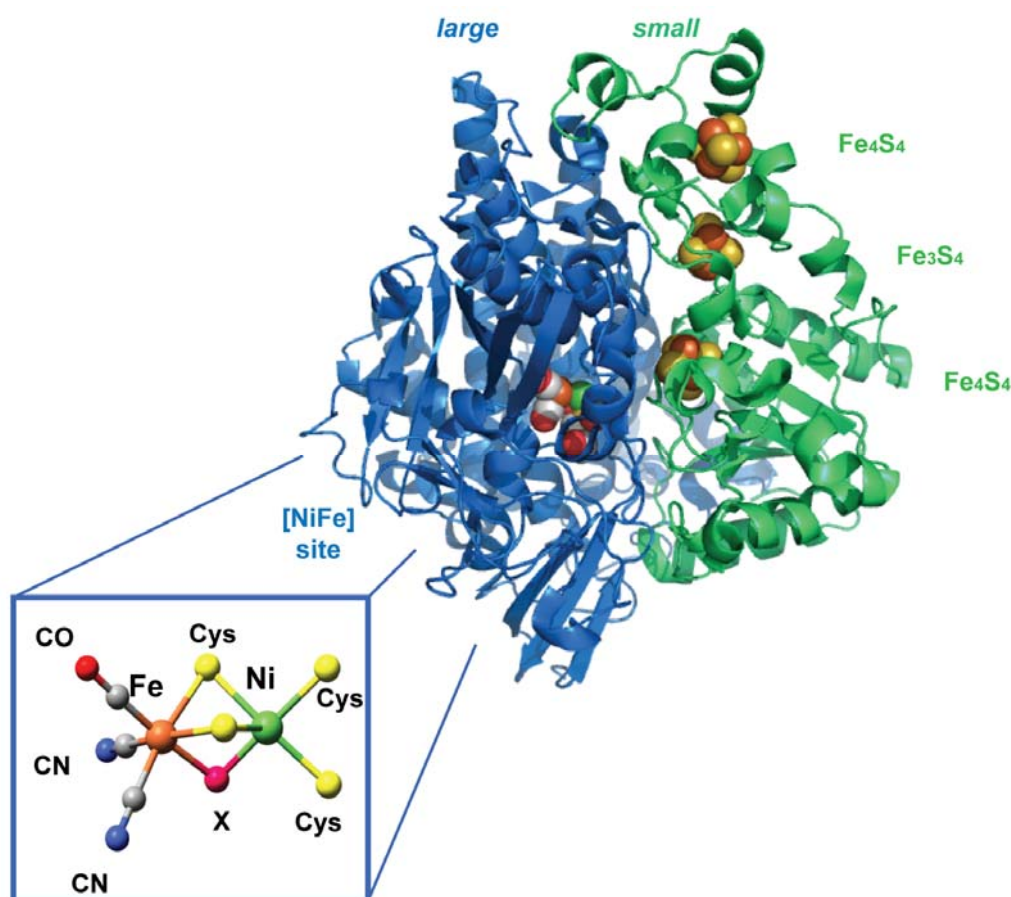


**Figure 1.** The crystal structure of the [NiFe] hydrogenase from *Desulfovibrio vulgaris* Miyazaki F (1WUJ pdb entry). The large subunit that harbours the heterobimetallic site (insert) is shown in blue and the small subunit carrying the iron-sulphur clusters in green.

The large subunit contains a [NiFe] active site. Its coordination in the protein is mediated by two Fe-Ni-bridging and two nickel-binding terminal cysteinyl thiolates. The iron atom is additionally coordinated by three diatomic molecules, one carbonyl and two cyanides, which were uniquely indentified by Fourier transform spectroscopic[12] and $^{13}C$, $^{15}N$ isotope labelling studies[13,14]. The nickel ion has a coordination site available (bridging and terminal) for binding exogenous ligands. An additional metal centre near to the active site was found in the C-terminus of the large subunit, which in the case of *D. vulgaris* Miyazaki F is a $Mg^{2+}$ ion in a distorted octahedral coordination environment with three amino acid residues (Glu62, His552, Leu498 - *D. vulgaris* numbering) and three water molecules[11]. This ion is believed to be involved in the maturation process[15].

The small subunit consists of three almost linearly situated iron-sulphur centres; a $[Fe_3S_4]^{1+/0}$ cluster in-between two low potential $[Fe_4S_4]^{2+/1+}$ clusters[16]. On the basis of their distance from the [NiFe] active site these are characterized as proximal, medial and distal. The distal cluster has a rather unusual coordination, in which one of the irons is ligated by a histidine that is exposed at the surface of the protein[6]. These iron-sulphur clusters are involved in the electron transport between the [NiFe] active site and the physiological partner of hydrogenase. The electron transfer is based on the propensity of Fe to formally switch between oxidative states +2 and +3. Depending on their protein surrounding and the cofactor properties, iron-sulphur clusters can have various redox potentials[17]. In the case of hydrogenases from *Desulfovibrio* and *Ralstonia* species these potentials have been determined by EPR titrations[16,18,19].

The proton pathway is not that straightforward. Protons are transported inside proteins via motions of water molecules and amino acid residues with acid-base properties, (i.e. histidine, glutamic acid, aspartic acid). Most of the experimental data support the general view that the proton acceptor group after heterolytic cleavage of $H_2$ in the active site is one of the terminal cysteine thiols[3,15,20]. Most likely this cysteine is the starting or the ending point of the proton transport pathway. A glutamic acid residue conserved in [NiFe] hydrogenases and hydrogen bonded to this cysteinyl bound to nickel was shown to be essential for proton transfer[21].
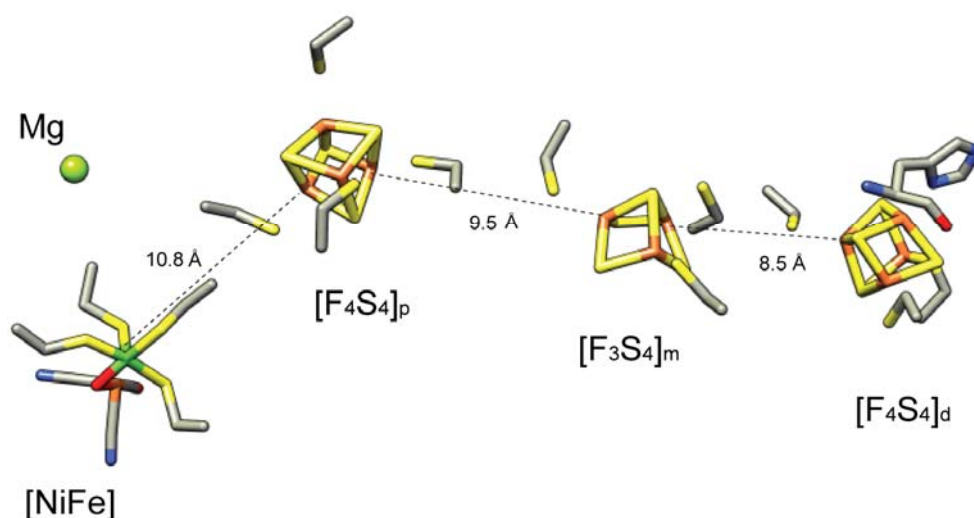
**Figure 2.** The FeS cofactors mediating electron transfer between the [NiFe] site and the cyt $c_3$ in the hydrogenase from *D. vulgaris* Miyazaki F. The approximate distances depicted are obtained from the crystal structure (1WUJ, pdb entry). The location of the $Mg^{2+}$ has been also included.

To probe the gas accessibility at the active site of the enzyme, Xenon binding experiments were carried out on single crystals of the [NiFe] hydrogenase from *D. gigas*[22]. These experiments showed that hydrogenases have hydrophobic channels that allow the substrates and the inhibitors to enter and circulate in the protein[22]. The end of the hydrophobic channel ends near a vacant terminal binding site at the nickel (approximately 4.5 Å), which is believed to be the point of heterolytic cleavage of dihydrogen.

**1.2 Anaerobic sulphate reducing bacteria**

**1.2.1 The [NiFe] hydrogenase from *Desulfovibrio vulgaris* Miyazaki F- Hydrogen metabolism**

Sulphate reducing bacteria are a biochemically diverse group of strictly anaerobic bacteria that share in common the ability to utilize sulphate as a terminal electron acceptor ($SO_4^{2-}$). The [NiFe] hydrogenase from *Desulfovibrio vulgaris* Miyazaki F is part of the energy pathway that couples dihydrogen oxidation to sulphate reduction, while the generated protons are imported through ATP synthase for ATP synthesis. It is a periplasmic hydrogenase, anchored to the membrane via a

soluble tetrahaem cytochrome $c_3$. The transient complex formation by [NiFe] hydrogenase and cyt $c_3$ was investigated by means of NMR in order to study the site of interaction between them[23].

The interaction (docking site) of this multi-haem centre with the [NiFe] hydrogenase is proposed to involve the histidine ligand of the distal [Fe$_4$S$_4$] cluster and the aromatic ring of a nearby conserved phenylalanine (His188, Phe197- *D. vulgaris* Miyazaki numbering)[23]. The respective macroscopic redox potentials of each haem of the cyt $c_3$ subunit have been determined and have been found to be unusually low (~ -300 mV)[24,25] compared to those of mitochondrial cyt $c$. At the first reduction step, the haem-specific redox potential of haem IV is the highest at pH 7, therefore this haem is most suitable for accepting an electron. This supports the idea that haem IV is the physiological interaction site in the electron transfer from hydrogenase to cyt $c_3$. Electrons are transferred from hydrogenase to cytochrome $c_3$, which can then be channelled through the cytoplasmic membrane for sulphate reduction, whereas haem III has a lower redox potential and is involved in the electron transport from cytc$_3$ to hydrogenase.
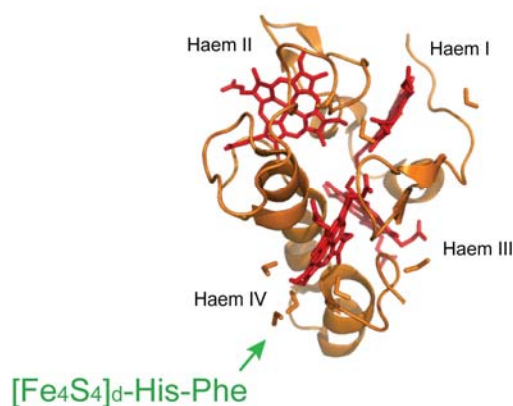


**Figure 3.** Crystal structure of the cyt $c_3$ and interaction site with the small subunit (1J0O, pdb entry).

The pathway of dissimilatory sulphate reduction involves three key enzymes. Sulphate is activated to adenylylsulphate (adenosine-5-phosphosulphate, APS) by ATP sulphurylase (Sat) at the expense of ATP; hereafter, APS reductase (Apr) converts APS to AMP and sulphite is reduced to sulphide by the sulphite reductase (Dsr).
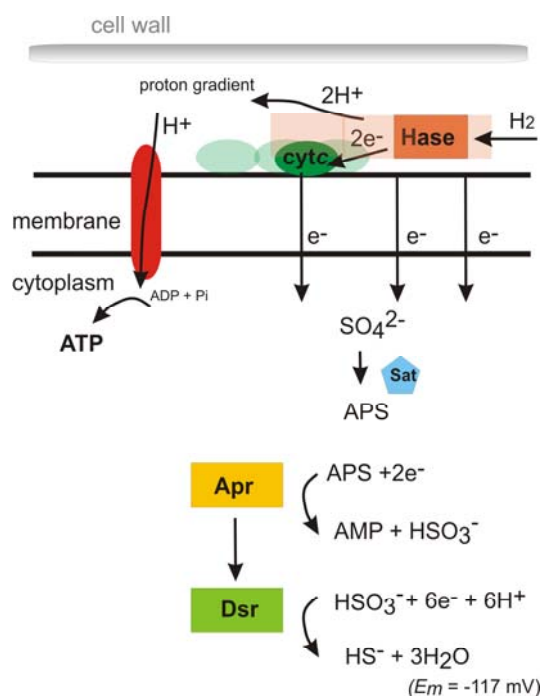
**Figure 4.** Hydrogen metabolism in *Desulfovibrio vulgaris* Miyazaki F; dihydrogen oxidation is coupled to sulphate reduction. Modified and adapted from [26].

On the basis of the formal reduction potential of electron donors and electron acceptors in electron transfer processes the midpoint redox potentials for the $SO_4^{2-}/HSO_3^-$ couple is -516 mV and the $HSO_3^-/HS^-$ couple is -117 mV[27].

## 1.2.2 The [NiFe] hydrogenase from *Desulfovibrio vulgaris* Miyazaki F-
## Redox Chemistry

The redox chemistry of the [NiFe] hydrogenases is rich and involves many intermediate states, both functional and inactive, since apart from catalysing $H_2$ oxidation/production, they can also interact with gaseous molecules (i.e. carbon monoxide, oxygen) and become inhibited[28-31]. It is thus important to gain an understanding into how hydrogenases catalyze $H_2$ production and oxidation, to determine the mechanisms by which they are inactivated under oxidizing conditions and how they may become re-activated. A combination of spectroscopic and electrochemical methods has provided structural knowledge on the oxidised and reduced forms of the enzyme, namely electron paramagnetic resonance (EPR) spectroscopy, Fourier transform infrared (FTIR) spectroscopy and protein film voltammetry (PFV).

The Ni ion can shuttle between the trivalent ($3d^7$, $S=1/2$) and the divalent state ($3d^8$, $S=0,1$), whereas it has been shown that it can have also a monovalent configuration ($3d^9$, $S=1/2$)[28-31]. The Fe ion remains low-spin $Fe^{2+}$ at all times. Electron paramagnetic resonance (EPR) can be used to study the properties of $Ni^{3+/1+}$ (the $S=1$ state of $Ni^{2+}$ is EPR-silent) and of the iron-sulphur centres in their paramagnetic oxidation states[16]. However, since not all states participating in the mechanism of hydrogenases are paramagnetic, the application of complementary techniques, (i.e. FTIR spectroscopy), have contributed in obtaining an overall picture on the activity of such enzymes. The further coupling of these techniques with electrochemistry has significantly contributed in characterising these enzymes[28,31,32].

In the presence of oxygen [NiFe] hydrogenases are reversibly inhibited. Purification is carried out aerobically and the protein is obtained in inactive states with oxygen based ligands present in the bimetallic site. The two most oxidised oxygen inhibited forms are denoted as Ni-A and Ni-B[33]. They are both paramagnetic ($Ni^{3+}$, $S=1/2$) but differ in their spectroscopic and catalytic properties. Ni-B is readily activated in the presence of $H_2$ or under reducing conditions, whereas Ni-A shows a long delay in its activation kinetics[34,35]. The difference in their activation rates has been ascribed to the presence of a different type of oxygenic bridging ligand, $OH^-$ for Ni-B[36] and a hypothetic hydroperoxide for Ni-A, since recent X-ray diffraction studies have revealed the ligand in the bridging position to be *diatomic*[37,38]. On the other hand, all iron-sulphur centres are in their oxidised form and thus only the $[Fe_3S_4]^{1+}$ is paramagnetic and can be observed by EPR as a nearly isotropic signal centred at g= 2.02[39].

One-electron reduction of Ni-B, Ni-A produces $Ni-SI_r$ and Ni-SU states respectively ($Ni^{2+}$, EPR silent). ($Ni-SI_r$) exists in two states that are in acid base equilibrium. $(Ni-SI_r)_I$ is proposed to have an $OH^-$ and $(Ni-SI_r)_{II}$ a water ligand loosely bound to the active site. At this redox level, the medial $[Fe_3S_4]$ cluster starts to become reduced. Upon activation, the oxygen ligand in the bridging position is lost and the enzyme makes a transition to the $Ni-SI_a$ state ($Ni^{2+}$, EPR silent)[28-31].
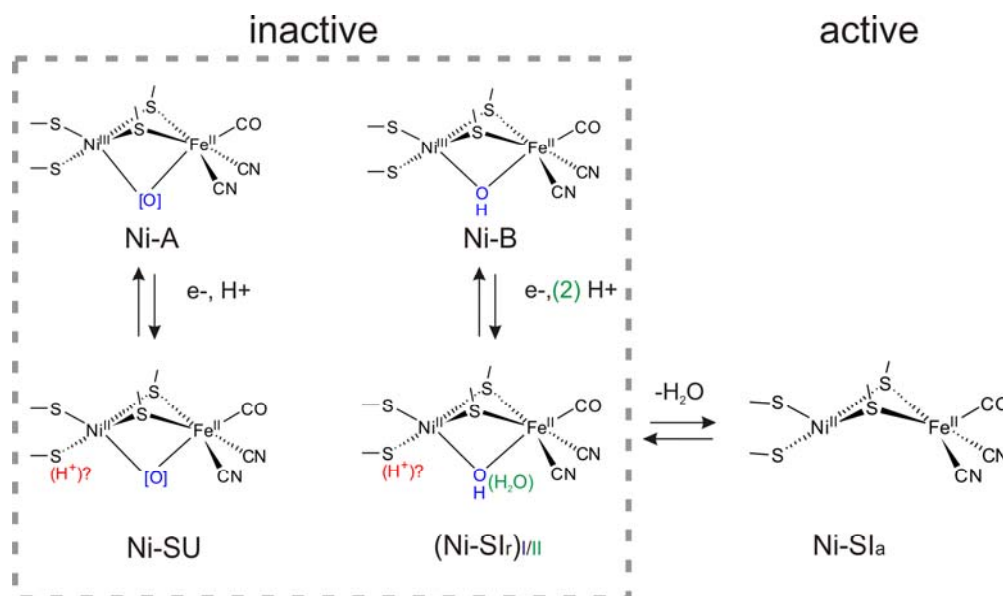
**Figure 5.** Proposed (re-)activation mechanism of the oxygen inhibited states for the [NiFe] hydrogenase from *Desulfovibrio vulgaris* Miyazaki F [30].

Further reduction leads to the Ni-C state (paramagnetic S = 1/2, $Ni^{3+}$). Ni-C is directly involved in the hydrogen converting mechanism and was shown to carry a hydrogenic species by Electron Nuclear Double Resonance (ENDOR) and Hyperfine Sublevel Correlation (HYSCORE) spectroscopy, first in *Ralstonia eutropha*[40] and later also in *D. vulgaris* Miyazaki F[41]. In these experiments a hydride ligand ($H^-$) in the bridging position between the two metals was detected.

At this redox level the [$Fe_4S_4$] clusters start to become reduced, which is inferred at low temperatures in the EPR spectra from the magnetic interaction of the reduced proximal [$Fe_4S_4$]$^{1+}$ cluster (S=1/2) with the nickel centre. This interaction changes the Ni-C signal into a complex EPR spectrum, the so-called split Ni-C signal that is visible only at low temperatures[42].
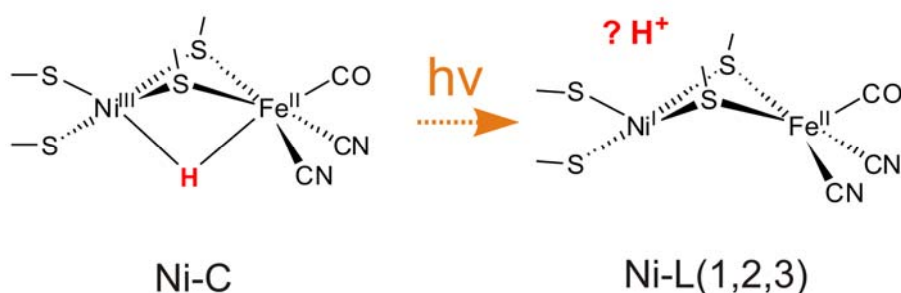
**Figure 6.** Light sensitivity of the Ni-C state is accompanied by photodissociation of the bridging hydride as a proton. The light-induced state is known as Ni-L, while the location of the proton after illumination has been suggested to be one of the coordinating thiols.

Illumination at cryogenic temperatures (T ≤ 170 K) converts Ni-C to the so-called Ni-L state with concomitant photo-dissociation of this bridging hydride[40,43]. Density functional calculations support a formal $Ni^{1+}$ oxidation state for Ni-L, indicating that upon illumination a proton is removed from the bridging position of the active site[44]. Further reaction of Ni-C with hydrogen produces Ni-R ($Ni^{2+}$, EPR silent S=0 or S=1), which can exist in more than one protonation state. Recent theoretical studies support that $Ni^{2+}$ is in the low spin state for the Ni-S states, whereas for the Ni-R a high spin $Ni^{2+}$ is suggested[45,46].

In addition to molecular oxygen, CO is well known to be a competitive inhibitor of [NiFe] hydrogenases. Already in 1962, CO inhibition was observed to be reversible by light or by flushing the protein with hydrogen[47]. In later years, FTIR and EPR studies showed that CO inhibition can be summarized into two distinct CO-bound enzyme conformations; a paramagnetic (Ni-CO) and an EPR-silent state (Ni-SCO)[48]. The carbon monoxide complex of the [NiFe] hydrogenase from *Desulfovibrio vulgaris* in the Ni-SCO state was characterized by crystallographic studies, in which CO was unambiguously shown to bind to the nickel in a terminal fashion[49]. Stopped flow EPR studies showed that Ni-CO can be formed when carbon monoxide binds to the active site of the Ni-L state at near cryogenic temperatures[50], whereas the EPR-silent Ni-SCO form results from reaction of the active enzyme with CO under physiological conditions. An overview of all the characterized states in sulphur reducing bacteria and in particular for the *Desulfovibrio vulgaris* hydrogenase (active, inactive) is given in Figure 7.
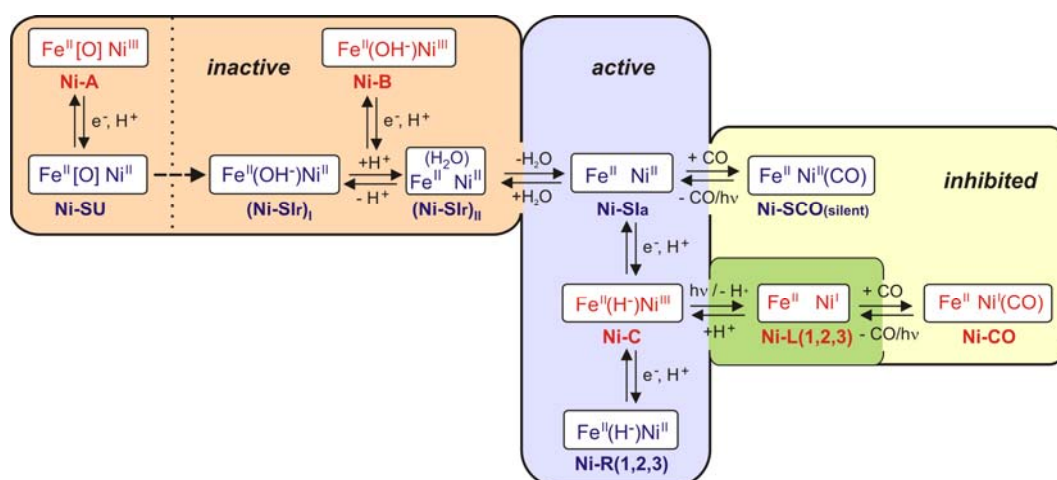
**Figure 7:** Overview of the possible nickel redox states in the [NiFe] hydrogenase from *D. vulgaris* Miyazaki F as adapted from[30].

**1.3 Microaerophilic hyperthermophilic bacteria**

**1.3.1 The [NiFe] hydrogenase(s) from *Aquifex aeolicus* –**

**Cofactors and hydrogen metabolism**

Hyperthermophilic bacteria and archea represent organisms that thrive at the upper-temperature limit of life. They optimally grow between 80°C and 100°C and are usually hosted in biotopes such as volcanic areas (terrestrial hot springs) and submarine hydrothermal vents[51,52]. Among these hyperthermophiles and on the basis of phylogenetic analysis, the *Aquificaceae* represent the most deeply branching family within the bacterial domain.
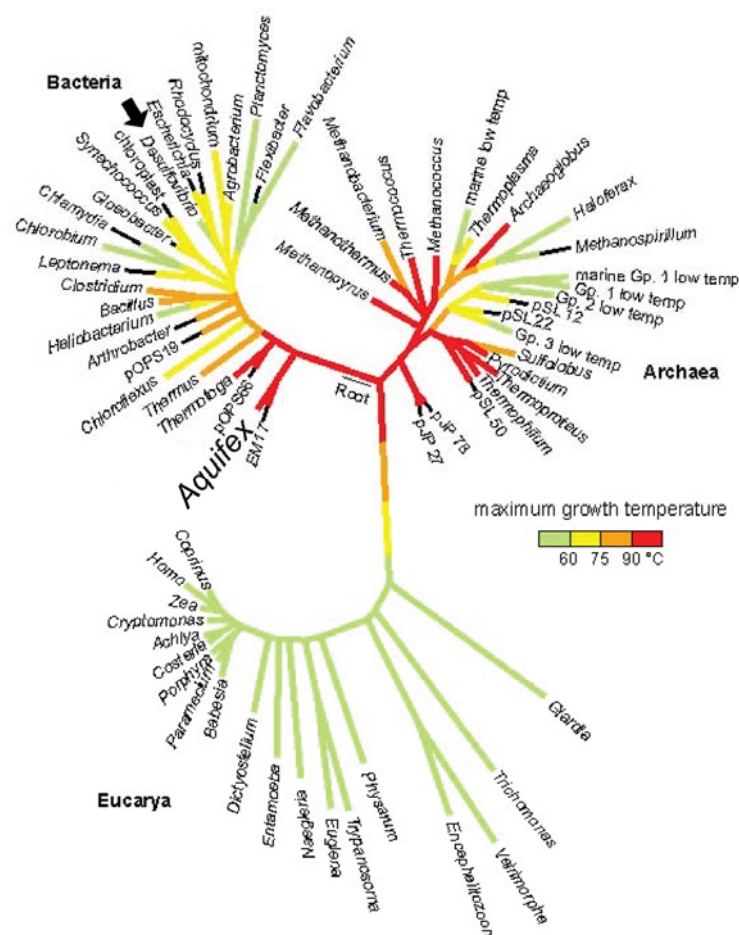


**Figure 8.** The genus *Aquifex* of the *Aquificaceae* phylum within the RNA-based phylogenetic tree[53]. The position of the *Desulfovibrio* species is indicated with an arrow.

The order *Aquificales* are all thermophilic or extremely thermophilic bacteria, and obtain energy by respirative hydrogen oxidation. This reaction is known as the "Knallgas" reaction. They are obligate aerobes, generally microaerophilic (the solubility of oxygen in water at the temperatures these organisms grow at is very low). Reduced sulphur compounds such as sulphide, thiosulphate ($S_2O_3^{2-}$), or elemental sulphur can generally replace hydrogen, but nitrate cannot replace oxygen as the terminal electron acceptor in most species. These organisms are autotrophic, fixing carbon dioxide via the reverse tricarboxylic acid cycle (TCA) cycle[54].

The present study is focused on *Aquifex aeolicus*, one of the most hyperthermophilic bacteria known. It is able to grow chemolithoautotrophically at 85-95 °C with hydrogen as the electron donor and oxygen as an electron acceptor in the presence of a sulphur compound (thiosulphate or elemental sulphur)[54]. Its complete genome was sequenced at 1998[55] and it is commonly found in the outflow of hot springs. It encodes three distinct [NiFe] hydrogenases[56]; Hydrogenase I and II that are membrane bound and involved in energy conservation mechanisms and Hydrogenase III that is cytoplasmic and involved in the $CO_2$ fixation mechanism. The use of oxygen as an electron acceptor (albeit at very low concentrations) is supported by the presence of a complex respiratory apparatus. Hydrogenase (Hase) I as part of this aerobic respiration pathway coupled to hydrogen oxidation is shown in Figure 9 and the individual components will be selectively described.
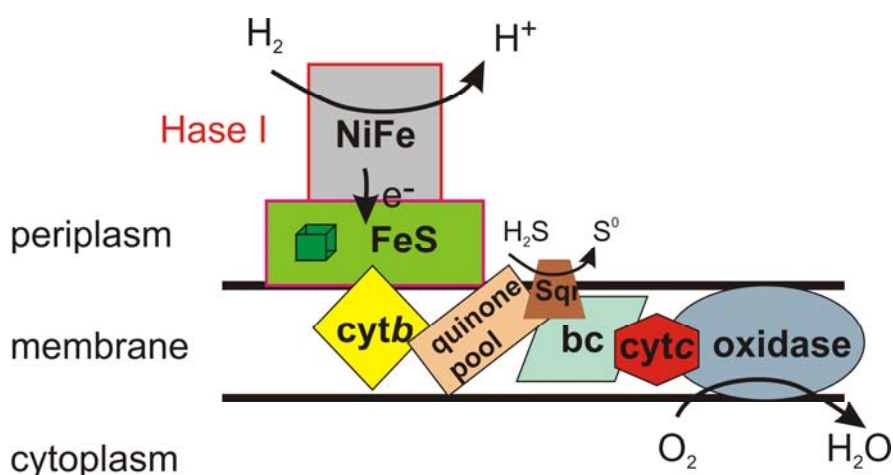


**Figure 9.** Hase I as part of the hydrogen metabolism in *Aquifex aeolicus* involved in the aerobic respiration[57].

The amino acid sequence of the large subunit of the [NiFe] hydrogenase from *Desulfovibrio vulgaris* is strongly homologous to Hase I; the [NiFe] site is ligated by four cysteinyl residues, found in pairs at the N- and C- terminal ends of the large subunit. These are surrounded by well-conserved sequence stretches denoted as L1 (N-terminal) and L2 (C-terminal) motifs. On the basis of these motifs hydrogenase I belongs to Group I according to the classification proposed by Vignais et al [5].

The electrons produced by heterolytic cleavage of dihydrogen at the catalytic site are transferred to the physiological redox partner by a chain of iron-sulphur clusters, situated in the small subunit. The crystal structure of Hase I is not yet available, but amino acid sequence alignments have shown the ten cysteines that bind three iron-sulphur centres in known hydrogenases to be conserved. The absence of a fourth ligand in the medial cluster and the histidine ligation in the distal iron-sulphur cluster implies a strong similarity between the iron-sulphur centres found in Hase I and the hydrogenases from sulphate reducing bacteria. On the other hand, the presence of two additional cysteines in the protein fold of the proximal to the [NiFe] site cluster was found, which is rather unusual by not entirely rare. An identical ligation has been also found for the membrane bound (MBH) hydrogenase from *Ralstonia eutropha*[58] as well as for a number of thermophilic and other not well-characterized enzymes. An amino acid sequence alignment for certain well-characterized species is shown in Figure 11.

Electrons are channelled through the iron-sulphur centres to the physiological acceptor, a di-haem *b*-type cytochrome. The $[Fe_4S_4]_d$-His-Phe motif proposed to be the interaction site of the small subunit with the cyt $c_3$ in *Desulfovibrio vulgaris* is also conserved, indicating a similar type of interaction in Hase I with cyt *b*. The cyt *b* contains two haems with different redox potentials and is strongly homologous to the cyt *b* in the respiratory chain of the *Wolinella succinogenes* [NiFe] hydrogenase that is connected to menaquinone reduction[59]. On the basis of their similarity, both haem groups are proposed to be involved in the electron transport towards the quinone pool. Hydrogenase I alone or as a Hydrogenase I-cyt *b* complex can couple $H_2$ uptake with the reduction of electron acceptors in a wide range of potentials (e.g. methyl viologen, methylene blue, phenazine methosulphate, DCIP)[56]. The reduction of high-potential electron acceptors was more efficient than the reduction of low-potential ones.
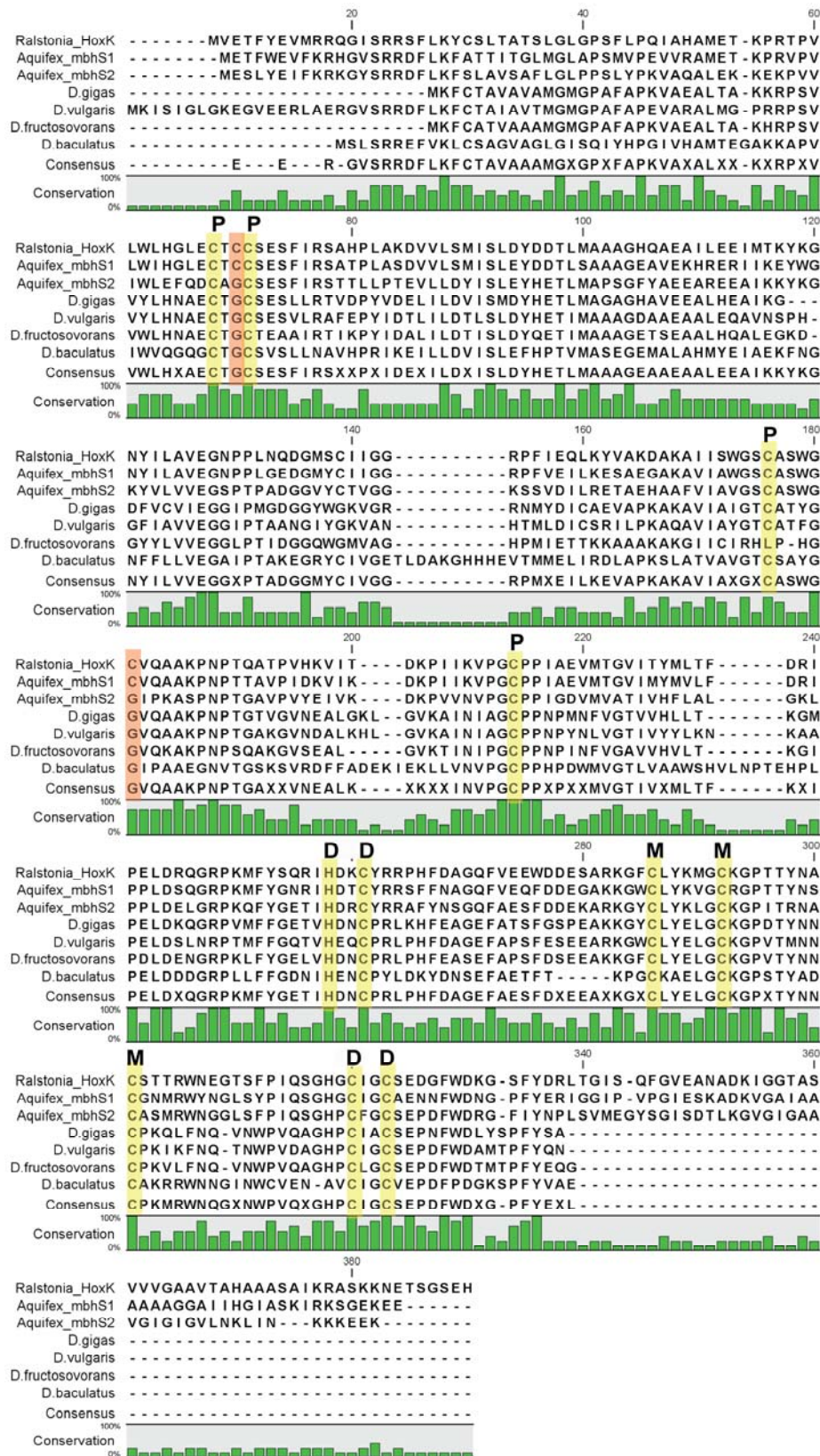
**Figure 11.** Sequence alignment (clystalW) of the small subunits of the [NiFe] hydrogenases from *Aquifex aeolicus* (Hase I/II), MBH from *R. eutropha*, *D. gigas*, *D. vulgaris*, *D. fructosovorans*, *D. baculatus*.

From an inspection of quinone genes in the *Aquifex* genome it was suggested that it uses ubiquinone (UQ) as a quinone pool. Recently however, *Aquifex aeolicus* has been identified by solution NMR to contain a demethylmenaquinone (DMK) pool, while there is evidence that it could also be a menaquinone (MK) type[60], similar to the one in *Wolinella succinogenes*. Such a difference is expected to be significant for the electron transfer pathway, since MK has a formal reduction potential of -74 mV and DMK of +36 mV[61].
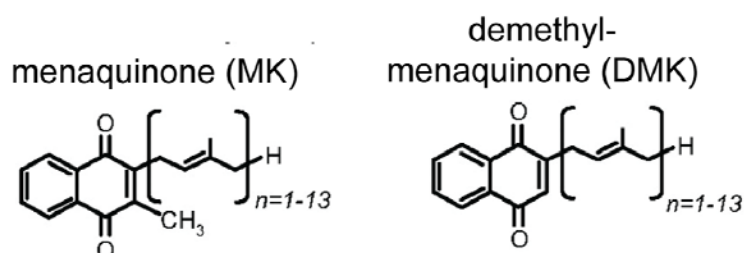


**Figure 12.** The two possible quinone pools in the *Aquifex aeolicus* aerobic respiration pathway.

In Figure 10 next to the quinone pool, a sulphide quinone reductase (Sqr) is situated[62]. However its position is merely schematic. It is a flavoprotein and a short time ago its structure was reported. Recent studies have proposed the coexistence of two models[57]; (a) Sqr catalyses the oxidation of sulphide to sulphur and reduces the quinone pool, whereas part of the quinol becomes reoxidised by the *bc* complex and (b) electrons are transferred from Hase I in interaction with the cyt *b* to the quinone, pass through the *bc* complex, the membrane bound cytochrome *c* and are used for the reduction of molecular oxygen. The fact that proteins associated with sulphide/hydrogen oxidation to oxygen reduction are found in the same position in native gels, suggests that these individual components can be organised *in vivo* in supramolecular structures. This organisation might be a way to regulate electron partitioning in the different pathways and contribute to the protein structure stabilisation at high temperatures.

The *bc* complex has been characterized by optical and EPR methods and contains two *b*-type cytochromes, a mono-haem cytochrome *c* and two Rieske centres

with distinct redox potentials[60]. It is the only naphthoquinol oxidising *bc* complex reported so far. The electron acceptor of the *bc* complex is the cytochrome $c_{555}$, for which within this year a crystal structure was reported in 1.15 Å resolution[63]. It is a mono-haem centre with a unique extra helix and an increased number of hydrogen bonds with the protein backbone. High thermostability and protection against denaturation is proposed to therefore take place due to the restricted conformational flexibility through hydrogen bonds and an extra-helix.
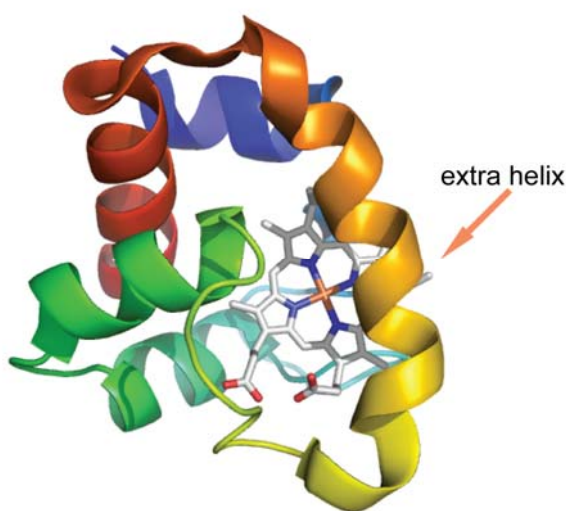


**Figure 13.** Crystal structure of the cytochrome $c_{555}$ in the 'Knallgas' pathway coupling hydrogen oxidation to molecular oxygen reduction (2ZXY, pdb entry).

### 1.3.2   The [NiFe] hydrogenase from *Aquifex aeolicus-*
### Physicochemical and redox properties

The aerobic respiration pathway that uses electrons from Hase I for the final reduction of molecular oxygen to water consists of cofactors that have been well characterized. On the contrary, there is not much information on the mechanism and structure of the [NiFe] Hase I. This knowledge is pivotal, on the basis that such hydrogenases have exhibited some unique physicochemical properties that make them ideal for biotechnological applications.

In contrast to the majority of [NiFe] hydrogenases, the Hase I from *Aquifex aeolicus* is quite tolerant to oxygen. It was shown that it can partially retain its activity in the presence of atmospheric oxygen, while a 50% loss in the activity was observed after 24h at 0°C[64]. EPR spectroscopic studies on the as purified enzyme showed

signals related only to the readily activated oxidised Ni-B state (ready) and not to the slowly activated Ni-A state (unready)[56]. In addition, the region of the iron-sulphur clusters contained more composite signals superimposed to a nearly isotropic signal at g = 2.02 from a $[Fe_3S_4]^{1+}$ cluster expected in standard hydrogenases. Similar signals for the iron-sulphur cofactors were found in the case of the oxygen-tolerant membrane bound hydrogenase from *Ralstonia eutropha*[19] and might be related to the enhanced $O_2$-tolerance exhibited.

Incubation of the Hase I for 10-15 min under aerobic conditions at the 'in vivo' physiological temperatures (85°C) resulted in the disappearance of the complex spectrum and of the nickel signals, demonstrating that the enzyme was being reduced[64]. This is rather extraordinary, as it shows that Hase I can be simply activated by increasing the temperature despite the presence of oxygen. Hase I is quite thermostable; its thermal stability increases if it is co-purified as a complex with its native electron acceptor cytochrome *b*.

The principal values of the g-tensors of the nickel signals corresponding to the oxidised and reduced states are comparable to those for well-characterized mesophilic hydrogenases, showing that the molecular structure of the active site in these enzymes is quite similar. Significant differences were found for the iron-sulphur cluster signals, though the presence of one $[Fe_3S_4]$ and possibly two $[Fe_4S_4]$ was deduced. In addition, the hydrophobic channel in Hase I is similar in size to the one of standard hydrogenases, precluding the possibility of a narrow gas channel hindering $O_2$ to reach the active site[65].

**1.4. Scope**

Up to date, there is no systematic study on the Hase I from *Aquifex aeolicus*. Neither the catalytic cycle of the enzyme nor the redox properties of the [NiFe] site and the iron-sulphur centres are known. The present work therefore focuses onto the study of the redox centres in Hase I by coupling different spectroscopic and electrochemical techniques in order to gain a better understanding of these oxygen tolerant thermophilic enzymes. Results are being compared to standard hydrogenases from sulphate reducing bacteria (i.e. *Desulfovibrio vulgaris*), for which additionally new aspects of the current mechanistic scheme have been added. The present work has a two-fold aim; (a) to improve our current knowledge on the standard [NiFe] hydrogenase from *Desulfovibrio vulgaris*, for which high resolved crystal structures for all states and extensive spectroscopic information is available and (b) to characterize the catalytic properties of the Hase I from *Aquifex aeolicus*, identify redox intermediates and redox components as well as propose the basis for its enhanced tolerance against oxygen inhibition.

# References

1. Brock, T.; Madigan, T.; Martinko, J. M.; Parker, J. *Biology of Microorganisms;* 7th ed.; Prentice-Hall International: **1994**.

2. Dworkin, M.; Falkow, S.; Rosenberg, E.; Schleifer, K. H. *The Prokaryotes; Ecophysiology and Biochemistry;* 3rd ed.; Springer: **2007**, Vol. 2.

3. Cammack, R.; Frey, M. *Hydrogen as a fuel;* Taylor and Francis: London, **2001**.

4. Vignais, P. M. *Coord. Chem. Rev.* **2005**, *249* (15-16), 1677-1690.

5. Vignais, P. M.; Billoud, B. *Chem. Rev.* **2007,** *107*, 4206-4272.

6. Volbeda, A.; Charon, M. H.; Piras, C.; Hatchikian, E. C.; Frey, M.; Fontecilla-Camps, J. C. *Nature* **1995**, *373* (6515), 580-587.

7. Nicolet, Y.; Lemon, B. J.; Fontecilla-Camps, J. C.; Peters, J. W. *Trends in Biochemical Sciences* **2000,** *25* (3), 138-143.

8. Shima, S.; Pilak, O.; Vogt, S.; Schick, M.; Stagni, M. S.; Meyer-Klaucke, W.; Warkentin, E.; Thauer, R. K.; Ermler, U. *Science* **2008**, *321* (5888), 572-575.

9. Kobayashi, K.; Morisawa, Y.; Ishituka, T.; Ishimoto, M. *J. Biochem.* **1975**, *78* (5), 1079-1085.

10. Huber, R.; Wilharm, T.; Huber, D.; Trincone, A.; Burggraf, S.; Konig, H.; Rachel, R.; Rockinger, I.; Fricke, H.; Stetter, K. O. *Systematic and Applied Microbiology* **1992**, *15* (3), 340-351.

11. Higuchi, Y.; Yagi, T.; Yasuoka, N. *Structure* **1997,** *5* (12), 1671-1680.

12. Bagley, K. A.; Vangarderen, C. J.; Chen, M.; Duin, E. C.; Albracht, S. P. J.; Woodruff, W. H. *Biochemistry* **1994**, *33* (31), 9229-9236.

13. Happe, R. P.; Roseboom, W.; Pierik, A. J.; Albracht, S. P. J.; Bagley, K. A. *Nature* **1997,** *385* (6612), 126.

14. Pierik, A. J.; Roseboom, W.; Happe, R. P.; Bagley, K. A.; Albracht, S. P. J. *J. Biolog. Chem.* **1999**, *274* (6), 3331-3337.

15. Matias, P. M.; Soares, C. M.; Saraiva, L. M.; Coelho, R.; Morais, J.; Le Gall, J.; Carrondo, M. A. *J. Biolog. Inorg. Chem.* **2001**, *6* (1), 63-81.

16. Cammack, R.; Patil, D. S.; Hatchikian, E. C.; Fernandez, V. M. *Biochim. Biophys. Acta* **1987**, *912* (1), 98-109.

17. Capozzi, F.; Ciurli, S.; Luchinat, C. *Metal Sites in Proteins and Models* **1998**, *90*, 127-160.

18. Asso, M.; Guigliarelli, B.; Yagi, T.; Bertrand, P. *Biochim. Biophys. Acta* **1992**, *1122* (1), 50-56.

19. Knuttel, K.; Schneider, K.; Erkens, A.; Plass, W.; Muller, A.; Bill, E.; Trautwein, A. X. *Bulletin of the Polish Academy of Sciences-Chemistry* **1994**, *42* (4), 495-511.

20. Sellmann, D.; Geipel, F.; Moll, M. *Angewandte Chemie-Intern. Ed.* **2000**, *39* (3), 561-+.

21. Dementin, S.; Burlat, B.; de Lacey, A. L.; Pardo, A.; dryanczyk-Perrier, G.; Guigliarelli, B.; Fernandez, V. M.; Rousset, M. *J. Biolog. Chem.* **2004**, *279* (11), 10508-10513.

22. Montet, Y.; Amara, P.; Volbeda, A.; Vernede, X.; Hatchikian, E. C.; Field, M. J.; Frey, M.; Fontecilla-Camps, J. C. *Nature Structural Biology* **1997**, *4* (7), 523-526.

23. Yahata, N.; Saitoh, T.; Takayama, Y.; Ozawa, K.; Ogata, H.; Higuchi, Y.; Akutsu, H. *Biochemistry* **2006**, *45* (6), 1653-1662.

24. Akutsu, H.; Takayama, Y. *Acc. Chem. Res.* **2007**, *40* (3), 171-178.

25. Park, J. S.; Kano, K.; Niki, K.; Akutsu, H. *FEBS Lett.* **1991**, *285* (1), 149-151.

26. Heidelberg, J. F.; Seshadri, R.; Haveman, S. A.; Hemme, C. L.; Paulsen, I. T.; Kolonay, J. F.; Eisen, J. A.; Ward, N.; Methe, B.; Brinkac, L. M.; Daugherty, S. C.; Deboy, R. T.; Dodson, R. J.; Durkin, A. S.; Madupu, R.; Nelson, W. C.; Sullivan, S. A.; Fouts, D.; Haft, D. H.; Selengut, J.; Peterson, J. D.; Davidsen, T. M.; Zafar, N.; Zhou, L. W.; Radune, D.; Dimitrov, G.; Hance, M.; Tran, K.; Khouri, H.; Gill, J.; Utterback, T. R.; Feldblyum, T. V.; Wall, J. D.; Voordouw, G.; Fraser, C. M. *Nature Biotechnology* **2004**, *22* (5), 554-559.

27. Thauer, R. K.; Jungermann, K.; Decker, K. *Bacteriological Reviews* **1977**, *41* (1), 100-180.

28. De Lacey, A. L.; Fernandez, V. M.; Rousset, M.; Cammack, R. *Chem. Rev.* **2007**, *107*, 4304-4330.

29. Fontecilla-Camps, J. C.; Volbeda, A.; Cavazza, C.; Nicolet, Y. *Chem. Rev.* **2007**, *107*, 4273-4303.

30. Lubitz, W.; Reijerse, E.; van Gastel, M. *Chem. Rev.* **2007**, *107*, 4331-4365.

31. Armstrong, F. A.; Belsey, N. A.; Cracknell, J. A.; Goldet, G.; Parkin, A.; Reisner, E.; Vincent, K. A.; Wait, A. F. *Chem. Soc. Rev.* **2009**, *38* (1), 36-51.

32. Leger, C.; Bertrand, P. *Chem. Rev.* **2008**, *108* (7), 2379-2438.

33. Albracht, S. P. J..*Biochim. Biophys. Acta Bioenergetics* **1994**, *1188* (3), 167-204.

34. Fernandez, V. M.; Hatchikian, E. C.; Cammack, R. *Biochim. Biophys. Acta* **1985**, *832* (1), 69-79.

35. Lamle, S. E.; Albracht, S. P. J.; Armstrong, F. A. *J. Am. Chem.Soc.* **2004**, *126* (45), 14899-14909.

36. van Gastel, M.; Stein, M.; Brecht, M.; Schroder, O.; Lendzian, F.; Bittl, R.; Ogata, H.; Higuchi, Y.; Lubitz, W. *J. Biolog. Inorg. Chem.* **2006**, *11* (1), 41-51.

37. Ogata, H.; Hirota, S.; Nakahara, A.; Komori, H.; Shibata, N.; Kato, T.; Kano, K.; Higuchi, Y. *Structure* **2005**, *13* (11), 1635-1642.

38. Volbeda, A.; Martin, L.; Cavazza, C.; Matho, M.; Faber, B. W.; Roseboom, W.; Albracht, S. P. J.; Garcin, E.; Rousset, M.; Fontecilla-Camps, J. C. *J. Biolog. Inorg. Chem.* **2005**, *10* (3), 239-249.

39. Fan, C. L.; Houseman, A. L. P.; Doan, P.; Hoffman, B. M. *J. Phys. Chem.* **1993**, *97* (12), 3017-3021.

40. Brecht, M.; van Gastel, M.; Buhrke, T.; Friedrich, B.; Lubitz, W. *J. Am. Chem. Soc.* **2003**, *125* (43), 13075-13083.

41. Foerster, S.; van Gastel, M.; Brecht, M.; Lubitz, W. *J. Biolog.Inorg. Chem.* **2005**, *10* (1), 51-62.

42. Guigliarelli, B.; More, C.; Fournel, A.; Asso, M.; Hatchikian, E. C.; Williams, R.; Cammack, R.; Bertrand, P. *Biochemistry* **1995**, *34* (14), 4781-4790.

43. Van der Zwaan, J. W.; Albracht, S. P. J.; Fontijn, R. D.; Slater, E. C. *FEBS Lett.* **1985**, *179* (2), 271-277.

44. Stein, M.; van Lenthe, E.; Baerends, E. J.; Lubitz, W. *J. Am. Chem. Soc.* **2001**, *123* (24), 5839-5840.

45. Jayapal, P.; Robinson, D.; Sundararajan, M.; Hillier, I. H.; McDouall, J. J. W. *Phys. Chem. Chem. Phys.* **2008**, *10* (13), 1734-1738.

46. Pardo, A.; De Lacey, A. L.; Fernandez, V. M.; Fan, H. J.; Fan, Y. B.; Hall, M. B. *J. Biolog. Inorg. Chem.* **2006**, *11* (3), 286-306.

47. Purec, L.; Krasna, A. I.; Rittenberg, D. *Biochemistry* **1962**, *1* (2), 270-&.

48. De Lacey, A. L.; Stadler, C.; Fernandez, V. M.; Hatchikian, E. C.; Fan, H. J.; Li, S. H.; Hall, M. B. *J. Biolog. Inorg. Chem.* **2002**, *7* (3), 318-326.

49. Ogata, H.; Mizoguchi, Y.; Mizuno, N.; Miki, K.; Adachi, S.; Yasuoka, N.; Yagi, T.; Yamauchi, O.; Hirota, S.; Higuchi, Y. *J. Am. Chem. Soc.* **2002**, *124*, 11628-11635.

50. Happe, R. P.; Roseboom, W.; Albracht, S. P. J. *Eur. J. Biochem.* **1999**, *259* (3), 602-608.

51. Huber, R.; Huber, H.; Stetter, K. O. *Fems Microbiol. Rev.* **2000**, *24* (5), 615-623.

52. Stetter, K. O. *Philosophical Transactions of the Royal Society B-Biological Sciences* **2006**, *361* (1474), 1837-1842.

53. Lineweaver, C. *Journal and Proceedings of the Royal Society of New South Wales* **2005**, *138* (Part 3-4), 93-98.

54. Guiral, M.; Tron, P.; Aubert, C.; Gloter, A.; Iobbi-Nivol, C.; Giudici-Orticoni, M. T. *J. Biolog. Chem.* **2005**, *280* (51), 42004-42015.

55. Deckert, G.; Warren, P. V.; Gaasterland, T.; Young, W. G.; Lenox, A. L.; Graham, D. E.; Overbeek, R.; Snead, M. A.; Keller, M.; Aujay, M.; Huber, R.; Feldman, R. A.; Short, J. M.; Olsen, G. J.; Swanson, R. V. *Nature* **1998**, *392* (6674), 353-358.

56. Brugna-Guiral, M.; Tron, P.; Nitschke, W.; Stetter, K. O.; Burlat, B.; Guigliarelli, B.; Bruschi, M.; Giudici-Orticoni, M. T. *Extremophiles* **2003**, *7* (2), 145-157.

57. Guiral, M.; Prunetti, L.; Lignon, S.; Lebrun, R.; Moinier, D.; Giudici-Orticoni, M. T. *Journal of Proteome Research* **2009**, *8* (4), 1717-1730.

58. Saggu, M.; Zebger, I.; Ludwig, M.; Lenz, O.; Friedrich, B.; Hildebrandt, P.; Lendzian, F. *J. Biolog. Chem.* **2009,** *284* (24), 16264-16276.

59. Gross, R.; Pisa, R.; Sanger, M.; Lancaster, C. R. D.; Simon, J. *J. Biolog. Chem.* **2004**, *279* (1), 274-281.

60. Schutz, M.; Schoepp-Cothenet, B.; Lojou, E.; Woodstra, M.; Lexa, D.; Tron, P.; Dolla, A.; Durand, M. C.; Stetter, K. O.; Baymann, F. *Biochemistry* **2003**, *42* (36), 10800-10808.

61. Hollander, R. *FEBS Lett.* **1976**, *72* (1), 98-100.

62. Nubel, T.; Klughammer, C.; Huber, R.; Hauska, G.; Schutz, M. *Archives of Microbiology* **2000**, *173* (4), 233-244.

63. Obuchi, M.; Kawahara, K.; Motooka, D.; Nakamura, S.; Yamanaka, M.; Takeda, T.; Uchiyama, S.; Kobayashi, Y.; Ohkubo, T.; Sambongi, Y. *Acta Crystallographica Section D-Biological Crystallography* **2009**, *65*,

64. Giudici-Orticoni, M.; Guiral, M.; Tron, P.; Belle, V.; Aubert, C.; Leger, C.; Guigliarelli, B. *International Journal of Hydrogen Energy* **2006**, *vol.31, no.11*, 1424-1431.

65. Buhrke, T.; Lenz, O.; Krauss, N.; Friedrich, B. *J. Biolog. Chem.* **2005**, *280* (25), 23791-23796.

# Chapter 2

# Theory and experimental methods

## 2.1 EPR spectroscopy

Electron paramagnetic resonance (EPR) is a powerful technique in the study of paramagnetic systems i.e. systems that contain one or more unpaired electrons and of diamagnetic systems with the use of spin-labels. EPR spectroscopy can provide in-depth information on the electronic structure, since magnetic parameters such as g-values, hyperfine couplings and nuclear quadrupole interactions are encoded in the electronic wavefunction[1]. The EPR spectrum can be interpreted in terms of the effectiv*e spin Hamiltonian* that describes the interactions of the electronic and nuclear spins with the applied magnetic field and with each other[2]. The spins are expressed in terms of operators and the interactions as coupling coefficients and by analysing the spectra, these interactions can be quantitatively determined. The concept of the spin Hamiltonian was developed in the early days of EPR and is elaborately described by Abragam and Bleaney[2].

## 2.1.1 Spin Hamiltonian

The static *spin Hamiltonian* describes the energies of the states of a paramagnetic species in the ground state with an effective electron spin $S$ and $m$ nuclei with nuclear spins I and is given by[3]:

$$\mathcal{H}_0 = \mathcal{H}_{EZ} + \mathcal{H}_{ZFS} + \mathcal{H}_{HF} + \mathcal{H}_{NZ} + \mathcal{H}_{NQ}$$

$$= \beta_e \widetilde{\mathbf{B}}_0 \mathbf{g} \mathbf{S} + h \widetilde{\mathbf{S}} \mathbf{D} \mathbf{S} + h \sum_{k=1}^{m} \widetilde{\mathbf{S}} \mathbf{A}_k \mathbf{I}_k - \beta_n \sum_{k=1}^{m} g_{n,k} \widetilde{\mathbf{B}}_0 \mathbf{I}_k + h \sum_{\substack{k=1;\\ I_k>1/2}}^{m} \widetilde{\mathbf{I}}_k \mathbf{P}_k \mathbf{I}_k \quad \text{(Eq. 1)}$$

$\mathcal{H}_0$ is called the *spin Hamiltonian* and contains phenomenological constants and spin coordinates described by the electron-spin vector operator $\widetilde{\mathbf{S}} = \left[ \hat{S}_x, \hat{S}_y, \hat{S}_z \right]$ and the nuclear spin vector operator $\widetilde{\mathbf{I}}_k = \left[ \hat{I}_{x,k}, \hat{I}_{y,k}, \hat{I}_{z,k} \right]$. $\widetilde{\mathbf{B}}_0$ is a 3 x 1 vector describing the direction and strength of the applied magnetic field. The terms in this equation describe; $\mathcal{H}_{EZ}$: the electron Zeeman interaction, $\mathcal{H}_{ZFS}$: the zero-field splitting, $\mathcal{H}_{HF}$:

the hyperfine interaction, $\mathcal{H}_{NZ}$ : the nuclear Zeeman interaction, $\mathcal{H}_{NQ}$ : the nuclear quadrupole interaction for spins with nuclear spin quantum number larger than ½. The term of the spin-spin interactions between pairs of nuclear spins has not been included in (Eq.1). The ~ is used to denote the transpose of a vector and in bold the vectors (tensors) are indicated.

In the following a brief introduction on the interactions dealt within the present study is given.


### 2.1.2 Electronic Zeeman Interaction

In the simple case of a two-level system for a paramagnetic centre with an electron spin $S = $ ½. The application of an external magnetic field $\boldsymbol{B}_0$ results in a splitting of the two energy levels as the electron spin $\boldsymbol{S}$ can only be oriented parallel or anti-parallel to the magnetic field vector. The interaction between an unpaired electronic spin (magnetic dipole) and an external magnetic field $B_0$ is described by the electron Zeeman term:

$$\mathcal{H}_{EZ} = \beta_e g_e \widetilde{B}_0 S \quad \text{(Eq.2).}$$

The energies for the two spin states, characterized by the spin quantum numbers $m_S = \pm$ ½, are given by the eigenvalues of $\mathcal{H}_{EZ}$:

$$E(m_S) = \beta_e g_e B_0 m_S \quad \text{(Eq.3).}$$

The splitting between these two energy states is called *electron Zeeman interaction* (EZI) and is proportional to the magnitude of the external magnetic field (Figure 1). The energy difference between the two Zeeman states is given by $\Delta E = E(m_S = +$½$) - E(m_S = -$½$) = \beta_e g_e B_0$. If the energy of the radiation field ($h\nu_{mw}$) matches the energy gap $\Delta E$, transitions between the two spin states can be induced. In this case the resonance condition is fulfilled:

$$\Delta E = \beta_e g_e B_0 \quad \text{(Eq. 4).}$$
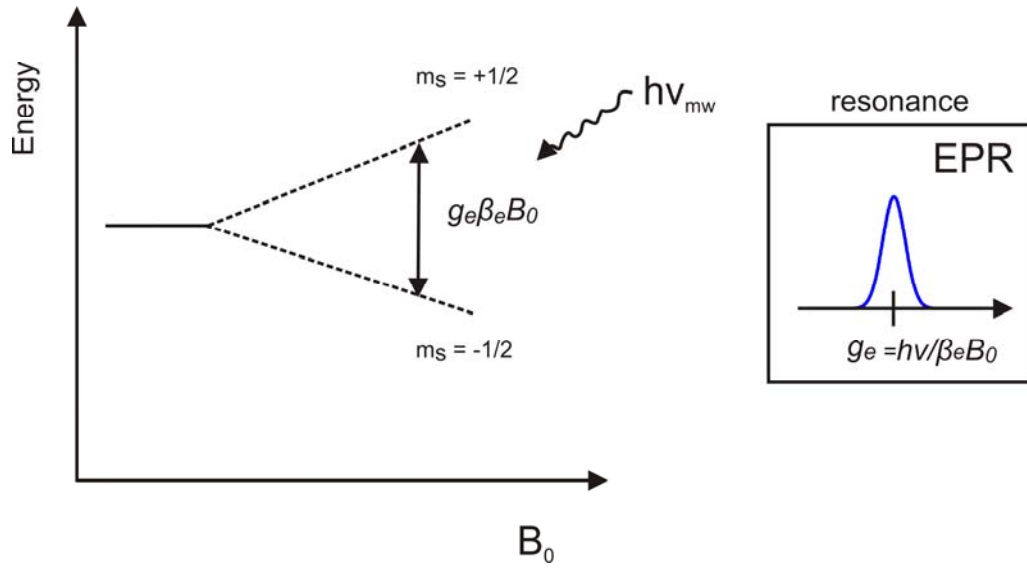
**Figure 1.** The behaviour of a electron spin S = ½ in the presence of an applied magnetic field. When the resonance condition is fulfilled, an EPR allowed transition is observed.

In most of the cases however, the g-value of the system under study deviates for the $g_e$ for a free electron spin and is orientation dependent (g-tensor). This is caused by an interaction of ground and excited states, which admixes the orbital momentum $L$ from the excited state into the ground state[1]. To account for this effect the *Hamiltonian* is modified to:

$$\mathcal{H}_{EZ} = \mathcal{H}_{Z} + \mathcal{H}_{LS}$$

$$= \beta_e \widetilde{\mathbf{B}}_0 (\mathbf{L} + g_e \mathbf{S}) + \lambda \widetilde{\mathbf{L}} \mathbf{S} \quad \text{(Eq.5)}.$$

The $\mathcal{H}_Z$ is the electron-Zeeman term that included the orbital angular momentum and $\lambda \widetilde{\mathbf{L}} \mathbf{S}$ is the spin-orbit interaction with $\lambda$ the spin-orbit coupling parameter.

### 2.1.3 Hyperfine Interaction

The hyperfine interaction between an electron and a nuclear spin is described by the *Hamiltonian* term, which for convenience has been divided with the planck constant (see eq. 1):

$$\mathcal{H}_{HF}/h = \widetilde{\mathbf{S}}\mathbf{A}\mathbf{I} \qquad \text{(Eq. 6)}.$$

The hyperfine tensor consists of an isotropic (Fermi contact) and an anisotropic part and can be written as:

$$\mathcal{H}_{HF}/h = a_{iso}\widetilde{\mathbf{S}}\mathbf{I} + \widetilde{\mathbf{S}}\mathbf{T}\mathbf{I} \text{ (Eq. 7), where}$$

$$a_{iso} = \frac{2}{3}\frac{\mu_0}{h}g_e\beta_e g_n\beta_n|\psi_0(0)|^2 \qquad \text{(Eq. 8)}$$

is the isotropic hyperfine coupling constant and $|\psi_0(0)|^2$ is the spin density at the nucleus. The isotropic interaction for an electron that is in a p, d or f orbital can be significant, since in this case the spin density at the nucleus (s orbital) is induced by spin polarisation mechanisms.

**T** is the dipolar hyperfine coupling tensor.

The electron-nuclear dipole-dipole coupling is described by:

$$\widetilde{\mathbf{S}}\mathbf{T}\mathbf{I} = \frac{\mu_0}{4\pi h}g_e\beta_e g_n\beta_n\left[\frac{(3\widetilde{\mathbf{S}}\mathbf{r})(\widetilde{\mathbf{r}}\mathbf{I})}{r^5} - \frac{\widetilde{\mathbf{S}}\mathbf{I}}{r^3}\right] \qquad \text{(Eq. 9)}$$

In the case of *spin only* electron-nuclear dipole-dipole interaction and considering only the wavefunction of the ground state, **T** is traceless and symmetric tensor with components:

$$\mathrm{T}_{ij} = \frac{\mu_0}{4\pi h}g_e\beta_e g_n\beta_n\left\langle\psi_0\left|\frac{3r_ir_j - \delta_{ij}r^2}{r^5}\right|\psi_0\right\rangle \qquad \text{(Eq. 10)}$$

**2.1.4 Nuclear quadrupole interaction**

Nuclei with spin equal to or larger than 1 are characterised by a non-spherical charge distribution, described by the electrical nuclear quadrupole moment Q. The interaction of this charge distribution with the electric field gradient, caused by electrons and nuclei in the close vicinity is given by the *Hamiltonian* term:

$$\mathcal{H}_{NQ}/h = \widetilde{\mathbf{I}}\mathbf{P}\mathbf{I} \qquad \text{(Eq. 11)},$$

where **P** is the nuclear quadrupole tensor that is traceless in its principal axes system. This interaction can be then written to first order as:

$$\mathcal{H}_{NQ}/h = \mathrm{P}_x\mathrm{I}_x^2 + \mathrm{P}_y\mathrm{I}_y^2 + \mathrm{P}_z\mathrm{I}_z^2 = \frac{e^2qQ}{4\mathrm{I}(2\mathrm{I}-1)h}\left[3\mathrm{I}_z^2 - \mathrm{I}(\mathrm{I}+1)^2 + \eta\left(\mathrm{I}_x^2 - \mathrm{I}_y^2\right)\right] \text{ (Eq. 12)},$$

with eq the electric field gradient and $\eta = \dfrac{\mathrm{P}_x - \mathrm{P}_y}{\mathrm{P}_z}$ the asymmetry parameter with

$|P_z| \geq |P_y| \geq |P_x|$ and $0 \leq \eta \leq 1$. As it follows from (Eq. 12), the largest value of the quadrupole tensor is given by

$$P_z = e^2qQ/2I(2I-1)h \qquad \text{(Eq. 13)}$$

It is quite common that only these two quantities are given: $K = e^2qQ/4h$ and $\eta$. The resulting energy diagrams taking into account the related interactions for a S=1/2, I=1/2 system and a S=1/2, I=1 system are given in Figure 2.
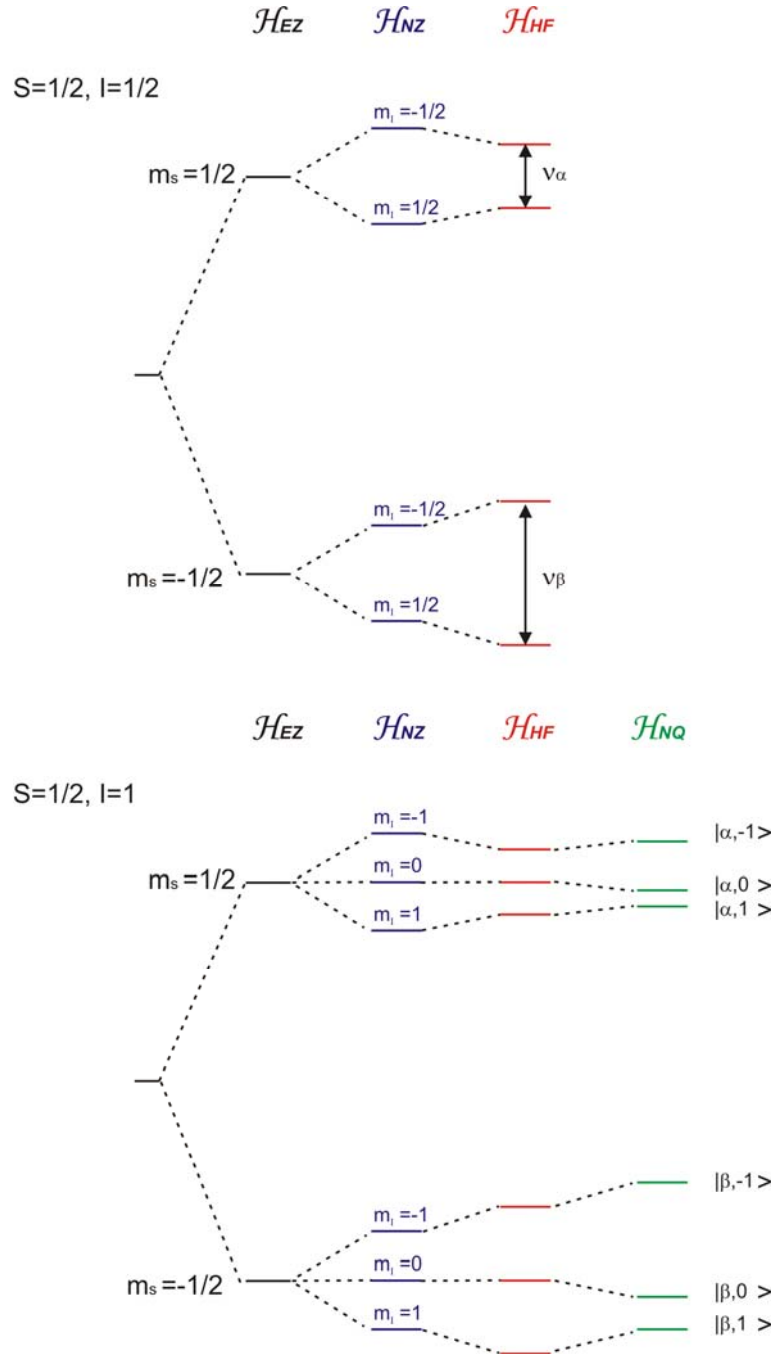


**Figure 2.** Energy diagrams for a S=1/2, I=1/2 system and a S=1/2, I=1 system.

**2.1.5 Weak coupling between electron spins**

In the case of weakly interacting unpaired electrons or generally two species with spins $S_1$ and $S_2$, these are more conveniently characterized by their individual spins ,an exchange coupling tensor **J** and a dipole-dipole coupling tensor $\mathbf{D}^4$. The complete *Hamiltonian* for such a two-spin system consists by the *Hamiltonians* for the individual spins and the *Hamiltonian* term for their interaction[3]:

$$\mathcal{H}_0(S_1,S_2) = \mathcal{H}_0(S_1) + \mathcal{H}_0(S_2) + \mathcal{H}_{int} \text{ (Eq. 14)}$$

with

$$\mathcal{H}_{int}/h = \widetilde{\mathbf{S}}_1\mathbf{J}\mathbf{S}_2 + \widetilde{\mathbf{S}}_1\mathbf{D}_{12}\mathbf{S}_2 \text{ (Eq. 15).}$$

The first term corresponds to the so-called Heisenberg exchange coupling, which becomes relevant when the orbitals of the two spins overlap significantly resulting in the exchange of the unpaired electrons of the two species. In solids an exchange may be observed if unpaired electrons are closer than about 1.5 nm or are strongly delocalised, whereas in solution an exchange can occur in biradicals[5]. For the case of of $S_1 = ½$ and $S_2 = ½$ it can be discussed in relation to chemical bonding[5]. A positive exchange coupling corresponds to a case where the triplet state of the two electrons is higher in energy than the singlet state. This antiferromagnetic coupling describes a weak bonding situation. Accordingly, a negative exchange coupling corresponds to a stabilisation of the triplet state over the singlet state, which is a ferromagnetic coupling describing a weak antibonding situation. The anisotropic part of **J**, which may be asymmetric, is caused by the spin-orbit coupling and can usually be neglected for organic radicals[3]. The second term in (Eq. 15) is the anisotropic spin-spin dipole-dipole interaction. The dipole-dipole coupling between two electron spins is analogous to the dipole-dipole coupling between an electron and a nuclear spin (Eq. 9). The contribution to the Hamiltonian is given by:

$$\mathcal{H}_{dd}/h = \widetilde{\mathbf{S}}_1\mathbf{D}_{12}\mathbf{S}_2 = \frac{1}{r_{12}^3}\frac{\mu_0}{4\pi h}g_1g_2\beta_e^2\left[\widetilde{\mathbf{S}}_1\mathbf{S}_2 - \frac{3}{r_{12}^2}\left(\widetilde{\mathbf{S}}_1\mathbf{r}_{12}\right)\left(\widetilde{\mathbf{S}}_2\mathbf{r}_{12}\right)\right] \text{ (eq. 16)}$$

where $\mathbf{r}_{12}$ is the vector connecting the two electron spins and $g_1$, $g_2$ are the g-values of the two electrons spins, respectively.

**2.1.6 Continuous wave EPR**

In continuous wave EPR the magnetic field is being linearly swept and the microwave frequency is constant. An EPR transition (absorption signal in Figure 1) occurs when the resonance condition described by equation 5 is fulfilled. For the improvement of the signal-to-noise ratio the magnetic field is modulated and the first harmonic of the signal is obtained (first derivative). In general, the magnetic moments of the spins and hence the g-factors of transition ions are usually very anisotropic; the EPR properties depend on the orientation of the molecule with the applied magnetic field.
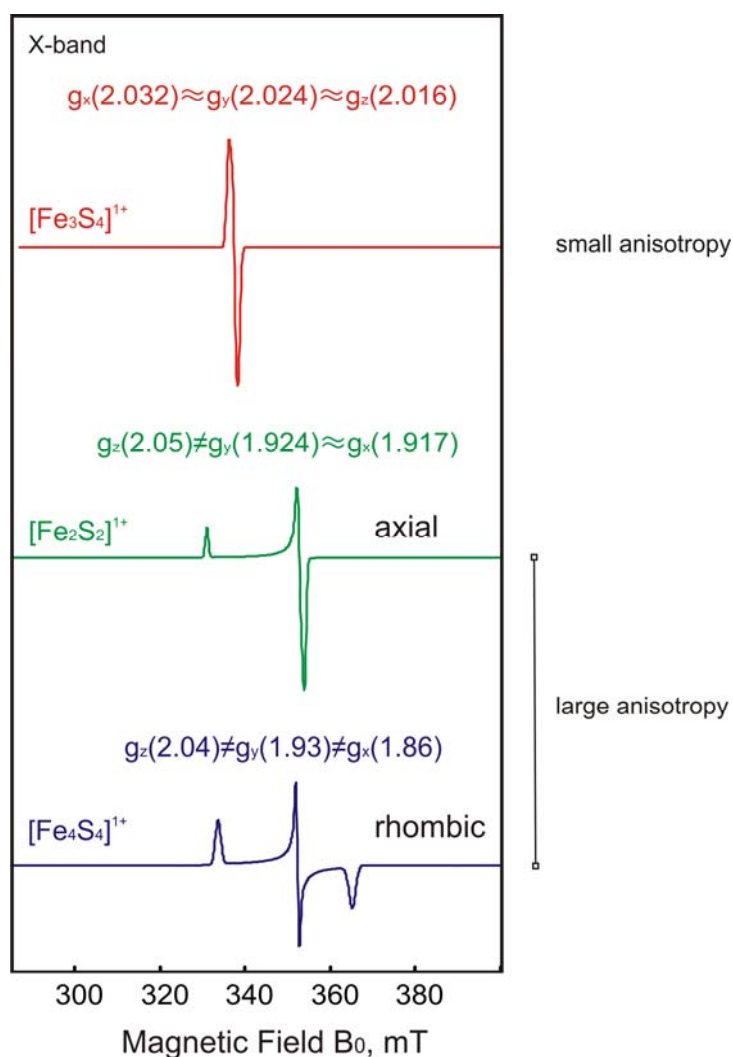


**Figure 3.** Simulated spectra of selected spectra of FeS clusters, exhibiting a nearly isotropic, axial and rhombic g-tensor. Principal values and line-width parameters for the $[Fe_3S_4]^{1+}$ cluster were obtained from Fan et al[6] and the ones for the $[Fe_2S_2]^{1+}$ and $[Fe_4S_4]^{1+}$ from Ohnishi[7].

In the case where the reference axis system is the principal axis system of the g-tensor (in which it is diagonal), the orientation dependence of the principal values of the g-tensor is given by[1],

$$g^2 = g_{xx}^2 l_x^2 + g_{yy}^2 l_y^2 + g_{zz}^2 l_z^2 \quad \text{(Eq. 17)},$$

where $l_x$, $l_y$ and $l_z$ are the direction cosines between the direction of **B**$_0$ and the principal g-tensor axes. Selected simulated EPR spectra corresponding to some know iron-sulphur centres are presented in Figure 3.

**2.1.7 Pulse EPR techniques**

**2.1.7.1 Two-pulse electron spin echo (ESE)**

Information similar to CW EPR can be obtained from the electron spin echo (ESE) detected EPR. In these experiments, a spin echo, usually a Hahn echo or a primary echo is generated using a specific microwave pulse sequence and the echo intensity is monitored as a function of the external magnetic field. For a S=1/2 system this approach generates a spectrum matching the integrated form of the corresponding CW spectrum[3].

The use of pulse EPR methods contributes greatly in the investigation of the local structure and dynamics of paramagnetic centres, by improving the limitations in spectral and time resolution imposed by traditional CW EPR methods. The EPR spectra of metal compounds and metalloproteins in frozen solution are usually inhomogeneously broadened. Within the exception of single-crystal studies, nuclear, hyperfine and quadrupole splitting are not resolved in the low temperature frozen solution EPR spectra. There are two EPR-based spectroscopies which can recover this information: (a) electron nuclear double resonance (ENDOR)[8] and (b) electron spin echo envelope modulation (ESEEM)[9]. In both ENDOR and ESEEM experiments, the nuclear transition (NMR) frequencies are detected indirectly through EPR transitions.

**2.1.7.2 Two- and three pulse ESE envelope modulation (ESEEM)**

ESEEM experiments are performed by recording the echo intensity generated by a sequence of resonant microwave pulses, separated by evolution times i.e. periods where the microwave power is off; the recorded echo-envelope modulation is the time-domain ESEEM signal. In the presence of nuclear spins weakly coupled with the electron-spin, the intensity of the echo is modulated at the nuclear transition

frequencies of the interacting nucleus. The standard one-dimensional ESEEM experiments consist of two-and three-pulse sequences, respectively (Figure 4)[3]. In the two-pulse experiment, at time $\tau$ after the second pulse, an electron spin-echo is generated. The modulation envelope, obtained as $\tau$ is incremented, is related to the nuclear transition frequencies within an electron spin manifold; in addition, the sum and difference of the basic nuclear frequencies also appear in the two-pulse ESEEM. A major disadvantage of the two-pulse method for metal spins is that the spin-spin relaxation time $T_2$ is usually short thereby limiting the time which modulations can be obtained.

An alternative procedure is given by the three-pulse ESEEM experiment. In this experiment two pulses, separated by time $\tau$, are applied followed by a third pulse after time T, and the stimulated echo is observed at time r after the third pulse (Figure 4). The echo envelope, obtained as T is incremented, is modulated by the nuclear transition frequencies of nuclei coupled with the electron spin. In contrast to the two-pulse ESEEM experiment, the three-pulse ESEEM spectra are free of sum and difference frequencies. The resolution is limited by the electron spin-lattice relaxation time $T_1$, which is usually much larger than the electronic spin-spin lattice relaxation time $T_2$. The spectrum is dependent on $\tau$ separation time and thus the three pulse ESEEM exhibits a blind spot behaviour. For $\omega_{\alpha,\beta} = 2\pi n/\tau$ (n=0,1,..) the modulation vanishes.
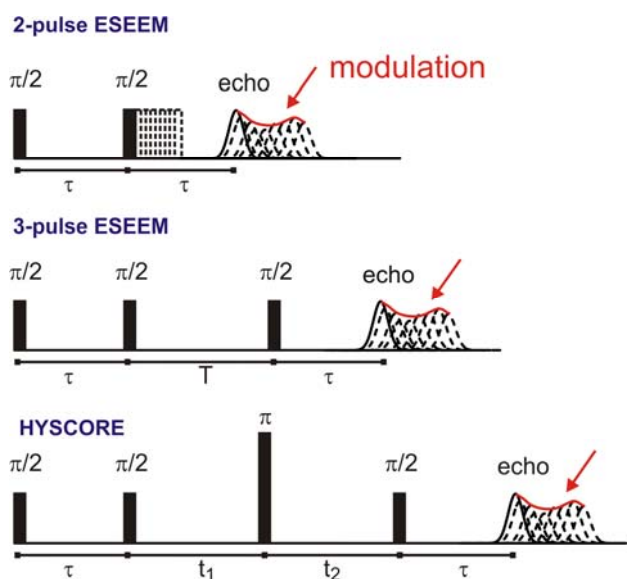


**Figure 4.** Pulse sequences making use of the ESEEM effect: two-pulse ESEEM, three pulse ESEEM and HYSCORE.

43

**2.1.7.3 Hyperfine sublevel correlation spectroscopy (HYSCORE)**

The HYSCORE sequence is based on the three pulse ESEEM experiment that consists of three $\pi/2$ microwave pulses, whereby the primary echo is detected as a function of the time between the last two pulses[3]. It is a four pulse ESSEM technique, where the two inter-pulse distances $t_1$ and $t_2$ are varied independently (Figure 4). Two-dimensional Fourier transformation leads to a 2D frequency-domain spectrum, where the nuclear frequencies belonging to $\alpha$ manifold are correlated to nuclear frequencies of the $\beta$ manifold (different $m_S$ manifolds). For the weak coupling case ($|v_I|>A/2$), where the $v_\alpha$ and $v_\beta$ have the same sign, the cross-peaks appear in the first quadrant (++). In the strong coupling case ($|v_I|<A/2$), peaks appear in the second quadrant (-+). These cases are illustrated in Figure 5 for an S=1/2, I=1/2 system. Due to non-ideality of the inversion $\pi$ pulse, correlations in the diagonal ($v_\alpha,v_\alpha$) and ($v_\beta,v_\beta$) can also be observed.
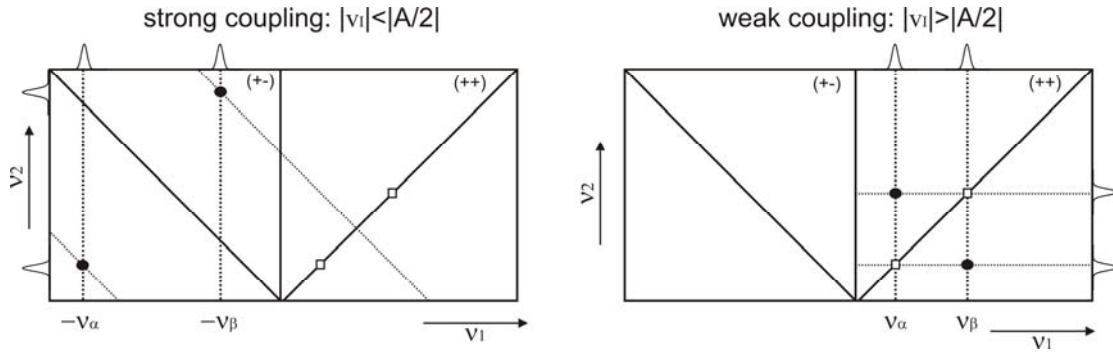


**Figure 5.** 2D HYSCORE spectra for a S=1/2, I=1/2 system in the strong coupling ($|v_I|<A/2$) and the weak coupling case ($|v_I|>A/2$).

**2.1.7.4 Special case: Cancellation condition**

For $^{14}$N nuclei (I=1) it is often found that the condition of the so-called cancellation condition is fulfilled ($|v_I| \sim A/2$)[10]; this occurs when the nuclear-Zeeman and electron–nuclear hyperfine interactions approximately cancel one another (see energy levels in Figure 6), so that the level splittings are primarily determined by the $^{14}$N nuclear quadrupole interaction (NQI). Three sharp transition frequencies are obtained in the 'cancelled' $m_S$ manifold, which correspond to zero-field nuclear quadrupole transitions. From these frequencies, which are given by[10]:

$$v_{\pm} = K(3 \pm \eta) \text{ and } v_0 = 2K\eta \qquad (Eq. 18),$$

the quadrupole coupling constant $K = \dfrac{e^2 qQ}{4h}$ and the asymmetry parameter $\eta$ can be calculated. In the spectra, the positions of the lines are determined by the values of K and $\eta$, while their relative intensities are sensitive to the relative orientation of the NQI principal axes system with respect to the hyperfine coupling tensor and the $\tau$ value used for the measurement. In the 'non-cancelled' manifold, where the nuclear-Zeeman and the hyperfine interactions are additive, much broader resonances are obtained and the only resolvable component is a double quantum transition line, $\Delta m_I = 2$, occurring at higher frequencies. The double-quantum transition has maximum intensity at a frequency[3]:

$$v_{dq} = 2\left[\left(\frac{|A|}{2} + v_I\right)^2 + K^2\left(3 + \eta^2\right)\right]^{1/2} \quad \text{(Eq. 19)},$$

where $|A|$ is a secular component of the hyperfine coupling tensor determined mainly by its isotropic part; a modest anisotropy of the hyperfine interaction affects mainly the line shape but not the frequency of the double quantum line.
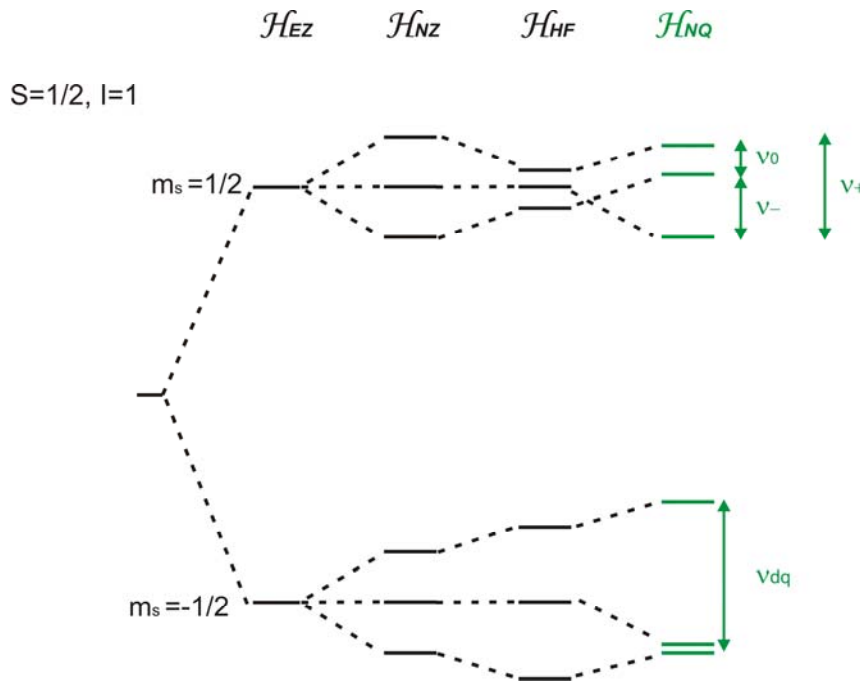


**Figure 6.** Energy level diagram for a S=1/2, I=1 nucleus in cancellation condition.

**2.1.7.5 Electron nuclear double resonance spectroscopy (ENDOR)**

Electron nuclear double resonance (ENDOR) is a technique that directly probes the nuclear transitions ($|\Delta m_S| = 0$, $|\Delta m_I| \geq 1$). For a S=1/2, I=1/2 system the nuclear frequencies (Figure 2) are given by[8]:

$$\nu_\alpha = \sqrt{\left(\frac{A}{2} + \nu_I\right)^2 + \frac{B^2}{4}} \quad \text{and} \quad \nu_\beta = \sqrt{\left(-\frac{A}{2} + \nu_I\right)^2 + \frac{B^2}{4}} \quad \text{(Eq. 20)},$$

where A and B are related to the secular part ($A_{zz}$) and to non-secular ($A_{zx}$, $A_{zy}$) hyperfine couplings and $\nu_I$ is the nuclear Larmor frequency. For isotropic hyperfine values and cases where $\nu_I \gg |A|$, B these equations reduce to:

$$\nu_{\alpha,\beta} = \left|\nu_I \pm \frac{A}{2}\right| \qquad \text{(eq. 21)}.$$

For nuclei I >1/2 the ENDOR frequencies depend additionally on the nuclear quadrupole interactions:

$$\nu_{\alpha,\beta} = \left|\nu_I \pm \frac{A}{2} + \frac{3}{2}P(2m_I - 1)\right| \quad \text{(eq. 22)}.$$

The pulsed ENDOR scheme introduced by Davies is based on selective microwave pulses (Figure 7)[8]. In Davies ENDOR, the first selective microwave pulse inverts the polarization of a particular EPR transition. Each time the frequency of the subsequent selective rf $\pi$ pulse becomes equal to a nuclear frequency, the population of the EPR transitions will be affected. This change is monitored via a two-pulse echo detection scheme. The ENDOR spectrum is then recorded by monitoring the primary echo intensity as the rf is incremented stepwise over the desired frequency range. The line intensities in a Davies ENDOR spectrum depend on the length of the first microwave $\pi$ pulse *($t_{mw}$)* and it can be described by introducing the selectivity parameter $\eta_S = A\,t_{mw}/2\pi$.
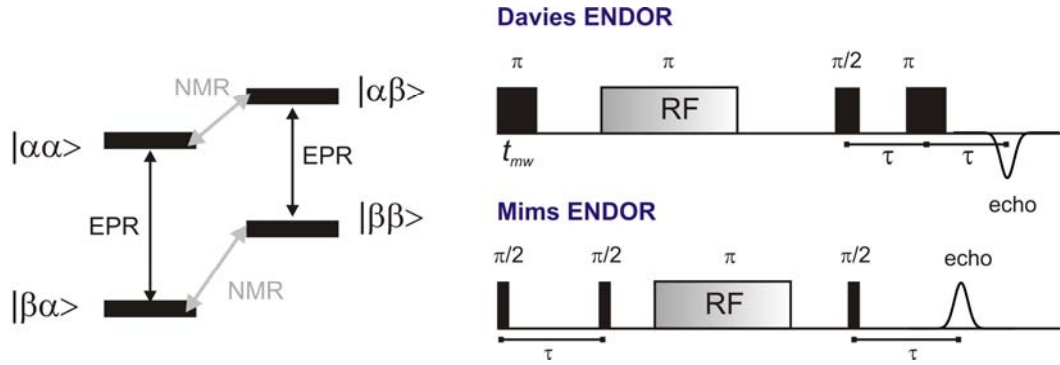
**Figure 7.** Energy level scheme for a S=1/2, I=1/2 (right). The Davies and Mims ENDOR sequences described in the text (left).

A second ENDOR technique frequently used for small hyperfine interactions is the scheme introduced by Mims and is based on the stimulated echo sequence with three non-selective microwave pulses[12]. The preparation part, $\pi/2$-$\tau$-$\pi/2$, creates a $\tau$ dependent grated polarization pattern. Next, the polarization is changed by a selective rf pulse if it is resonant with a nuclear transition. The electron polarization is then detected via a stimulated echo created at a time $\tau$ after the last $\pi/2$ mw pulse. The ENDOR efficiency of Mims ENDOR is given by:

$$F_{ENDOR} = \frac{1}{4}(1 - \cos(A\tau)) \text{ (Eq. 23)}$$

and depends upon the hyperfine coupling constant $A$ and the time $\tau$. It is maximum for $\tau = (2n+1)\pi/A$ and zero for $\tau = 2n\pi/A$, with n=0,1,2,etc.

Mims ENDOR thus exhibits blind-spot behaviour similar to the three pulse ESEEM and HYSCORE but which now depends on $A$ (in a three-pulse ESEEM the blind spots depend on $\nu_\alpha$ and $\nu_\beta$).

*Chapter 2*

**2.2 FTIR Spectroscopy**

**2.2.1 Vibration of a diatomic molecule**

A diatomic molecule is the simplest system that can show a molecular vibration. The classical frequency of an oscillation is given by Hooke's law[13]:

$$\nu = \frac{1}{2\pi}\sqrt{\frac{k}{\mu}} \text{ (Eq. 24)},$$

where $k$ is the force constant for the bond between two atoms in their equilibrium distance and $\mu$ is the reduced mass. This equation provides a link between the strength of the covalent bond between two atoms, the mass of the interacting atoms and the frequency of vibration. In diatomic molecules, the vibration of the nuclei occurs only along the line connecting the two nuclei. In general these oscillations are to a good approximation harmonic. From the masses of the atoms the force constant can be calculated by the equation[14]:

$$k = 0.58915 \times 10^{-4} \nu^2 \mu \text{ (Eq. 25)},$$

where the masses of the atoms are expressed in atomic units, the frequency in cm$^{-1}$ and the force constant in N/m.

**2.2.2 Interactions of diatomic molecules with light – Absorption in the infrared**

Light passing through a molecule imposes an oscillating electric dipole. Within the electric dipole approximation for light, the vibrations of a diatomic molecule that give rise to a change in the dipole moment are infrared-active, therefore in order for a molecule to absorb infrared radiation a net change in the dipole moment must occur. Infrared absorption spectroscopy uses a continuum of incident radiation that includes light of the same frequency as these vibrations. The infrared spectrum is then obtained as a consequence of the absorption of electromagnetic radiation at frequencies that correlate with the vibration of the chemical bond of the diatomic molecule[14]. The intensity of the absorption depends, among other things, on the square of the oscillating molecular dipole. Two factors contribute to its size; the charges on the moving atoms and the orbital following of the valence electrons.

48

## 2.2.3 Modes of IR sampling

The basic procedures for infrared measurements can be divided in transmission and reflectance methods[15]. These are illustrated in Figure 8.
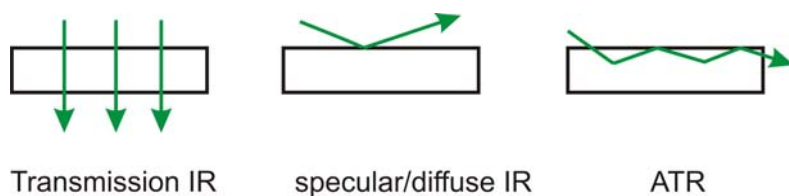


**Figure 8.** Overview of the basic methods used in Infrared Spectroscopy.

*Reflectance Infrared.* This method can be subdivided into two categories; external and internal measurements[15]. In external reflectance, incident irradiation is focused onto the sample and two forms of reflectance can occur; specular and diffuse. External reflectance measures the radiation reflected from a surface. On the other hand an internal reflection method is ATR (Attenuated Total Reflectance). In particular, ATR spectroscopy measures the changes that occur when a totally reflected infrared beam comes into contact with the sample. A beam of radiation entering a crystal will undergo a total internal reflection, when the angle of the incidence at the interface between the sample and the crystal is greater than a critical angle that is a function of the refractive indices of the two surfaces. The beam penetrates a fraction of a wavelength beyond the reflecting surface and when a material selectively absorbs radiation in close contact with the reflecting surface, the beam loses energy at the wavelength where the material absorbs. The resulting attenuated irradiation is measured and plotted as a function of wavelength and gives rise to the absorption spectral characteristics of the sample.

*Transmission Infrared.* The transmission sampling method involves passing the infrared energy through the sample and detecting the fraction of the beam that is transmitted (i.e. not absorbed). This is the method used extensively within the present study in solution samples. The infrared beam passes through the sample and the energy that comes through is measured versus the respective wavelength to generate a spectrum. The Beer-Lambert law relates the amount of light transmitted by a sample to its thickness and concentration according to the relation[15,16]:

$$A_{abs} = \varepsilon c l \quad \text{(eq. 26)},$$

where $A_{abs}$ is the absorbance of the solution, $c$ is the concentration, $l$ the path length of the sample and $\varepsilon$ the molar absorptivity. The absorbance is equal to the difference between the logarithms of the intensity entering the sample ($I_0$) and the intensity of the light transmitted ($I$) and is dimensionless:

$$A_{abs} = \log(I_0 / I) = -\log(I / I_0) = -\log(T) \quad \text{(eq. 27)},$$

where $T$ is the transmittance.

### 2.2.4 FTIR spectroscopy- Interferometer and interferrogram

The principle of the infrared experimental techniques is based on the Michelson interferometer[16] (see Figure 9). Light from an infrared source impinges upon a beamsplitter that transmits 50% of the light to one mirror and reflects 50% onto a second mirror. The light reflected off the two mirrors is passed through the beamsplitter for a second time and the two beams recombine, go through the sample and are focused on the infrared detector. One of the mirrors is movable and scans back and forth relative to the beamsplitter. During this scan, the path length between them changes relative to the path length between the stationary mirror and the beamsplitter. This path difference is known as the optical retardation ($\delta$) and is a function of the moving mirror position. What is produced then is the interferrogram; a digital plot of the light intensity versus the mirror position. The two domains of distance and frequency are inter-convertible by the mathematical method of Fourier transformation expressed as:

$$I(\bar{v}) = \int_{-\infty}^{+\infty} I(\delta)\cos(2\pi\bar{v}\delta)d\delta \quad \text{(Eq. 28)}$$

The Fourier transform converts the $I(\delta)$ information in the interferrogram to a $I(\bar{v})$ plot of intensity versus wavenumber (frequency).
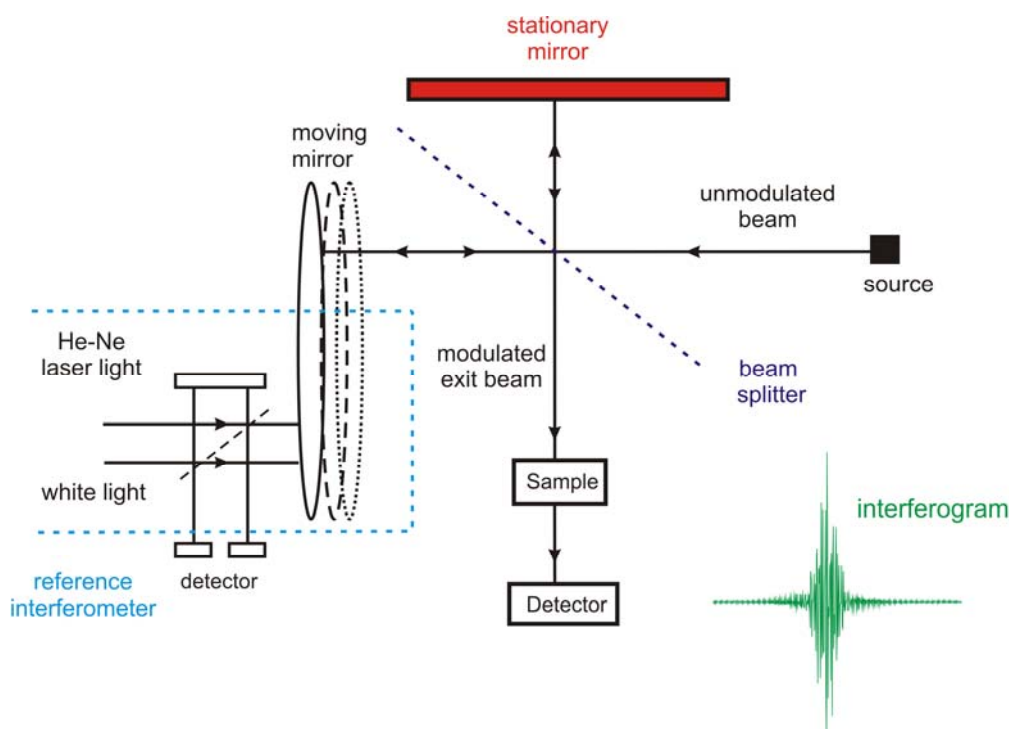
**Figure 9.** Illustration of the Michelson interferometer as an integrated part of an FTIR spectrometer. Adapted and modified from Griffiths[16]

The FTIR spectrum therefore consists of bands at the frequencies in which the sample absorbed the incident radiation. Band positions are presented as wavenumbers ($\bar{v}$) whose unit is the reciprocal centimeter (cm$^{-1}$). This unit is proportional to the energy of the vibration. The wavenumbers are commonly referred to as 'frequencies' in the majority of the scientific works, though such annotation is not entirely correct. These 'frequencies' are characteristic of each molecular group within the molecular environment in which, the latter is located. Vibrating dipole moments are sensitive to structure, conformation or physical state and can be distinguished from similar groups in a complex biological matrix. In this way they serve as probes changes in the local molecular environment and thus provide information about a specific molecular site.

**2.2.5 Surface enhanced infrared absorption spectroscopy (SEIRA)**

The SEIRA method couples immobilization of a protein sample onto a gold electrode with *in-situ* characterization via infrared spectroscopy in an ATR configuration[22,23]. The infrared absorption of molecules adsorbed on the metal surface is enhanced (10 to 1000 times) and thus it is possible to record infrared spectra on a

single protein monolayer. The observed enhancement is predominantly caused by the electromagnetic interactions of the incident photon field with the metal and the molecules. The SEIRA effect is not yet perfectly understood, but it has been accepted that at least two mechanisms are responsible for it. The band intensity can be increased by increasing (1) the dynamic dipole moment (chemical mechanism) and (2) the electric filed along the given dynamic dipole moment (electromagnetic mechanism). The second mechanism is related to plasmon excitation. In a simplified picture, this can be understood in terms of that the electrons inside of the gold nanoparticles follow the applied electric field and transmit dipole radiation. The transmitted electric field has the frequency and wavelength similar to the applied electric field. Within certain size ranges of the nanoparticles there is a resonance and certain phase relation between the electrons in the nanoparticles and the light wave. This resonance and phase relation is proposed to cause the effect of enhanced absorption. In a simplified picture, the nanoparticles act like little antennas, which are tuned for a high interaction with the light wave. In addition, the immobilization on a gold electrode offers the possibility of direct redox experiments and time-resolved electrochemical reactions.

**2.2.6 FTIR spectroscopy in the study of hydrogenases**

The active site of metalloproteins such as hydrogenases is coordinated by diatomic molecular groups, namely carbonyls and cyanides[17]. The stretching vibrations of these two diatomic molecules occur in a region free of other vibrations and can provide valuable information on the system under study.

Most carbonyls exhibit strong and sharp bands in the region between 2100 and 1800 cm$^{-1}$. The free CO 'frequency' is at 2155 cm$^{-1}$. CO bonding is a synergic effect between $\sigma$ donation and $\pi$ acceptance[13]. $\sigma$-bonding is formed by donation of the 5$\sigma$ electrons of CO to the empty orbital of the metal. This tends to raise the $\bar{\nu}$ (CO), since the 5$\sigma$ orbital is weakly anti-bonding. On the other hand, $\pi$-bonding occurs by a back donation of $d_\pi$ electrons from the metal orbitals to the empty anti-bonding 2p$\pi^*$ orbital of CO. This tends to lower $\bar{\nu}$ (CO). The CO is a better $\pi$-acceptor and the net result is a drift of electrons from the metal to CO, when the metal is in a relatively low oxidation state. Thus the $\bar{\nu}$ (CO) in hydrogenases are lower than the value of free CO.

In the case where CO forms a bridge between two metals its $\bar{\nu}$(CO) is much lower than that for a terminal CO group.

On the other hand, cyanides in complexes exhibit sharp $\bar{\nu}$(CN) at 2200 - 2000 cm$^{-1}$ and the $\bar{\nu}$(CN) for the free CN$^-$ in an aqueous solution is 2080 cm$^{-1}$. Upon coordination to a metal the $\bar{\nu}$(CN) shifts to higher wavenumbers. The CN$^-$ ion acts as a σ-donor by donating electrons to the metal and as a π-acceptor by accepting electrons[13]. σ-donation tends to raise the $\bar{\nu}$(CN), because the electrons enter into the 5σ orbital, which is weakly anti-bonding, while π- back bonding tends to decrease the $\bar{\nu}$(CN). CN$^-$ is a better σ-donor and a poorer π-acceptor compared to CO. The $\bar{\nu}$(CN) are higher than the value of the free CN$^-$, while the opposite holds for the $\bar{\nu}$(CO).

In particular, the FTIR spectrum of a [NiFe] hydrogenase is shown in Figure 10, where the bands of the carbonyl and cyanides ligands are found in the related positions. Based on the discussion above, it is evident that changes in the electronic structure and charge distribution at the active site of hydrogenases as well as hydrogen bonding interactions with surrounding amino acids greatly affect the vibrations of the CO, CN$^-$ molecules, resulting in unique spectra for each enzymatic state (structure). In some cases it is useful to obtain the first, second or higher derivative of the infrared bands. This results in a resolution enhancement, since changes in the gradient are examined. The second derivative gives a negative peak for each band in the FTIR spectrum. With differentiation the sharp bands are enhanced at the expense of broad ones and this may allow for the selection of a suitable peak or the 'flattening' of the broad envelope background that can mask the desired peaks.
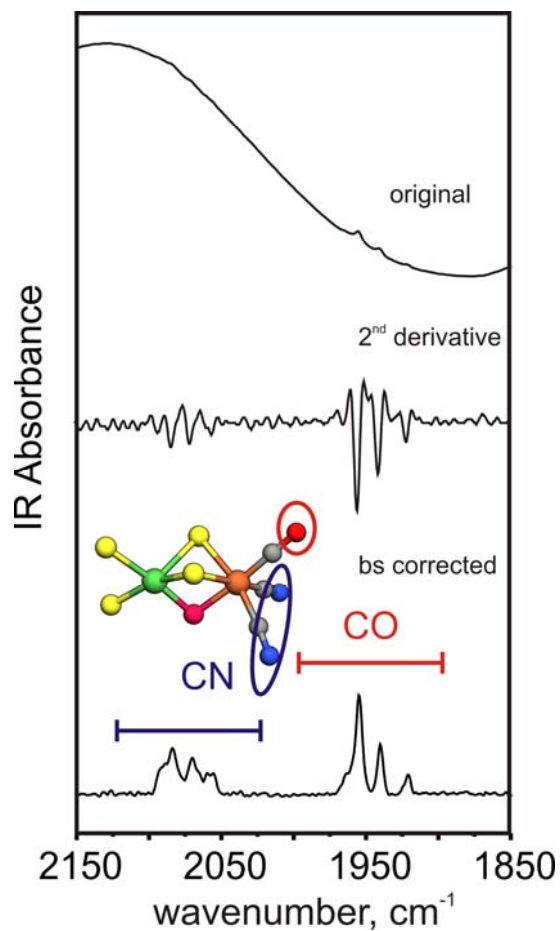
**Figure 10.** FTIR absorbance spectrum, the second derivative and the baseline corrected spectrum in a sample of a [NiFe] hydrogenase, in which the protein molecules show a mixture of redox states. Each redox state is described by one CO stretching vibration and two CN stretching vibrations.

**2.3 Electrochemistry**

Electrochemistry is important in understanding the kinetics and energetics of biological electron transfer processes as well as reactions coupled to redox transitions. There are two strategies for studying electrochemical reactions in redox enzymes[18]; dynamic electrochemistry and electrochemistry on proteins in solution and in the presence of redox mediators.

**2.3.1 Protein film voltammetry**

The first approach is known as protein film voltammetry (PFV), where a monolayer of the enzyme is adsorbed onto an electrode, which plays the role of its redox partner[19,20]. The adsorption of proteins takes place on a metal electrode with the help of redox linker molecules (Self-Assembled Monolayers - SAMs) or surfactants and on pyrolytic graphite electrodes (PGE), in which the rough, oxidised surface is effective for non-covalent adsorption. Reversible electron transfer occurs with the electrode and the enzyme's catalytic activity is controlled by the electrode potentials. Two main experiments are used in the study of catalytic electron transport: cyclic voltammetry and chronoamperometry[21]. In cyclic voltammetry, the potential of the electrode is cycled between two limiting values and the resulting current is monitored. In chronoamperometry, the current is monitored as a function of time after initiating a reaction, i.e. stepping the potential to a specific value or injecting gases in the PFV cell. The current is directly proportional to the rate of the catalytic electron flow. By scanning or stepping the electrode potential, the rates and direction of electron flow can be changed and specific sites in the enzyme can be inter-converted between different redox states, while activation or inactivation processes can be also induced.

**2.3.2 Electrochemistry in solution – Theory and nature of information obtained**

Electroactive centres in proteins in solution can be dynamically studied by coupling electrochemical and spectroscopic techniques[24].

A redox component or 'couple' $A_{red}/A_{ox}$ can be represented undergoing the reaction:

$$A_{red} = A_{ox} + n e^- \quad \text{(eq. 29),}$$
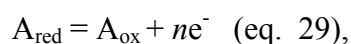
where $n$ is the number of electrons. Such equation represents only half of the complete oxidation-reduction reaction and is called a half cell. The complete cell (reaction) is:

$$A_{red} + B_{ox} = A_{ox} + B_{red} \quad \text{(eq. 30).}$$
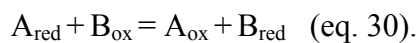
The equilibrium constant $K_{eq} = [A_{ox}][B_{red}]/[A_{red}][B_{ox}]$ of equation 30 depends on the individual affinities for electrons of the A and B couples. In the case that B has a higher affinity for electrons this reaction will tend to the right. Since the standard free energy of the reaction will be negative (i.e. $\Delta G^o = -RT \ln K_{eq}$), $K_{eq}$ is expected to be larger than unity. Because of the nature of the measurement, the electrical potential unit can be used and the standard free energy of the reaction can be given using the equation:

$$\Delta G^o = -nF\Delta E \text{ (eq. 31),}$$

where $\Delta E$ is the redox potential difference between two half cells and $F$ the Faraday constant (96.493 JV$^{-1}$). The negative sign is a matter of convention; a positive redox potential change represents a low to high redox potential change for which, $\Delta G^o$ is always negative. The redox potential of the redox couple or half cell of B is given by the Nernst equation:

$$E = E_m + \frac{RT}{nF} \ln \frac{[B_{ox}]}{[B_{red}]} = E_m + 2.303 \frac{RT}{nF} \log \frac{[B_{ox}]}{[B_{red}]} \text{ (eq. 32),}$$

where $E_m$ is the standard redox potential (midpoint potential) of the B couple, i.e. the potential $E$ when $[B_{ox}] = [B_{red}]$. Figure 11 shows a typical Nernst curve for $n = 1$ and $n = 2$ plotted against the applied potential for a fictitious [red] system. At the half reduction point, where [ox]=[red], $E = E_m$.
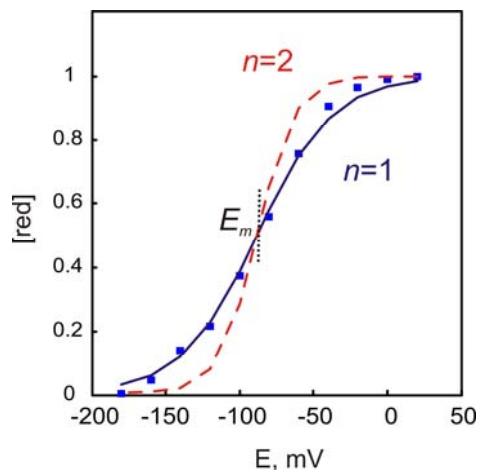
**Figure 11.** The Nernst curve for one- and two-electron redox couples for a process with a midpoint potential -84 mV.

Two mechanisms by which the observed midpoint reduction potential can exhibit a pH dependence are: (1) oxidation-reduction equilibria involving hydrogen ion ($H^+$) binding and (2) pH-dependent conformational changes. A pH dependence can be incorporated in the Nernst equation using the model of two equivalent sites as shown in Figure 12, for the case of an [Fe₄S₄] cluster. This diagram is schematic, since it is not required that the proton binding site is the iron-sulphur cluster. The only requirement is only that the equilibrium for binding is pH dependent. $pK_{ox}$ and $pK_{red}$ are the $pK$ values for proton association to the oxidised and the reduced form, respectively.

Taking into consideration the Henderson-Hasselbalch expression[25]

(i.e. pH = p$K$ +log([base]/[acid])) the pH dependence of the first formal potential (low pH) can be obtained by the relation:

$$E_{m,(\text{pH})} = E_{m,(lowpH)} + \frac{RT}{nF} \ln\left( \frac{K_a^{red} + [H^+]}{K_a^{ox} + [H^+]} \right) \quad (\text{eq. 33})$$
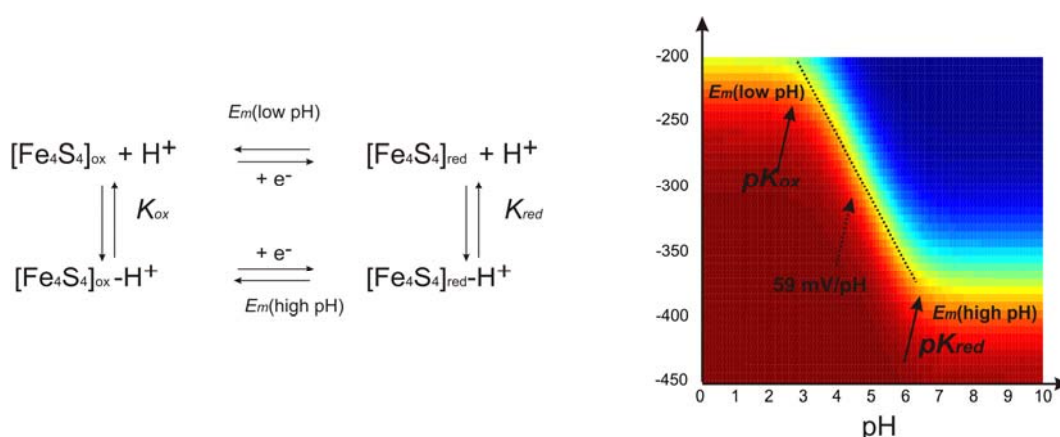
**Figure 12.** Schematic diagram of the $E_m$/ pH relationship and an example of a plot of the midpoint potential versus pH for a species with p$K_{red}$ 6.1 and p$K_{ox}$ 3.2 (Pourbaix diagram). Three regions can be seen: pH< p$K_{ox}$, where $E_m$ approaches pH independence; p$K_{ox}$<pH< p$K_{red}$, where $E_m$ varies by 59 mV/pH unit (25°C); and pH > p$K_{red}$, where $E_m$ becomes again pH independent.

### 2.3.3 FTIR and EPR integrated electrochemistry

For the FTIR electrochemistry employed in this study the Optical Transparent Thin Layer (OTTLE) cell described by Moss et al[26,27] has been used.
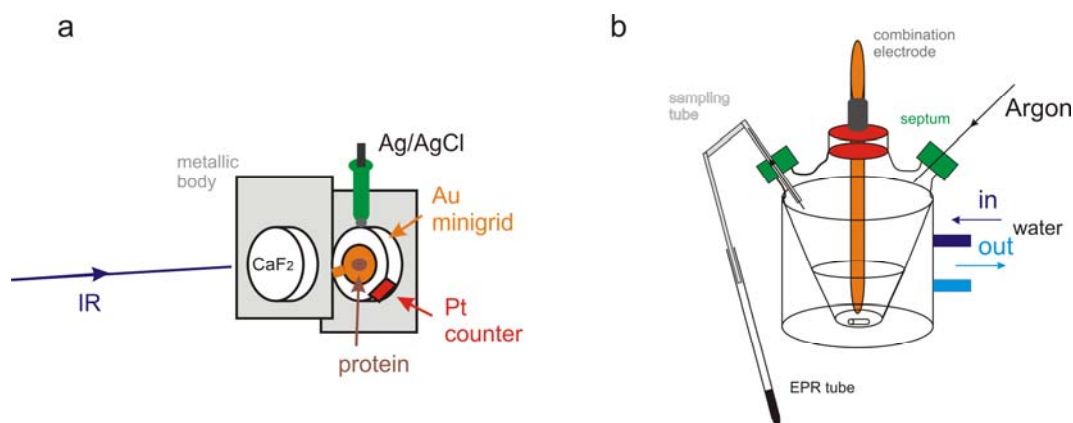


**Figure 13.** a) OTTLE cell designed by Moss[26] for FTIR electrochemistry, b) A vessel for potentiometric titrations in which samples are taken anaerobically and frozen for EPR studies at low temperatures[24].

The working electrode consists of a 8.5 μm thick, 70% transparent gold mini-grid, which together with a platinum (Pt) foil counter and a Ag/AgCl reference electrodes

complete the three electrode geometry. The outer cavity of the cell is filled with buffer/salt solution. For the improvement of the heterogeneous electron transfer, electron transfer reagents may be added to the sample solution.

The high electrode surface leads to a fast equilibration of the system within minutes. A schematic representation of the Moss cell is shown in Figure 13a. For the EPR titrations the electrochemical cell designed by Dutton was used (Figure 13b). In this type of cell a solution of the protein and the redox mediators is added, which is being stirred during the titration. The anaerobic conditions required are ensured by flushing the cell through one of the septums with high purity argon gas that has prior been hydrated so that the biological suspension does not evaporate. At the second septum (sampling point), a tube (usually from stainless steel) is inserted that is directed into the EPR tube and removes any traces of $O_2$ from the latter. After being flushed, the metallic tube is dipped into the protein solution. Since there is no exit for the incoming gas, a pressure builds up and pushes the protein solution through the metallic capillary into the EPR tube. The sample is then removed and promptly frozen. During the titration, the temperature of the solution is maintained by water passing through the outer body of the cell in a closed circuit with a thermostat. The potentials are adjusted by addition of stoichiometric amounts of sodium dithionite or potassium ferricyanide and the potential value is measured by a combination micro-electrode (i.e. a combination of an ion-selective and an external reference electrode).

# References

1. Atherton, N. M. *Principles of Electron Spin Resonance;* Ellis Horwood Limited: **1993**.

2. Abragam, A.; Bleaney, B. *Electron Paramagnetic Resonance of Transition Ions;* Dover Publication Inc: New York, **1970**.

3. Schweiger, A.; Jeschke G. *Priniciple of pulse electron paramagnetic resonance;* Oxford University Press: New York, **2001**.

4. Bencini, A.; Gatteschi, D. *EPR of Exchange coupled systems;* Springer-Verlag: **1990**.

5. Pilbrow, J. R. *Transition Ion Electron Paramagnetic Resonance;* Oxford University Press: New York, **1990**.

6. Fan, C. L.; Houseman, A. L. P.; Doan, P.; Hoffman, B. M. *J. Phys. Chem.* **1993,** *97* (12), 3017-3021.

7. Ohnishi, T. Iron-sulfur clusters semiquinones in Complex I. *Biochim. Biophys. Acta-Bioenergetics* **1998,** *1364* (2), 186-206.

8. Gemperle, C.; Schweiger, A. Pulsed Electron Nuclear Double-Resonance Methodology. *Chem. Rev.* **1991,** *91* (7), 1481-1505.

9. Dikanov, S. A.; Tsvetkov, Y. D. *Echo Envelope Modulation (ESEEM) spectroscopy;* CRC Press: **1992**.

10. Flanagan, H. L.; Singel, D. J. Analysis of N-14 ESEEM Patterns of Randomly Oriented Solids. *J. Chem. Phys.* **1987,** *87* (10), 5606-5616.

11. Agrawal, A. G.; van, G. M.; Gartner, W.; Lubitz, W. *J. Phys. Chem. B* **2006**, *110* (15), 8142-8150.

12. Mims, W. B. Pulsed ENDOR Experiments. *Proceedings of the Royal Society of London Series A-Mathematical and Physical Sciences* **1965,** *283* (1395), 452-&.

13. Nakamoto, K. *Infrared and Raman Spectra of Inorganic and Coordination Compounds;* 5th ed.; John wiley & Sons, Inc: **1997**; Vol. B.

14. Braterman, P. S. *Metal carbonyl spectra;* Academic Press Inc: London, **1975**.

15. Stuart, B. *Infrared Spectroscopy Fundamentals and applications;* Wiley: **2004**.

16. Griffiths, P. R.; de Haseth, J. A. *Fourier Transform Infrared Spectrometry;* John Wiley & Sons: **1986**.

17. Pierik, A. J.; Roseboom, W.; Happe, R. P.; Bagley, K. A.; Albracht, S. P. J. *J. Biolog. Chem.* **1999**, *274* (6), 3331-3337.

18. Kaim,W.; Klein, A. *Sperctroelectrochemistry;* RSC Publishing: **2008**.

19. Armstrong, F. A.; Heering, H. A.; Hirst, J. *Chem. Soc. Rev.***1997**, *26* (3), 169-179.

20. Vincent, K. A.; Armstrong, F. A. *Inorg. Chem.* **2005,** *44* (4), 798-809.

21. Leger, C.; Elliott, S. J.; Hoke, K. R.; Jeuken, L. J. C.; Jones, A. K.; Armstrong, F. A. *Biochemistry* **2003**, *42* (29), 8653-8662.

22. Aroca, R. *Surface-Enhanced Infared spectroscopy;* Wiley: 2006.

23. Osawa, M. *Bulletin of the Chemical Society of Japan* **1997**, *70* (12), 2861-2880.

24. Dutton, P. L. *Methods Enzymol.* **1978**, *54*, 411-435.

25. Murray, R. K.; Granner, D. K.; Mayes, P. A. R. V. W. *Harper's Illustrated Biochemistry;* 26th ed.; McGraw-Hill Companies, Inc.: 2003.

26. Moss, D. A.; Leonhard, M.; Bauscher, M.; Mantele, W. *FEBS Lett.* **1991,** *283* (1), 33-36.

27. Baymann, F.; Moss, D. A.; Mantele, W. *Anal. Biochem.* **1991**, *199* (2), 269-274.

*Chapter 2*

# Chapter 3

## Spectroelectrochemical study of the [NiFe] hydrogenase from *Desulfovibrio vulgaris* Miyazaki F in solution and immobilized on biocompatible gold surfaces
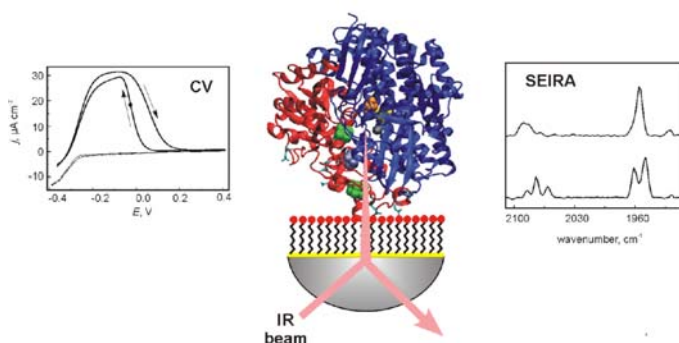


**Graphical abstract.** Spectroelectrochemical experiments monitored by surface enhanced absorption infrared spectroscopy (SEIRA)

*Chapter 3*

# Spectroelectrochemical study of the [NiFe] hydrogenase from *Desulfovibrio vulgaris* Miyazaki F in solution and immobilized on biocompatible gold surfaces[†]

Diego Millo[a], Maria-Eirini Pandelia[b], Tillmann Utesch[a], Nattawadee Wisitruangsakul[a], Maria A. Mroginski[a], Wolfgang Lubitz[b], Peter Hildebrandt[a], Ingo Zebger[a]

[a] *Institut für Chemie, Technische Universität Berlin, Str. des 17. Juni 135, Sekr. PC14, D-10623 Berlin, Germany*
[b] *Max-Planck-Institut für Bioanorganische Chemie, Stiftstrasse 34-36, D-45470 Mülheim/Ruhr, Germany*

## Abstract

The catalytic cycle of the anaerobic [NiFe] hydrogenase from *Desulfovibrio vulgaris* Miyazaki F (*Dv*MF) both in solution and immobilised on an Au electrode was studied by IR spectroscopic and electrochemical methods. IR spectroelectrochemistry in solution at different pH-values allows the identification of the various redox-states of the active site, and the determination of the midpoint potentials, as well as, their acid-base equilibria. The spectroscopic characterisation was based on the unique marker bands of the CN and CO stretching modes of the Fe-Ni center, and served as reference for the surface enhanced IR absorption (SEIRA) study of the immobilised enzyme. Using structural models of hydrogenases from *Dv*MF and *Desulfovibrio gigas*, dipole moment calculations were carried out to guide the immobilisation strategy. In view of the high dipole moment of ca. 1100 Debye pointing through the negatively charged area surrounding the distal [FeS] cluster, the Au electrode was coated by a self-assembled monolayer of amino-terminated mercaptanes which, due to the positively charged head groups, permit a durable electrostatic binding of the protein. SEIRA spectroscopy revealed a structurally and functionally intact active site as demonstrated by the reversible activation and inactivation under hydrogen and argon, respectively. Cyclic voltammetry on the immobilised enzyme demonstrate a reversible anaerobic inactivation upon changing the applied potential. The "switch" potential ($E_{switch}$) associated with the reductive reactivation was determined to be -33 mV (vs. normal hydrogen electrode). However, the catalytic current decreased on the time scale of hours during continuous cycling. SEIRA experiments demonstrate that the loss of catalytic activity is not due to protein desorption, but is rather related to a slow degradation of the active site, possibly initiated by the attack of reactive species electrochemically generated from residual traces of oxygen in solution.

---

## Introduction

Hydrogenases are metalloenzymes that catalyze the interconversion of molecular $H_2$ and protons and thus play a crucial role for the energy metabolism in many anaerobic microorganisms.[1,2] The [NiFe] hydrogenase from *Desulfovibrio vulgaris* Miyazaki F (*Dv*MF) is a heterodimeric enzyme, consisting of two subunits.[3,4] The large subunit (534 residues) contains the active site, a Ni-Fe center, whereas the small one (267 residues) accommodates three Fe-S clusters, which act as an electron transfer chain connecting the buried active site with the protein surface.[5-8] In the active site, the Fe atom is bound to one CO and two $CN^-$ ligands, whereas the Ni atom is coordinated by four cysteinyl residues, among which Cys549 and Cys84 serve as bridges to the Fe atom.[5,9] A third bridging position between the Ni and the Fe atoms is free for coordination and can bind different exogeneous ligands during the catalytic cycle.[2,10,11]

The highest oxidized states are denoted as $Ni_u$-A and $Ni_r$-B, which are catalytically inactive, be activated by exposing the enzyme to hydrogen.[2,9,12,13] $Ni_u$-A is referred to as the "unready" and $Ni_r$-B as the "ready" state, as they require different times for activation. This heterogeneity in the activation rates between the two states is ascribed to a different extra bridging ligand between the Ni and the Fe atoms. For the $Ni_r$-B state a hydroxyl group ($OH^-$) was identified[14], while for $Ni_u$-A a hydroperoxide ($OOH^-$) was suggested from crystallographic studies,[6,15] which is however still under discussion[2,10,16] One-electron reduction of $Ni_u$-A and $Ni_r$-B leads to the $Ni_u$-S and $Ni_r$-S states, respectively. Further reduction results in the formation of the $Ni_a$-S, $Ni_a$-C and $Ni_a$-SR states, which are catalytically active.[17-22]

EPR and IR spectroscopy have contributed to the identification of the various states of hydrogenases and, together with electrochemical methods, have provided important insight into the catalytic mechanism.[2,16,23-30] EPR spectroscopy allows analysing the paramagnetic states of the catalytic site and of the FeS cluster and provides information about structural and electronic properties.[28-30] IR spectroscopy, however, is applicable to both paramagnetic and EPR-silent states. It probes the CN and CO stretching modes, which are sensitive spectral markers for the oxidation state of the catalytic center, its ligation pattern, and its molecular environment.[2,9,31] These modes appear in a frequency range (1890 – 2110 $cm^{-1}$) that is free of any spectral contribution from the protein and

thus can be directly monitored in the absolute spectra. These techniques are applied to proteins in (frozen) solutions using either a controlled hydrogen pressure or chemical reductants and oxidants to accumulate and stabilize specific states of the enzyme[32-34].

DeLacey and coworkers have pioneered IR spectro-electrochemical titrations of hydrogenases in bulk solution using redox mediators.[2,31,35-37] Alternatively, the enzyme can be wired to an electrode to drive the catalytic process.[10,27,38-40] This approach is particularly interesting in view of potential biotechnological applications of hydrogenases in biofuel cells.[10,13,41] For such devices, protein film voltammetry can control and monitor the catalytic process, thereby revealing information about the redox properties and the functional integrity of the immobilized proteins. This technique, however, does not provide insight into the molecular structure of the active site of the immobilised enzyme and its changes during the catalytic reaction cycle.

In this respect, surface enhanced infrared absorption (SEIRA) spectroscopy represents a promising tool to bridge cyclic voltammetry (CV) and classical IR spectroscopy. SEIRA spectroscopy takes advantage of the enhanced absorption by ca. two orders of magnitude experienced by molecules in close vicinity of nanostructured Au films, such that it is possible to probe the IR bands of molecules even at sub-monolayer coverages.[42-44] This technique has been recently applied to immobilised proteins[45-48] and can be performed in a time-resolved mode in conjunction with the step-scan and rapid scan techniques.[49] Furthermore, using the Au support as a working electrode, electrochemical and spectroscopic analysis can be combined using the same experimental setup. A prerequisite for applying this technique to proteins is the appropriate immobilisation under preservation of the native structure and function. Such biocompatible immobilisation is usually achieved by coating the metal surface with self-assembled monolayers (SAMs) that are designed for a specific and uniform binding of the protein, excluding a direct contact with the metal surface.[50-52]

We have previously shown that SEIRA spectroscopy can be successfully applied to the membrane-bound hydrogenase from *Ralstonia eutropha*. On the basis of the CN and CO stretching modes, it was possible to monitor the enzyme activation and de-activation by a variation of the hydrogen pressure.[6,47] In this work, we have extended such studies to the [NiFe] hydrogenase from *Desulfovibrio vulgaris* Miyazaki F (*Dv*MF), for which

high resolution crystallographic data[6], allow a rational design of the immobilisation strategy. SEIRA experiments have been complemented on one hand by CV measurements to probe the catalytic activity of the immobilised enzyme and on the other hand by IR spectro-electrochemistry in bulk solution, in order to identify the various redox states of the active site and determine the midpoint potentials of the respective transitions.

*Chapter 3*

## Materials and methods

*Materials.* Cysteamine (HSCH$_2$CH$_2$NH$_2$, hereby indicated as C$_2$-NH$_2$) was purchased from Sigma Aldrich. 6-amino-1-hexanethiol, hydrochloride (C$_6$-NH$_2$), 8-amino-1-hexanethiol, hydrochloride (C$_8$-NH$_2$), and 11-amino-1-hexanethiol, hydrochloride (C$_{11}$-NH$_2$) were purchased from Dojindo and used without further purification. Purified Milli-Q water (Millipore, Massachusetts, USA) was used for all preparations and procedures.

*Sample purification and preparation.* The [NiFe] hydrogenase from *Dv*MF has been isolated and purified in 50 L cultures as described previously.[9,53] The pH of the enzyme solution was kept at pH 7.4 in Tris/HCl buffer. For the preparation of the Ni-A state, the hydrogenase was incubated with an excess of Na$_2$S under aerobic conditions, which was subsequently removed from the protein solution.[6] The pH of the protein solution for Ni$_u$-A at 4°C was 8.2.

*IR spectro-electrochemistry.* IR measurements were carried out on a Bruker IFS 66v/s FTIR spectrometer (2 cm$^{-1}$ resolution), equipped with a photoconductive MCT detector. IR spectro-electrochemistry was performed in an OTTLE (optically transparent thin-layer electrochemical) cell described by Moss.[54] A layer of the protein solution was formed between two CaF$_2$ windows on an 8.5 μm thick gold mesh in electrical contact with a Pt counter electrode. As a reference electrode an Ag/AgCl electrode (1 M KCl) was employed. All potentials cited in this work refer to the standard hydrogen electrode. For the spectroelectrochemical measurements, a 50 mM acetate (pH 5.5) buffer was used, containing a mixture of 11 redox mediators (125 μM) and KCl (100 mM). The mediators were methylviologen, $E_m$ = -448 mV (Acros), benzylviologen, $E_m$ = -359 mV (Acros), safranine T, $E_m$ = -289 mV (Acros), phenosafranine, $E_m$ = -252 mV (Acros), anthraquinone-2-sulfonate, $E_m$ = - 225 mV (Acros), anthraquinone-1,5-disulfonate, $E_m$ = -170 mV (Sigma), 2-hydroxy-1,4-naphthoquinone, $E_m$ = -145 mV (Sigma), potassium indigo tetrasulfonate, $E_m$ = -46 mV (Acros), methylene blue, $E_m$ = +11 mV (Acros), phenazine methosulfat, $E_m$ = +92 mV (Acros), 1,2 naphthoquinone, $E_m$ = + 145 mV (Sigma). The pH-dependence of the redox potentials for the various mediators, here

given at pH 7, has been previously described by Prince et al[55]. The measured intensity of the bands was divided by the enzyme concentration and the optical path length. In this way the apparent normalised absorbance (B, mM$^{-1}$ cm$^{-1}$) was obtained.

*SEIRA spectroscopy.* SEIRA measurements were performed in the Kretschmann-ATR configuration using a semi-cylindrical shaped Si crystal (20 x 25 x 10 mm of W x L x H) under an angle of incident of 60$^{\circ}$.[45] Thin Au films were formed on the flat surface of the Si substrate by electroless (chemical) deposition.[42] SEIRA spectra were recorded from 4000 to 1000 cm$^{-1}$ with a spectral resolution of 4 cm$^{-1}$ on a Bruker IFS66v/s spectrometer equipped with a photoconductive MCT detector. 400 scans were co-added for a spectrum. Further details are given elsewhere.[47,49]

*Protein Immobilisation.* SAMs were formed by immersing the Au electrode in a 1 mM ethanolic solution of the respective mercaptane for 18 hours. Subsequently, the coated electrode was rinsed with ethanol and finally dried under a stream of nitrogen. The protein was electrostatically immobilised by covering the chemically modified electrode inside the spectroelectrochemical SEIRA cell with 1 μM solution *Dv*MF in 10 mM phosphate buffer at pH 7. Covalent protein immobilization was achieved by adding a large excess of 1-ethyl-3-[3-(dimethylamino)propyl]carbodiimide hydrochloride (EDC) (5-10 mM) to the protein solution.[57] Alternatively, the protein was first incubated in a solution of EDC and

N-hydroxysuccinimide (NHS) (10 mM) for esterification of the protein carboxylate side chains in order to increase the yield of the coupling reaction.[40,57]

*Cyclic voltammetry.* CV measurements were carried out in the SEIRA cell connected to an Autolab PGSTAT 12 potentiostat which was controlled by the GPES software. The Au-film on the ATR crystal (0.8 cm$^2$ geometric area), a Pt wire, and a Ag/AgCl (3.0 M KCl) electrode served as working, counter, and reference electrode, respectively. The total filling volume of the cell was 3 mL. Further details are given elsewhere.[47,50] A disadvantage of this set-up is that, due to the rigidly fixed working electrode, mass transport limitations impair detailed studies on the enzyme kinetics [10].

*Chapter 3*

*Dipole moment calculations.* For the dipole moment calculations we have used the crystallographic data set of the oxidized [NiFe]-hydrogenases of *D. gigas* (2 FRV) and *Dv*MF (1 WUK).[6] The calculations were restricted to the small and large subunit of a hydrogenase heterodimer including the [NiFe] centre, the three [FeS] clusters and the $Mg^{2+}$ ion. All missing hydrogen atoms were added with the HBUILD[58] routine of CHARMM.[59] The protonation state of the His residues was chosen by visual inspection and the charges of ionisable groups were set appropriate for pH 7.0 assuming standard $pK_A$ values. For dipole moment calculations with VMD 1.8.6, partial charges of the CHARMM 27 force field were used for the protein and the $Mg^{2+}$ ion.[58,60,61] For *D. gigas* (2 FRV) partial charges for the metal clusters were taken from previous quantum mechanical calculations by Teixeira *et al.* [62], considering all the [FeS] clusters oxidized and the active center in the $Ni_a$-S state. In the case of *Dv*MF, partial charges for the metal clusters were not available, and were therefore replaced by dummy atoms positioned in the centre of the iron atoms for each [FeS] cluster. The [NiFe] dummy atom carried a total negative charge of two electrons ($-2e^-$), while the [4Fe4S] and the [3Fe4S] were positively charged ($+2e^-$ and $+1e^-$, respectively). The ligating Cys residues at the [FeS] cluster were deprotonated at the sulphur atom, corresponding to a charge of $-1e^-$ per Cys residue. The calculations for the static structures afford a total charge of the enzyme of $-10e^-$ and $-8e^-$ for *D. gigas* and *Dv*MF, respectively. However, the dipole moments were determined to be quite similar with 1052 Debye for *D. gigas* and 1112 Debye for *Dv*MF.

## Results and discussion

The intermediate states involved in the redox chemistry of the [NiFe] hydrogenase from *Dv*MF were monitored by FTIR electrochemistry. IR can identify all the redox intermediates by probing the stretching modes corresponding to the three diatomic ligands bound to Fe. Bands in the frequency region between 1890 and 1970 cm$^{-1}$, are assigned to the CO modes, whereas bands in the region between 2040 and 2110 cm$^{-1}$ correspond to the coupled CN stretching vibrations (vide supra). Following these modes as a function of a controlled applied potential, the redox transitions among the various redox states can be monitored. Figure 1 shows a three dimensional representation of such a potentiometric titration at pH 5.5. In these spectra the bands of the inactive $Ni_r$-B, $Ni_r$-S, as well as, of the active $Ni_a$-S, $Ni_a$-C, $Ni_a$-SR states could be identified (Table 1). All redox processes were reversible and could be described Nernst curves corresponding to one-electron transfer.
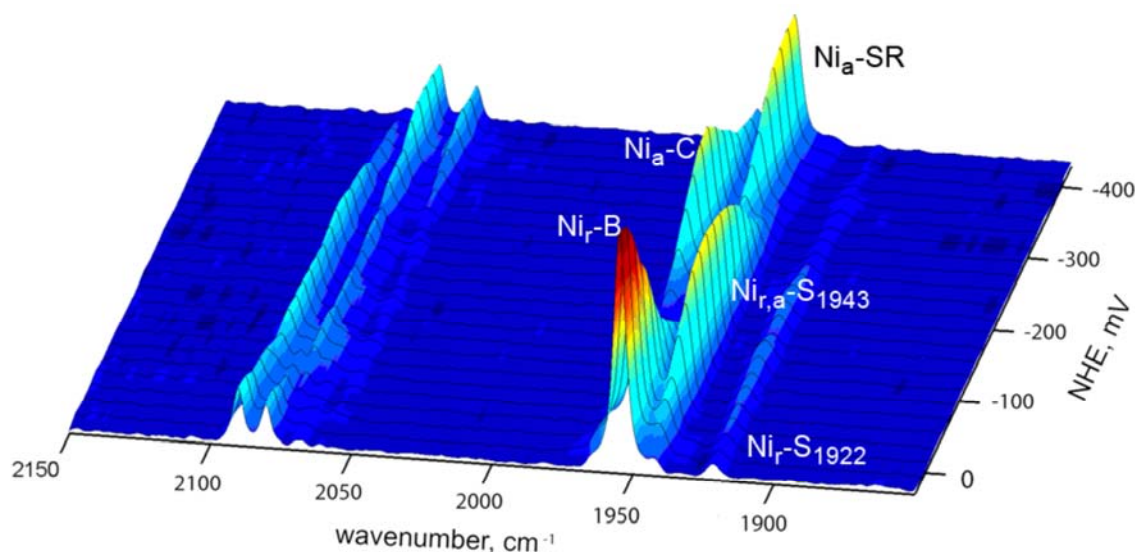


**Figure 1**. Three dimensional representation of the potentiometric titration of the [NiFe] hydrogenase from *Dv*MF in solution at pH 5.5 (25 °C). Each slice of this plot represents a spectrum recorded with 400 scans.

In Figure 2A the titration curves at pH 5.5 are shown, where the normalised intensities of the CO bands have been plotted versus the applied potential. For the $Ni_r$-B / $Ni_{r,a}$-S, $Ni_{r,a}$-S / $Ni_a$-C, $Ni_a$-C / $Ni_a$-SR redox couples the apparent midpoint potentials

were determined to be -58, -226 and -333 mV, respectively. The error was estimated to be ± 5 mV. These potentials were found to be pH-dependent, showing that these redox transitions are coupled also to a proton transfer.[9,32,31] The infrared spectra of the respective states are shown in Figure 2B. The positions of the bands at pH 5.5 are slightly shifted compared to the values obtained at physiological relevant pH (*i. e.* pH 7.4, Table 1). These frequencies are in agreement with the ones reported previously for the NiFe hydrogenase from *Dv*MF [9,63]. In the same work only the $Ni_u$-S was observed to be different from other enzymes. Therefore, the redox transition between the $Ni_u$-A / $Ni_u$-S was re-examined in the present study to account for this discrepancy.

**Table 1**. The vibrational frequencies of the CO and CN stretchings of the [NiFe] hydrogenase of *Dv*MF at pH 7.4 (25 °C).

| State | IR frequencies , $cm^{-1}$ | | |
|-------|----------------------------|---|---|
| | **CO stretching** | **CN stretching** | |
| $Ni_u$-A | 1956 | 2085 | 2094 |
| $Ni_r$-B | 1955 | 2081 | 2090 |
| $Ni_u$-S | 1958 | 2089 | 2100 |
| $Ni_r$-S | 1922 | 2061 | 2070 |
| $Ni_r$-S | 1943 | 2074 | 2086 |
| $Ni_a$-S | 1943 | 2074 | 2086 |
| $Ni_a$-C | 1961 | 2074 | 2085 |
| $Ni_a$-SR | 1948 | 2061 | 2074 |
| $Ni_a$-SR' | 1932 | 2052 | 2066 |

In this respect an additional potentiometric titration of a sample containing 90 % of $Ni_u$-A and 10% of $Ni_r$-B (determined by EPR spectroscopy , see Figure S1 Appendix A) was carried out. The IR spectrum of the same sample is shown in Figure 3A. Besides the $Ni_r$-B, also the EPR-silent states $Ni_r$-$S_{1922}$ and $Ni_r$-$S_{1943}$ were present. These states were persistent even after applying higher potentials prior to the titration. The titration was then carried out at pH 8.2 and 4 °C, in order to suppress a further conversion to the $Ni_r$-S states. Figure 3B shows the IR spectrum of the $Ni_u$-S state, which was found to be similar to the respective spectra of other oxygen-sensitive hydrogenases.[2]

However, even at 4 °C transition to the $Ni_r$-S states could not be completely avoided. An apparent midpoint potential of -278 ± 5 mV for the $Ni_u$-A/$Ni_u$-S transition was obtained (Figure 3C), which is comparable to those determined by Asso et al. in EPR investigations.[64] This process was fully reversible and consistent with a one-electron transfer. The electrochemical characterization of the *Dv*MF hydrogenase in solution (summarized in Scheme S1) showed that the redox transitions are similar to those observed for other standard [NiFe] hydrogenases from sulphate reducing and photosynthetic purple bacteria.

Thus the observed spectral and electrochemical deviations reported in previous investigations could be explained by a reduced stability of the $Ni_u$-S at a lower pH and a higher temperature of 15°C, leading to the concomitant rapid conversion to the $Ni_r$-S states. Furthermore, the obviously weaker signal to noise ration complicated an unambiguously band assignment of the CO stretching around 1943 (± 3) $cm^{-1}$ and guided together with the pH-dependence , shifted the redox potentials to -96 mV vs. NHE to a wrong assignment of the $Ni_u$-S state.
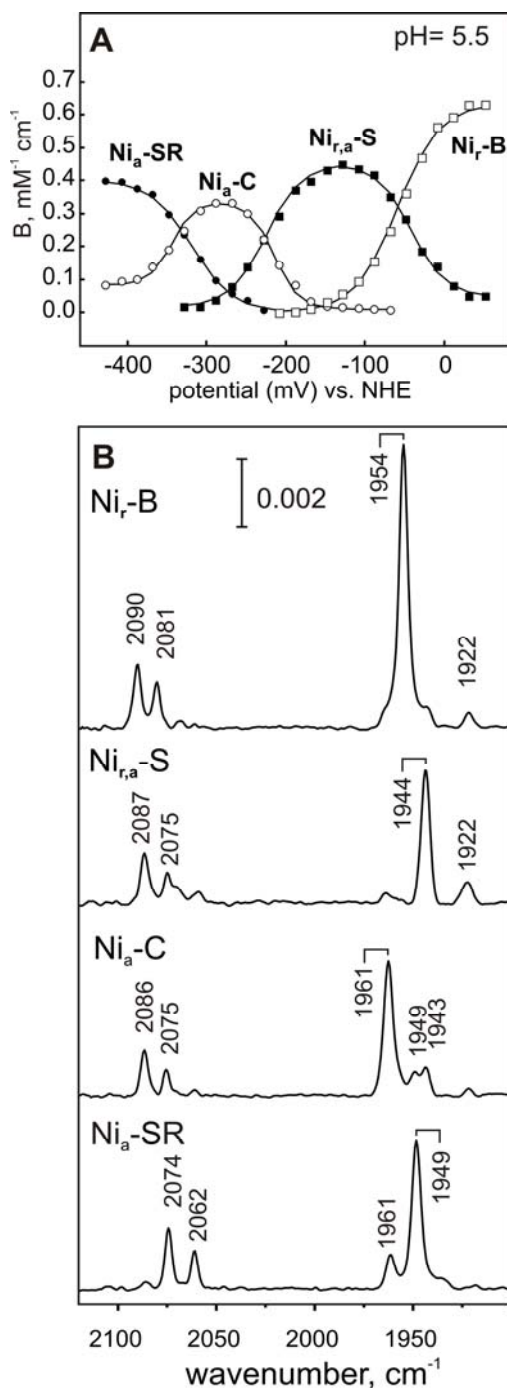
**Figure 2**. A potentiometric titration of the [NiFe] hydrogenase from *Dv*MF in solution at pH 5.5 (25 °C), obtained by plotting the normalised intensity of the CO bands of the individual states as a function of the applied potential. The solid lines represent a fit of the Nernst equation to the experimental data. B: IR spectra of the individual states (pH 5.5, 25 °C).
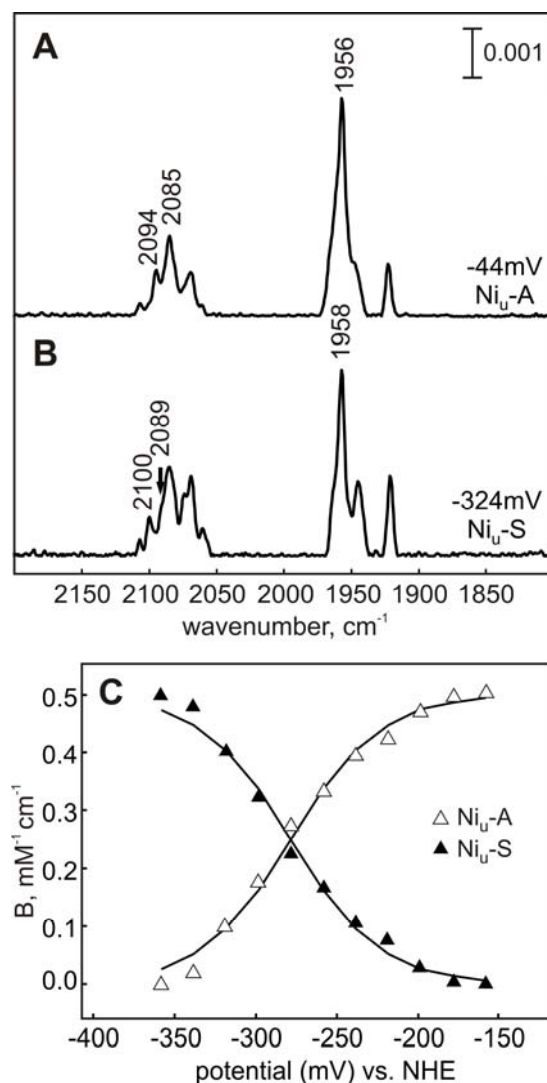
**Figure 3.** IR spectra of the [NiFe] hydrogenase from *Dv*MF in solution at pH 8.4 and 4°C. A: spectrum obtained at an applied potential of -44 mV where the $Ni_u$-A state (1956 cm$^{-1}$) is the major component, B: IR spectrum obtained at an applied potential at -324 mV where the transition to $Ni_u$-S (1958 cm$^{-1}$) is complete. In all spectra, small fractions of the $Ni_r$-S (1922 cm$^{-1}$) and $Ni_{r,a}$-S (1943 cm$^{-1}$) states are present. C: Potentiometric titration of the $Ni_u$-A/$Ni_u$-S couple of the [NiFe] hydrogenase from *Dv*MF in solution at pH 8.4 (4°C). The normalised intensity of the CO bands of the $Ni_u$-A and $Ni_u$-S states are plotted against the applied potential. The solid lines represent a fit of the Nernst equation to the experimental data yielding the number of transferred electrons, n = 1 and an apparent midpoint potential of -278 ± 5 mV.

There are various approaches to immobilise proteins on electrodes using SAM coatings that allow binding via electrostatic or hydrophobic interactions, covalent or coordinative bonds, respectively. An appropriate immobilisation strategy has to guarantee a high and durable surface coverage, a largely uniform orientation, and an efficient electrical contact between the electrode and the enzyme, as a prerequisite for a successful application of CV and SEIRA spectroscopy. An optimisation of the immobilisation conditions may be either achieved empirically or guided by rational concept, as we have employed in the present case. For the static structures of both *D. gigas* and *Dv*MF, calculations reveal a molecular dipole moment around 1100 Debye. The negative end of the dipole vector points through the glutamate-rich region located on the protein surface close to the distal [4Fe4S] cluster, which serves as the interaction domain with the natural electron acceptor of the enzyme, cytochrome $c_3$ (Figure S2).[9] Therefore, this protein part appears to be ideal for an attachment to a positively charged SAM surface (vide infra). In this way, one may expect a highly uniform orientation of the enzyme, since a large dipole moment is likely to cause a homogeneous alignment of the protein on the surface. Furthermore, the electrode may adopt the role of the physiological redox partner of hydrogenase, thereby promising an efficient electronic coupling.

After identifying the target domain on the protein surface, three approaches were used to immobilise the protein either electrostatically or covalently. In all cases, amino-terminated mercaptanes of different chain lengths ($C_x$-$NH_2$ with x = 2, 6, 8, 11 denoting the number of methylene groups) were used as biocompatible coatings for the Au surface. For these SAMs, pKa values between 6 and 7.5 were reported for the amino groups, which increased slightly with the chain length.[65,66] Thus, these amino groups are largely protonated in the present experiments carried out at pH 7 or lower. As a first approach, this resulting high positive charge density on the SAM surface was used for the formation of tight and stable electrostatic complexes with the negatively charged domain of *Dv*MF. Second, it was possible to crosslink the electrostatic complex via EDC coupling between the amino groups of the SAM and the carboxylate side chains in the putative binding domain of hydrogenase. As a third approach, a combination of EDC and NHS was used in order to achieve a more efficient covalent immobilisation.

In all three cases, immobilisation of hydrogenase was monitored by SEIRA by following the intensity of the amide I and amide II bands in the absolute spectra, which gradually increased until it reached a maximum after ca. 45 min (Figure 4). The same time constant allows describing the temporal evolution of the CO stretching, ruling out any major re-arrangement processes of the immobilised proteins and coverage-dependent differences in the protein orientations.

The degree of surface coverage at equilibrium is similar for both covalent and electrostatic binding, as concluded from the SEIRA spectra measured before and after EDC coupling. The absolute intensities reveal only minor variations of less than 15%. Furthermore, the amide I / amide II intensity ratio and the overall shape of these bands are not altered after covalent cross-linking. This indicates that the overall structure and orientation of the hydrogenase on the electrode is largely the same in both modes of immobilisation. In addition, the stability of both immobilisation methods is comparable, as shown by the SEIRA intensities, which did not decrease after prolonged exposure of the electrostatic SAM/*Dv*MF complex to a 1.0 molar KCl solution for 36 hours, similar to the covalently bound hydrogenase. Moreover, the voltammetric traces obtained under $H_2$ atmosphere on electrodes previously exposed to a 1.0 M KCl solution are similar to those recorded before addition of KCl, thereby showing that the catalytically active enzyme is still present on the electrode. In contrast, at such a high ionic strength and at pH 7 the cationic protein cytochrome *c* electrostatically bound to carboxyl-terminated SAMs was nearly completely desorbed.[50] This difference may be attributed to the significantly higher surface charge density of amino-terminated SAMs as compared to carboxyl-terminated SAMs at pH ≤ 7.[58,67]
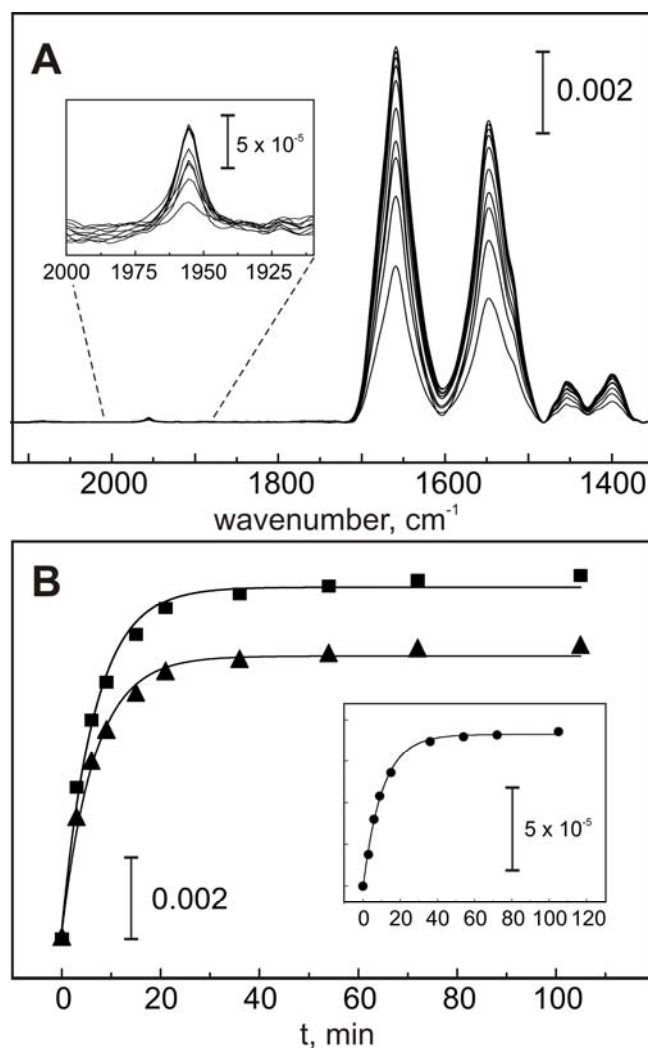
**Figure 4.** A) Time-dependent SEIRA spectra of *Dv*MF measured during immobilization on a SAM-coated electrode after adding a *Dv*MF-containing solution at pH 7.0 under aerobic atmosphere. B) Time-dependent changes of the integrated amide I (squares)/II (triangles) and CO (circles, inset) band intensities derived from the SEIRA spectra.

In addition, the thickness of the SAM was varied using amino-terminated thiols of different chain lengths. Here, a compromise had to be made between optimum enhancement of the IR signals that decreases with increasing distance from the electrode,[44] compactness and homogeneity of the SAM structure that are improved with increasing length of the aliphatic chain,[44] and a good SAM-mediated electrical contact between the electrode and the enzyme. The highest SEIRA intensity was observed for the $(C_2-NH_2)$-SAM. In this case, CV measurements showed some catalytic activity of the

enzyme, however the shape of the signal could not be evaluated, most likely due to the largely disordered SAM structure and the limited potential window as compared to ($C_6$-$NH_2$)-SAM.[40] For SAMs of $C_{11}$-$NH_2$, the distance-dependent drop of the SEIRA intensity was so pronounced that the vibrational bands of the diatomic inorganic ligands (*i.e.* CO, $CN^-$) could not be anymore detected. Thus, we have chosen amino-terminated SAMs with six methylene units, which allow both good and reproducible SEIRA spectra and CVs.

The SEIRA spectrum of *Dv*MF immobilised on the coated electrode at open circuit reveals the characteristic CO and CN stretching bands of the inactive oxidised $Ni_u$-A, $Ni_r$-B and a minor contribution of their respective EPR-silent states $Ni_u$-S/$Ni_r$-S. The two latter states were only identified via their CO stretchings. The spectrum is very similar to the IR spectrum of the "as-isolated" enzyme in solution, which due to the higher spectral resolution displays a more clearly detectable fine structure in the CN stretching region (Figure 5).
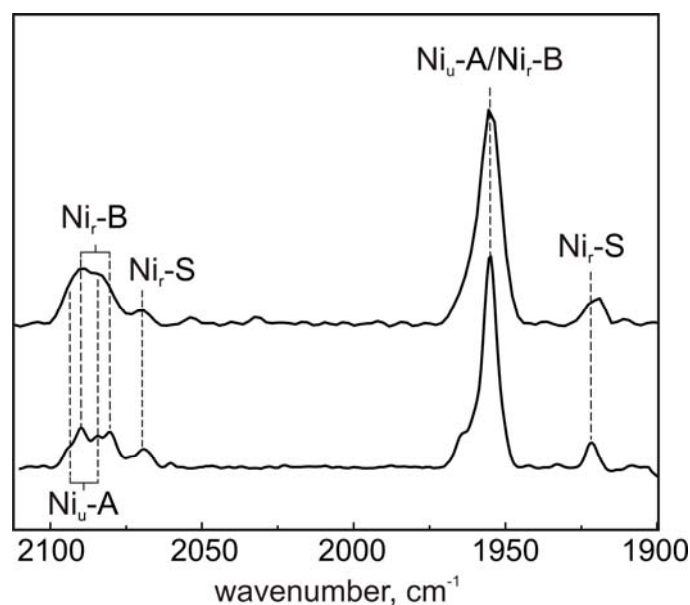


**Figure 5.** SEIRA (upper trace) and IR spectra (lower trace), obtained from *Dv*MF immobilised on a coated electrode at open circuit and in bulk solution, respectively, both measured at pH 7.0. The spectral resolution of the SEIRA and the IR measurements was 4 and 2 cm$^{-1}$, respectively. For a better comparison, the intensity of the IR spectrum was divided by 100.

Reductive activation of the immobilized enzyme was achieved by increasing the temperature of the buffered solution to 39 °C under $H_2$ atmosphere at open circuit potential. The activation process, as monitored by SEIRA spectroscopy was slow and requires ca. 5 hours to reach equilibrium conditions. This finding is illustrated in the spectra measured immediately after exposing the protein to $H_2$ and after keeping the sample under $H_2$ atmosphere for 5 hours. Selected spectra in Figure 6A show that the CO stretching at 1955 cm$^{-1}$, indicative for the inactive $Ni_u$-A and $Ni_r$-B, is replaced by two bands at 1961 and 1948 cm$^{-1}$, characteristic for the catalytically active forms $Ni_a$-C and $Ni_a$-SR, respectively. The corresponding CN stretchings are observed at 2061 / 2074 cm$^{-1}$ ($Ni_a$-SR) and 2075 / 2085 cm$^{-1}$ ($Ni_a$-C). In addition, the two minor peaks at 1922 and 2070 cm$^{-1}$, which are assigned to the $Ni_r$-$S_{1922}$ state, decrease largely upon $H_2$ activation.

The quantitative analysis of the time-dependent SEIRA measurements affords time constants of 0.03 and 0.02 min$^{-1}$ for the increase of $Ni_a$-SR and $Ni_a$-C, respectively. The best fit to the data for the 1955 cm$^{-1}$ band could be achieved by using two exponential functions reflecting the decay of both the $Ni_u$-A and $Ni_r$-B states with time constants of 0.01 and 0.1 min$^{-1}$, respectively (Figure 6B).

After demonstrating the structural integrity of the immobilised enzyme and its conversion into the active states, the catalytic process itself was monitored by CV for the same samples as studied by SEIRA spectroscopy. The voltammograms of the immobilised *Dv*MF at pH 5.5 recorded under $H_2$, display sigmoidally shaped oxidation currents characteristic of catalytically active enzymes (Figure 7).[10,40] Such a response was not obtained on bare Au or SAM-coated Au electrodes in the absence of the enzyme. Whereas in the case of $H_2$ oxidation (thick solid line) the complete voltammetric wave could be measured, proton reduction could only be probed within a restricted potential range, due to reductive desorption of the SAM at potentials < -0.45 V. Purging the solution with Ar (Figure 7, thin solid line) causes an immediate and complete suppression of the oxidation current, and a small negative catalytic current ascribed to proton reduction is detected at -0.25 V. After purging the solution with $H_2$, the characteristic CV plot featuring a large oxidation current was immediately restored, indicating that loss of the catalytic activity ($H_2$ oxidation) is reversible. However, a slight

decrease in the absolute height of the catalytic current was observed, *vide infra*. A similar tendency was observed for gas-exchange experiments using $H_2$ and $O_2$ atmosphere.
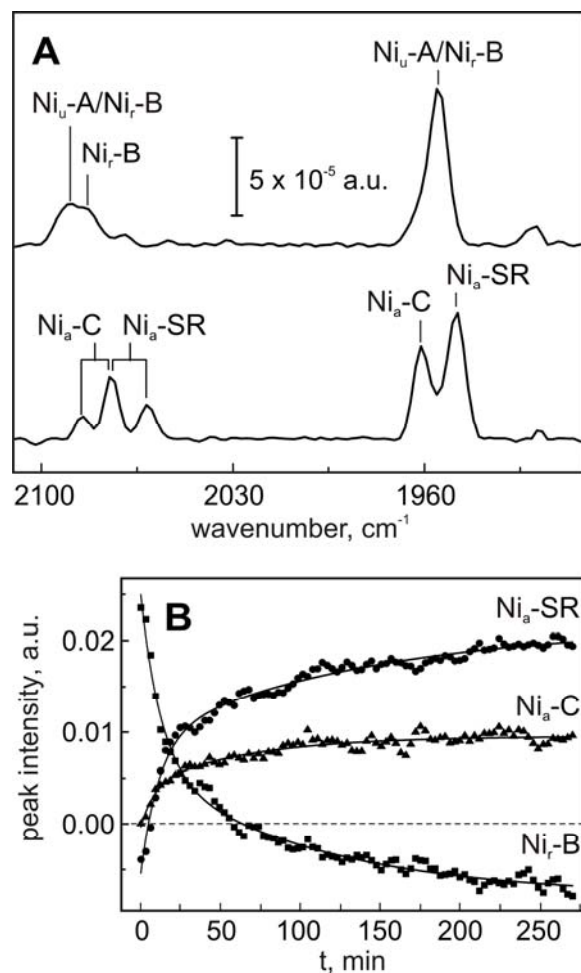


**Figure 6.** A Reductive activation of *Dv*MF immobilized on SAM-coated Au electrodes in a solution at pH 5.5. Activation was achieved under $H_2$ atmosphere at 39 °C. Panel **A** shows the absolute spectrum obtained immediately after purging the solution with $H_2$ (upper spectrum), and the spectrum obtained after keeping the sample under $H_2$ for 5 hours (lower spectrum). Panel B displays the variations of peak intensities of second derivative spectra with time during reductive activation multiplied by a factor of -1. Circle, triangle and square symbols correspond to the intensities of the bands at 1948, 1961 and 1955 $cm^{-1}$, assigned to $Ni_a$-SR, $Ni_a$-C and $Ni_u$-A/$Ni_r$-B, respectively.
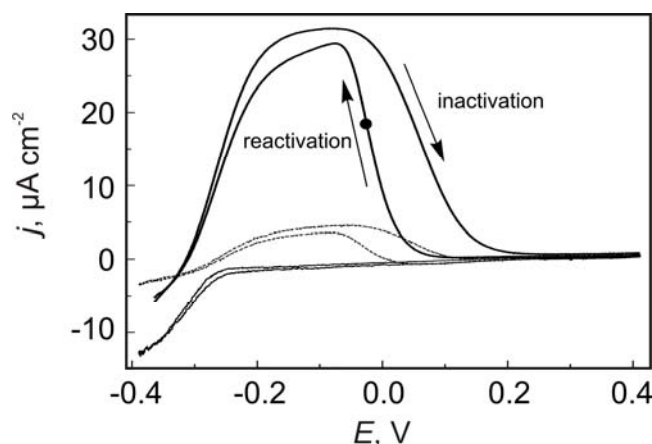
**Figure 7.** Anaerobic inactivation and reactivation of *Dv*MF immobilized on coated Au electrodes monitored by CV under $H_2$ atmosphere. The thick solid line refers to the first voltammetric scan whereas the dotted line was obtained after 14 hours of continuous potential scanning. The black dot shows the point of inflection of the ascending current having an $E_{switch}$ = -33 mV. The thin solid line describes the corresponding CV scans under Ar. Measurements were carried out at pH 5.5. The scan rate was 1 mV s$^{-1}$

The CV demonstrates that the anaerobic oxidative inactivation of the enzyme is followed by reductive reactivation. This behaviour is characteristic for hydrogenases immobilized on electrodes. The "switch" potential ($E_{switch}$) associated with the anaerobic reductive activation is (-33 ± 8) mV (Figure 7). This is similar to the value obtained by Vincent et al. for *Dv*MF immobilized onto graphite electrodes.[68] As shown in Figure 7 (dashed trace), the catalytic current of $H_2$-oxidation decreases with increasing the number of voltammetric scans, such that the CV signal is almost entirely lost after 24 hours of continuous scanning. The decay of the catalytic activtiy can be described by an exponetial function with a time constant of 5.7 ± 0.4 hrs. Remarkably, further attempts to restore catalytic activity, such as a prolonged reductive activation, did not improve the CV signal. At first sight, these observations could be interpreted in terms of enzyme desorption. However, no intensity decrease of the amide bands and no changes of their band shape and positions are observed in SEIRA spectra recorded after long-term CV measurements (Figure 8, inset). The time- and potential- invariant amide band intensities

in the SEIRA spectra, therefore, imply that there are no major orientational changes of the enzyme with respect to the electrode and no severe structural changes of that part of the protein that is close to the surface. This conclusion is consistent with the fact that the decrease of the catalytic current is not accompanied by changes in the shape of the CVs.[10] Such changes would be detectable in the case of a diminished electronic coupling with the electrode, caused by a re-orientation of the enzyme or a structural perturbation in the interaction domain.
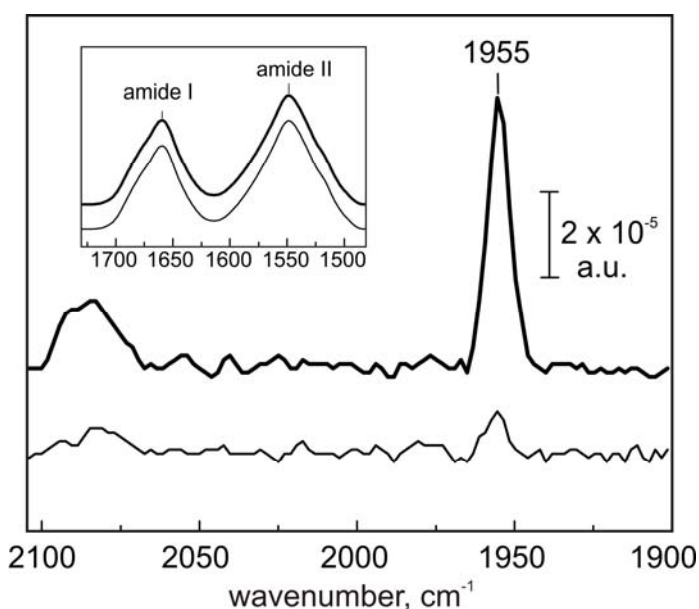


**Figure 8.** SEIRA spectra of *Dv*MF in the CO and CN stretching region measured at open circuit (dark line) and after performing CV (240 minutes later, lighter line). The inset shows the respective amide band regions, which remain unchanged. Spectra are shifted for clarity.

Thus, the loss of catalytic activity may be due to a structural perturbation of the active site, which does not affect changes of the amide bands. In fact, after long-term CV experiments, the CN and CO stretching modes cannot be detected anymore. Moreover, SEIRA spectra measured after applying a potential to the working electrode display a steady intensity decrease of the bands of the ligand stretchings (Figure 8). Since the SEIRA intensities of these modes are already rather low at open circuit, *i.e.* 0.8 % of the amide I band intensity, no quantitative analysis of the time-dependent decay is possible.

Nevertheless, it is likely that an intensity loss of these bands is correlated with a time-dependent decrease of the catalytic current as observed in the CV experiments. No potential-dependent changes of the band positions due to oxidation or reduction of the active site were detected under $H_2$ or Ar atmosphere which, however, may at least in part be due to the concomitant loss of SEIRA intensity of these modes. This fact impairs a reliable spectral analysis.

These findings point to a degradation of the active site which eventually leads to a loss of the diatomic ligands. Since this process is not observed at open circuit, we assume that degradation is initiated by reactive oxygen species electrochemically generated on the working electrode. Taking into account the small number of adsorbed enzyme, even steady state concentrations of oxygen in the sub-picomolar range, unavoidable under the present anaerobic conditions, might be sufficient to induce the chemical degradation of the active site on the time-scale of hours. This is confirmed by a loss in the integrated intensity of the CO stretching mode within the IR spectroelectrochemical experiments in the bulk phase, as displayed in Figure 2.

## Conclusions

The present spectroscopic and electrochemical study represents a detailed characterisation of the catalytic process of the [NiFe] hydrogenase of *Dv*MF in solution and in the immobilised state. The various species of the enzymatic process in solution were identified by IR spectroscopy which, in combination with potentiometric titrations, allowed also the determination of the midpoint potentials of the respective redox couples. On the basis of these data the active and inactive states of the immobilised enzymes were found to be $Ni_u$-A/$Ni_r$-B, minor amounts of $Ni_u$-S/$Ni_r$-S and $Ni_a$-C/$Ni_a$-SR, respectively. Interconversion between these states by hydrogen and oxygen/argon could be monitored by SEIRA spectroscopy indicating that the immobilised enzyme is functionally intact. Electrochemically driven anaerobic activation and deactivation was monitored by CV indicating a slow time-dependent decay of the catalytic activity which is tentatively attributed to a chemical degradation of the active site via reactive oxygen species formed in the electrochemical cell.

This work constitutes a starting point for analysing the interfacial processes of hydrogenases on electrodes as a prerequisite for optimising the long-term structural and functional stability of the immobilised enzyme. In this sense, the study has an impact for elucidating the molecular functioning of hydrogenases and for improving the design of hydrogenase-based bio-electronic devices for technological applications such as biofuel cells.

## Acknowledgments

# References

1.  Adams, M. W. W.; Mortenson, L. E.; Chen, J. S. *Biochim. Biophys. Acta* **1980**, *594* (2-3), 105-176.

2.  De Lacey, A. L.; Fernandez, V. M.; Rousset, M.; Cammack, R. *Chem. Rev.* **2007**, *107* (10), 4304-4330.

3.  Lubitz, W.; van Gastel, M. Nickel Iron Hydrogenases. In *Metal Ions in Life Science* 2 ed. John Wiley & Son. Ltd: pp 279-322.

4.  Ogata, H.; Lubitz, W.; Higuchi, Y. *Dalton Trans.* **2009**, DOI:10.1039/b903840j, 7577-7587

5.  Higuchi, Y.; Yagi, T.; Yasuoka, N. *Structure* **1997**, *5* (12), 1671-1680.

6.  Ogata, H.; Hirota, S.; Nakahara, A.; Komori, H.; Shibata, N.; Kato, T.; Kano, K.; Higuchi, Y. *Structure* **2005**, *13* (11), 1635-1642.

7.  Ogata, H.; Mizoguchi, Y.; Mizuno, N.; Miki, K.; Adachi, S.; Yasuoka, N.; Yagi, T.; Yamauchi, O.; Hirota, S.; Higuchi, Y. *J. Am. Chem. Soc.* **2002**, *124* (39), 11628-11635.

8.  Happe, R. P.; Roseboom, W.; Pierik, A. J.; Albracht, S. P. J.; Bagley, K. A. *Nature* **1997**, *385* (6612), 126.

9.  Fichtner, C.; Laurich, C.; Bothe, E.; Lubitz, W. .*Biochemistry* **2006**, *45* (32), 9706-9716.

10. Vincent, K. A.; Parkin, A.; Armstrong, F. A. *Chem.Rev.***2007**, *107* (10), 4366-4413.

11. Armstrong, F. A.; Albracht, P. J. *Philosophical Transactions of the Royal Society A-Mathematical Physical and Engineering Sciences* **2005**, *363* (1829), 937-954.

12. Cammack, R.; Fernandez, V. M.; Hatchikian, E. C. *Inorganic Microbial Sulfur Metabolism* **1994,** *243*, 43-68.

13. Dementin, S.; Belle, V.; Champ, S.; Bertrand, P.; Guigliarelli, B.; De Lacey, A. L.; Fernandez, V. M.; Leger, C.; Rousset, M. *Int. J. Hydrogen Energy* **2008**, *33* (5), 1503-1508.

14. van Gastel, M.; Stein, M.; Brecht, M.; Schroder, O.; Lendzian, F.; Bittl, R.; Ogata, H.; Higuchi, Y.; Lubitz, W. *J. Biolog. Inorg. Chem.* **2006**, *11* (1), 41-51.

15. Volbeda, A.; Martin, L.; Cavazza, C.; Matho, M.; Faber, B. W.; Roseboom, W.; Albracht, S. P. J.; Garcin, E.; Rousset, M.; Fontecilla-Camps, J. C. *J. Biolog. Inorg. Chem.* **2005**, *10* (3), 239-249.

16. Lubitz, W.; Reijerse, E.; van Gastel, M. *Chem. Rev.* **2007**, *107* (10), 4331-4365.

17. Cammack, R.; Patil, D.; Aguirre, R.; Hatchikian, E. C. *FEBS Lett.* **1982**, *142* (2), 289-292.

18. Coremans, J. M. C. C.; Van der Zwaan, J. W.; Albracht, S. P. J. *Biochim. Biophys. Acta* **1992**, *1119* (2), 157-168.

19. Teixeira, M.; Moura, I.; Xavier, A. V.; Moura, J. J. G.; Legall, J.; Der Vartanian, D. V.; Peck, H. D.; Huynh, B. H. *J. Biolog. Chem.* **1989**, *264* (28), 16435-16450.

20. Roberts, L. M.; Lindahl, P. A. *J. Am. Chem. Soc.* **1995,** *117* (9), 2565-2572.

21. Roberts, L. M.; Lindahl, P. A. *Biochemistry* **1994**, *33* (47), 14339-14350.

22. Coremans, J. M. C. C.; Vangarderen, C. J.; Albracht, S. P. J. *Biochim. Biophys. Acta* **1992**, *1119* (2), 148-156.

23. Hoeben, F. J. M.; Meijer, F. S.; Dekker, C.; Albracht, S. P. J.; Heering, H. A.; Lemay, S. G. *Acs Nano* **2008**, *2* (12), 2497-2504.

24. Hoeben, F. J. M.; Heller, I.; Albracht, S. P. J.; Dekker, C.; Lemay, S. G.; Heering, H. A. *Langmuir* **2008**, *24* (11), 5925-5931.

25. Pershad, H. R.; Duff, J. L. C.; Heering, H. A.; Duin, E. C.; Albracht, S. P. J.; Armstrong, F. A. *Biochemistry* **1999**, *38* (28), 8992-8999.

26. Pershad, H. R.; Duff, J. L. C.; Heering, H. A.; Duin, E. C.; Albracht, S. P. J.; Armstrong, F. A. *J. Inorg. Biochem.* **1999**, *74* (1-4), 264.

27. Leger, C.; Elliott, S. J.; Hoke, K. R.; Jeuken, L. J. C.; Jones, A. K.; Armstrong, F. A. *Biochemistry* **2003**, *42* (29), 8653-8662.

28. van Gastel, M.; Fichtner, C.; Neese, F.; Lubitz, W. *Biochem. Soc. Trans.* **2005**, *33*,7-11.

29. Foerster, S.; Stein, M.; Brecht, M.; Ogata, H.; Higuchi, Y.; Lubitz, W. Single crystal *J. Am. Chem. Soc.* **2003**, *125* (1), 83-93.

30. Dole, F.; Fournel, A.; Magro, V.; Hatchikian, E. C.; Bertrand, P.; Guigliarelli, B. *Biochemistry* **1997**, *36* (25), 7847-7854.

31. De Lacey, A. L.; Hatchikian, E. C.; Volbeda, A.; Frey, M.; Fontecilla-Camps, J. C.; Fernandez, V. M. *J. Am. Chem. Soc.* **1997**, *119* (31), 7181-7189.

32. Burgdorf, T.; Loscher, S.; Liebisch, P.; Van der Linden, E.; Galander, M.; Lendzian, F.; Meyer-Klaucke, W.; Albracht, S. P. J.; Friedrich, B.; Dau, H.; Haumann, M. *J. Am. Chem. Soc.* **2005,** *127* (2), 576-592.

33. Knuttel, K.; Schneider, K.; Erkens, A.; Plass, W.; Muller, A.; Bill, E.; Trautwein, A.X. *Bulletin of the Polish Academy of Sciences-Chemistry* **1994**, *42* (4), 495-511.

34. Saggu, M.; Zebger, I.; Ludwig, M.; Lenz, O.; Friedrich, B.; Hildebrandt, P.; Lendzian, F.. *J. Biolog. Chem.* **2009**, *284* (24), 16264-16276.

35. Bleijlevens, B.; van Broekhuizen, F. A.; De Lacey, A. L.; Roseboom, W.; Fernandez, V. M.; Albracht, S. P. J. *J. Biolog. Inorg. Chem.* **2004**, *9* (6), 743-752.

36. De Lacey, A. L.; Stadler, C.; Cavazza, C.; Hatchikian, E. C.; Fernandez, V. M. *J. Am. Chem. Soc.* **2000**, *122* (45), 11232-11233.

37. De Lacey, A. L.; Pardo, A.; Fernandez, V. M.; Dementin, S.; Dryanczyk-Perrier, G.; Hatchikian, E. C.; Rousset, M. *J. Biolog. Inorg. Chem.* **2004**, *9* (5), 636-642.

38. Armstrong, F. A.; Belsey, N. A.; Cracknell, J. A.; Goldet, G.; Parkin, A.; Reisner, E.; Vincent, K. A.; Wait, A. F. *Chem. Soc. Rev.* **2009**, *38* (1), 36-51.

39. Leger, C.; Elliott, S. J.; Hoke, K. R.; Jeuken, L. J. C.; Jones, A. K.; Armstrong, F. A. *Biochemistry* **2003**, *42* (29), 8653-8662.

40. Rudiger, O.; Abad, J. M.; Hatchikian, E. C.; Fernandez, V. M.; De Lacey, A. L. *J. Am. Chem. Soc.* **2005**, *127* (46), 16008-16009.

41. Vincent, K. A.; Cracknell, J. A.; Clark, J. R.; Ludwig, M.; Lenz, O.; Friedrich, B.; Armstrong, F. A. *Chem. Comm.* **2006**, (48), 5033-5035.

42. Miyake, H.; Ye, S.; Osawa, M. *Electrochem. Comm.* **2002**, *4* (12), 973-977.

43. Osawa, M. *Bulletin of the Chemical Society of Japan* **1997**, *70* (12), 2861-2880.

44. Osawa, M. Surface-enhanced infrared absorption. *Near-Field Optics and Surface Plasmon Polaritons* **2001**, *81*, 163-187.

45. Ataka, K.; Heberle, J. *J. Am. Chem. Soc.* **2004**, *126* (30), 9445-9457.

46. Ataka, K.; Heberle, J. *Analytical and Bioanalytical Chemistry* **2007,** *388* (1), 47-54.

47. Wisitruangsakul, N.; Lenz, O.; Ludwig, M.; Friedrich, B.; Lendzian, F.; Hildebrandt, P.; Zebger, I. *Ang. Chem. Int. Ed.* **2009**, *48* (3), 611-613.

48. Ataka, K.; Giess, F.; Knoll, W.; Naumann, R.; Haber-Pohlmeier, S.; Richter, B.; Heberle, J. *J. Am. Chem. Soc.* **2004**, *126* (49), 16199-16206.

49. Wisitruangsakul, N.; Zebger, I.; Ly, K. H.; Murgida, D. H.; Ekgasit, S.; Hildebrandt, P. *Phys. Chem. Chem. Phys.* **2008**, *10* (34), 5276-5286.

50. Love, J. C.; Estroff, L. A.; Kriebel, J. K.; Nuzzo, R. G.; Whitesides, G. M. *Chem. Rev.* **2005**, *105* (4), 1103-1169.

51. Murgida, D. H.; Hildebrandt, P. *Acc. Chem. Res.* **2004**, *37* (11), 854-861.

52. Murgida, D. H.; Hildebrandt, P. *Phys. Chem. Chem. Phys.* **2005**, *7* (22), 3773-3784.

53. Yagi, T.; Kimura, K.; Daidoji, H.; Sakai, F.; Tamura, S.; Inokuchi, H. *J. Biochem.* **1976**, *79* (3), 661-671.

54. Baymann, F.; Moss, D. A.; Mantele, W. *Anal. Biochem.* **1991**, *199* (2), 269-274.

55. Prince, R. C.; Linkletter, S. J. G.; Dutton, P. L. *Biochim. Biophys. Acta* **1981**, *635* (1), 132-148.

56. Murgida, D. H.; Hildebrandt, P. *J. Molec. Struct.* **2001**, *565*, 97-100.

57. Patel, N.; Davies, M. C.; Hartshorne, M.; Heaton, R. J.; Roberts, C. J.; Tendler, S. J. B.; Williams, P. M. *Langmuir* **1997**, *13* (24), 6485-6490.

58. Brunger, A. T.; Karplus, M. *Proteins-Structure Function and Genetics* **1988**, *4* (2), 148-156.

59. Brooks, B. R.; Bruccoleri, R. E.; Olafson, B. D.; States, D. J.; Swaminathan, S.; Karplus, M. *J. Comput. Chem.* **1983**, *4* (2), 187-217.

60. Foloppe, N.; MacKerell, A. D. *J. Comput. Chem.* **2000**, *21* (2), 86-104.

61. Humphrey, W.; Dalke, A.; Schulten, K. *J. Molec. Graph.* **1996**, *14* (1), 33-&.

62. Teixeira, V. H.; Baptista, A. M.; Soares, C. M. *Biophys. J.* **2006**, *91* (6), 2035-2045.

63. Fichtner,C. Spectroskopische und electronische Untersuchung der [NiFe]-Hydrogenase aus *Desulfovibrio vulgaris* Miyazaki F.PhD Thesis, Heinrich-Heine-Universität, Düsseldorf, June **2005**

64. Asso, M.; Guigliarelli, B.; Yagi, T.; Bertrand, P. *Biochim. Biophys. Acta* **1992**, *1122* (1), 50-56.

65 Campina, J. M.; Martins, A.; Silva, F. *J. Phys. Chem. C* **2007**, *111* (4), 5351–5362.

66 Degefa, T. H.; Schon, P.; Bongard, D.; Walder, L. *J. Electroanal. Chem.* **2004**, *574* (1), 49–62.

67 White, H. S.; Peterson, J. D.; Cui, Q.; Stevenson, K. J. *J. Phys. Chem. B* **1998**, *102* (16), 2930–2934.

68 Vincent, K. A.; Belsey, N. A.; Lubitz, W.; Armstrong, F. A. *J. Am. Chem. Soc.* **2006**, *128* (22), 7448–7449.

# Chapter 4

# Inhibition of the [NiFe] Hydrogenase from *Desulfovibrio vulgaris* Miyazaki F by Carbon Monoxide: An FTIR and EPR Spectroscopic Study
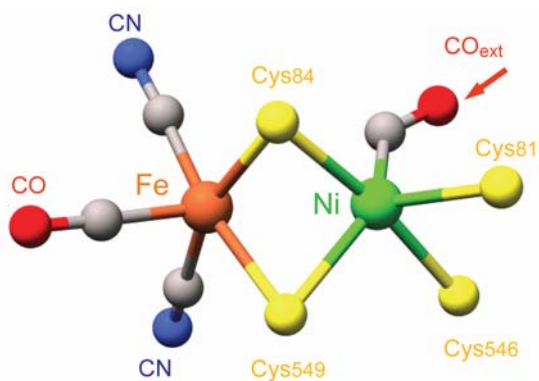


**Graphical Abstract.** The CO inhibited states of the [NiFe] hydrogenase from *Desulfovibrio vulgaris* Miyazaki F have been studied by a combination of FTIR spectroelectrochemistry, low temperature photodissociation kinetics and EPR and discussed in the framework of a high resolution crystal structure (1UBJ, pdb entry).

# Inhibition of the [NiFe] Hydrogenase from *Desulfovibrio vulgaris* Miyazaki F by Carbon Monoxide: An FTIR and EPR Spectroscopic Study[†]

Maria-Eirini Pandelia, Hideaki Ogata, Leslie J. Currell, Marco Flores[§], Wolfgang Lubitz

*Max-Planck-Institut für Bioanorganische Chemie, Stiftstrasse 34-36, D 45470, Mülheim a.d. Ruhr, Germany.*
[§] *Present address: Department of Chemistry and Biochemistry, Arizona State University, Tempe, Arizona 85287-1604*

## Abstract

X-ray crystallographic studies (Ogata et al, *J. Am. Chem. Soc.* 124 (2002) 11628-11635) have shown that carbon monoxide binds to the nickel of the active site of the [NiFe] hydrogenase from *Desulfovibrio (D.) vulgaris* Miyazaki F and inhibits its catalytic function. In the present work spectroscopic aspects of the CO inhibition for this bacterial organism are reported for the first time and enable a direct comparison with the existing crystallographic data. The binding affinity of each specific redox state for CO is probed by FTIR spectroelectrochemistry. It is shown that only the state $Ni-SI_a$ reacts physiologically with CO. The CO-inhibited product state is EPR-silent ($Ni^{2+}$) and exists in two forms, Ni-SCO and $Ni-SCO_{red}$. At very negative potentials, the exogenous CO is electrochemically detached from the active site and the active Ni-R state(s) are obtained. At temperatures below 100 K, photodissociation of the extrinsic CO from the Ni-SCO state results in $Ni-SI_a$ that is identified to be the only light-induced state. In the dark, rebinding of CO takes place; the recombination rate constants are of bi-exponential character and the activation barrier is determined to be approximately 9 kJ mol$^{-1}$. In addition, formation of a paramagnetic CO-inhibited state (Ni-CO) was observed that

results from the interaction of carbon monoxide with the Ni-L state. It is proposed that the nickel in Ni-CO is in a formal monovalent state ($Ni^{1+}$).

## Introduction

Hydrogenases are metalloenzymes that catalyze the reversible conversion of molecular hydrogen according to [1]: $H_2 \rightleftharpoons 2H^+ + 2e^-$. They are part of an energy converting mechanism found in the metabolic pathway of a wide variety of micro-organisms [2]. They can be classified according to their metal content as: (a) [NiFe] hydrogenases with a hetero-binuclear Ni-Fe active center[3,4,5] (b) [FeFe] hydrogenases with a binuclear iron site connected to a $[Fe_4S_4]$ cubane[6] forming the so-called H-cluster[7] and (c) iron-sulfur cluster- free hydrogenases (Hmd) consisting of a mononuclear iron site[8].
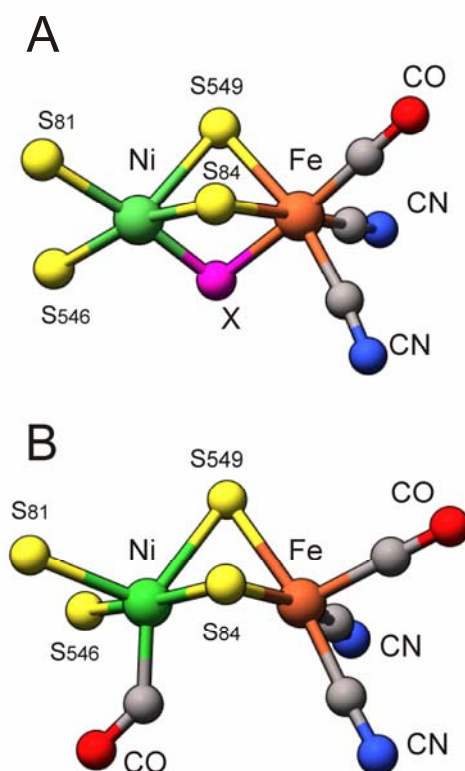


**Figure 1.** (A) Representation of the active site of the [NiFe] hydrogenase from *D. vulgaris* Miyazaki F in the oxidized and $H_2$ reduced forms that carry an oxygenic or hydrogenic species, respectively. (B) The active site of the CO inhibited hydrogenase (entry 1UBJ, protein databank). The elements are represented with the following colors:

Fe (orange), Ni (green), S (yellow), C (grey), O (red), N (blue). The third bridging ligand X is shown in magenta.

The [NiFe] hydrogenase from the sulfate reducing bacterium *Desulfovibrio (D. ) vulgaris*  Miyazaki F is a membrane attached enzyme with a molecular weight of 91.3 kDa [9], consisting of two subunits [10]. The large subunit (62.5 kDa) contains the Ni-Fe center [11]. This is shown in Figure 1A. The two metals are connected via two cysteinyl residues and depending on the redox state of the enzyme, a third non-protein ligand is present at the active site (labeled X in Figure 1A). The nickel ion is coordinated by two more cysteines (terminal) and changes during catalysis its redox state ($Ni^{3+}$, $Ni^{2+}$ and presumably $Ni^{1+}$) [12]. The iron, in all intermediate states of the enzymatic cycle, maintains a low oxidation state ($Fe^{2+}$) and is coordinated by three diatomic inorganic ligands [13]; one carbonyl surrounded by hydrophobic residues and two cyanides that are hydrogen bonded to nearby amino acids [14]. The small subunit (28.8 kDa) harbors a $[Fe_3S_4]^{1+/0}$ center situated between two low potential $[Fe_4S_4]^{2+/1+}$ clusters[11,15,16]. These three clusters mediate the electron transfer between the [NiFe] center and the native electron acceptor cytochrome $c_3$[1,17]. Proton transfer involves several possible pathways, among which the most predominant is via the glutamate residue (Glu34, D. vulgaris numbering) located near the nickel center [18].

In the presence of oxygen, reversible inhibition of the enzyme takes place. Purification is carried out aerobically and thus the protein is obtained in inactive states containing oxygen-based ligands in the bimetallic site. The two most oxidized forms are known as Ni-A and Ni-B [4,5] (Scheme 1). They are both paramagnetic ($Ni^{3+}$, S = 1/2)[19], but differ in their spectroscopic and catalytic properties [20,21]. Ni-B is readily activated in the presence of $H_2$ or under reducing conditions, whereas Ni-A shows a long delay in its activation kinetics [21,22]. The difference in their activation rates has been recently ascribed to the different identities of the oxygenic ligands, $OH^-$ for Ni-B [19,23], and a proposed $OOH^-$  for Ni-A[24]. One-electron reduction of Ni-A and Ni-B leads to the Ni-SU and Ni-$SI_r$ inactive states ($Ni^{2+}$, EPR silent[‡]) [25,26], respectively. For Ni-$SI_r$, two states have been

---

[‡] Integer spin ground states can be characterized as EPR-silent either if they are diamagnetic (S=0) or if they cannot be observed by conventional microwave frequencies

94

observed, $(Ni\text{-}SI_r)_I$ – carrying an $OH^-$ bridge - and $(Ni\text{-}SI_r)_{II}$ – with an $H_2O$ bridge[27] -, which co-exist in acid-base equilibrium (Scheme 1). Catalytic activity is recovered in the $Ni\text{-}SI_a$ state ($Ni^{2+}$, EPR silent) by liberation of the oxygenic species. Further reduction leads to Ni-C, a paramagnetic state ($Ni^{3+}$, $S = 1/2$) with a hydride ($H^-$) bridging the two metals [28,29]. Ni-C is photosensitive at low temperatures, leading to the dissociation [28,30] of the bridging $H^-$. Further reaction of Ni-C with hydrogen produces Ni-R ($Ni^{2+}$, EPR silent), which can exist in more than one protonation states [27,31].
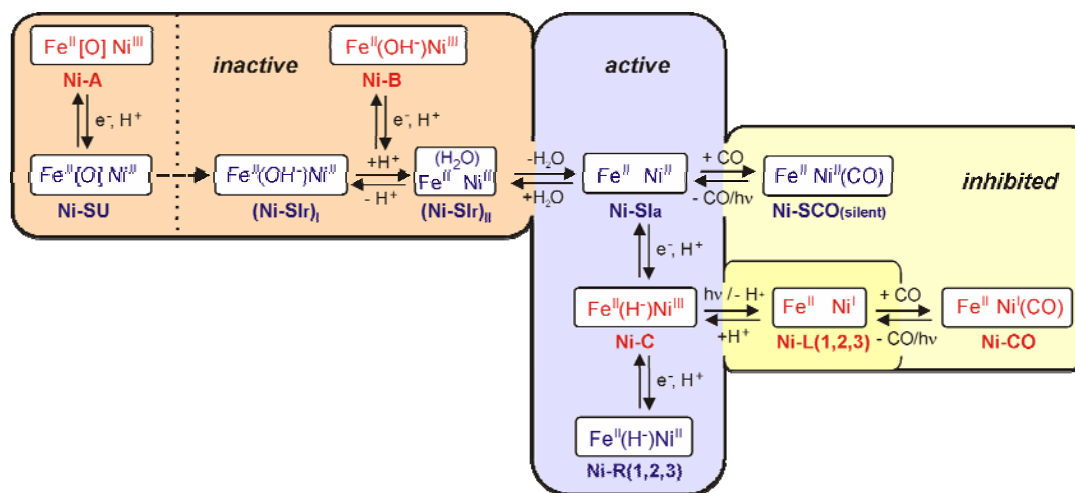


**Scheme 1.** Proposed mechanism for the [NiFe] hydrogenase from *D. vulgaris* Miyazaki F, including both active and inactive intermediate states. The orange shaded frame contains the oxygen-inhibited inactive states, the light blue frame contains the active states, the light yellow the CO-inhibited and the dark yellow frame contains the light-induced state(s).

It has been shown that carbon monoxide also inhibits the catalytic function[32,33] of hydrogenase enzymes. X-ray crystallographic experiments[34] have demonstrated that the

---

X/Q/W band frequencies (i.e. $S \geq 1$, where the zero field splitting is larger than the microwave quantum). So far no experimental evidence exists from high field EPR for the reduced hydrogenase states, whether they are associated with a high spin or low spin state for $Ni^{2+}$.

exogenous CO ligand coordinates to the nickel (Figure 1B). Two different CO-inhibited states have been observed, with distinct electronic structures and properties[32,36]. The formation of these states depends on the redox state and the coordination number of nickel. The paramagnetic form is known as Ni-CO[32,35], whereas the EPR-silent forms as Ni-SCO/Ni-SCO$_{red}$ [36]. In all the above states, the exogenous CO ligand can be photodissociated from the active site at near cryogenic temperatures[32,34,35,37]

The present work presents an extensive spectroscopic characterization of the interaction between carbon monoxide and the [NiFe] hydrogenase from D. vulgaris Miyazaki F, for which, apart from a high resolution crystal structure [34], no previous information exists on the properties of the CO-adduct. A thorough investigation consisting of infrared spectroelectrochemistry, rapid scan FTIR and EPR is described and results are compared to those corresponding to hydrogenases from other organisms[36,37,38]. In particular, the activation barrier for the rebinding of CO to the active site of hydrogenases is determined and the paramagnetic Ni-CO state is described for the first time for a [NiFe] hydrogenase from sulfate reducing bacteria. Results are discussed within the framework of structural models proposed for the oxygen-sensitive hydrogenases.

## Material and Methods

*Purification of the enzyme.* Hydrogenase from *D. vulgaris* Miyazaki F was purified from 50 L cultures as previously described [9]. The pH of the enzyme solutions was kept at pH 7.4 in Tris-HCl buffer for all experiments. In sample preparations, where the enzyme was incubated with carbon monoxide at 0 °C, with consideration of the temperature dependence of the Tris buffer, the pH for that case was calculated to be 8.12.

*Reactions with gases.* Reduction with $H_2$ (N 50, Air Liquide), treatment with carbon monoxide gas (N 47, Air Liquide) and $^{13}CO$ labeled gas ( < 10 % $^{18}O_2$, Cambridge Isotopes) were performed using a home-built gas-mixer. Mixtures of gases ($H_2$, CO) were regulated with a manometer in a steel chamber of 30 $cm^3$.

*Preparation of the Ni-SCO state.* Two preparation procedures were used. The first consists of adding methyl viologen (-448 mV, Sigma Aldrich) as an electron acceptor to 50 µL of *D. vulgaris* hydrogenase. Final concentration of methyl viologen was 1.6 mM and of the protein 1 mM. Reduction for 3 min with $H_2$ (1.1 bar, ~ 22 °C) was followed by an incubation for 15 min with CO (2.5 bar, ~ 0 °C). 15 µL were transferred into the FTIR sample cell and immediately frozen in liquid $N_2$. The remaining sample was used for control measurements (EPR spectroscopy). In the second procedure 50 µL hydrogenase (1 mM) were activated with $H_2$ (1.1 bar, ~ 22 °C) for 40 min and further incubated for 15 min with CO gas (2.5 bar, ~ 0 °C).

*Preparation of the Ni-SCO$_{red}$ state.* The Ni-SCO state was prepared according to the second preparation procedure described above. The sample was further reduced by sodium dithionite (Sigma Aldrich) yielding mainly the Ni-SCO$_{red}$ state.

*Preparation of the paramagnetic Ni-CO state.* Degassed hydrogenase samples were reduced for 30 - 50 min with hydrogen (1.1 bar, ~ 22 °C) and further incubated with either CO or CO/$H_2$ gas mixtures. Interaction solely with CO was restricted to 1 minute; whereas interaction with gas mixtures of 20 % CO / 80 % $H_2$ was carried out for 30 min. Samples were frozen in liquid nitrogen under green light.

*FTIR spectroscopy.* Infrared measurements were carried out with a Bruker IFS 66v/S FTIR spectrometer equipped with a mercury-cadmium-telluride (MCT) photoconductive detector (Kolmar Technologies). For the experiments at 100 K and below, an Oxford Instruments OptistatCF cryostat with an ITC 503 temperature controller was used. The spectral resolution of the low temperature measurements was 2 cm$^{-1}$.

*FTIR electrochemistry.* Infrared electrochemical measurements were performed in an OTTLE (optically transparent thin-layer electrochemical cell described by Moss [39,40], with 1 cm$^{-1}$ spectral resolution. The mediators used for the titrations were: methylviologen, benzylviologen, neutral red, phenosafranine, anthraquinone-2-sulfonate, anthraquinone-1,5-disulfonate, 2-hydroxy-1,4-naphthoquinone, potassium indigo tetrasulfonate, methylene blue. The midpoint potentials of these mediators at pH 7.0 are given elsewhere [41]. Solubilization of the mediators was achieved by sonication on ice and addition of 5 – 10 % glycerol. The protein solution for the electrochemical measurements contained 1 mM of hydrogenase, 125 $\mu$M of each mediator and 100 mM KCl (final concentrations). The enzyme-redox mediators solution was saturated for 15 min with carbon monoxide (2.5 bar, $\sim$ 0 °C) and transferred to the electrochemical Moss cell under 100 % CO atmosphere (glove bag). In the electrochemical cell [39], a layer of the protein-redox mediator solution is formed between two CaF$_2$ windows on an 8.5 $\mu$m thick gold mesh in electrical contact with a platinum counter electrode. An Ag/AgCl electrode (1 M KCl) was used as a reference, which was calibrated prior to and after each measurement by the reduction of methyl viologen. In the titrations the potential was controlled with a potentiostat (Princeton Applied Research / EG&G Model 283) and the temperature was maintained with a thermostat (RML6 LAUDA) at the desired value. After full activation of the enzyme a time period of 3-5 minutes was required to reach redox equilibrium at each applied potential. All potentials in this work are quoted versus the normal hydrogen electrode (NHE). Data were collected and baseline corrected using the OPUS software (Bruker). Data fitting was performed using MATLAB 7.0. The measured areas of the bands were normalized by dividing with the enzyme concentration and the optical path-length. In this way the apparent integrated absorbance (B, mM$^{-1}$ cm$^{-1}$) was obtained.

*Rapid scan FTIR.* 15 µL hydrogenase samples were placed between sapphire windows (80 µm path-length) and inserted in the cryostat at low temperatures. The samples were illuminated in situ for 5 min (halogen lamp 24 V, 250 W) prior to measuring the recombination kinetics in the rapid scan mode. The time resolution of the rapid scan measurements was in the order of one second. The temperature dependence of the measured kinetic rates was fitted with the Arrhenius equation ($\ln k = \ln A_0 - E_a/RT$) [42], where k is the rate constant ($s^{-1}$), $A_0$ is the frequency factor ($s^{-1}$), $E_a$ is the activation energy ($kJ\,mol^{-1}$), R is the ideal gas constant ($8.314\,J\,K^{-1}\,mol^{-1}$) and T the temperature in K.

*EPR spectroscopy.* EPR measurements were carried out with a Bruker E-300 cw X-band spectrometer using a rectangular cavity ($TE_{102}$) and an Oxford Instruments helium flow cryostat with an ITC 503 temperature controller. Illumination of the samples at low temperatures was performed in the EPR resonator with a halogen lamp (12 V, 50 Watt) until maximum conversion was obtained (~ 5 min).

## Results

### FTIR electrochemistry at room temperature (inactivated enzyme)

The redox chemistry of the [NiFe] hydrogenase from *D. vulgaris* was investigated by infrared electrochemical studies in enzyme solutions with and without carbon monoxide. FTIR probes changes in the active site (e.g. electron density at the Fe, coordination number, hydrogen bonding) [43,44], by means of monitoring the stretching vibrations of the CO and $CN^-$ ligands. Each redox state is thus characterized by three IR bands [13], one for a terminally bound carbonyl in the region 1900 to 1970 $cm^{-1}$, and two corresponding to the coupled vibrations of the two cyanide ligands in the region 2100 to 2040 $cm^{-1}$. The infrared absorption bands of all redox intermediates at room temperature are collected in Table 1. In the text, the characteristic stretching vibration of the CO band for each state is given in parenthesis.

Figure 2a shows the FTIR spectrum of the aerobically isolated hydrogenase from *D. vulgaris* at +229 mV (25 °C). In this spectrum the bands corresponding to the oxygen inhibited forms Ni-A, Ni-B and $(Ni\text{-}SI_r)_I$ could be identified[26] (Scheme 1, Table 1). The Ni-B and Ni-A states were shown by EPR experiments to occur in a ratio 7 : 3. The CO band in Figure 2a results from the overlap of Ni-B (1955 $cm^{-1}$) and Ni-A (1956 $cm^{-1}$) and is thus centered at 1955 $cm^{-1}$. The Ni-SU state could not be resolved in these spectra (Table 1). A CO band of small intensity at 1964 $cm^{-1}$ was observed, but the corresponding $CN^-$ bands could not be identified. This state, denoted as $Ni\text{-}S_{1964}$, is EPR-silent. It can be electrochemically reduced irreversibly and its yield does not depend on pH. The FTIR spectrum in the case of the aerobically purified hydrogenase in a carbon monoxide saturated buffer solution under 100 % CO atmosphere was identical (Figure S1 of the Appendix B).

Figure 2b shows the spectrum of hydrogenase partially activated for 53 min at -295 mV in the absence of CO. Reduction of Ni-B (1955 $cm^{-1}$) resulted in the increase of the $(Ni\text{-}SI_r)_I$ (1921 $cm^{-1}$) state and the appearance of $(Ni\text{-}SI_r)_{II}$ and/or $Ni\text{-}SI_a$ (1943 $cm^{-1}$)[§].

---

[§] The $(Ni\text{-}SI_r)_{II}$ inactive state has a water molecule as ligand weakly bound at its active site. The active $Ni\text{-}SI_a$ state has no additional X ligand (see Figure 1) and the divalent nickel is four-coordinated. However, both states are described by the same FTIR spectrum[26], indicating a very similar electronic distribution in the [NiFe] center of these states.
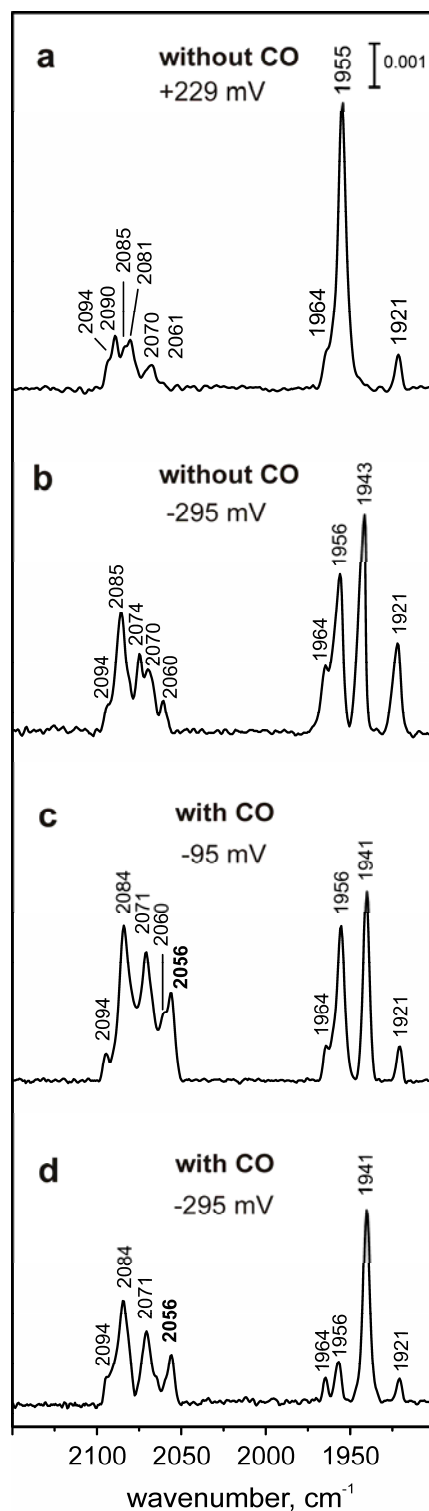
**Figure 2.** FTIR spectra of the *D. vulgaris* Miyazaki F [NiFe] hydrogenase in the absence of CO in the solution (a) at +229 mV and (b) partially activated for 53 min at -295 mV. In the presence of CO in solution (c) partially activated sample for 53 min at -95 mV and (d) a second sample partially activated for 30 min at -295mV. All redox potentials are quoted vs NHE and the temperature is 25 °C.

**Table 1.** Stretching vibrations of the CO and CN⁻ ligands for each redox state of the [NiFe] hydrogenase from *D. vulgaris* Miyazaki F at 25 °C (298 K). Values at 100 K are given in brackets.

| State | IR Frequencies, cm$^{-1}$ | | | |
|---|---|---|---|---|
| | $\bar{v}_{CO}(Fe)$ | $\bar{v}^{asym}_{CN}(Fe)$ | $\bar{v}^{sym}_{CN}(Fe)$ | $\bar{v}_{CO}(Ni)$ |
| Ni-A | 1956 | 2085 | 2094 | - |
| Ni-B | 1955 | 2081 | 2090 | - |
| Ni-SU | 1958 | 2089 | 2100 | - |
| (Ni-SI$_r$)$_I$ | 1921 | 2061 | 2070 | - |
| (Ni-SI$_r$)$_{II}$ | 1943 | 2074 | 2086 | - |
| Ni-SI$_a$ | 1943 | 2074 | 2086 | - |
| | (1946) | (2077) | (2090) | (-) |
| Ni-C | 1961 | 2074 | 2085 | - |
| Ni-R(1) | 1948 | 2061 | 2074 | - |
| Ni-R(2) | 1932 | 2052 | 2066 | - |
| Ni-SCO$_{1941}$ | 1941 | 2071 | 2084 | 2056 |
| | (1941) | (2072) | (2086) | (2061) |
| Ni-SCO$_{red}$ | 1939 | 2070 | 2083 | 2054 |
| | (1940) | (2071) | (2086) | (2060) |

Figure 2c shows the spectrum of the CO saturated hydrogenase after 53 min at -95 mV. A second sample of CO saturated hydrogenase poised for 30 min at -295 mV is shown in Figure 2d. In both spectra the dominant species is the CO inhibited state Ni-SCO (1941 cm$^{-1}$), as confirmed by the appearance of an additional fourth band at 2056 cm$^{-1}$, originating from the binding of exogenous CO to nickel[34,37,38]. Activation of the [NiFe] hydrogenase is observed to take place at much lower negative redox potentials and is faster in the presence of carbon monoxide. (Figure 3d, right). At the more negative

potential of -739 mV (Figure 3e, right), Ni-SCO$_{red}$ has completely disappeared and the sample contains a mixture of the catalytically active states

(Ni-C, Ni-R(1), Ni-R(2)).


**FTIR electrochemistry at room temperature (fully activated enzyme)**

Figure 3 collects the infrared spectra of the fully activated [NiFe] hydrogenase from *D. vulgaris* without CO (left) and with CO (right) in solution, poised at different redox potentials. At a potential of -228 mV (Figure 3a, left), the hydrogenase is predominantly at the onset of its catalytic cycle with its major fraction in the Ni-SI$_a$ state (1943 cm$^{-1}$). A small band corresponding to the (Ni-SI$_r$)$_I$ (1921 cm$^{-1}$) is also present. In the carbon monoxide saturated protein at the same potential (Figure 3a, right), all of the enzyme molecules are in the EPR-silent Ni-SCO state (1941 cm$^{-1}$).

At a potential of -419 mV (Figure 3b, left), the main state observed in the activated enzyme is Ni-C (1961 cm$^{-1}$). A second state with its CO band centered at 1948 cm$^{-1}$ corresponds to Ni-R(1). At the same redox potential in the CO saturated protein (Figure 3b, right), hydrogenase remains in the Ni-SCO state. However, the bands are now shifted by approximately 0 to 1 cm$^{-1}$ to lower wavenumbers. At a potential of -499 mV (Figure 3c, left), the most reduced Ni-R(1) state (1948 cm$^{-1}$) increases in intensity relative to Ni-C (1961cm$^{-1}$). At the same redox potential (Figure 3c, right) in the CO saturated enzyme, the bands corresponding to Ni-SCO shift again towards lower frequencies. The intrinsic CO band is now centered at 1939 cm$^{-1}$ and the band of the exogenous CO at 2054 cm$^{-1}$. The bands corresponding to the coupled cyanides are also shifted by 1 cm$^{-1}$ with respect to the spectrum at -228 mV (Figure 3a, right). This small but consistent shift has been associated previously with a state denoted as Ni-SCO$_{red}$ in the hydrogenase from *Desulfovibrio (D.) fructosovorans* [36]. This effect is fully reversible upon electrochemical re-oxidation. EPR experiments showed that the Ni-SCO$_{red}$ state is EPR-silent (data not shown, see Discussion). In addition, in this spectrum a small fraction of Ni-C (1961 cm$^{-1}$) is also observed (Figure 3c, right).

At a potential of -639 mV in the absence of CO (Figure 3d, left**),** most of the sample is in the Ni-R(1) state (1948 cm$^{-1}$, ~ 53 %), while smaller fractions are in Ni-C (1961 cm$^{-1}$, ~ 23 %) and Ni-R(2) (1933 cm$^{-1}$, ~ 24 %). Lowering the potential to -739 mV
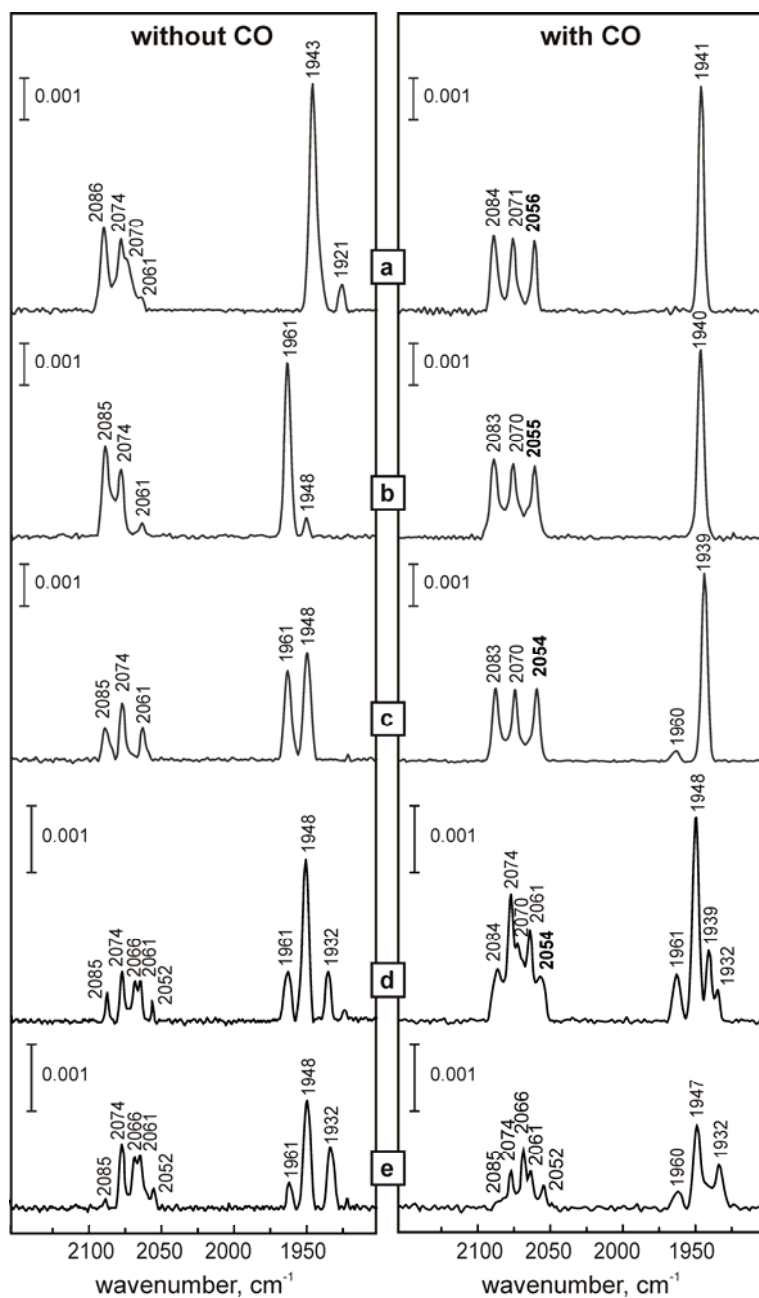
**Figure 3.** FTIR spectra of the *D. vulgaris* Miyazaki F [NiFe] hydrogenase poised at different potentials. In the absence of CO in solution (left): (a) at -228 mV the Ni-SI$_a$ is the major species, (b) at -419 mV the Ni-C is maximized, (c) at -499 mV a mixture of the Ni-C/Ni-R(1) states co-exist, (d) at -639 mV the Ni-R(1) state has maximal intensity and the Ni-R(2) appears, whose intensity increases (e) at -739 mV. For the CO saturated hydrogenase (right): (a) at -228 mV all the enzyme is in the Ni-SCO state, (b) at -419 mV and (c) at -499 mV the Ni-SCO$_{red}$ is observed. At even lower potentials (d) at -639 mV and (e) at -739 mV hydrogenase appears to have recovered from CO inhibition.

(Figure 3e, left**)**, results in an increase of the intensity of Ni-R(2) relative to Ni-C and Ni-R(1). In the CO saturated enzyme at -639 mV, Ni-R(1) becomes the species with the largest intensity and only a small fraction of the sample remains in Ni-SCO$_{red}$

Assuming that Ni-SCO (1941 cm$^{-1}$) and Ni-SCO$_{red}$ (1939 cm$^{-1}$) are two different forms of the same redox state, their apparent integrated intensity was plotted against the applied potential (Figure 4). The data obtained from deconvolution of the two bands are best fitted with Nernst curves corresponding to a one-electron transfer. The apparent midpoint potential of such a process at 25°C was determined by the mean value of the two curves to be -421 mV ± 5 mV. In the same figure the potentiometric titration corresponding to the transition from Ni-SCO$_{red}$ to Ni-R(1) is also shown. The apparent midpoint potential of this process was determined to be -596 mV ± 5 mV.
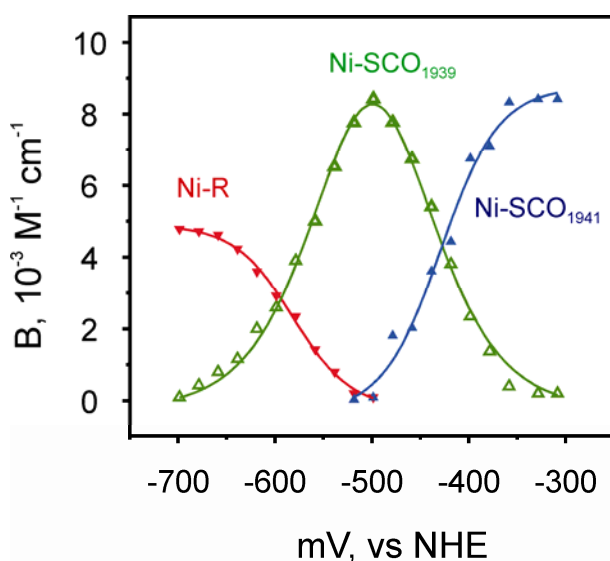


**Figure 4.** Potentiometric titration at 25 °C for the Ni-SCO/Ni-SCO$_{red}$ and Ni-SCO$_{red}$/ Ni-R(1) pairs. The integrated absorption bands corresponding to Ni-SCO and Ni-SCO$_{red}$ are plotted against the potential, corresponding to a one- electron transfer with apparent midpoint potential of -421 mV ± 5 mV. The data obtained from integration of the absorption bands corresponding to Ni-SCO$_{red}$ and Ni-R(1) in the range between -499 mV and -719 mV are described by curves with an apparent midpoint potential of -596 mV ± 5 mV. The titration was fully reversible at 25 °C.

Re-oxidation of the sample containing the active states (Ni-C, Ni-R(1,2)) in the presence of CO at 25 °C in the electrochemical cell yielded the Ni-SCO state. Binding of CO was faster than the insertion of oxygen in the active site. However, re-oxidation of the sample from the active states in the presence of CO at 4°C resulted in the formation of Ni-B in approximately one third of the hydrogenase molecules in the sample (Figure S2 of the Appendix B).

**FTIR experiments at low temperatures: photodissociation of CO from Ni-SCO**

Figure 5a shows the FTIR spectrum of the Ni-SCO state at 40 K. The shifts observed in the positions of the bands with respect to those measured at room temperature (Figure 3a, right), result from the more restricted vibrational motion of the diatomic molecules [45]. Four bands can be clearly observed in the spectra. The absorption band at 1941 cm$^{-1}$ corresponds to the CO terminally bound to iron and the two peaks at 2072 and 2086 cm$^{-1}$ are assigned to the conjugate CN$^{-}$ ligands. A fourth additional band at 2061 cm$^{-1}$ corresponds to the externally added CO bound to nickel. A similar spectrum has been obtained for the Ni-SCO state of the [NiFe] hydrogenase from *Allochromatium (A.) vinosum*[37,38], in which an absorption band at 2060 cm$^{-1}$ was ascribed to the extrinsic CO.

Inhibition of hydrogenase using isotope labeled $^{13}$CO, results in the spectrum shown in Figure 5b. The absorption band corresponding to the externally added CO shifts by 46 cm$^{-1}$ to 2015 cm$^{-1}$, whereas the positions corresponding to the intrinsic ligands bound to iron remain unchanged.

It is known that the external CO can be photodissociated from the active site at temperatures below 100 K[32,34, 37]. The spectrum after illumination at 40 K is shown in Figure 5c. In this spectrum only three bands are observed, which correspond to the CO and the CN$^{-}$ ligands bound to Fe. The fourth band associated with the external CO at 2061 cm$^{-1}$ (or at 2015 cm$^{-1}$, Ni-S$^{13}$CO) is absent, showing that the external CO is no longer attached to the active site. The light-induced state corresponds to the Ni-SI$_{a}$ state (Table 1). Dissociation of the exogenous CO ligand occurs at temperatures equal to or lower than 100 K, but a complete photoconversion to Ni-SI$_{a}$ (100 % of the molecules in Ni-SCO) takes place only below 50 K.
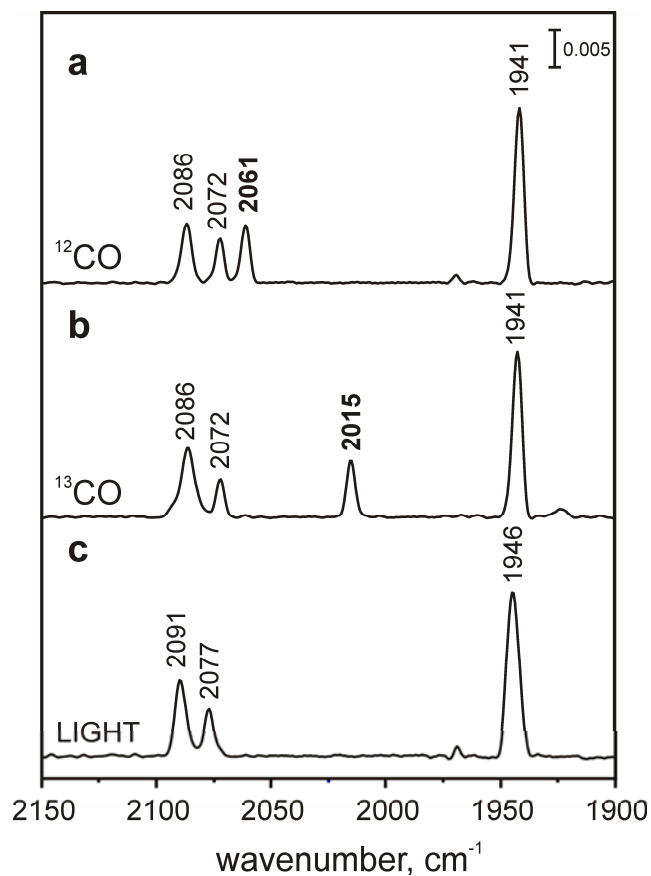
**Figure 5.** (a) FTIR spectrum of the CO inhibited enzyme from *D. vulgaris* Miyazaki F at 40 K in the dark. The absorption band of the exogenous CO is found at 2061 cm$^{-1}$. (b) $^{13}$CO inhibited hydrogenase in the dark at 40 K. The band of the exogenous $^{13}$CO shifts by 46 cm$^{-1}$ towards lower frequencies with respect to the exogenous $^{12}$CO band. (c) After illumination, the absorption bands at 2061 cm$^{-1}$ (and 2015 cm$^{-1}$, respectively) disappear, corresponding to the light dissociation of the externally added CO molecule. The light excited state is the Ni-SI$_a$ state (1946 cm$^{-1}$).

.

**Rapid scan FTIR: kinetics and activation energy for the reassociation of CO in the Ni-SI$_a$ state**

In the absence of light, the dissociated carbonyl ligand rebinds to the active site and the Ni-SCO state is reformed. This process is completely reversible. Figure 6a shows the time dependence of a light-minus-dark difference infrared spectrum in a three

dimensional representation at 78 K. The positive bands correspond to the Ni-SI$_a$ state (light product) and the negative bands correspond to Ni-SCO

(educt state). At time t = 0, the first slice of the spectrum represents the maximum difference, i.e. the maximum conversion from Ni-SCO to Ni-SI$_a$. As the time of dark adaptation is incremented, Ni-SCO recovers and Ni-SI$_a$ decreases in intensity. The resulting kinetics are bi-exponential, consisting of fast and slow components.
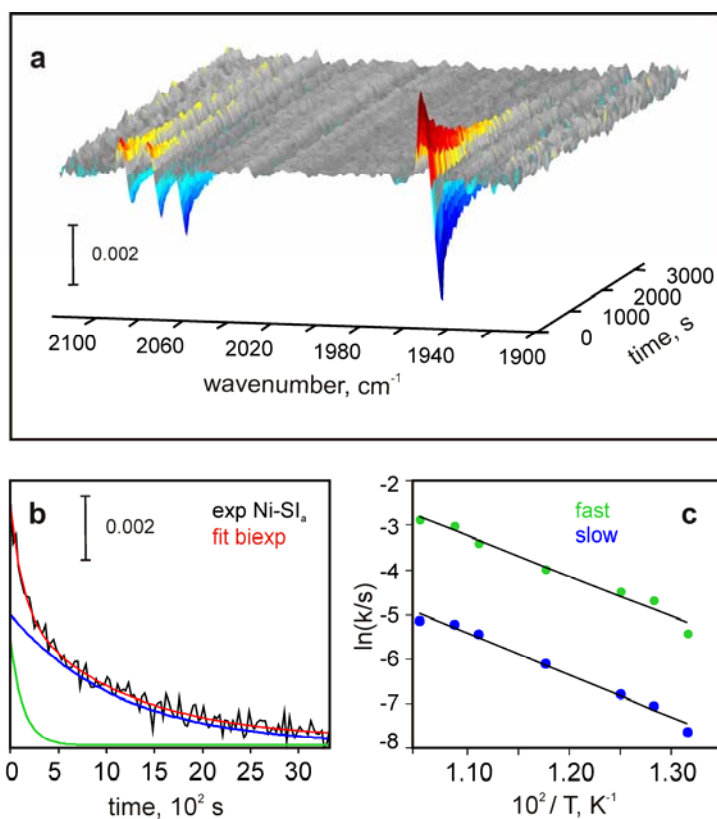


**Figure 6.** (a) Three dimensional representation of a FTIR light-minus-dark difference spectrum corresponding to the back-conversion from Ni-SI$_a$ to Ni-SCO as a function of the dark adaptation time at 78 K. (b) Time dependent kinetics of the disappearance of the Ni-SI$_a$ state in the dark was exponential and fitted by a bi-exponential model. The respective slow and fast components are shown in green and light blue. (c) Arrhenius plot for the fast and slow rebinding processes between 78 K and 95 K.

In Figure 6b the kinetics of the disappearance of the Ni-SI$_a$ state are shown along with the corresponding data fits and components. No other intermediate states were detected within the time resolution of these experiments. The temperature dependence of the rate constants was examined in the range between 78 and 95 K for both slow and fast re-association processes (Figure 6c). The activation barrier for the reassociation of the extrinsic CO ligand was estimated by analyzing the kinetics of both the Ni-SCO recovery and the Ni-SI$_a$ disappearance, which were the same (within experimental error). The activation energy corresponds to approximately 9 kJ mol$^{-1}$. Results are summarized in Table 2. Activation energies assuming single exponential back conversion kinetics are also included.

**Table 2.** Activation energies (E$_a$) for the rebinding of exogenous CO. The error in the determination of energies is ± 8 %

| State | Type of fitting | E$_a$ , kJ mol$^{-1}$ |
|---|---|---|
| | bi-exponential (fast) | 8.0 |
| Ni-SCO / Ni-SI$_a$ | bi-exponential (slow) | 8.8 |
| | single exponential | 9.2 |

*Chapter 4*

**EPR experiments: formation of the paramagnetic Ni-CO state**

In the present study, the interaction of CO with the [NiFe] hydrogenase from D. vulgaris Miyazaki F under physiological conditions yielded only one state in two different EPR-silent forms (Ni-SCO and Ni-SCO$_{red}$). Ni-SCO was shown to be light sensitive, which was also found for the catalytically active Ni-C state. However, reassociation of CO to the active site takes place at lower temperatures as compared to the rebinding of the hydrogenic species in the Ni-C state [30]. On the basis of this observation, the hydrogen reduced hydrogenase (Ni-C) was allowed to interact for only one minute with carbon monoxide. The respective EPR spectrum at 40 K (Figure 7a) shows no changes in the Ni-C state signal ($g_x = 2.20$, $g_y = 2.15$, $g_z = 2.01$)[29], except for a decrease of approximately 20 % in its signal intensity (data of Ni-C without CO in the frozen solution are not shown). Illumination of the sample for 5 min at 40 K in the resonator of the EPR spectrometer, resulted in the formation of the Ni-L state , described by a signal with values $g_x = 2.30$, $g_y = 2.12$, $g_z = 2.05$ (Figure 7b). An additional rhombic signal was also present in both spectra ($g_x = 2.21$, $g_y = 2.09$ and $g_z = 2.03$). This corresponds to a non-light sensitive state and its amount depends on the purification procedure; it has previously been observed when the enzyme was treated with CO or Na$_2$S [24,58]. Based on the g-values and its relaxation behavior, it is most likely associated with different conformation of the [NiFe] active site.  To create the paramagnetic Ni-CO state, CO has to compete with the hydron for binding to the site of the Ni-L state[35]. Dark adaptation of Ni-L at 77 K showed along with the Ni-C state, a new rhombic signal. This signal is similar to the one observed in *A. vinosum*[32,35] and in *Methanococcus (M.) voltae* [46] hydrogenases treated with CO and is associated with a paramagnetic Ni-CO state. Dark adaptation after a second illumination of the sample yielded the maximum amount of EPR-detectable Ni-CO in the spectrum (Figure 7c), in which all g-values can be clearly identified ($g_x = 2.13$, $g_y = 2.08$ and $g_z = 2.02$).
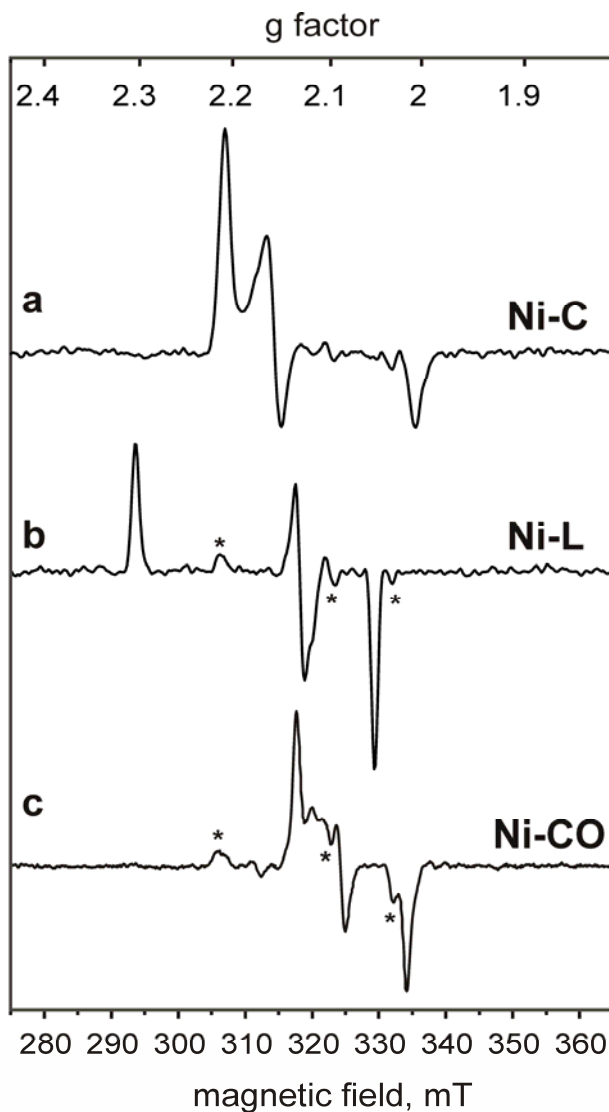
**Figure 7.** EPR spectra of the [NiFe] hydrogenase from *D. vulgaris* Miyazaki F at 40 K. (a) Enzyme of the H$_2$ reduced sample (Ni-C) after interaction for 1 min with carbon monoxide, (b) same as (a) but after illumination for 5 min (Ni-L state). A rhombic non-light sensitive signal often observed, is denoted with an asterisk (see text), (c) The same sample after a second illumination - dark adaptation cycle (dark adaptation was carried out at 77 K). The majority of the enzyme is in the Ni-CO state described by a rhombic g-tensor with principal values g$_x$ = 2.13, g$_y$ = 2.080 and g$_z$ = 2.019. Experimental conditions: T = 40 K, microwave frequency 9.454 GHz, modulation amplitude 0.7 mT, microwave power 2 mW, except for (c) which was 6 mW.

## Discussion

### Electrochemical titrations and redox equilibria

Carbon monoxide has a large affinity for binding to transition metals[47]. In the case of the [NiFe] hydrogenases, binding of CO to the active site[34] is a process that hinders catalytic function and renders the enzyme inactive[33]. In the present work, a series of electrochemical measurements were carried out for the [NiFe] hydrogenase from *D. vulgaris* Miyazaki F and redox changes were followed by FTIR. The results can be summarized as follows:

(i) Carbon monoxide interacts only with the catalytically active state Ni-SI$_a$. The FTIR spectrum of Ni-SCO strongly resembles that of Ni-SI$_a$ with respect to the bands of the diatomic Fe ligands, which show a constant shift of 2 to 3 cm$^{-1}$. This suggests that the active site conformation is only slightly distorted after binding extrinsic CO to nickel. The stretching vibration of the external CO centered at 2056 cm$^{-1}$ suggests a weak $\pi$ back-bonding, further supported by the X-ray structures of the CO-adduct in *D. vulgaris*, which showed a terminally bound CO ligand with a bond length of 1.136 Å [34], close to the one for a free CO molecule (1.13 Å ).

CO does not bind to the oxygen inhibited states (*e.g.* Ni-A, Ni-B, (Ni-SI$_r$)$_l$) or to the active Ni-C / Ni-R states due to the presence of more electronegative ligands in the active site of these states and the overall electronic properties of the [NiFe] complex, which has a distorted octahedral geometry. In Ni-SI$_a$ however, the nickel ion is in the divalent state and most of the proposed catalytic schemes are consistent with a four coordinated nickel in a high spin state (S=1), which would retain the octahedral geometry of the complex [5,48]. A recent theoretical study showed that only models of Ni-SCO, considering a high spin nickel state, could reproduce the FTIR experimental results[49]. Therefore the absence of additional non-protein ligands in the active site and the electronic configuration of the nickel ion govern the interaction of CO with the [NiFe] center resulting in binding of carbon monoxide only to the active Ni-SI state.

(ii) Hydrogenase is shown to be reactivated from the oxygen inhibited forms faster in the presence of CO. It was observed that in the presence of CO, transition to the functional intermediates occurs at much lower negative redox potentials (Figure 2). This finding has been reported in various studies[51,52] but so far, to date no definite explanation

for this acceleration in the activation times has been substantiated. Most probably, CO displaces the oxygen from the protein surrounding resulting in a faster recovery from oxygen 'contamination' in the hydrophobic channels. In addition it does not form reactive species as does $O_2$ and thus might be easier to remove from the protein environment.

(iii) At an applied potential of -419 mV, a small shift in the bands of Ni-SCO (1 to 2 $cm^{-1}$ towards lower frequencies) was observed, which was maximized at -499 mV (Ni-SCO$_{red}$). All four vibrational bands shifted slightly, suggesting a redistribution of the delocalized electronic density at the [NiFe] site[53]. To correlate formation of Ni-SCO$_{red}$ (1939 $cm^{-1}$) with a possible redox change of nickel, the Ni-SCO state was reduced with sodium dithionite and the EPR spectrum was recorded. No additional signals could be observed, except for a weak Ni-C signal (data not shown). Both Ni-SCO, Ni-SCO$_{red}$ are thus EPR-silent, as previously demonstrated [36]. Conversion from Ni-SCO to Ni-SCO$_{red}$ was reversible and could be titrated as a one-electron process. Such a transition involves no redox change in the bi-nuclear active site, but is suggested to be connected with reduction of the proximal $[Fe_4S_4]^{2+/1+}$ cluster. This has been shown previously for the [NiFe] hydrogenase from *D. fructosovorans*, by comparing the UV/VIS spectra of the Ni-SCO/Ni-SCO$_{red}$ states[36]. The midpoint potential found here is in good agreement with the redox potential for the reduction of the $[Fe_4S_4]^{2+/1+}$ proximal cluster in *D. vulgaris*[54]. A change in the electrostatic interaction between the proximal $[Fe_4S_4]^{2+/1+}$ cluster and the [NiFe] site, therefore alters the electron density distribution on the bimetallic site, resulting in the small shift of the infrared bands.

(iv) At -499 mV, the Ni-C state is present in the spectrum of Ni-SCO$_{red}$ (Figure 3c, right), whereas at more negative potentials a small increase of Ni-C and a larger increase of the Ni-R states is observed (Figure 3d,f right). A form of electrochemical cleavage of the Ni-C bond of the externally added CO appears to take place, which is complete at -739 mV. At this potential only the active states (i.e. Ni-C, Ni-R(1,2)) were detected (Fig. 3e, right). Transition from Ni-SCO$_{red}$ to Ni-R(1) was fitted as a one-electron process with a midpoint potential of -596 mV (Figure 4). The appearance first of the Ni-C state and the involvement of one electron from the Ni-SCO$_{red}$ to the Ni-R transition, leads to the conclusion that upon removal of the external CO ligand, hydrogenase is left

in the Ni-SI$_a$ state. Depending on the potential and on the amount of redox equivalents, transition to Ni-R from the Ni-SI$_a$ state takes place with or without Ni-C as a detectable intermediate. This has been shown by stopped-flow infrared studies on *A. vinosum*[38,48], where in the presence of excess hydrogen and with both [Fe$_4$S$_4$] clusters reduced, a direct transition of Ni-SI$_a$ to Ni-R was observed. Most likely, at such very negative potentials, Ni-C is an extremely short-lived intermediate. A further increase of Ni-C at the most negative potential is a result of the [NiFe] hydrogenase turnover (H$_2$ evolution) activity.

### $^{13}$CO isotope labeling

Isotopic labeling of Ni-SCO with $^{13}$CO, shifts the band of the extrinsic carbonyl by 46 cm$^{-1}$ towards lower wavenumbers (larger reduced mass relative to $^{12}$CO). This shift is in agreement with that theoretically predicted for a 'pure' CO vibration ($\bar{v}_{13CO} = 0.97771 \cdot \bar{v}_{12CO}$)[55]. In this case, the Cotton Kraihanzel Force Field (CKFF)[56,57] approximation permits calculation of the stretching parameters, by taking into account only the CO displacement and ignoring the metal carbonyl frequencies. An estimation of the force constants and the extent of metal-to-carbon $\pi$ donation can be made. A relatively small force constant k ~ 1665 N/m$^{**}$ was obtained, showing a weak $\pi$-back bonding with a small degree of metal-to-carbon electron donation. The FTIR bands corresponding to the intrinsic carbonyl and cyanide ligands bound to iron do not shift upon labeling. This shows that there is no vibrational coupling between these diatomic oscillators and the externally added CO bound to nickel.

**Photodissociation and reassociation kinetics of the external CO ligand to nickel**

In Ni-SCO, the extrinsic CO is photolabile at temperatures ≤ 100 K. The light-induced state corresponds to Ni-SI$_a$. The infrared bands of the Fe ligands associated with Ni-SI$_a$, occur at higher frequencies compared to those of Ni-SCO. This indicates that dissociation of the carbonyl ligand (2061 cm$^{-1}$) at the nickel results in a small decrease of the electron density at the iron. Illumination of Ni-SCO$_{red}$ (data not shown), also resulted in the formation of Ni-SI$_a$, but was only effective at temperatures below 80 K. These

---

$^{**}$ The force constant k for a free CO molecule considering an infrared frequency $\bar{v}$ = 2153 cm$^{-1}$ is 1872 N/m.

results show that Ni-SI$_a$ and not Ni-R(1,2) binds CO, leading to formation of the EPR silent Ni-SCO / Ni-SCO$_{red}$ states.

The cleavage of the Ni-CO bond upon illumination is reversible at T $\leq$ 100 K. Rebinding of CO takes place in the dark following bi-exponential kinetics, consisting of a slow and a fast component. Such a biphasic nature could have a physical interpretation, since the CO ligand does not bind in a linear form to nickel, but the bonding is governed by an angle distribution 161° $\leq$ $\varphi$ $\leq$ 136° [34]. This spread in the bonding modes could account for the composite nature of the recombination kinetics observed. Due to the restricted mobility of the bound carbonyl at these temperatures, the slightly different conformations are almost degenerate. This is illustrated in the activation energies for the rebinding of CO, which are very similar (Table 2). The activation barrier was estimated to between 8 and 9 kJ·mol$^{-1}$. Transition from Ni-SI$_a$ to Ni-SCO is a first order process without intermediates. The back conversion kinetics for the disappearance of Ni-SI$_a$ and increase of Ni-SCO are exponential, in contrast to the rebinding of CO to myoglobin (Mb)[58,59] in a similar temperature range. Activation energies for CO rebinding in Mb are between 5 to 30 kJ/mol[59,61], which are comparable to or even larger than the energy threshold required for the carbonyl to rebind to nickel in hydrogenases. These results show a considerable degree of similarity in the rebinding of CO to divalent transition metals (*i.e.* Ni$^{2+}$, Fe$^{2+}$), which may be of significance as both proteins are reversibly inhibited by CO.

**The paramagnetic Ni-CO state**

In the present work, the paramagnetic Ni-C state was shown not to interact with CO, in agreement with previous studies [35]. Incubation with carbon monoxide results in the gradual disappearance of the EPR signal corresponding to Ni-C (Figure 7a). This occurs as the concentration of CO in the protein solution becomes high enough to shift the redox equilibrium towards the Ni-SI$_a$ state (Ni$^{2+}$, EPR silent), in which CO can bind.

Ni-C is light sensitive and illumination leads to the paramagnetic Ni-L state. The bridging hydride has been proposed to be dissociated as a proton, which would leave the

nickel in a formally monovalent state ($Ni^{1+}$) [2,35,62,††] in Ni-L. Dark adaptation of Ni-L in the presence of CO leads to the paramagnetic Ni-CO state (Figure 7c), as rebinding of CO to the active site occurs at lower temperature with respect to the recombination of the hydrogenic species[30]. The paramagnetic Ni-CO has been well studied in *A. vinosum* [32,35] and *M. voltae* [46], whereas the present study is the first report for sulfate reducing species such as *D. vulgaris* Miyazaki F. Ni-CO is described by a rhombic spectrum with g-values significantly smaller than those of the other paramagnetic states of hydrogenase (i.e. Ni-A, Ni-B, Ni-C) [4]. This is a consequence of the binding of CO to nickel, which results in a larger ligand field splitting of the molecular orbitals involved and thus in smaller

g-values.

Furthermore, from a chemical point of view, CO would not bind to $Ni^{3+}$. The reason is that carbon monoxide is a weak $\sigma$ donor and a strong $\pi$ acceptor. Therefore in a $Ni^{3+}$ situation, CO would have to donate the lone pair to nickel, but the back donation from nickel to CO, which would stabilize the bond, is not feasible due to the large positive charge on the $Ni^{3+}$. Density functional theoretical studies are also consistent with a monovalent nickel center in both Ni-CO and Ni-L states [62], where the g-values and the $^{13}CO$ hyperfine parameters were in good agreement with the experimental data[32,62]. We thus conclude that the Ni in the Ni-CO and Ni-L states is formally monovalent $Ni^{1+}$ and therefore the paramagnetic Ni-CO can be obtained only upon interaction of carbon monoxide with the light-induced Ni-L state.

---

†† $Ni^{1+}$ spectra of model compounds are described by an axial g-tensor, but depending on the ligands they can also show a rhombic g-tensor. The distinction between $Ni^{1+}$ and $Ni^{3+}$ is not straightforward from EPR. $Ni^{1+}$ would be in agreement with a $d^9$ configuration and the unpaired electron in the $d_{x^2-y^2}$ orbital. However the energy difference between the $d_{z^2}$ and $d_{x^2-y^2}$ orbitals might not be large in this case, which would result in a significant mixing of these two orbitals [63].

## Conclusions

The current study presents results on the characterization of the CO inhibited states in the [NiFe] hydrogenase from *D. vulgaris* Miyazaki F by FTIR and EPR spectroscopies. A paramagnetic CO inhibited state can be formed by treating Ni-C with carbon monoxide prior to illumination to generate Ni-L, in which the nickel ion is in the 1+ state (monovalent). Based on the different rebinding kinetics during dark adaptation, binding of CO to Ni-L is favored as compared to the insertion of the hydride. The resulting Ni-CO state is proposed to be monovalent since it can be obtained only upon interaction of CO with Ni-L. On the other side, two diamagnetic CO-bound complexes; Ni-SCO and Ni-SCO$_{red}$ can be formed by the binding of carbon monoxide to the active form of Ni-SI. The one-electron difference between the latter is attributed to the reduction of the proximal [Fe$_4$S$_4$] cluster. At negative redox potentials below -500 mV, the Ni-CO bond can be 'electrochemically cleaved' and the enzyme can recover its enzymatic activity despite the presence of CO in solution. Comparison with previous studies for enzymes derived from different organisms exhibited similar results. Differences are found for the absolute values of the redox potentials of the respective processes and to the extent of the CO 'electrochemical detachment'. Furthermore, in our experiments neither (Ni-SI$_r$)$_I$ nor Ni-C were shown to interact with CO. A rapid scan FTIR study on the kinetics of the CO rebinding to the active site quantified for the first time the activation barrier for such a process, showing a weak metal carbonyl in the [NiFe] hydrogenases consistent with values reported for other metalloproteins such as myoglobin.

## Acknowledgments

**References**

1  P.M. Vignais, B. Billoud, Chem. Rev. 107 (2007) 4206-4272.

2  L.G. Ljungdahl, M.W. Adams, L.L. Barton, J.G. Ferry, M.K. Johnson, B Springer, New York, 2007.

3  S.P.J. Albracht, Nickel hydrogenases: in search of the active site, Biochim. Biophys. Acta 1188 (1994) 167-204.

4  W. Lubitz, , E.J. Reijerse, M. van Gastel,  Chem. Rev. 107 (2007) 4331-4365.

5  J.C. Fontecilla-Camps, A. Volbeda, C. Cavazza, Y. Nicolet,  Chem. Rev. 107 (2007) 4273-4303.

6  Y. Nicolet,  B.J. Lemon, J.C. Fontecilla-Camps, J.W. Peters, Trends in Biochemical Sciences 25 (2000) 138-143.

7  A. Silakov, E.J. Reijerse, S.P.J. Albracht, E.C. Hatchikian, W. Lubitz,  J. Am. Chem. Soc. 129 (2007) 11447-11458.

8  S. Shima, O. Pilak, S. Vogt, M. Schick, M. S. Stagni, W. Meyer-Klaucke, E. Warkentin, R.K. Thauer, U. Ermler,  Science 321 (2008) 572-575.

9  T. Yagi, K. Kimura, H. Daidoji, F. Sakai, S. Tamura, H. Inokuchi,  J. Biochemistry 79 (1976) 661-671.

10  Y. Higuchi, T. Yagi, N. Yasuoka, Structure 5 (1997) 1671-1680.

11  A. Volbeda, M.H. Charon, C. Piras, E.C. Hatchikian, M. Frey, J.C. Fontecilla-Camps, Nature 373 (1995) 580-587.

12  S.P.J. Albracht,  Recueil des Travaux Chimiques des Pays-Bas-Journal of the Royal Netherlands Chemical Society 106 (1987) 173.

13  A.J. Pierik, W. Roseboom, R.P. Happe, K.A. Bagley, S.P.J. Albracht, J. Biolog. Chem. 274 (1999) 3331-3337.

14   A. Volbeda, C. Piras, A.L. De Lacey, V.M. Fernandez, E.C.  Hatchikian, M. Frey, J.C. Fontecilla-Camps, J. Am. Chem. Soc. 118 (1996) 12989-12996.

15    Y. Higuchi, H. Ogata, K. Miki, N. Yasuoka, T. Yagi, Structure 7 (1999) 549-556.

16   J.M.C. Coremans, J.W. Van der Zwaan, S.P.J. Albracht, Biochim. Biophys. Acta 1119 (1992) 157-168.

.   17   Y. Higuchi, S. Bando, M. Kusunoki, Y. Matsuura, N. Yasuoka, M. Kakudo, T. Yamanaka, T. Yagi, H. Inokuchi, J. Biochem. 89 (1981) 1659-1662.

18   S. Dementin, B. Burlat, A.L. De Lacey, G.  Adryanczyk-Perrier, B. Guigliarelli, V.M. Fernandez, M.  Rousset, J. Biolog. Chem. *279* (2003) 10508-10513.

19   M. van Gastel,C. Fichtner, F. Neese, W. Lubitz,  Biochem. Soc. Trans. 33 (2005) 7-11.

20   A.K.  Jones,  S.E.  Lamle,  H.R.  Pershad,  K.A.Vincent,S.P.J.  Albracht,  F.A. Armstrong, J. Am. Chem. Soc. 125 (2003) 8505-8514.

21   S.E. Lamle, S.P.J Albracht, F.A. Armstrong, J. Am. Chem. Soc. 126 (2004) 14899-14909.

22   V.M. Fernandez, E.C. Hatchikian, D.S. Patil, R. Cammack, Biochim. Biophys. Acta 883 (1986) 145-154.

23   A.Volbeda, L. Martin, C. Cavazza, M. Matho, B.W. Faber, W. Roseboom, S.P.J. Albracht, E. Garcin, M. Rousset, J.C. Fontecilla-Camps, J. Biolog. Inorg. Chem. 10 (2005) 239-249.

24   H. Ogata, S. Hirota, A. Nakahara, H. Komori, N. Shibata,T. Kato, K. Kano, Y. Higuchi, Structure 13 (2005) 1635-1642.

25   A.L. De Lacey, E.C. Hatchikian, A. Volbeda, M. Frey, J.C. Fontecilla-Camps, V.M. Fernandez,  J. Am. Chem. Soc. 119 (1997) 7181-7189.

26   C. Fichtner, C. Laurich, E. Bothe, W. Lubitz, Biochemistry 45 (2006) 9706-9716.

27   B. Bleijlevens, F.A. van Broekhuizen, A.L. De Lacey, W. Roseboom, V.M. Fernandez, S.P.J. Albracht, J. Biolog. Inorg. Chem. 9 (2004) 743-752.

28   M. Brecht, M. van Gastel, T. Buhrke, B. Friedrich, W. Lubitz, J. Am. Chem. Soc. 125 (2003) 13075-13083.

29   S. Foerster, M. van Gastel, M. Brecht, W. Lubitz, J. Biolog. Inorg. Chem. 10 (2005) 51-62.

30   P. Kellers, M.E. Pandelia, L.J. Currell, H. Görner, W. Lubitz, Phys. Chem. Chem. Phys.,(2009), 11, 8680 - 8683

31   A.L. De Lacey, V.M. Fernandez, M. Rousset, R. Cammack, Chem. Rev. 107 (2007) 4304-4330.

32   J.W. van der Zwaan, S.P.J. Albracht, R.D. Fontijn, Y.B.M. Roelofs, Biochim. Biophys. Acta 872 (1986) 208-215.

33   G.D. Fauque, Y.M. Berlier, E.S. Choi, H.D. Peck, J. LeGall, P.A. Lespinat, Biochem. Soc. Trans. 15 (1987) 1050-1051.

34   H. Ogata, Y. Mizoguchi, N. Mizuno, K. Miki, S. Adachi, N. Yasuoka, T. Yagi, O. Yamauchi, S. Hirota, Y. Higuchi, J. Am. Chem. Soc. 124 (2002) 11628-11635.

35   R.P. Happe, W. Roseboom, S.P.J. Albracht, Eur. J. Biochem. 259 (1999) 602-608.

36   A.L. De Lacey, C. Stadler, V.M. Fernandez, E.C. Hatchikian, H.J. Fan,S.H. Li, M.B. Hall, J. Biolog. Inorg. Chem. 7 (2002) 318-326.

37   K.A. Bagley, C.J. van Garderen, M. Chen, E.C. Duin, S.P.J. Albracht, W.H. Woodruff, Biochemistry 33 (1994) 9229-9236.

38   S.J. George, S. Kurkin, R.N.F. Thorneley,S.P.J. Albracht, A stopped-flow infrared study, Biochemistry 43 (2004) 6808-6819.

39   D.A. Moss, M. Leonhard, M. Bauscher, W. Mantele, FEBS Lett. 283 (1991) 33-36.

40   F. Baymann, D.A. Moss, W. Mantele, Anal. Biochem. 199 (1991) 269-274.

41   M.L. Fultz, R.A. Durst, Analytica Chimica Acta 140 (1982) 1-18.

42   P. Atkins,J. Paula. *Atkins' Physical Chemistry,* Oxford University Press, 2006.

43   M.Y. Darensbourg, E.J. Lyon, J.J. Smee, Coord. Chem. Rev. 206 (2000) 533-561.

44   M.E. Pandelia, H. Ogata, L.J. Currell, M. Flores, W.  Lubitz, J. Biolog. Inorg. Chem. (2009) DOI: 10.1007/s00775-009-0566-9.

45   R.A. Nyquist, Appl. Spectrosc. *40* (1986) 79-85.

46   O. Sorgenfrei, A. Klein, S.P.J. Albracht, FEBS Lett. 332(1993) 291-297.

47   J.P. Collman, J.I. Brauman, K.M. Doxsee,  Proc Natl Acad Sci USA 76 (1979) 6035-6039.

48   M. Bruschi, L. De Gioia, G. Zampella, M. Reiher, P. Fantucci, M. Stein, J. Biolog. Inorg. Chem. 9 (2004) 873-884.

49   A. Pardo, A.L. De Lacey, V.M. Fernandez, H.J. Fan, Y. Fan, M.B. Hall, J. Biolog. Inorg. Chem. 11 (2006) 286-306.

50   S. Kurkin, S.J. George, R.N.F Thorneley, S.P.J. Albracht, Biochemistry 43 (2004) 6820-6831.

51   Y.M. Berlier, G.D. Fauque, J. LeGall, P.A. Lespinat, P. A.,H.D. Peck, FEBS Lett. 221 (1987) 241-244.

52  S.E. Lamle, S.P.J. Albracht, F.A. Armstrong, J. Am. Chem. Soc.  127 (2005) 6595-6604.

53  C.H. Lai, W.Z., Lee, M.L. Miller, J.H. Reibenspies, D.J. Darensbourg, M.Y. Darensbourg,  J. Am. Chem. Soc. 120 (1998) 10103-10114.

54  M. Asso, B. Guigliarelli, T. Yagi, P. Bertrand, Biochim. Biophys. Acta 1122 (1992) 50-56.

55  P.S. Braterman, Metal Carbonyl Spectra, Academic Press London, 1975.

56  F.A. Cotton, Inorg. Chem. 3 (1964) 702-711.

57  C.S. Kraihanzel, F.A. Cotton, Inorg. Chem. 2 (1963) 533-540.

58  C. Fichtner, M. van Gastel, W. Lubitz, Phys. Chem. Chem.  Phys. 5 (2003) 5507-5513.

59  H. Frauenfelder, S.G. Sligar, P.G.Wolynes,  Science 254 (1991) 1598-1603.

60  F. Parak, H.Frauenfelder, Physica A 201 (1993) 332-345.

61  R.H. Austin, K.W. Beeson, L. Eisenstein, H. Frauenfelder, I.C. Gunsalus , Dynamics of Ligand Binding to Myoglobin, Biological Physics, 1993

62  M. Stein, E. van Lenthe, E.J. Baerends, W. Lubitz,  J. Am. Chem. Soc. 123 (2001) 5839-5840.

63  M. van Gastel, W. Lubitz, in High Resolution EPR: Applications to Metalloenzymes and Metals in Medicine, Biol. Magn. Res. 28 (2009) 441-470, G.R. Hanson and L.J. Berliner (Eds), Springer, New York

# Chapter 5

# Probing Intermediates in the Activation Cycle of [NiFe] Hydrogenase by Infrared Spectroscopy: The Ni-SI$_r$ State and its Light Sensitivity
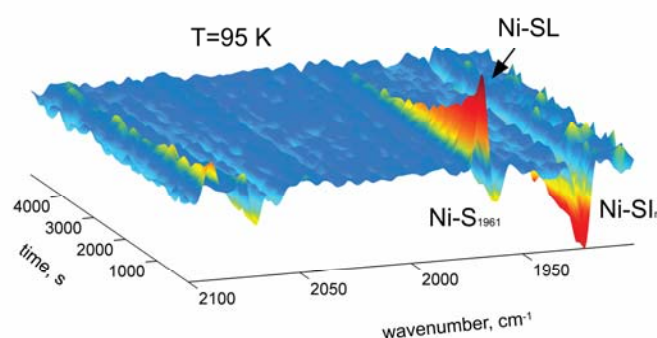


**Graphical Abstract**

The Ni-SI$_r$ state reversibly converts to a light-induced state denoted as Ni-SL. Reappearance and decay of Ni-SI$_r$ and Ni-SL, respectively, take place with single-exponential kinetics. The structural effects associated with the photoinduced transition involve displacement of the oxygenic ligand bound to the active site of Ni-SI$_r$

*Chapter 5*

# Probing Intermediates in the Activation Cycle of [NiFe] Hydrogenase by Infrared Spectroscopy: The Ni-SI$_r$ State and its Light Sensitivity[†]

Maria-Eirini Pandelia, Hideaki Ogata, Leslie J. Currell, Marco Flores[§],
Wolfgang Lubitz

*Max-Planck-Institut für Bioanorganische Chemie, Stiftstrasse 34-36, D-45470, Mülheim an der Ruhr, Germany.*
*[§] Current address: Department of Chemistry and Biochemistry, Arizona State University, Tempe, Arizona 85287-1604*

## Abstract

The [NiFe] hydrogenase from the sulphate reducing bacterium *Desulfovibrio vulgaris* Miyazaki F is reversibly inhibited in the presence of molecular oxygen. A key intermediate in the re-activation process, Ni-SI$_r$, provides the link between fully oxidised (Ni-A, Ni-B) and active forms of hydrogenase (Ni-SI$_a$, Ni-C, and Ni-R). In this work Ni-SI$_r$ was found to be light sensitive (T $\leq$ 110 K), similar to the active Ni-C and the CO-inhibited states. Transition to the final photo-product state (Ni-SL) was shown to involve an additional transient light-induced state (Ni-SI$_{1961}$). Rapid scan kinetic infrared measurements provided activation energies for the transition from Ni-SL to Ni-SI$_r$ in protonated as well as deuterated samples. The inhibitor carbon monoxide was found not to react with the active site of the Ni-SL state. Wavelength dependence of the Ni-SI$_r$ photo-conversion was examined in the range between 410 and 680 nm. Light induced effects were associated with a nickel centred electronic transition, possibly involving a change in the spin state of nickel (Ni$^{2+}$). In addition, at T $\leq$ 40 K the CN$^-$ stretching vibrations of Ni-SL were found to be dependent on the colour of the monochromatic irradiation, suggesting a change in the interaction of the hydrogen bonding network of the surrounding amino acids. A possible mechanism of the photochemical process, involving displacement of the oxygen based ligand, is discussed.

## Introduction

Hydrogenases are metalloenzymes found in the metabolic pathway of a wide variety of anaerobic and hydrogen oxidising micro-organisms[1]. They catalyze the elementary reversible reaction

$$H_2 \rightleftharpoons 2H^+ + 2e^-.$$

Such enzymes couple either oxidation of dihydrogen or reduction of protons to $H_2$ to the activity of nearby redox centres. According to the metal content of their active site, they can be classified into three major categories: (a) [NiFe] hydrogenases, with Ni and Fe forming a hetero binuclear active centre[2,3,4,5],(b) [FeFe] hydrogenases, with a bimetallic Fe centre linked to a $[Fe_4S_4]$ cubane forming the so-called H-cluster[6,7] and (c) iron-sulphur-cluster free hydrogenases (Hmd) or [Fe] hydrogenases from methanogenic archea consisting of a mononuclear Fe[8].

The [NiFe] hydrogenase from the sulphate reducing bacterium *Desulfovibrio (D.) vulgaris* Miyazaki F is a periplasmic membrane attached enzyme[9]. It has a molecular mass of 91 kDa and consists of two subunits. The hetero-nuclear Ni-Fe centre is located at the heart of the large subunit; with two cysteinyl ligands linking the two metal ions (Figure 1). Nickel is coordinated further by two other cysteinyl residues in a terminal fashion and has an open co-ordination site opposite to the bridging Cys549. The free coordination site is believed to serve as the contact position for dihydrogen during the catalytic process, as the enzyme cycles through the different redox states. In this process the nickel changes oxidation state whereas the Fe remains always in the divalent state ($Fe^{2+}$). The iron is bridged to nickel by the Cys84 and Cys549 residues (Figure 1) and is further coordinated by strong σ- and π- ligands, *i.e.* two cyanides and one carbonyl[10], which stabilise the Fe into a low oxidation and low spin state ($Fe^{2+}$, S = 0). Each cyanide ligand ($CN^-$) is proposed to form up to two hydrogen bonds with the surrounding amino acids (*e.g.* Arg479, Pro478, Pro501, Ser502 - *D. vulgaris* numbering), whereas the carbonyl (CO) is surrounded by more hydrophobic residues (*e.g.* Leu482, Val500). A third bridging ligand is often present (labelled as X in Fig. 1), whose identity and composition varies depending on the catalytic state of the enzyme[4,5]. The small subunit contains one $[Fe_3S_4]^{1+/0}$ cluster and two $[Fe_4S_4]^{2+/1+}$clusters[3,11]. These clusters mediate the electron transfer between the active site and the redox partner of the hydrogenase (e.g. cytochrome $c_3$)[1].
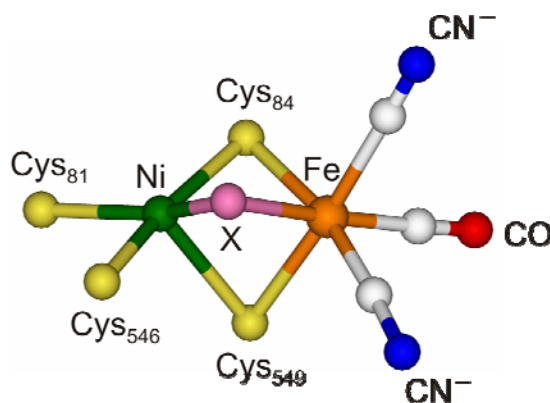
**Figure 1.** Active site of the [NiFe] hydrogenase from *D. vulgaris* Miyazaki F in the oxidised forms. The elements are represented with the following colours: Fe (orange), Ni (green), S (yellow), C (white), O (red) and N (blue). The third bridging ligand X is shown in pink. The numbering of the cysteine ligands from the protein is given.

The function of the [NiFe] hydrogenases can be inhibited in the presence of oxygen[12,13,14], carbon monoxide[15,16] and other substances[17,8]. Thus, aerobic isolation of the enzyme results in inactive states with oxygen based ligands bound to the bimetallic site. The most oxidised states are called Ni-A and Ni-B (Figure 2). They are both paramagnetic states (S = 1/2) related to a $Ni^{3+}$ in the $d_{z^2}$ ground state, but exhibit different spectroscopic properties[2] and activation kinetics[12,19]. Ni-B (ready) is quickly activated in the presence of $H_2$ or under reducing conditions, whereas Ni-A (unready) requires longer times[12] and is suggested not to interact directly with $H_2$[16,20]. It has been proposed that the differences between Ni-A and Ni-B are associated with the identity of the third ligand bridging Ni and Fe (labelled as X in Fig. 1). For Ni-B the ligand was identified as $OH^-$[21], whereas for Ni-A this position is suggested to be occupied by a di-oxo species (presumably $OOH^-$) as shown by X-ray crystallographic experiments[14, 22].

One electron reduction of Ni-B produces the Ni-SI$_r$ state (Ni$_r$-S/Ni-SI$_I$ by other authors). This reaction is pH dependent[23,24,25] , showing that the transition from Ni-B to Ni-SI$_r$ is coupled to a proton transfer[23,25]. Electron paramagnetic resonance (EPR) experiments have shown that Ni-SI$_r$ is an EPR-silent‡ species ($Ni^{2+}$)[26,27]. In addition,

---

‡ Integer spin ground states can be characterized as EPR-silent either if they are diamagnetic (S=0) or if they cannot be observed by conventional microwave frequencies X/Q/W band (i.e. S ≥ 1, where the zero field splitting is larger than the microwave quantum). So far no experimental evidence exists from high field EPR for the reduced hydrogenase states, whether they are associated with a high spin or low spin state for $Ni^{2+}$.

other spectroscopic data have shown the presence of a third bridging ligand that hinders the functional ability of Ni-SI$_r$[5,24,28,29]. Thus, two different mechanisms have been proposed to explain the transition from Ni-B to Ni-SI$_r$. Some authors have suggested that the proton is directly transferred to OH$^-$ resulting in a water molecule as the third bridging ligand in Ni-SI$_r$ [30,31], which can then be easily removed. Others have suggested that the proton is transferred to one of the co-ordinating cysteinyl residues that acts as a base, which facilitates the posterior protonation of OH$^-$ to water (H$_2$O) [29]. The second mechanism considers that OH$^-$ remains as the third bridging ligand in the active site of Ni-SI$_r$. In this scheme Ni-SI$_r$ is in acid-base equilibrium with a transient state (Ni-SI$_r$)$_{II}$ (state in brackets in Fig. 2), which retains the H$_2$O ligand loosely bound to the active centre.
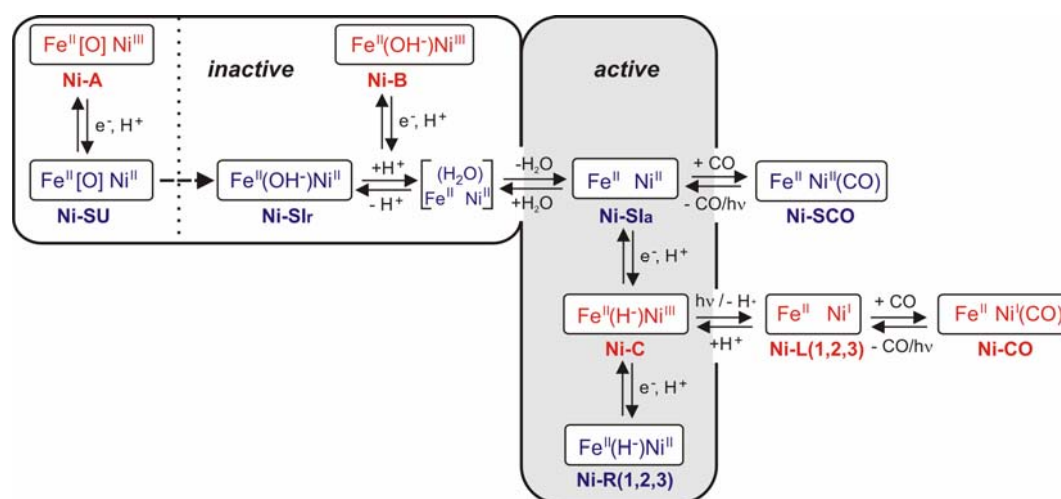


**Figure 2.** Proposed activation and catalytic mechanism for the standard, oxygen sensitive [NiFe] hydrogenases. The inhibition by CO and the light sensitivity of specific states are also depicted. The formal oxidation state of the nickel and iron ions are shown for each state along with the proposed inorganic bridging ligand X present in the active site. Note that for Ni-A and Ni-SU the exact identity of X is not yet known. The red colour denotes the EPR-active states, while the EPR-silent states are given in blue.

After removal of the H$_2$O ligand, the enzyme is able to enter the functional cycle. This cycle is comprised of three catalytically active states (Figure 2), in which the redox components (active site and iron sulphur centres) change their oxidation levels. Ni-SI$_a$ is the most oxidised active state and is EPR-silent (Ni$^{2+}$). Further one

electron reduction of Ni-SI$_a$ leads to the paramagnetic active state Ni-C (Ni$^{3+}$, S=1/2), with the substrate bound to the Ni-Fe site. This was shown by Electron Nuclear Double Resonance (ENDOR) and Hyperfine sublevel correlation (HYSCORE) spectroscopies, first for the regulatory hydrogenase from *Ralstonia (R.) eutropha*[32] and later for the standard hydrogenase from *D. vulgaris* Miyazaki F[33], where a hydride (H$^-$) was identified as the third bridging ligand in Ni-C. At cryogenic temperatures ($T \leq 170$ K) the Ni-C state has been shown to be light sensitive[34]. Illumination at such temperatures converts Ni-C into a new paramagnetic state denoted as Ni-L. This light-induced transition was shown by EPR spectroscopy to be associated with the loss of the hydride bridging ligand upon conversion to Ni-L. This reaction is fully reversible in the dark at higher temperatures ($\geq 200$ K). Further reduction of Ni-C produces the Ni-R states that are again EPR-silent. Up to three different Ni-R states have been observed by infrared spectroscopic studies[31]. For all divalent reduced states (Ni-SI, Ni-R) L-edge X-ray absorption (XAS)[35] and L-edge X-ray magnetic circular dichroism (XMCD)[36] studies are consistent with a high spin nickel state. However, recent theoretical studies suggest a low spin state for Ni$^{2+}$ in the Ni-SI states[37].

Furthermore, [NiFe] hydrogenases can be inhibited by carbon monoxide. It has been shown that in the active enzyme extrinsic CO binds terminally to Ni at the open co-ordination site[38]. An EPR-silent CO-inhibited state (Ni-SCO)[26,39] is formed if CO binds to the Ni-SI$_a$ state, whereas a paramagnetic CO-inhibited state (Ni-CO) results from binding of CO to the Ni-L state[40] (Figure 2). Similar to the Ni-C state, Ni-SCO (EPR-silent, inactive) and Ni-CO (paramagnetic, inactive) are also light sensitive at cryogenic temperatures. This effect can be directly correlated with structural changes in the active site upon illumination (*i.e.* dissociation of the extrinsic CO)[26]. However, up to present there is little information on the light sensitivity of the states related to the oxygenic inhibition of the enzyme. This kind of property, if observed, can be used to characterize structural features of the active site in such states and thus provide insight in the re-activation process of the enzyme, in particular for the study of the inactive EPR-silent states (e.g. Ni-SI$_r$).

Since some of the states participating in the catalytic cycle of the enzyme (*i.e.* Ni-SI states, Ni-R (1,2,3) states) shown in Fig.2 are EPR-silent[26,27,30], their structural and chemical properties cannot be studied by EPR spectroscopy. In such cases

Fourier transform infrared (FTIR) spectroscopy has proved to be very valuable for following redox changes in the active site of hydrogenases, as the strong $\pi$- and $\sigma$-ligands (CO, CN$^-$) [26] are sensitive probes of electronic changes (*i.e.* electron density on Fe, solvent interactions and intermolecular hydrogen bonding of the CN$^-$ ligands with nearby proton-donor amino acids)[26]. Infrared vibrational spectroscopy can thus provide an effective means to identify each redox state, to follow them in the reaction cycle and reveal associated structural and electronic changes.

In this work we have investigated the Ni-SI$_r$ state and its light sensitivity using FTIR spectroscopy. Temperature dependent back-conversion kinetics, study of the isotope effect (H/D) on the kinetic rates, wavelength dependence of the photo-conversion and effect of carbon monoxide are reported. The light induced effects are discussed and related to structural re-arrangements in the active site of the *D. vulgaris* Miyazaki F hydrogenase.

*Chapter 5*

## Materials and Methods

*Sample preparation.* Hydrogenase from the anaerobic bacterium *D. vulgaris* Miyazaki F was isolated from 50 L cultures as previously described[41]. The pH of the purified enzyme was kept at pH 7.4 in Tris/HCl buffer solutions.

*Samples in D₂O.* The aerobically purified enzyme was 20-fold diluted and re concentrated in $D_2O$ (99, 9 %, Deutero GmbH ) based Tris buffer with pD = pH + 0.41. This procedure was repeated five times. The sample was finally concentrated and fully reduced with $D_2$ gas (N27, Air Liquide). Reduction with $D_2$ was performed using a home-built gas-mixer, in which the pressure was controlled with a manometer in a steel chamber of 30 $cm^3$. Oxidation of the sample was obtained by exposure to atmospheric air.

*CO inhibited enzyme.*The aerobically purified hydrogenase was reduced with $H_2$ in the presence of methyl viologen ($E_m$ = -448 mV, Aldrich) for 10 min. Hydrogen was flushed out of the solution which was subsequently saturated with carbon monoxide (N47, Air Liquide) for 15 min on ice. The sample was transferred to the FTIR cell under 100 % CO atmosphere (glove bag) and immediately frozen in liquid $N_2$.

*FTIR spectroscopy.* Low temperature measurements (10 K ≤ T ≤ 110 K) were carried out in a Bruker IFS 66v/S FTIR spectrometer with a 2 $cm^{-1}$ spectral resolution using an Oxford Optistat CF cryostat. The spectrometer is equipped with an MCT photo-conductive detector. Temperature was controlled using an ITC 503 gas flow controller. Kinetic measurements were carried out in rapid scan mode. Samples were irradiated in situ for 5 minutes with a slide projector (250 W halogen lamp, 24 V) equipped with an electronic shutter (Compor). The temperature dependence of the measured kinetic rates was fitted with the Arrhenius equation ($lnk = lnA-E_a/RT$)[42], where **k** is the rate constant ($sec^{-1}$), A is a constant, $E_a$ is the activation energy (kJ/mol), R is the ideal gas constant (8.31445 J $K^{-1}$ $mol^{-1}$) and T the temperature in K. Illumination for variable times at different wavelengths in the range between 410 and 680 nm was carried out with an OPO Laser (OPOTEK Vibrant 355 II). A conversion of ~ 100 % could be achieved at T = 40 K after 10 min of illumination. This temperature was chosen since a complete conversion took place faster as compared to

higher temperatures. The laser repetition rate was 10 Hz. The total energy of the excitation light was measured with a calibrated power meter. The excitation energy was chosen so that the number of photons was the same for all selected wavelengths and corresponded to the number of photons present with excitation light at 630 nm and 1.5 mJ/pulse total energy. The excitation energy at an arbitrary wavelength λ can be then calculated according to the equation:

$$P(\lambda) = P(630) \cdot \frac{630}{\lambda}$$

15 µL samples were placed between sapphire windows (80 µm path-length) and inserted in the cryostat at low temperatures. Measurements at room temperature were carried out in a 50 µL transmission cell equipped with calcium fluoride ($CaF_2$) windows with 1 $cm^{-1}$ resolution. The temperature was regulated and kept to the desired value with the help of a thermostat (RML, LAUDA). In a FTIR spectrometer a low power output He-Ne laser (λ = 633 nm, red light) passes through the sample compartment and monitors the position of the moving mirror. In some cases an anti-reflection coated Ge-filter was placed between the sample and the interferometer. This filter serves to shield the sample from the He-Ne laser and its transmission is greater than 80 % between 5000 and 500 $cm^{-1}$. Usually it is omitted so as to increase the sensitivity of the infrared measurements as it is not entirely transmissive to infrared. Data were collected and baseline corrected using the OPUS software (Bruker). Kinetic data fitting was performed using MATLAB 7.0.

*EPR spectroscopy.* EPR measurements were carried out in a Bruker ESP-300 cw X-band spectrometer equipped with an Oxford Instruments helium flow cryostat and an ITC 503 temperature controller.

*Chapter 5*

## Results

**Room temperature FTIR measurements**

Figure 3a shows the FTIR spectrum of the aerobically isolated [NiFe] hydrogenase from *D. vulgaris* Miyazaki F at a temperature of 297 K (24 °C). In this spectrum we identified the bands corresponding to the Ni-A, Ni-B and Ni-SI$_r$ states. The vibrational frequencies corresponding to these states as well as of all the redox intermediate states present in *D. vulgaris* are summarized in Table 1. These values are similar to the ones described previously for *D. vulgaris* with the exception of the Ni-SU state[25], which has been now accurately resolved and is in agreement with data reported for other known hydrogenases[31]. All other EPR-silent states which do not correspond to known redox intermediates will be denoted with their CO vibration as a subscript. The bands in the region from 2000 to 1900 cm$^{-1}$ are associated with the CO vibrations of three different states, (*i.e.* Ni-A at 1956 cm$^{-1}$, Ni-B at 1955 cm$^{-1}$ and Ni-SI$_r$ at 1922 cm$^{-1}$)[25]. The bands in the region from 2100 to 2050 cm$^{-1}$ are associated with the CN$^-$ stretching vibrations (2 per state). The high frequency absorption band is assigned to the in-phase (symmetric) vibration of the CN$^-$ ligands and the low frequency absorption band is assigned to the out-of-phase (asymmetric) vibration. Those corresponding to Ni-A, Ni-B and Ni-SI$_r$ are well resolved (Figure 3a, Table 1).

An additional CO band at 1964 cm$^{-1}$ was observed in all sample preparations. The intensity of this CO band did not increase in preparations with different pH, whereas the CN$^-$ stretching vibrations that are probably related to such a state (Ni-S$_{1964}$, EPR-silent) could not be resolved. However, it can be electrochemically reduced and re-oxidised. The re-oxidised fraction was significantly smaller (~ 40 % of the initial intensity). Additional states in the as isolated enzyme preparations have been observed also in *Allochromatium (A.) vinosum*[24], where they were attributed to completely inactive species or states that carry a sulphur based ligand[24]. This state in the case of *D. vulgaris* is presumably an oxygen inhibited state, conformationally different from the Ni-SI$_r$ as a result of the purification procedure. From the apparent integrated intensities of these peaks and assuming equal absorption coefficients, we estimated that 80 % of the sample contains a mixture of the paramagnetic Ni-A and Ni-B states (~ 30 % Ni-A and 50 % Ni-B). The rest of the sample (~ 20 %) contains mostly the Ni-SI$_r$ and in lesser amount the Ni-S$_{1964}$ state.
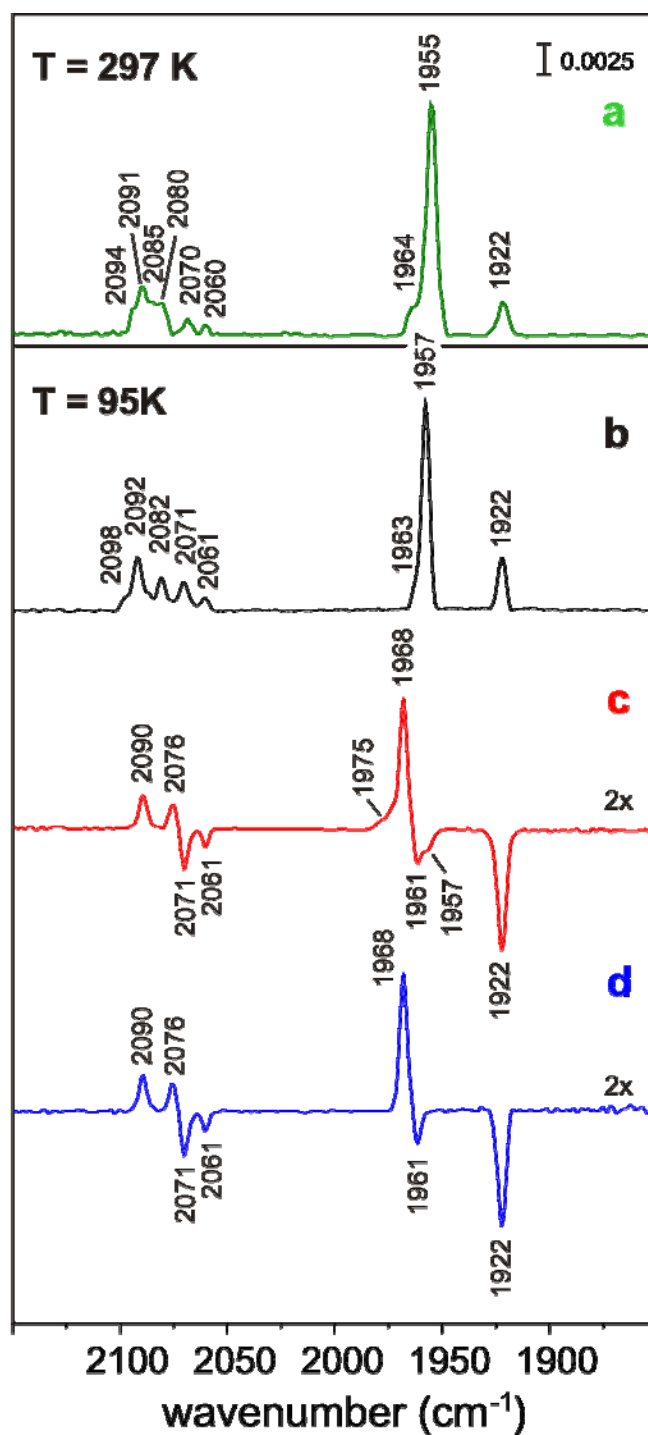
**Figure 3.** FTIR spectra of the aerobically isolated [NiFe] hydrogenase from *D.vulgaris* Miyazaki F, at 297 K (a) and 95 K (b). Light-minus-dark difference spectrum at 95 K (c) and after dark adaptation and re-illumination (d). Ni-SI$_r$ and Ni-SI$_{1961}$ are the dark educts (negative signals), which upon illumination convert to the Ni-SL product state (positive signals). The vibrational frequencies for the CO and CN$^-$ stretching vibrations are given on all spectra (see Table 1). The y axis in these figures represents the IR absorbance.

*Chapter 5*

**Low temperature FTIR measurements**

Figure 3b shows the FTIR spectrum of the aerobically isolated [NiFe] hydrogenase from *D. vulgaris* Miyazaki F at 95 K. The positions of the absorption bands at low temperatures are shifted by 0 - 5 cm$^{-1}$ in comparison to those obtained at room temperature (297 K, Table 1). This is a general property of the stretching bands observed in infrared and Raman spectroscopies [43] and is related to the restricted vibrational freedom of the oscillators.

Figure 3c shows a FTIR difference spectrum (light-minus-dark). This spectrum shows only the bands of the light sensitive states (educts, negative absorption bands) and those of the light-induced states (products, positive absorption bands). The negative CO bands observed in the spectrum correspond to Ni-SI$_r$ (1922 cm$^{-1}$) and to a new state named as Ni-SI$_{1961}$ in this work (denoted by its CO vibration at 1961 cm$^{-1}$). As a product we observed only one positive CO band (1968 cm$^{-1}$), which was associated with a new light-induced state (named Ni-SL) (Fig. 3c). The infrared spectra show that both Ni-SI$_r$ and Ni-SI$_{1961}$ convert to a light-induced product state (*i.e.* Ni-SL). However, it is not possible at this point to affirm whether Ni-SI$_{1961}$ is present in the initial dark spectrum (Fig. 3b). The presence of this band and its possible involvement in the photochemical processes observed will be described in a later section of this work. The light sensitivity observed by FTIR spectroscopy in the aerobically isolated sample was also monitored by EPR spectroscopy (X-band, ~ 9 GHz). No new EPR signals were observed upon illumination (data not shown). This suggests that the light-induced Ni-SL state is EPR-silent (Ni$^{2+}$).

In addition, Figure 3c shows a small negative CO band at 1957 cm$^{-1}$, which is associated with the fully oxidised enzyme (*i.e.* Ni-A, Ni-B), and the corresponding positive CO band (product state) at 1975 cm$^{-1}$. This indicates that a small fraction of the oxidised enzyme is also light sensitive. This effect was not reversible, when irradiation was performed with white light. Therefore, it might be related to a form of photo-degradation. Quantification based on the integrated intensity of these peaks shows that this corresponds to 4 (± 2) % of the initial amount of oxidised states. Similar light effects at cryogenic temperatures have been previously observed in the cyanobacterial-like uptake hydrogenase from *Acidithiobacillus ferrooxidans*[44].

Figure 3d shows the light-minus-dark difference spectrum after dark adaptation and re-illumination of the sample. Since the small effect on the fully oxidised enzyme was

not reversible (when illuminating with white light[§]), their corresponding bands (educts and products) do not appear in this spectrum. A similar light-minus-dark difference spectrum as for the aerobically isolated enzyme was also obtained for hydrogenase samples partially reduced with $H_2$ (data not shown), in which the amount of Ni-SI$_r$ was ~ 90 %.

**Table 1.** Stretching vibrations of the CO, CN⁻ ligands for the different states of the [NiFe] hydrogenase from *D. vulgaris* Miyazaki F measured in this work and in [25] , at 297 and 100 K.

| Frequencies IR States | T = 297 K | | | | T = 100 K | | | |
|---|---|---|---|---|---|---|---|---|
| | $\bar{v}_{CO}$ $cm^{-1}$ | $\bar{v}_{CN}$ (asym, sym) $cm^{-1}$ | | $\bar{v}_{CO}$ (ext) $cm^{-1}$ | $\bar{v}_{CO}$ $cm^{-1}$ | $\bar{v}_{CN}$ (asym, sym) $cm^{-1}$ | | $\bar{v}_{CO}$ (ext) $cm^{-1}$ |
| **Ni-B** | 1955 | 2081 | 2090 | - | 1957 | 2082 | 2092 | - |
| **Ni-A** | 1956 | 2085 | 2094 | - | 1957 | 2087 | 2098 | - |
| **Ni-SU** | 1958 | 2089 | 2100 | - | - | - | - | - |
| **Ni-SI$_r$** | 1922 | 2060 | 2070 | - | 1922 | 2061 | 2071 | - |
| **Ni-SI$_a$** | 1943 | 2074 | 2086 | - | 1946 | 2077 | 2090 | - |
| **Ni-C** | 1961 | 2074 | 2085 | - | 1963 | 2076 | 2088 | - |
| **Ni-L** | not observed | | | - | 1911 | 2048 | 2063 | - |
| **N-SL** | not observed | | | - | 1968 | 2076 | 2090 | - |
| **Ni-SI$_{1961}$** | not observed | | | - | 1961 | 2067 | 2084 | - |
| **Ni-SCO** | 1941 | 2071 | 2084 | 2056 | 1941 | 2072 | 2087 | 2061 |

**Light conversion as a function of the illumination time**

The light sensitivity of the Ni-SI$_r$ state is clearly observed in the FTIR spectra, in which this state is shown to convert to the product state Ni-SL (Fig. 3). However, the appearance of Ni-SI$_{1961}$ was unexpected. The question arises as to whether this

---

[§] These light effects were reversible when illuminating with monochromatic light (laser illumination).
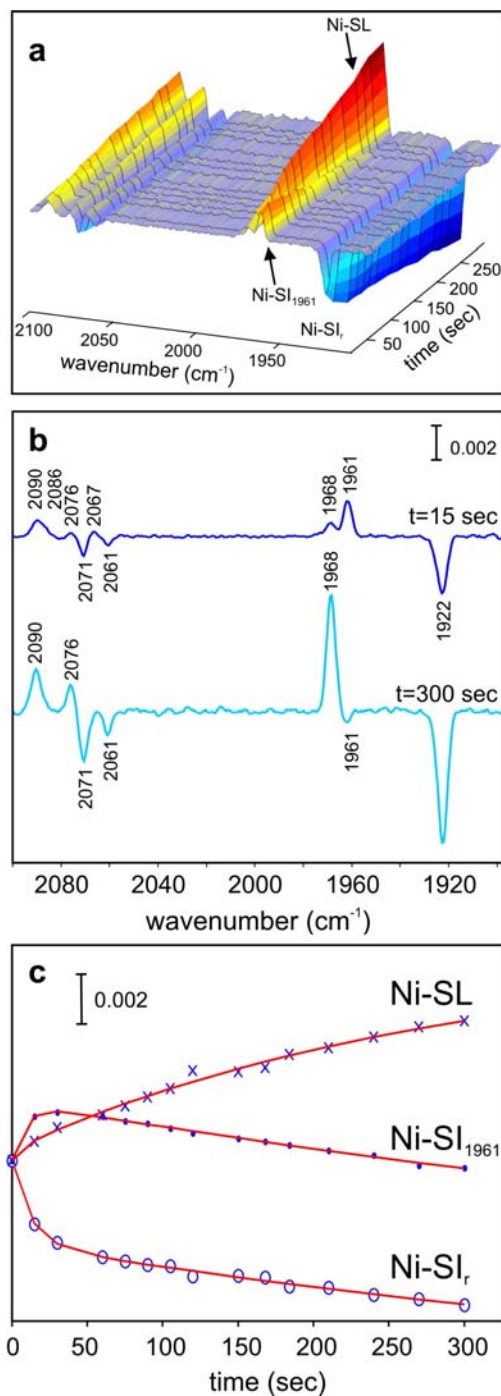
**Figure 4.** FTIR light-minus-dark difference spectra recorded at 75 K for different irradiation times: (a) 3D representation of the photo-conversion of the Ni-SI$_r$ state (1922 cm$^{-1}$) to Ni-SI$_{1961}$ and Ni-SL using white light as a function of the illumination time; (b) slices of the 3D representation at t = 15 sec and 300 sec illustrating Ni-SI$_{1961}$ as an intermediate in the reaction sequence; (c) time evolution of the light product and educt states as function of illumination time.

state was already present in the as isolated sample or whether it is somehow related to the photochemistry observed. Figure 4a shows the light-induced conversion process from $Ni\text{-}SI_r$ to Ni-SL. The three dimensional spectrum was obtained by measuring the light-minus-dark difference spectra at different intervals of illumination (from 15 sec to 300 sec) at T = 75 K. Upon illumination there is a fast conversion from $Ni\text{-}SI_r$ to $Ni\text{-}SI_{1961}$ and simultaneously, as illumination time increases, both $Ni\text{-}SI_r$ and $Ni\text{-}SI_{1961}$ convert to Ni-SL.

Figure 4b shows the light-minus-dark difference spectrum after 15 sec of illumination at T = 75 K. The negative CO peak at 1922 $cm^{-1}$ corresponds to the dark educt ($Ni\text{-}SI_r$). The two positive CO bands correspond to the light products $Ni\text{-}SI_{1961}$ and Ni-SL. The peak at 1961 $cm^{-1}$ is of larger intensity, clearly showing that $Ni\text{-}SI_r$ converts initially to $Ni\text{-}SI_{1961}$. The vibrational frequencies of the conjugate $CN^-$ corresponding to $Ni\text{-}SI_{1961}$, 2086 and 2067 $cm^{-1}$, could be identified from this spectrum (Table 1). Figure 4b shows also the light-minus-dark difference spectrum after 300 sec of illumination at 75 K, in which only the Ni-SL state is observed as the final light product.

Figure 4c shows the time-dependent forward conversion of the three states; transient rise/decay of $Ni\text{-}SI_{1961}$, formation of Ni-SL and disappearance of $Ni\text{-}SI_r$. These curves were obtained from the apparent integrated intensity of the respective CO bands. The time axis represents illumination time in seconds. The decrease of $Ni\text{-}SI_{1961}$ to negative values shows that a small fraction of $Ni\text{-}SI_r$ converted to the $Ni\text{-}SI_{1961}$ state, already in the absence of an external light source (dark conditions). This partial conversion was due to the spectrometer-integrated He-Ne laser ($\lambda = 633$ nm, see Materials and Methods). The $Ni\text{-}SI_{1961}$ state is suggested to be a local minimum in the potential surface of the transition from $Ni\text{-}SI_r$ to its final product Ni-SL.

**Kinetic measurements and isotope (H/D) exchange effect**

Figure 5a depicts the recovery of the absorption bands in the light-minus-dark difference FTIR spectrum at T = 95 K. Continuous illumination was carried out for 5 min as described in Material and Methods. The first slice of the three-dimensional spectrum corresponds to time t = 0, when the light source was switched off
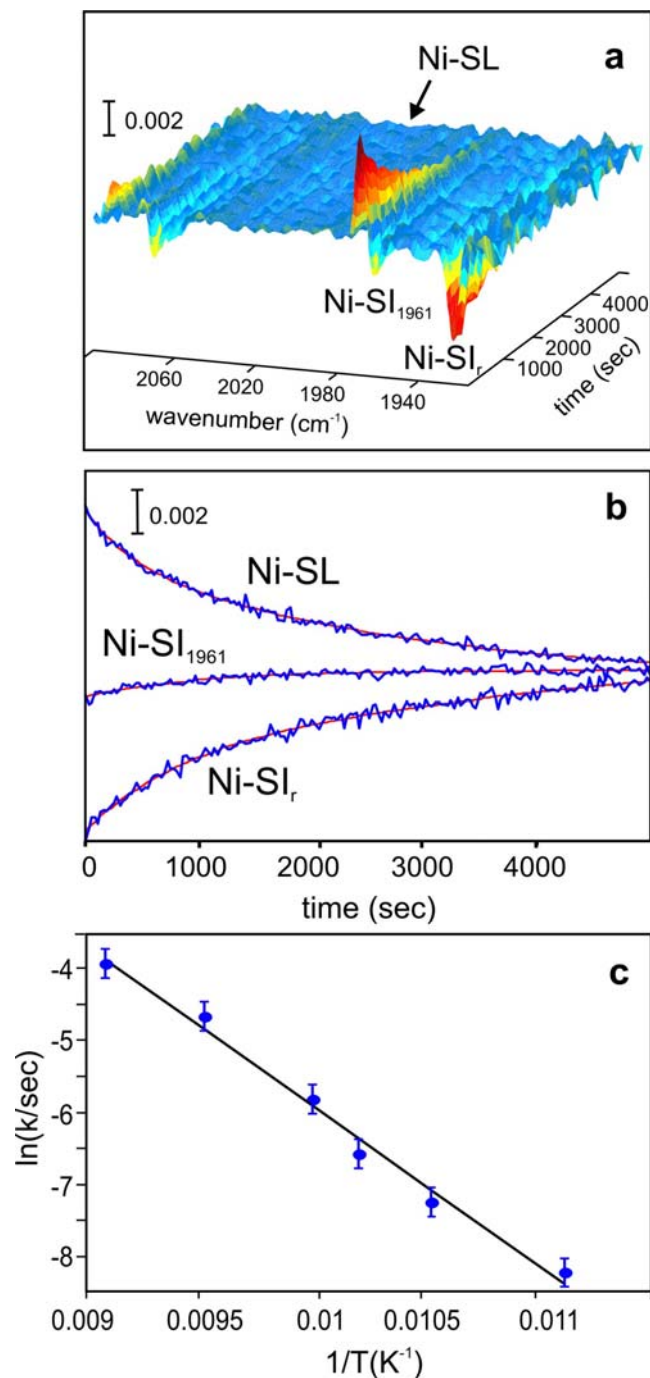
**Figure 5.** Time dependence of the recovery of the Ni-SI$_r$, Ni-SI$_{1961}$ states and the decay of the Ni-SL state at T = 95 K directly after switching off the light (a) 3D representation of the FTIR light-minus-dark difference rapid scan spectrum. (b) Decay kinetics of Ni-SL (1968 cm$^{-1}$, $\tau$ = 1394 sec) and recovery kinetics of Ni-SI$_r$ (1922 cm$^{-1}$, $\tau$ = 2203 sec) and Ni-SI$_{1961}$ (1961 cm$^{-1}$, $\tau$ = 1305 sec). The y axis represents the IR absorbance. (c) Temperature dependence (90 K $\leq$ T $\leq$ 110K) of the decay rate constants for the Ni-SL state (Arrhenius plot).

(maximum light-minus-dark difference) and the subsequent slices show how the FTIR absorption bands disappear/recover in the dark (Ni-SL, Ni-SI$_r$ and Ni-SI$_{1961}$).

The light-induced effects associated with these states are fully reversible. During back conversion there is no transient increase of the Ni-SI$_{1961}$, which indicates that only Ni-SL to Ni-SI$_r$/Ni-SI$_{1961}$ conversion and vice versa can be observed at temperatures T $\geq$ 80 K. The transition from Ni-SL to Ni-SI$_r$ presumably still occurs via the Ni-SI$_{1961}$ state, but under these conditions is too fast to be resolved.

Figure 5b shows the kinetics during dark adaptation of the educt and product states after 5 min of continuous illumination at 95 K. Assuming a single exponential decay/increase of the signals, the corresponding rate constants were estimated. The Ni-SI$_{1961}$ state recovers 1.5 times faster than the Ni-SI$_r$ state. The kinetics of the Ni-SL disappearance has intermediate values between the recovery kinetics observed for Ni-SI$_r$ and Ni-SI$_{1961}$. The rate constants exhibited a temperature dependence, which shows that the light-induced processes are associated with an activation energy barrier (E$_a$).

Figure 5c shows the temperature dependence of the measured rate constants corresponding to the decay of the Ni-SL state in the temperature range between 90 and 110 K. Similar plots were obtained for the Ni-SI$_r$ and Ni-SI$_{1961}$ (see Appendix C). The activation energies for Ni-SI$_r$, Ni-SI$_{1961}$ and Ni-SL were obtained from the linear behaviour of the temperature dependence of all rate constants using the Arrhenius equation (see Materials and Methods). Similar activation energies were obtained within the error for the Ni-SI$_r$, Ni-SI$_{1961}$ and Ni-SL states (Table 2).

To study a possible isotope effect on the rate constants, samples were prepared in which the potential third bridging ligand (*e.g.* OH$^-$) [4,5,24] was exchanged with its deuterated form (OD$^-$). The activation energies for the isotopically (H/D) exchanged samples were also determined from the Arrhenius dependence of the kinetic rates. The results showed slightly larger activation energies for the samples containing the deuterated form of this ligand (Table 2 and Appendix C).

**Table 2.** Activation energies for the recovery of the Ni-SI$_r$ and Ni-SI$_{1961}$ states and for the decay of Ni-SL, obtained by the temperature dependence of the rate constants (see text).

| | H$_2$O | D$_2$O |
|---|---|---|
| Activation energy | E$_a$ (kJ/mol) | E$_a$ (kJ/mol) |
| State | | |
| Ni-SI$_r$ | 18.9 ± 1.4 | 20.3 ±0 .8 |
| Ni-SI$_{1961}$ | 17.6 ± 1.5 | 19.8 ± 1.1 |
| Ni-SL | 18.5 ± 0.8 | 20.6 ± 0.7 |

**Reversible light effects in the presence of CO**

In the light-induced process from Ni-SI$_r$ to Ni-SL the fate of the oxygen based bridging ligand is not clear. This ligand is either completely dissociated from the active site or displaced towards Ni, presumably as a consequence of loss of its bond to Fe (as reflected by the shift of the infrared frequencies, see Discussion). It is known from extensive stopped-flow studies on *A. vinosum*[20,29,40] that the oxidised states Ni-A, Ni-B and Ni-SI$_r$ are not CO sensitive. However, Ni-SI$_a$ and Ni-L are CO sensitive, allowing its binding to the active site (Figure 2). This suggests that for CO binding to take place, the bridging ligand must be absent[38]. In the case of complete dissociation of the bridging ligand dark adaptation of the Ni-SL in the presence of CO would lead to formation of a CO inhibited state, whereas in the case of its displacement towards nickel this ligand would still block the entrance to the active site precluding binding of CO. An experiment was thus designed in which the solution of reduced hydrogenase (ca -300 mV, *vs* NHE), containing mainly the Ni-SI$_r$ and Ni-SI$_a$ states, was saturated with carbon monoxide.

A high yield of the Ni-SCO state (approximately 80 %) was obtained with the rest of the hydrogenase molecules being in the Ni-SI$_r$ state. Illumination with white light at T = 40 K converted simultaneously Ni-SCO to Ni-SI$_a$, as described earlier[26], and Ni-SI$_r$ to Ni-SL. After dark adaptation at higher temperatures no decrease in the intensity of the Ni-SI$_r$ band was observed within error (data not shown). This shows that exogenous CO does not have the affinity to bind to the active site in the Ni-SL state.

**Wavelength dependence of the Ni-SI$_r$ light sensitivity**

The transition from Ni-SI$_r$ to the Ni-SI$_{1961}$ and Ni-SL states was also studied as a function of the excitation wavelength ($\lambda$) of the incident light. The results (*i.e.* the 'action spectrum') at 40 K are depicted in Figure 6. This 'action' spectrum describes the overall efficiency of the irradiation at a specific wavelength for the photochemical conversion (*i.e.* %) from Ni-SI$_r$ to Ni-SL to occur. Two local maxima at 490 and 600 nm were observed, which can be associated with Ni centred electronic transitions (see Discussion).

In addition, the wavelength dependence of the transient appearance of the Ni-SI$_{1961}$ state was studied at 75 K, as at temperatures below 60 K, the lifetime of this state was too short to be observed as an intermediate in the forward light conversion.
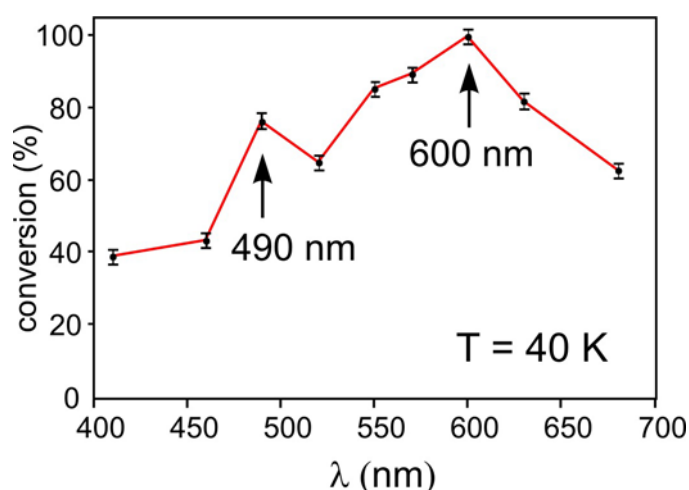


**Figure 6.** Photo-conversion (%) of the Ni-SI$_r$ state as a function of the irradiation wavelength ($\lambda$) at 40 K. The resulting 'action spectrum' shows local maxima at 490 nm and 600 nm, that can be associated with Ni centred d-d transitions upon light excitation.
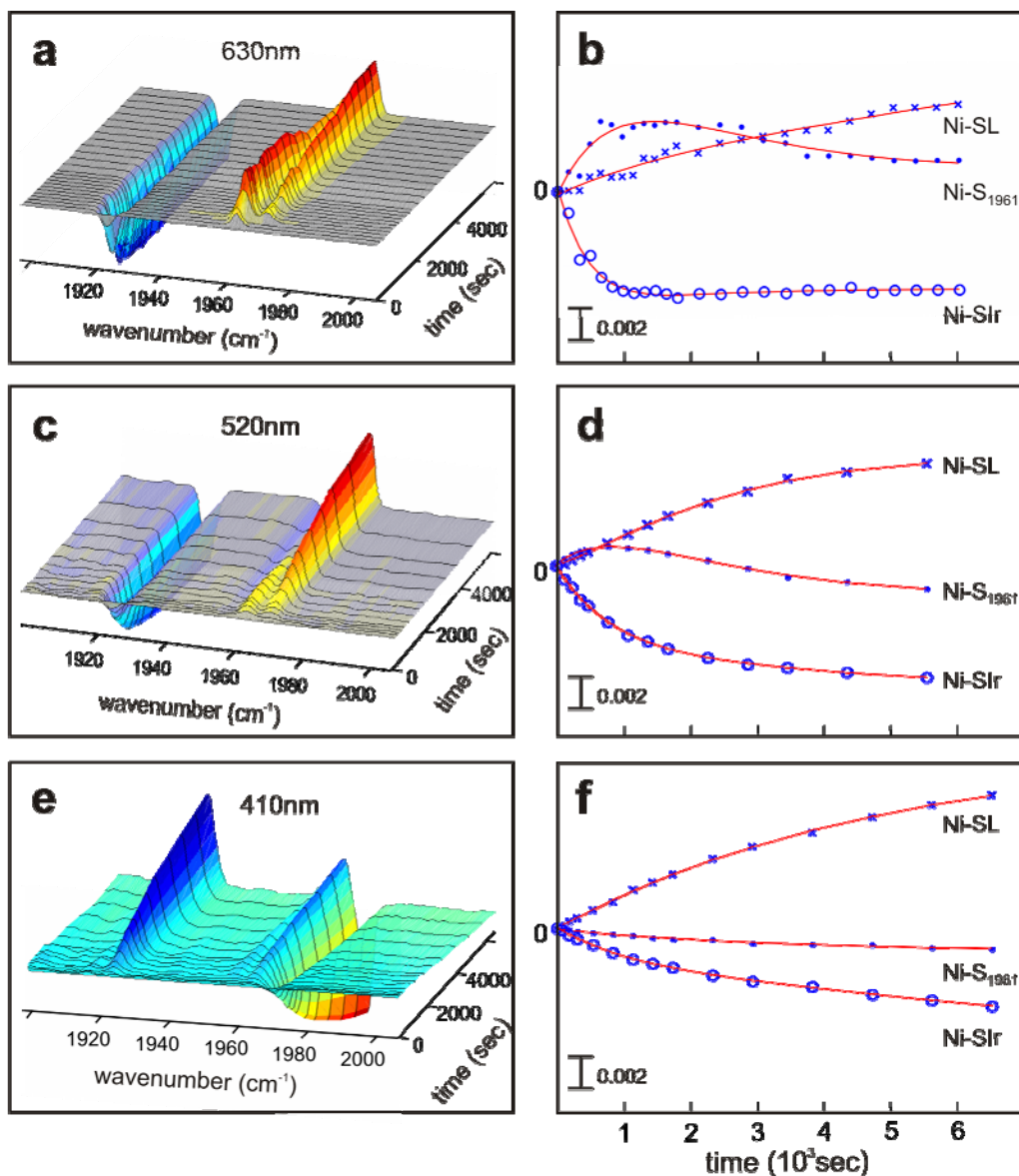
**Figure 7.** Representation of the forward photo-conversion of the Ni-SI$_r$ state to the product states Ni-SI$_{1961}$ and Ni-SL at three selected wavelengths $\lambda$ = 630 nm (a, b), $\lambda$ = 520 nm (c, d) and $\lambda$ = 410 nm (e, f) at 40 K. Both the 3D spectra are given (a, c, e) and plots of the time-dependent kinetics of the appearance/disappearance of the product/educt states, respectively as function of time (b, d, f). In (e) the 3D spectrum has been inverted (educt/product states as positive/negative signals, respectively), to better visualise the disappearance of the Ni-SI$_{1961}$ state.

Figure 7 shows the development of light-minus-dark difference spectra as a function of the irradiation time at three selected wavelengths. At $\lambda = 630$ nm (red light), the Ni-SI$_r$ state rapidly converts first to the transient Ni-SI$_{1961}$ state and to a smaller extent to the Ni-SL state. Subsequently, Ni-SI$_{1961}$ is depleted and Ni-SL is populated. The Ni-SI$_{1961}$ state can therefore be considered as a true intermediate state in this reaction. At $\lambda = 520$ nm (green), light transition from Ni-SI$_r$ to Ni-SI$_{1961}$ takes place to a much smaller extent, while both states convert to Ni-SL. It can be seen that the CO band corresponding to Ni-SI$_{1961}$ becomes positive but decreases to negative values, as a small fraction of this state is already present under dark conditions. For $\lambda = 410$ nm (violet), the spectrum is depicted as a dark-minus-light spectrum to better illustrate the observed processes. Illumination at this wavelength shows that in this transition the Ni-SI$_{1961}$ could not be resolved as an intermediate of the photo-reaction. These results demonstrate that the conversion of Ni-SI$_r$ to Ni-SI$_{1961}$ and subsequently to Ni-SL is strongly temperature and wavelength dependent.

Figure 8 shows that for the Ni-SL state, depending on the excitation wavelength, the stretching modes for the coupled CN$^-$ ligands were shifted, while the frequency position of the CO band remained the same. For irradiation with red light (Figure 8a) the coupled CN$^-$ of Ni-SL are observed at 2075, 2084 cm$^{-1}$, while at $\lambda = 410$ nm (Figure 8b) four overlapping CN$^-$ bands are present in the spectra corresponding to a conjugate CN$^-$ pair with frequency values of 2075, 2084 cm$^{-1}$ and to a second pair of coupled stretching vibrations with 2076, 2090 cm$^{-1}$. If illumination is carried out with white light (halogen lamp, Figure 8c) only the pair with stretching vibrations at 2076, 2090 cm$^{-1}$ is observed. In all cases, the CO absorption band appears at the same frequency position (1968 cm$^{-1}$). The invariance of the CO band upon $\lambda$-dependent illumination precludes a change of the electron density at the Fe between these two light induced forms of Ni-SL, as this would lead to a shift of all three stretching bands (CO and CN$^-$). The temperature and $\lambda$-dependence of only the CN$^-$ modes therefore indicates a change of the hydrogen bonding with the surrounding amino acids, as described in the Discussion section.
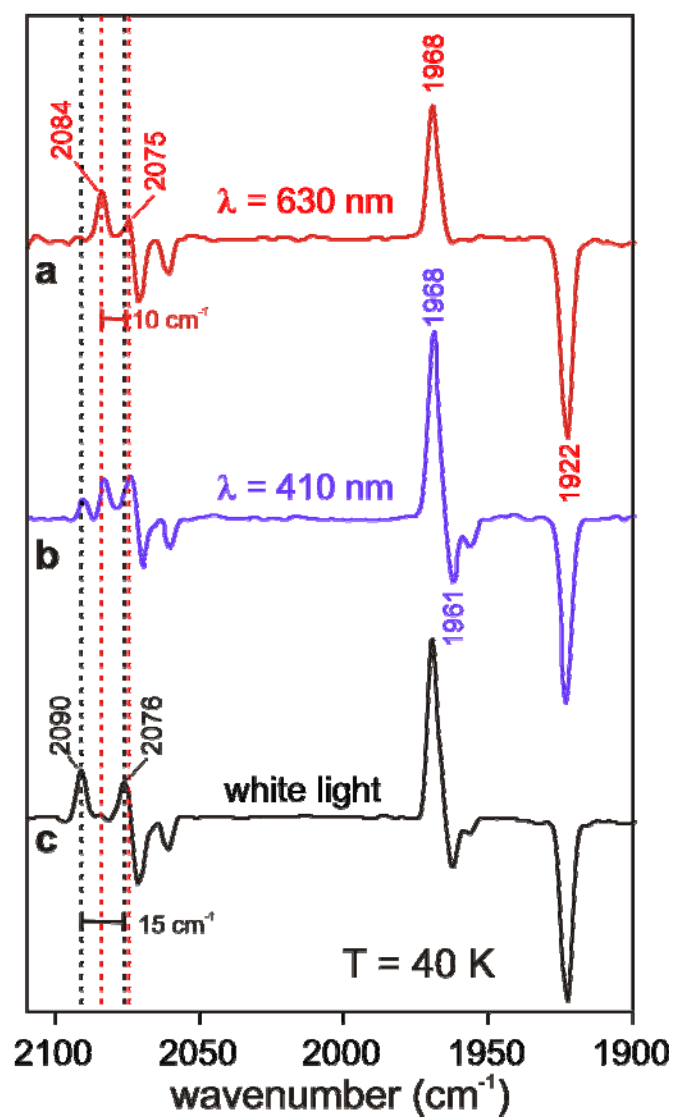
**Figure 8.** FTIR light-minus-dark difference spectra for incident irradiation with (a) red light ($\lambda$ = 630 nm), (b) violet light ($\lambda$ = 410 nm) and (c) white light (halogen lamp) at 40 K. Note that dependent on the colour of the light the Ni-SL state shows different pairs of conjugate CN$^-$ stretching vibrations, as indicated with dashed lines (see text).

## Discussion

### i) **Light-associated effects on the structure of Ni-SI$_r$**

The silent ready state Ni-SI$_r$ in the [NiFe] hydrogenases represents the link between the fully oxidised and the reduced active enzyme. However, up to date the characterization of this state has been rather elusive due to its inaccessibility to EPR studies and the difficulty to create pure states for other structural investigations[45]. In this work possible structural and electronic properties of Ni-SI$_r$ are discussed on the basis of its light sensitivity.

The infrared spectrum of the aerobically isolated enzyme from *D. vulgaris* contains mainly bands corresponding to Ni-A, Ni-B and Ni-SI$_r$. An additional band at 1964 cm$^{-1}$ was ascribed to a not-identified state (Ni-SI$_{1964}$), which presumably originates from the enzyme purification procedure. The Ni-A and Ni-B states (Ni$^{3+}$) exhibited a small light sensitivity (*i.e.* 4 % ± 2 % of their overall intensity, Fig. 3c). This shows that the bridging ligand present in these oxidised states (a hydroxide (OH$^-$) in Ni-B[4,21] and the proposed hydroperoxide (OOH$^-$) in

Ni-A[13,14]) is thus quite tightly bound to the Ni$^{3+}$- Fe$^{2+}$ centre.

On the other hand, upon illumination at cryogenic temperatures (T ≤ 110K), Ni-SI$_r$ was shown to convert to a new light-induced state (Ni-SL). Our experiments showed that this light-induced transition involves an intermediate transient state (Ni-SI$_{1961}$), which was best detected in the temperature range between 60 and 80 K (Fig. 4). EPR spectroscopy showed that Ni-SL is EPR-silent, indicating that the photochemical process is not related to a change in the oxidation state of nickel, which remains divalent (d$^8$, Ni$^{2+}$). The light-induced process was fully reversible.

The CO and CN$^-$ stretching bands corresponding to the Ni-SL state are all shifted to higher wavenumbers as compared to those from Ni-SI$_r$ (Figure 3 and Table 1). This correlates with a decrease in the electron density at the Fe[46] in the light-induced state (Ni-SL). Since all the photochemical properties observed so far in the [NiFe] hydrogenases are associated with dissociation of a non-protein ligand bound to the active site[26,32,38], this effect can, in principle, be associated with the removal or displacement of a negatively charged ligand. Since the Fe$^{2+}$ ion is strongly coordinated to the π- and σ- ligands (two CN$^-$ and one CO) and to the sulphurs from Cys84 and Cys549 residues (Figure 1), the most likely candidate is the bridging hydroxide (OH$^-$).

A shift towards higher vibrational frequencies has been also observed during the light-induced transition from Ni-SCO to Ni-SI$_a$[26], which is associated with the dissociation of the extrinsic CO. However, in the photo-conversion from Ni-C to Ni-L[46], a shift towards lower wavenumbers was observed. To explain the difference in the direction of shift, it has been proposed that the dissociation of H$^-$ is followed by a protonation of a co-ordinating cysteinyl ligand, which would affect the electron density at the Fe$^{2+}$ ion in a different way. The question arising now is whether the OH$^-$ ligand remains bound to Ni in the Ni-SL state. To answer this question, additional experiments in the presence of CO were performed (see Results). The results showed that CO does not bind to the active site in the Ni-SL state. This indicates that the active site remains blocked by the OH$^-$ ligand precluding thus the binding of CO.

Based on these observations and the detected shift in the stretching vibrations, we propose that the light-induced transition from Ni-SI$_r$ to Ni-SL involves an opening of the OH$^-$ bridge as depicted in Scheme 1. This displacement of the hydroxide ligand is facilitated by the weakening of the OH$^-$ binding to the more electron-rich nickel Ni$^{2+}$. The shift in the vibrational bands observed for Ni-SI$_{1961}$ is smaller than that observed for Ni-SL. Thus, the intermediate state might represent a structure, in which the OH$^-$ ligand is far less dislocated from the iron. The absolute intensity of the CN$^-$ bands with respect to the CO band between Ni-SI$_{1961}$ and Ni-SL is different, which might also indicate a change in the hydrogen bonds with the nearby amino acids[47].
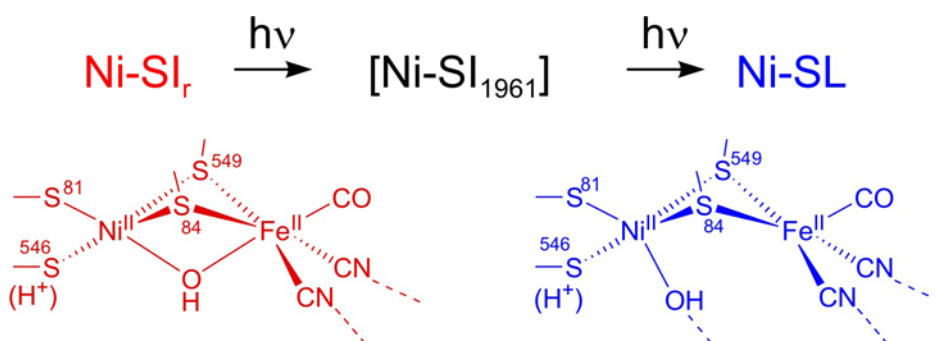


**Scheme 1.** Schematic chemical structures for the Ni-SI$_r$ and Ni-SL states.

The temperatures dependence of the kinetic rates corresponding to the back conversion processes (Ni-SL→Ni-SI$_r$, Ni-SL→Ni-SI$_{1961}$), provided the activation

energies ($E_a$), a measure of the energy barrier required to get back from the photoproduct (Ni-SL) to the initial state(s). Even though the recovery rates corresponding to Ni-SI$_r$ and Ni-SI$_{1961}$ are different (Fig. 5b) the activation energies are very similar (Table 2). Furthermore, the (H/D) isotope effect on the recovery kinetic rates was studied (Table 2). The magnitude of the isotope effect in our experiments (KIE = 0.6 - 1.4, see Appendix C) was too small to be related to the dissociation of a single hydron/deuteron species[48,**] as observed for the Ni-C to Ni-L transition. This result therefore suggests that the light induced effect is not related to a (de)protonation of a co-ordinating cysteine[30] or a release of a hydron located in the active site[49]. Thus, the (H/D) isotope effect observed in this work, can be better explained considering the dislocation of an oxygen based species[5,14,50] that has the potential to be deuterated (e.g. OH$^-$).

The small increase in mass introduced by the isotope labelling (e.g. OD$^-$) is expected to affect slightly the values of the kinetic rates. This is in agreement with our results, supports the proposed reaction shown in scheme 1 and further rules out processes involving a (de)protonation of a co-ordinating cysteine[30] or the release of a hydron located in the active site[49].

The activation barrier for the transition of Ni-SL→Ni-SI$_r$ and Ni-SL→Ni-SI$_{1961}$ was found to be 18-19 kJ/mol. Such a value lies well within the range of energies corresponding to related hydrogen bonds (15 - 40 kJ/mol)[51]. This would mean that back conversion from Ni-SL to the Ni-SI$_r$/Ni-SI$_{1961}$ states could involve the breaking of a hydrogen bond to surrounding amino acids. From the crystal structure of the Ni-B state it can be deduced that the OH$^-$ ligand at the nickel might be in a favourable position to form a hydrogen bond to Arg479 (see below).

**ii) Wavelength-dependence of the Ni-SI$_r$ photo-conversion**

It was found that light excitation of Ni-SI$_r$ is described by a broad absorption in the visible region between 410 and 680 nm (Figure 6). In this 'action spectrum' two local maxima were observed at 490 and 600 nm. Optical studies on Ni$^{2+}$ complexes with sulphur based ligands [52,53] showed bands in MCD spectra close to these values, which were associated with d-d transitions of the Ni d$^8$ ion. It can thus be assumed that in the case of Ni-SI$_r$ the 'action spectrum' shows that the photochemical process

---

** In such a case the kinetic isotope effect should be between 5-7 [48].

is associated with electronic excited states of the Ni ion. While Ni-L-Edge XAS spectroscopy cannot clearly discern whether the nickel ion in Ni-SI$_r$ is in a low (S = 0) or a high spin (S = 1) configuration[36], theoretical data[37] indicate a low spin Ni$^{2+}$. The light-induced electronic transitions (Fig. 6) could involve a change in the spin state of Ni from a low spin (d$^8$, S = 0) to a high spin (d$^8$, S = 1) configuration as a result of the redistribution of the electronic charge in the d-orbitals of the metal. Such light induced spin crossover transitions have been shown to involve a ligand rearrangement[54]. A change from low spin to high spin could in turn trigger a structural change of the ligand sphere effectively leading to the observed opening of the bridge of the NiFe centre.

At T = 40 K and at all excitation wavelengths, Ni-SI$_{1961}$ was not observed as an intermediate in the forward transition of Ni-SI$_r$ to Ni-SL. At higher temperatures, however, (*e.g.* in the range 60 K < T < 80 K) the λ- dependent forward photo-conversion of Ni-SI$_r$ involved the Ni-SI$_{1961}$ as a detectable intermediate (Ni-SI$_r$ → Ni-SI$_{1961}$→ Ni-SL) (Fig. 7). The amount of the light-induced Ni-SI$_{1961}$ species depended greatly on the excitation wavelength, being maximal in the red ( > 600 nm). However, since the optical transitions of the Ni$^{2+}$- Fe$^{2+}$ site are not known, it is difficult at present to elucidate a mechanism for the light-triggered evolution of the different states observed in our experiments.

**iii) H-bond network in the active site surroundings**

The putative hydrogen bonds between the active centre of the [NiFe] hydrogenase from *D. vulgaris* Miyazaki F and the surrounding amino acids are shown in Fig. 9. The formation of a H-bond between the sulphur of the bridging Cys549 and His88 is well established and has been studied for different states[55,56,57]. In addition, each of the CN$^-$ ligands at the Fe can potentially form up to two H-bonds as indicated in Fig. 9, whereas the CO ligand is surrounded by more hydrophobic residues and is thus not hydrogen bonded. It is well known that the environment of such iron ligands greatly affects the redox properties of the central metal[58,59].

Among the amino acids in the surrounding of the active site, an arginine residue (Arg479) is located very close to the bridging OH$^-$ ligand (Figure 9). This arginine is highly conserved among the various hydrogenases and is believed to be protonated and positively charged[60]. It is hydrogen bonded to one of the CN$^-$ ligands and to two negatively charged aspartates (Asp123, Asp544). The light-induced transition from
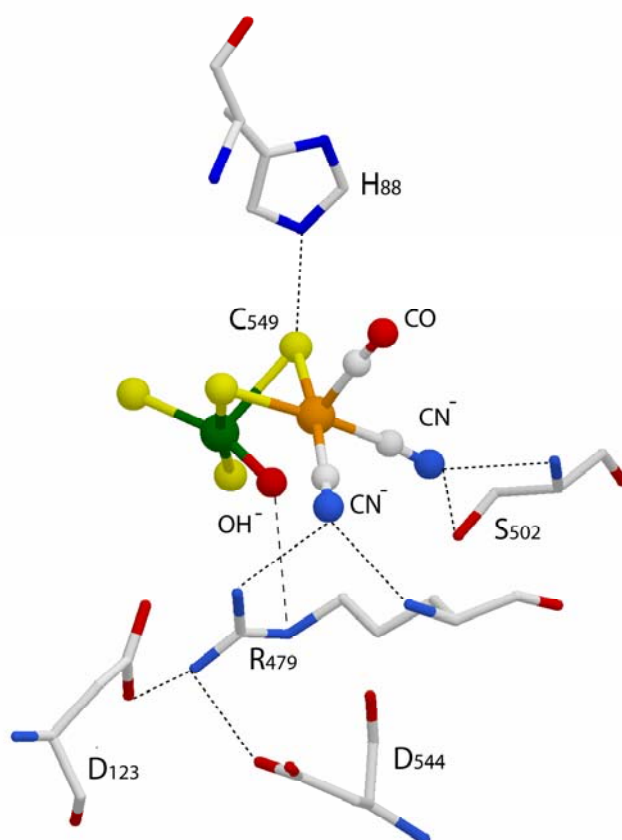
**Figure 9.** Proposed structure of the active site of the NiFe hydrogenase from *D. vulgaris* Miyazaki F in the Ni-SL state (based on the structure of Ni-B; 1WUJ pdb). The amino acid residues His88, Arg479 and Ser502 and part (backbone) of Pro480 and Pro501 are shown. The putative hydrogen bonds to the direct ligands of the Ni-Fe complex are represented with dashed lines. Note that the hydroxide bridge, present in Ni-SI$_r$ has been opened in this structure and the OH$^-$ ligand at the nickel is H-bonded to Arg479.

Ni-SI$_r$ to Ni-SL is proposed to involve a displacement of the hydroxide ligand to a position closer to Ni (Scheme 1). Since Arg479 is considered to be protonated (pK$_a$ ~ 12), this ligand re-arrangement would result in a hydrogen bond between the oxygen of the hydroxide and the NH of Arg479 (see Figure 9), with an O-N distance in the range of 3.0 - 3.4 Å. It can be speculated that the intermediate Ni-SI$_{1961}$ in the reaction sequence represents a pathway species with an opened OH$^-$ bridge that has

no - or weaker - H-bond interactions with the surrounding compared to the final Ni-SL state.

In the same figure the putative hydrogen bonds between the $CN^-$ ligands and the amino acid residues Arg479 and Ser502 as well as with the backbone NH of the two prolines[††] are shown. The vibrational frequencies of these ligands depend therefore, not only on the electron density on the Fe but also on the strength of the hydrogen bonding network[61]. In our experiments the stretching vibrations of the $CN^-$ in Ni-SL were observed to be affected by the wavelength of the exciting light (Figure 8). On the other hand, the respective $\bar{v}_{CO}$ were not sensitive to the colour of the monochromatic irradiation. Since the $CN^-$ ligands – but not the CO – are H-bonded to surrounding amino acids, it can be assumed that a change of the hydrogen bonding network is responsible for this observation. In support of our experiments, a shift in the infrared frequencies only of the $CN^-$ was observed in a study where the Ser residue (Ser502 in *D. vulgaris*; Ser499 in *D. fructosovorans*) was mutated to an alanine[47], which is incapable of forming a H-bond.

Figure 8a shows that at 40 K illumination in the red shifts the $CN^-$ bands to lower frequencies compared to illumination with white light (Fig. 8c). Such a shift to lower values indicates a weakening in the hydrogen bonding[61,62,63] interactions of these ligands with the surrounding amino-acid residues. Illumination in the violet ($\lambda = 410$ nm, Figure 8b) on the other hand, resulted in the simultaneous appearance of two pairs of vibrationally coupled $CN^-$. This observation is important as it shows that transition from one form of Ni- SL (red light-induced spectrum) to the second form (white light-induced) is characterized by distinct electronic levels. In co-ordination chemistry there are examples of Fe compounds, ligated by cyanides and nitrosyls, where light-induced isomers of the diatomic ligands can be observed at low temperatures. In such light-induced 'linkage isomers' (metastable states) the metal is co-ordinated (*e.g.* in nitrosyls) by the oxygen instead of the nitrogen[64,65]. It might be speculated that in the case of hydrogenase, a Fe-N-C could be realised[66,67] upon increasing the irradiation wavelength and decreasing the temperature ($T \leq 40$ K). This would result in the loss of the hydrogen bond to one of the amino acid residues and the concomitant shift of the $CN^-$ vibrations towards lower frequencies[47], as observed

---

[††] Hydrogen bonds with the backbone of Pro480 and Pro501 are considered less likely as mutation experiments have shown that substitution of Pro480 with alanine had no effect in the infrared spectra.[48]

in our experiments. Such a situation however, is purely hypothetical as it is not known whether it is possible to occur in a protein environment.

In addition, the CN⁻ vibrations shift in the same direction, but the magnitudes and intensities are different (Figure 8). This indicates a change in the coupling between the CN⁻ oscillators, which however remain conjugated. From these results and the invariance of the CO frequency band between these two Ni-SL forms, it becomes evident that changing the irradiation wavelength affects only the CN⁻ stretching vibrations, *i.e.* the hydrogen bonding interactions, and not the electron density at the Fe metal. The existence of the surrounding

H-bond network and /or electrostatic interactions is therefore important for stabilising and 'tuning' the active site conformation.

*Chapter 5*

## Summary and Conclusions

The FTIR data presented in this work provided an effective means to characterize the active site of Ni-SI$_r$. Conformational changes upon exposing Ni-SI$_r$ to light (T $\leq$ 110 K) are observed by the appearance of new product states. These changes consist of a structural re-arrangement of the negatively charged hydroxide ligand (OH$^-$), proposed to ligate the active site. The light-induced re-orientation of the oxygen based species involves a transient intermediate (Ni-SI$_{1961}$) prior to reaching Ni-SL as final steady state. Such a displacement is facilitated by the weakening of the OH$^-$ binding to the more electron-rich nickel Ni$^{2+}$, in contrast to the more oxidised Ni$^{3+}$ species. In support of this statement, only a minor light sensitivity was observed for the Ni-A and Ni-B states. Based on the X-ray diffraction data of the Ni-B state, we propose that the position of the hydroxide in Ni-SL can be stabilised by the formation of a hydrogen bond to Arg479. From this position, the oxygen based ligand is still blocking access to the active site, as it remains presumably coordinated to the nickel ion. This was presented by the inability of extrinsic carbon monoxide to bind to nickel. Therefore, upon illumination the oxygenic ligand is being spatially displaced rather than fully dissociated. Wavelength dependent irradiation showed indeed nickel centred electronic transitions, which could involve a light-induced spin crossover from a low spin Ni$^{2+}$ (S = 0) to a high spin Ni$^{2+}$ (S = 1). However, to uniquely assign these transitions further MCD measurements are needed. The hydrogen bonding and/or electrostatic interactions of the active site with the neighbouring amino acid residues were shown to be modulated by the colour of the monochromatic light. Spectral changes associated only with the CN$^-$ and not with the CO, preclude a change in the Fe electron density, as the CO has been shown to be approximately 2-3 times more sensitive to electronic changes compared to the cyanides[63]. We propose that the reason for the 'perturbation' of the H-bond network around the CN$^-$ ligands as presented in our experiments could be caused by a light-induced isomerisation. To prove this assumption further experiments including labelling of the intrinsic CN with $^{13}$C, $^{15}$N are required.

In the re-activation scheme, the oxygenic species has to be released from the active centre in order for the enzyme to be functional. From the results of the present study we conclude that an oxygen based ligand (*i.e.* OH$^-$) is still bound to the active site,

which hinders the enzymatic activity. In Ni-SI$_r$ the binding strength of this species is found to be attenuated compared to Ni-A and Ni-B. Illumination of Ni-SI$_r$ with light at T $\leq$ 110 K was adequate to overcome the activation energy barrier for the displacement of this ligand.

## Acknowledgements

# References

1. Vignais, P. M. and Billoud, B. (2007) Chem Rev **107,** 4206-4272

2. Albracht, S. P. (1994) Biochim Biophys Acta **1188,** 167-204

3. Volbeda, A., Charon, M. H., Piras, C., Hatchikian, E. C., Frey, M., and FontecillaCamps, J. C. (1995) Nature **373,** 580-587

4. Lubitz, W., Reijerse, E., and van Gastel, M. (2007) Chem Rev **107,** 4331-4365

5. Fontecilla-Camps, J. C., Volbeda, A., Cavazza, C., and Nicolet, Y. (2007) Chem Rev **107,** 4273-4303

6. Nicolet, Y., Lemon, B. J., Fontecilla-Camps, J. C., and Peters, J. W. (2000) Trends Biochem Sci **25,** 138-143

7. Silakov, A., Reijerse, E. J., Albracht, S. P. J., Hatchikian, E. C., and Lubitz, W. (2007) J Am Chem Soc **129,** 11447-11458

8. Shima, S., Pilak, O., Vogt, S., Schick, M., Stagni, M. S., Meyer-Klaucke, W., Warkentin, E., Thauer, R. K., and Ermler, U. (2008) Science **321,** 572-575

9. Higuchi, Y., Yagi, T., and Yasuoka, N. (1997) Structure **5,** 1671-1680

10. Pierik, A. J., Roseboom, W., Happe, R. P., Bagley, K. A., and Albracht, S. P. J. (1999) J Biol Chem **274,** 3331-3337

11. Higuchi, Y., Ogata, H., Miki, K., Yasuoka, N., and Yagi, T. (1999) Structure **7,** 549-556

12. Lamle, S. E., Albracht, S. P. J., and Armstrong, F. A. (2004) J Am Chem Soc **126,** 14899-14909

13. Volbeda, A., Martin, L., Cavazza, C., Matho, M., Faber, B. W., Roseboom, W., Albracht, S. P. J., Garcin, E., Rousset, M., and Fontecilla-Camps, J. C. (2005) J Biol Inorg Chem **10,** 239-249

14. Ogata, H., Hirota, S., Nakahara, A., Komori, H., Shibata, N., Kato, T., Kano, K., and Higuchi, Y. (2005) Structure **13,** 1635-1642

15. van der Zwaan, J. W., Albracht, S. P. J., Fontijn, R. D., and Roelofs, Y. B. M. (1986) Biochim Biophys Acta **872,** 208-215

16. Lamle, S. E., Albracht, S. P. J., and Armstrong, F. A. (2005) J Am Chem Soc **127,** 6595-6604

17. Zorin, N. A., Dimon, B., Gagnon, J., Gaillard, J., Carrier, P., and Vignais, P. M. (1996) Eur J Biochem **241,** 675-681

18. Vincent, K. A., Belsey, N. A., Lubitz, W., and Armstrong, F. A. (2006) J Am Chem Soc **128,** 7448-7449

19. Fernandez, V. M., Hatchikian, E. C., Patil, D. S., and Cammack, R. (1986) Biochim Biophys Acta **883,** 145-154

20. Kurkin, S., George, S. J., Thorneley, R. N. F., and Albracht, S. P. J. (2004) Biochemistry **43,** 6820-6831

21. van Gastel, M., Stein, M., Brecht, M., Schroeder, O., Lendzian, F., Bittl, R., Ogata, H., Higuchi, Y., and Lubitz, W. (2006) J Biol Inorg Chem **11,** 41-51

22. Volbeda, A. and Fontecilla-Camps, J. C. (2005) Coord Chem Rev **249,** 1609-1619

23. De Lacey, A. L., Hatchikian, E. C., Volbeda, A., Frey, M., FontecillaCamps, J. C., and Fernandez, V. M. (1997) J Am Chem Soc **119,** 7181-7189

24. Bleijlevens, B., van Broekhuizen, F. A., de Lacey, A. L., Roseboom, W., Fernandez, V. M., and Albracht, S. P. J. (2004) J Biol Inorg Chem **9,** 743-752

25. Fichtner, C., Laurich, C., Bothe, E., and Lubitz, W. (2006) Biochemistry **45,** 9706-9716

26. Bagley, K. A., Vangarderen, C. J., Chen, M., Duin, E. C., Albracht, S. P. J., and Woodruff, W. H. (1994) Biochemistry **33,** 9229-9236

27. Dole, F., Fournel, A., Magro, V., Hatchikian, E. C., Bertrand, P., and Guigliarelli, B. (1997) Biochemistry **36,** 7847-7854

28. Jones, A. K., Lamle, S. E., Pershad, H. R., Vincent, K. A., Albracht, S. P. J., and Armstrong, F. A. (2003) J Am Chem Soc **125,** 8505-8514

29. George, S. J., Kurkin, S., Thorneley, R. N. F., and Albracht, S. P. J. (2004) Biochemistry **43,** 6808-6819

30. Bruschi, M., Zampella, G., Fantucci, P., and De Gioia, L. (2005) Coord Chem Rev **249,** 1620-1640

31. De Lacey, A. L., Fernandez, V. M., Rousset, M., and Cammack, R. (2007) Chem Rev **107,** 4304-4330

32. Brecht, M., van Gastel, M., Buhrke, T., Friedrich, B., and Lubitz, W. (2003) J Am Chem Soc **125,** 13075-13083

33. Foerster, S., van Gastel, M., Brecht, M., and Lubitz, W. (2005) J Biol Inorg Chem **10,** 51-62

34. van der Zwaan, J. W., Albracht, S. P. J., Fontijn, R. D., and Slater, E. C. (1985) FEBS Lett **179,** 271-277

35. Wang, H. X., Ralston, C. Y., Patil, D. S., Jones, R. M., Gu, W., Verhagen, M., Adams, M., Ge, P., Riordan, C., Marganian, C. A., Mascharak, P., Kovacs, J., Miller, C. G., Collins, T. J., Brooker, S., Croucher, P. D., Wang, K., Stiefel, E. I., and Cramer, S. P. (2000) J Am Chem Soc **122,** 10544-10552

36. Wang, H., Patil, D. S., Ralston, C. Y., Bryant, C., and Cramer, S. P. (2001) *Journal of* Electr Spectrosc Rel Phenom **114,** 865-871

37. Jayapal, P., Robinson, D., Sundararajan, M., Hillier, I. H., and McDouall, J. J. W. (2008) Phys Chem Chem Phy*s* **10,** 1734-1738

38. Ogata, H., Mizoguchi, Y., Mizuno, N., Miki, K., Adachi, S., Yasuoka, N., Yagi, T., Yamauchi, O., Hirota, S., and Higuchi, Y. (2002) J Am Chem Soc **124,** 11628-11635

39. De Lacey, A. L., Stadler, C., Fernandez, V. M., Hatchikian, E. C., Fan, H. J., Li, S., and Hall, M. B. (2002) J Biol Inorg Chem **7,** 318-326

40. Happe, R. P., Roseboom, W., and Albracht, S. P. J. (1999) Eur J Biochem **259,** 602-608

41. Yagi, T., Kimura, K., Daidoji, H., Sakai, F., Tamura, S., and Inokuchi, H. (1976) J Biochem **79,** 661-671

42. Atkins, P. a. D. J. (2006) Atkins' Physical Chemistry, 8th Ed. Ed., Oxford University Press,

43. Nyquist, R. A. (1986) Appl Spectrosc **40,** 79-85

44. Schröder, O., Bleijlevens, B., de Jongh, T. E., Chen, Z., Li, T., Fischer, J., Förster, J., Friedrich, C. G., Bagley, K. A., Albracht, S. P. J., and Lubitz, W. (2007) J Biol Inorg Chem **12,** 212-233

45. Davidson, G., Choudhury, S. B., Gu, Z. J., Bose, K., Roseboom, W., Albracht, S. P. J., and Maroney, M. J. (2000) Biochemistry **39,** 7468-7479

46. Bagley, K. A., Duin, E. C., Roseboom, W., Albracht, S. P. J., and Woodruff, W. H. (1995) Biochemistry **34,** 5527-5535

47. De Lacey, A. L., Fernandez, V. M., Rousset, M., Cavazza, C., and Hatchikian, C. E. (2003) J Biol Inorg Chem **8,** 129-134

48. De Lacey, A. L., Pardo, A., Fernandez, V. M., Dementin, S., Adryanczyk-Perrier, G., Hatchikian, E. C., and Rousset, M. (2004) J Biol Inorg Chem **9,** 636-642

49. Fan, H. J. and Hall, M. B. (2001) J Biol Inorg Chem **6,** 467-473

50. Armstrong, F. A. (2004) Current Opinion in Chemical Biology **8,** 133-140

51. Jeffrey, G. A. (1997) An Introduction to Hydrogen Bonding, Oxford University Press Ed., Oxford University Press, New York

52. Kozlowski, H., Ravarend, B. D.-L., Ficheux, D., Loucheux, C., and Sovago, I. (1987) J Inorg Biochem **29,** 187-197

53. Kulon, K., Wozniak, D., Wegner, K., Grzonka, Z., and Kozlowski, H. (2007) J Inorg Biochem **101,** 1699-1706

54. Khalil, M., Marcus, M. A., Smeigh, A. L., Mc Cusker, J. K., Chong, H. H., and Schoenlein, R. W. (2006) J Phys Chem A **110,** 38-44

55. Chapman, A., Cammack, R., Hatchikian, C. E., McCracken, J., and Peisach, J. (1988) FEBS Lett **242,** 134-138

56. Buhrke, T., Lenz, O., Porthun, A., and Friedrich, B. (2004) Mol Microbiol **51,** 1677-1689

57. Agrawal, A. G., van, G. M., Gartner, W., and Lubitz, W. (2006) J Phys Chem B **110,** 8142-8150

58. Pereira, M. M. and Teixeira, M. (2004) Biochim Biophys Acta **1655,** 340-346

59. Pylypenko, O. and Schlichting, I. (2004) Annu Rev Biochem **73,** 991-1018

60. Lill, S. O. and Siegbahn, P. E. (2009) Biochemistr*y* **48,** 1056-1066

61. Darensbourg, M. Y., Lyon, E. J., and Smee, J. J. (2000) Coord Chem Rev **206,** 533-561

62. Liaw, W. F., Chiang, C. Y., Lee, G. H., Peng, S. M., Lai, C. H., and Darensbourg, M. Y. (2000) Inorg Chem **39,** 480-484

63. Lai, C. H., Lee, W. Z., Miller, M. L., Reibenspies, J. H., Darensbourg, D. J., and Darensbourg, M. Y. (1998) J Am Chem Soc **120,** 10103-10114

64. Carducci, M. D., Pressprich, M. R., and Coppens, P. (1997) J Am Chem Soc **119,** 2669-2678

65. Morioka, Y., Takeda, S., Tomizawa, H., and Miki, E. (1998) Chem Phys Lett **292,** 625-630

66. Braunstein, P., Herberich, G. E., Neusch³tz, M., and Schmidt, M. U. (1999) J Organometal Chem **580,** 66-71

67. Woike, T., Dahaoui, S., Schaniel, D., Ponou, S., Hansen, N. K., and Petrick, V. (2004) Zeitschrift fur Kristallographie **219,** 558-566

*Chapter 5*

# Chapter 6

# FTIR study on the light sensitivity of the [NiFe] hydrogenase from *Desulfovibrio vulgaris* Miyazaki F: Ni-C to Ni-L photoconversion, kinetics of proton rebinding and H/D isotope effect
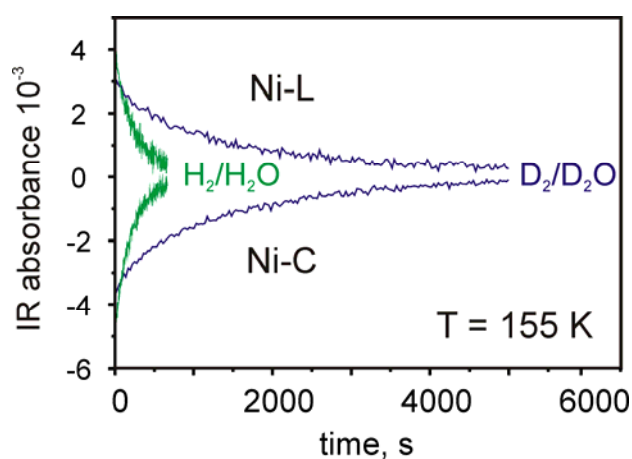


**Graphical Abstract.** (H/D) isotope effect on the Ni-L to Ni-C back conversion shows the rebinding of a proton as rate determining step.

# FTIR study on the light sensitivity of the [NiFe] hydrogenase from *Desulfovibrio vulgaris* Miyazaki F: Ni-C to Ni-L photoconversion, kinetics of proton rebinding and H/D isotope effect[†]

Petra Kellers[*][ab], Maria-Eirini Pandelia[*][a], Leslie J. Currell[a], Helmut Görner[a] and Wolfgang Lubitz[a]

[*] These Authors contributed equally to this work
[a]*Max-Planck-Institut für Bioanorganische Chemie, Stiftstraße 34-36, D-45470 Mülheim an der Ruhr, Germany.*
[b]*Department of Photochemistry and Molecular Science, The Ångström Laboratories, Uppsala University, Box 523, SE-751 20 Uppsala, Sweden*

## Short Abstract

The light-induced Ni-C to Ni-L transition results in the dissociation of a hydrogenic species, originating from the dihydrogen splitting at the active site. Back conversion in the dark to form Ni-C was investigated by studying the rebinding kinetics of this ligand in protonated ($H_2/H_2O$) and deuterated ($D_2/D_2O$) samples using time resolved FTIR spectroscopy.

## Introduction

Hydrogenases are bidirectional enzymes that play a key role in the cellular energy metabolism of a wide variety of micro-organisms.[1] The [NiFe] hydrogenase from the anaerobic sulfate reducing bacterium *Desulfovibrio* (*D.*) *vulgaris* Miyazaki F is a membrane attached protein consisting of two subunits.[2] *In vivo*, it works preferably as an uptake hydrogenase. Heterolytic splitting of dihydrogen takes place at the [NiFe] active site located in the large subunit, while electrons are transferred to the physiological redox partner cytochrome $c_3$[2] *via* three FeS centres; one $Fe_3S_4$ and two $Fe_4S_4$ clusters, located in the small subunit. The catalytic cycle of the *D. vulgaris* hydrogenase comprises a number of intermediate states[3], among which, Ni-C is pivotal for the enzymatic mechanism. The Ni-C state ($Ni^{3+}$, paramagnetic $S = 1/2$) is directly involved in the hydrogen conversion and was shown to carry a hydrogenic

species (Fig. 1). Electron nuclear double resonance (ENDOR) and hyperfine sublevel correlation (HYSCORE) spectroscopic experiments on the regulatory hydrogenase from *Ralstonia eutropha*[4] and on *D. vulgaris* Miyazaki F[5] combined with single crystal EPR[6] and theoretical[7] studies detected a hydride ligand (H⁻) in the bridging position between the two metals in the Ni-C state. This ligand is absent in the oxidised states of the enzyme and proposed to be derived from the substrate hydrogen that is split heterolytically at the active site.
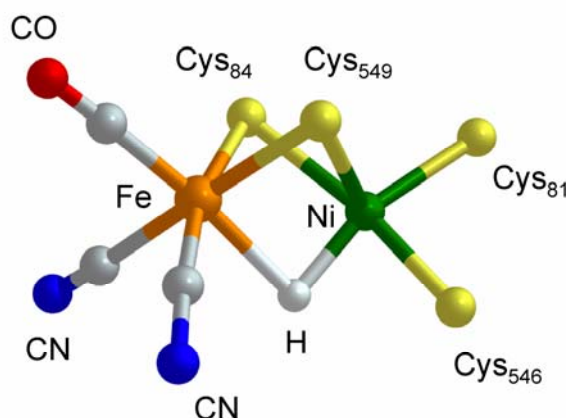


**Figure 1.** The active site of the *D. vulgaris* Miyazaki F [NiFe] hydrogenase in the Ni-C state. Ni and Fe are bridged by two cysteinyl residues. Fe is further coordinated by three inorganic ligands, one carbonyl and two cyanides. Ni is additionally coordinated by two terminally bound thiolate ligands. The substrate in the form of a hydride (H⁻) is located in the bridging position between the two metals.

Illumination at temperatures below 180 K converts Ni-C to the Ni-L state, with concomitant photodissociation of the bridging hydride[8–10], as shown by EPR studies. This light-induced transition can also be followed by Fourier transform infrared (FTIR) spectroscopy by monitoring the stretching vibrations of the CO and CN⁻ ligands attached to the Fe[11–13] (Fig. 1), as has been recently shown for the more oxidised intermediate state (Ni-SIr) of this enzyme.[14]

In this work, we report the first infrared investigation of the Ni-C to Ni-L photoconversion for [NiFe] hydrogenases from sulfate reducing bacteria and a novel rapid scan FTIR study on the kinetics of the proton rebinding. The activation barrier

for the re-association of the proton was determined and the H/D isotope effect examined over the accessible temperature range.

## Materials and Methods

*Sample preparation.* The [NiFe] hydrogenase was isolated from the sulfate reducing bacterium *D. vulgaris* Miyazaki F and was purified as described previously.[15] The Ni-C state was prepared in 50 mM $H_2O$ (pH 7.4) and $D_2O$ based Tris/Cl (pD 7.4) buffers, respectively. Degassing of the samples (concentration 1 mM) was followed by incubation at room temperature for 50 min with 1 bar of $H_2$ or $D_2$ gas, respectively. Transfer of the samples into the infrared cell was carried out anaerobically prior to freezing in liquid $N_2$.

*FTIR spectroscopy.* The spectra were recorded on a Bruker IFS 66v/S FTIR spectrometer equipped with a MCT photoconductive detector (Kolmar Technologies). A continuous flow cryostat system (Optistat CF, Oxford Instruments) with an ITC 503S controller (Oxford Instruments) was used. The spectral resolution was 2 $cm^{-1}$. The samples were illuminated *in situ* for 3 min (halogen lamp 250 W, 24 V) prior to measuring the recombination kinetics in the rapid scan mode. The time resolution of the rapid scan measurements was in the order of one second.

## Results and discussion

Infrared spectroscopy probes the [NiFe] active site by monitoring the vibrational frequencies of the diatomic ligands at the Fe, *i.e.* one carbonyl and two cyanides.[16] These frequencies are reliable sensors for changes in the electron density, coordination number on the Fe as well as changes in the hydrogen bonding.[17]

Figure 2a shows a light-minus-dark difference infrared spectrum of the $H_2$ reduced hydrogenase at 150 K. In such a spectrum the light sensitive states (educts) appear as negative bands and the light-induced states (products) as positive bands. The Ni-C state is described by three negative bands, one in the low frequency region that is associated with the CO vibration (1963 $cm^{-1}$) and two in the high frequency region associated with the coupled $CN^-$ oscillators (2077, 2087 $cm^{-1}$). Conversion from Ni-C to Ni-L upon illumination results in a shift of all bands towards lower

frequencies, similar to what has been observed for the *Allochromatium* (*A.*) *vinosum* hydrogenase.[11] The spectrum of Ni-L consists of a CO band at 1911 cm$^{-1}$ and two conjugate CN$^-$ bands at 2048 and 2061 cm$^{-1}$. Such a uniform shift of all three vibrational frequencies shows an enhancement of the $\pi$-back bonding character of the CN$^-$ and the CO ligands to Fe.[18] Lower vibrational frequencies of the diatomic ligands therefore suggest an increase in the electron density at the Fe as a result of the dissociation of the bridging ligand.
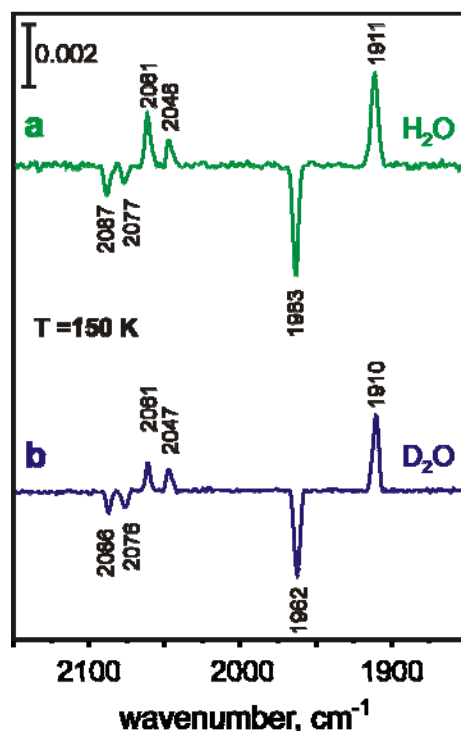


**Figure 2.** Light-minus-dark difference FTIR spectra of the *D. vulgaris* Miyazaki F hydrogenase H$_2$ reduced in H$_2$O (a) and D$_2$ reduced in D$_2$O (b) at 150 K.

A wavelength dependent EPR study of the Ni-C to Ni-L conversion showed a correlation with absorption bands in the visible spectrum that could be associated with electronic transitions of the [NiFe] centre.[9] Therefore, upon illumination, electronic excitation of the Ni-Fe site results in the dissociation of the bridging ligand. Based on results from previous theoretical studies,[19] the chemical form of the dissociated ligand is proposed to be a proton. This suggests that the complex becomes fairly acidic resulting in its light-induced deprotonation facilitated presumably by a nearby base. In the current work no SH vibrations in Ni-L were detected in the range between 2520-2590 cm$^{-1}$, which would indicate a protonation of one of the coordinating cysteinyl residues.[20] However, the absence of SH stretching bands in the present work does not

exclude their existence, since they may be too weak to be detected. Fig. 2b shows a light-minus-dark FTIR difference spectrum of the deuterated ($D_2/D_2O$) form of the reduced hydrogenase. Apart from slight shifts (0-1 $cm^{-1}$) of the infrared bands no other changes were detected.

Conversion from Ni-C to Ni-L was observed to be reversible in the dark,[8] involving dissociation of the bridging hydrogenic species upon illumination and its rebinding to the active site as a proton during dark adaptation.

Recombination rate constants for this process were studied using rapid scan FTIR. Fig. 3 shows a three-dimensional representation of the back conversion kinetics at 150 K. The first slice of the spectrum corresponds to the time $t = 0$, where the amount of hydrogenase molecules in the Ni–L state is maximum. At subsequent times the Ni-C state reappears, as rebinding of the ligand occurs.
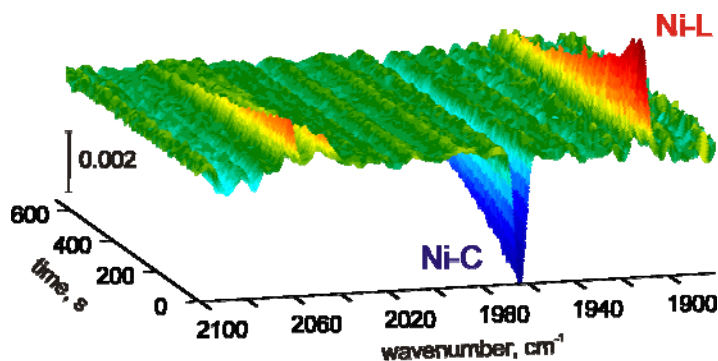


**Figure 3.** Three dimensional plot of the time evolution of the light-minus-dark FTIR difference spectra of the $H_2$ reduced hydrogenase from *D. vulgaris* Miyazaki F at 150 K after switching off the light. The positive bands correspond to Ni-L, negative bands to Ni-C.

All the kinetics have a single-exponential behaviour (see insert of Fig. 4 and the example in the graphical abstract). This shows that the rebinding is a first-order process and no transient intermediates were detected within the time resolution of these experiments. The temperature dependence of the rate constants ($k$) follows the Arrhenius equation $k = A_0 \exp(-E_a/RT)$ [21] between 140 and 180 K (Table 1, Fig. 4, open circles), where $A_0$ is the frequency factor in $s^{-1}$, $E_a$ is the activation energy in kJ $mol^{-1}$, $R$ is the universal gas constant 8.3144 J $K^{-1}$ $mol^{-1}$ and $T$ is the temperature in K.
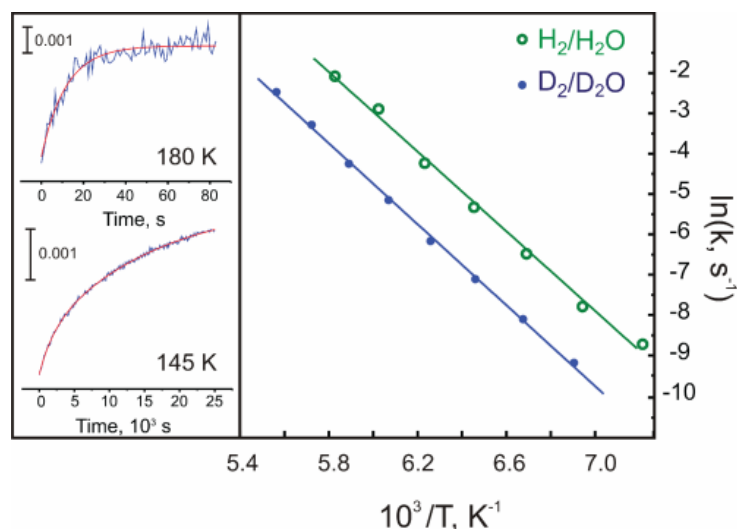
**Figure 4.** Temperature dependence of the rate constants for the back- conversion from Ni-L to Ni-C in $H_2$ (open circles) and $D_2$ reduced (full circles) samples. Insert: kinetics of the recovery of the Ni-C state ($D_2$ reduced) at 180 and 145 K by following the absorption band at 1962 cm$^{-1}$.

The activation barrier for the rebinding of the proton was estimated by analysing the kinetics of both the Ni-C recovery and the Ni-L disappearance, which were the same within experimental error. The averaged values of the lifetimes (inverse rate constants) at each temperature are included in Table 1. The activation barrier corresponds to $E_a$ ~46 kJ mol$^{-1}$ (Table 2).

**Table 1.** Inverse rate constants and kinetic isotope effect for the $H_2$ and $D_2$ reduced samples ($k_H/k_D$) in the range from 180 to 140 K

| $T$/K | $\tau_H$/s | $\tau_D$/s | $k_H/k_D$ |
|---|---|---|---|
| 180 | — | 12 | — |
| 175 | — | 27 | — |
| 170 | 10 | 70 | 7.0 |
| 165 | 27 | 175 | 6.5 |
| 160 | 78 | 480 | 6.2 |
| 155 | 210 | 1240 | 5.9 |
| 150 | 600 | 3350 | 5.6 |
| 145 | 1940 | 9860 | 5.1 |
| 140 | 4400 | — | — |

Isotopic substitution of the bridging species in the Ni-C state was carried out as described above. The kinetic isotope effect on the rebinding rate constants is substantial. Recombination of the ligand is 5-7 times slower in the $D_2$ reduced compared to the $H_2$ reduced sample (Table 1), in accordance with a primary isotope effect.[22] This shows that the rate-limiting step of the back conversion to Ni-C is the re-association of the proton in the active site. The activation energy for the back conversion from Ni-L to Ni-C in the deuterated sample was found to be somewhat larger and approximately 48 kJ mol$^{-1}$ (Table 2). The zero-point energy of the deuteride ligand is slightly smaller than that of the hydride ligand and a higher activation barrier would thus be anticipated, in accordance with our results. A comparison of the frequency factors (intercept of the Arrhenius plot in the limit where $1/T \rightarrow 0$) showed that the probability for the rebinding of the deuterium and the hydrogen based ligands is very similar.

**Table 2.** Activation energies ($E_a$) and frequency factors for the back conversion from Ni-L to Ni-C. The experimental error in the energies is $\pm 7\%$ and the error in the frequency factor is one order of magnitude

| Sample | $E_a$/kJ mol$^{-1}$ | $A_0$/s$^{-1}$ |
|---|---|---|
| $H_2$ reduced | 46 | $10^{12}$ |
| $D_2$ reduced | 48 | $10^{12}$ |

In our experiments only one light-induced state (Ni-L) for the *D. vulgaris* hydrogenase was observed in the temperature range studied. Therefore, other Ni-L states, which have been described to exist at lower temperatures[9,10] are outside the scope of this work. They probably reflect a different binding position of the $H^+/D^+$ ion after photodissociation. No marked effect on the yield of the photoproduct was found in our experiments at the given temperatures, indicating the same efficiency of photoconversion for both $H_2$ and $D_2$ reduced samples. Assuming a linear Arrhenius dependence, the extrapolated lifetimes for Ni-L at room temperature (297 K) are 57 and 220 μs for $H_2$ and $D_2$ reduced samples, respectively.

In this work we report the first FTIR investigation of the Ni-L state for a [NiFe] hydrogenase from a sulfate reducing bacterial organism. The spectra resemble the ones observed previously for the photosynthetic bacterium *A. vinosum*[11] and for the cyanobacterial-like uptake [NiFe] hydrogenase from *Acidithiobacillus ferrooxidans*,[13] showing a similar structure of the light-induced Ni–L state among different organisms. In addition, the present study confirmed, using FTIR spectroscopy and H/D isotope labelling, that the photosensitivity of the catalytically active Ni-C state is related to the dissociation of the bridging hydrogenic species. Rapid scan kinetic measurements showed that rebinding of this substrate ligand as a proton is a first-order process with no intermediates being formed. The activation barrier determined for this process is 46 kJ mol$^{-1}$. The primary isotope effect on the re-association rate constants demonstrated that the proton transfer is the rate-limiting step during back conversion from Ni-L to the Ni-C state. These results contribute to a better understanding of the character of the metal hydride binding in the catalytic mechanism of the [NiFe] hydrogenases and will help to elucidate its function.

## Acknowledgements

# References

1   P. M. Vignais and B. Billoud, *Chem. Rev.*, 2007, **107**, 4206.

2   Y. Higuchi, T. Yagi and N. Yasuoka, *Structure*, 1997, **5**, 1671.

3   W. Lubitz, E. Reijerse and M. van Gastel, *Chem. Rev.*, 2007, **107**, 4331.

4   M. Brecht, M. van Gastel, T. Buhrke, B. Friedrich and W. Lubitz, *J. Am. Chem. Soc.*, 2003, **125**, 13075.

5   S. Foerster, M. van Gastel, M. Brecht and W. Lubitz, *JBIC, J. Biol. Inorg. Chem.*, 2005, **10**, 51.

6   S. Foerster, M. Stein, M. Brecht, H. Ogata, Y. Higuchi and W. Lubitz, *J. Am. Chem. Soc.*, 2003, **125**, 83.

7   M. Stein and W. Lubitz, *Phys. Chem. Chem. Phys.*, 2001, **3**, 2668.

8   J. W. Van der Zwaan, S. P. J. Albracht, R. D. Fontijn and E. C. Slater, *FEBS Lett.*, 1985, **179**, 271.

9   C. Fichtner, M. van Gastel and W. Lubitz, *Phys. Chem. Chem. Phys.*, 2003, **5**, 5507.

10  M. Medina, E. C. Hatchikian and R. Cammack, *Biochim. Biophys. Acta*, 1996, **1275**, 227.

11  K. A. Bagley, E. C. Duin, W. Roseboom, S. P. J. Albracht and W. H. Woodruff, *Biochemistry*, 1995, **34**, 5527.

12  A. J. Pierik, W. Roseboom, R. P. Happe, K. A. Bagley and S. P. J. Albracht, *J. Biol. Chem.*, 1999, **274**, 3331.

13  O. Schröder, B. Bleijlevens, T. E. de Jongh, Z. Chen, T. Li, J. Fischer, J. Förster, C. G. Friedrich, K. A. Bagley, S. P. J. Albracht and W. Lubitz, *JBIC, J. Biol. Inorg. Chem.*, 2007, **12**, 212.

14  M.-E. Pandelia, H. Ogata, L. J. Currell, M. Flores and W. Lubitz, *JBIC, J. Biol Inorg. Chem.* 2009, **14(8)**, 1227

15  T. Yagi, K. Kimura, H. Daidoji, F. Sakai, S. Tamura and H. Inokuchi, *J. Biochem.*, 1976, **79**, 661.

16  C. H. Lai, W. Z. Lee, M. L. Miller, J. H. Reibenspies, D. J. Darensbourg and M. Y. Darensbourg, *J. Am. Chem. Soc.*, 1998, **120**, 10103.

17  M. Y. Darensbourg, E. J. Lyon and J. J. Smee, *Coord. Chem. Rev.*, 2000, **206–207**, 533.

18  K. Nakamoto, *Infrared and Raman Spectra of Inorganic and Coordination Compounds*, John Wiley & Sons Inc, New York, 5th edn, 1997.

19  M. Stein, E. van Lenthe, E. J. Baerends and W. Lubitz, *J. Am. Chem. Soc.*, 2001, **123**, 5839–5840.

20  H. Li and G. J. Thomas, *J. Am. Chem. Soc.*, 1991, **113**, 456–462.

21  P. Atkins, *Atkins Physical Chemistry*, Oxford University Press, 8th edn, 2006.

22  A. L. De Lacey, A. Pardo, V. M. Fernandez, S. Dementin, G. Adryanczyk-Perrier, E. C. Hatchikian and M. Rousset, *JBIC, J. Biol. Inorg. Chem.*, 2004, **9**, 636.

# Chapter 7

# Hydrogenase I from the hyperthermophilic bacterium *Aquifex aeolicus*: Activation process, redox intermediates and oxygen tolerance studied by FTIR spectroelectrochemistry and protein film electrochemistry
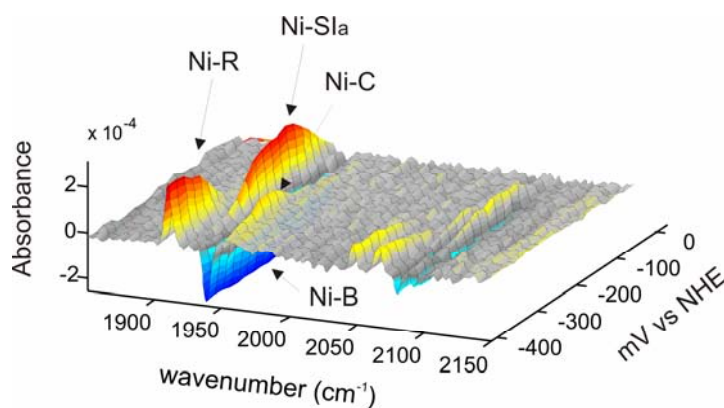


**Graphical abstract.** The redox intermediate states involved in the mechanism of the Hase I from *Aquifex aeolicus* and their redox properties have been followed by IR spectroelectrochemstry. One inactive and three catalytically active states have been detected.

*Chapter 7*

# Hydrogenase I from the hyperthermophilic bacterium *Aquifex aeolicus*: Activation process, redox intermediates and oxygen tolerance studied by FTIR spectroelectrochemistry and protein film voltammetry[†]

Maria-Eirini Pandelia[*], Pascale Tron-Infossi[‡], Vincent Fourmond, Christophe Leger, Marie-Thérèse Giudici-Orticoni[‡], and Wolfgang Lubitz[*]

[*]*Max-Planck-Institut für Bioanorganishe Chemie, Stiftstrasse 34-36, D45470, Mülheim a.d. Ruhr*
[‡]*Laboratoire de Bioenergetique et Ingenierie des Proteines, IBSM-CNRS, 13402 Marseille France*

## Abstract

Hydrogenase I (Hase I) is one of the three [NiFe] hydrogenases encoded in the hyperthermophilic bacterium *Aquifex (A.) aeolicus* and belongs to an intriguing class of redox enzymes that show enhanced thermostability and oxygen tolerance. On the basis of these properties, protein film voltammetry is employed to portray the interaction of Hase I with the $O_2$ inhibitor and obtain an overall picture of the catalytic activity. Fourier transform infrared (FTIR) spectroscopy integrated with *in-situ* electrochemistry is used to identify structural properties of the [NiFe] site and the intermediate states implicated in its redox chemistry. The active site coordination is found similar to that of standard hydrogenases with a conserved $Fe(CN)_2CO$ moiety. The results indicate a simple reaction mechanism, consisting of four detectable intermediates. These can be associated with the Ni-B, Ni-SI$_a$, Ni-C and Ni-R states found in other catalytic hydrogenases. Transition from Ni-B to Ni-SI$_r$ could not be resolved; instead a direct conversion to Ni-SI$_a$ was observed. Furthermore, only one Ni-R state was formed irrespective of temperature (4 - 40 °C) or pH (6.4 - 8.4), respectively. The midpoint potentials were notably more positive with respect to those observed in their mesophilic counterparts. A scheme for the enzymatic mechanism of Hase I is presented and the results are discussed in view of the proposed structural models for oxygen sensitive hydrogenases.

---

[†] *To be submitted* **2009**

## Introduction

Hydrogenases are enzymes that couple the reversible oxidation of molecular hydrogen to the activity of redox-related partners according to the elemental reaction[1]: $H_2 \rightleftharpoons 2H^+ + 2e^-$. They can be classified according to their metal ion content in three distinct classes[2]; [NiFe], [FeFe] and iron-sulphur cluster-free hydrogenases (Hmd), for which structural information has been derived[3,4,5]. Oxygen inhibition is reversible for the representatives of the [NiFe] class, whereas for the other two groups exposure to oxygen leads to irreversible degradation. Recently the strict requirement for anaerobic conditions has been reexamined on the grounds of the discovery of enzymes that can perform catalysis under atmospheric conditions. In particular, [NiFe] hydrogenases from hyperthermophilic (i.e *Aquifex (A.) aeolicus*)[6] or Knallgas (i.e. *Ralstonia (R.) eutropha*)[7] bacteria have shown increased oxygen tolerance and have allegedly a strong potential use for biotechnological purposes[8].

*A. aeolicus* VF5 belongs to the family of the most hyperthermophilic bacteria known to date with an optimum growing temperature of 85 °C[9]. It is a micro-aerobic, obligate chemolithoautotrophic bacterium that encodes three distinct [NiFe] hydrogenases[10]. Among these enzymes, Hydrogenase I (Hase I) is a membrane attached hydrogenase, which is part of the aerobic respiratory hydrogen oxidation pathway. It consists of two subunits; a large subunit (70 kDa) that contains the nickel-iron centre and a small subunit (40 kDa) that harbours the electron relaying iron-sulphur centres. It can be co-purified with its native electron acceptor, a di-haem cytochrome *b* (20 kDa) as a Hase I-cyt*b* complex[10].

Though, up to present, there is no crystal structure information available, a combination of techniques has been put forward to characterize the electronic and physicochemical properties of *A. aeolicus*. The sequence motif for binding the active centre in the large subunit is well preserved and electron paramagnetic resonance (EPR) studies have exhibited nickel signals typical of mesophilic hydrogenases[10]. This suggests a similar electronic structure and molecular symmetry of the spin carrying [NiFe] centre. Additionally, in the small subunit, the existence of one [Fe$_3$S$_4$] and two [Fe$_4$S$_4$] clusters has been suggested by the presence of the ten conserved cysteines, though the EPR signals of the latter were found to be more complex[10,11].

In oxygen sensitive hydrogenases the as isolated enzyme is a mixture of two states namely Ni-A (unready) and Ni-B (ready)[12]. They are both paramagnetic but

differ in their spectroscopic and catalytic properties[13,14,15]. Ni-B is readily activated by $H_2$ or reducing conditions, whereas Ni-A requires prolonged times. Their difference has been attributed to the chemical identity of the oxygenic species present in each state (OH⁻ for Ni-B[16] and a proposed OOH⁻ for Ni-A[17,18]). One electron reduction of Ni-A and Ni-B produces the states Ni-SU and (Ni-SI$_r$)$_I$, respectively[19,20,21] (Scheme 1), which are EPR-silent ($Ni^{2+}$). (Ni-SIr)$_I$ is in an acid-base equilibrium with a (Ni-SI$_r$)$_{II}$ state, proposed to loosely coordinate a water ligand[20]. After removal of the oxygenic species, the enzyme enters its functional cycle, comprised of three catalytically active states. The most oxidised Ni-SI$_a$ is EPR-silent ($Ni^{2+}$) and its one electron reduction leads to the paramagnetic Ni-C ($Ni^{3+}$, S=1/2), with a hydride bridge between nickel and iron[22,23]. Further reaction of Ni-C with $H_2$ yields Ni-R ($Ni^{2+}$). Up to three different Ni-R states can be observed depending on the pH of the protein solution[20].
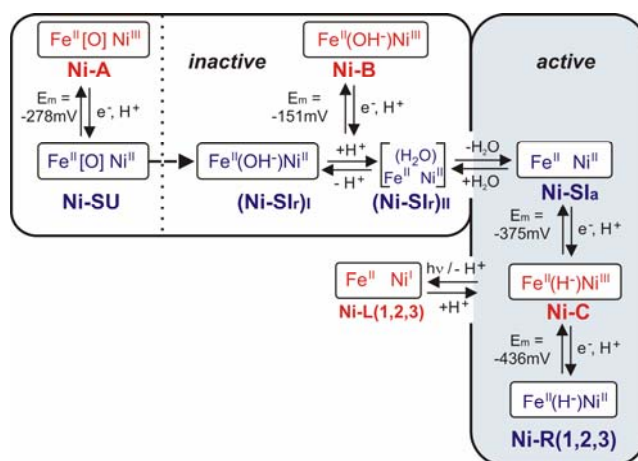


**Scheme 1.** Schematic overview of the redox intermediates in oxygen sensitive [NiFe] hydrogenases. The paramagnetic states are denoted in red and the EPR-silent states in blue. The midpoint potentials for the respective transitions are given for the sulphate reducing bacterium *D. vulgaris* Miyazaki F at pH 7.4, except for the Ni-A / Ni-SU couple which is given at pH 8.2

Electrochemical approaches such as protein film voltammetry[24] and electrochemistry in solution[19] have been proved to be indispensable in the characterization of redox enzymes. In particular, adsorption of hydrogenases on an electrode that mimics the function of their direct redox partner provides a dynamic

approach for studying inherent catalytic properties and delineates reactions both with the substrate and inhibitors[25]. Furthermore, in-situ electrochemistry integrated Fourier transform infrared (FTIR) spectroscopy has contributed greatly to the characterization of all intermediate states by relating redox changes in the active site with detectable shifts of the infrared absorption bands, corresponding to the CO, $CN^-$ ligands to iron[26]. The exact coordination of the metal ions in Hase I, however, could deviate from the one described in standard hydrogenases, as oxygen tolerant enzymes have been proposed to have more than three such ligands bound to the [NiFe] site[27].

In the present study, after examining the oxygen tolerance of *A. aeolicus* by means of protein film voltammetry, its structural and redox properties are extensively investigated. The coordination of the active site is probed by FTIR and in combination with electrochemistry information about the redox intermediates generated in solution is obtained. This study is important for elucidating the enzymatic function of hyperthermophilic hydrogenases and for discussing possible reasons for the marked oxygen tolerance of the Hase I(-cyt*b*) from *A. aeolicus*.

## Chapter 7

## Experimental procedures

*Protein purification.* Isolation and purification of the Hase I from *A. aeolicus* separately or together with its native electron acceptor, a di-haem *b*-type cytochrome was carried out as previously described[10] in a 50 mM Tris- HCl buffer pH 7.0 in the presence of 5 -10 % glycerol and 0.01 % n-dodecyl -β-D-maltoside (DDM).

*Electrochemical measurements.* Electrochemical measurements in solution were carried out in an Optically Transparent Thin Layer Electrochemical (OTTLE) cell designed by Moss et al[28,29]. 25 µL of 250 µM protein were placed on a 8.5 µm thick gold (Au) mini-grid (70% transparent to infrared), which serves as the working electrode. A platinum (Pt) foil is used as the counter and a Ag/AgCl (1 M KCl) as the reference electrode. Calibration of the reference electrode prior to and after each measurement was performed by monitoring the reduction of methyl viologen with cyclic voltammetry (-448 mV, pH 7.0). The temperature was regulated in the range between 4 and 40 ° C by water passing through the metallic body of the cell in a closed external circuit with a thermostat (LAUDA). For the pH dependent redox titrations the buffering solutions used (50 mM concentration) were: MES-NaOH (pH 6.4), Hepes-NaOH (pH 7.4) and Tricine-NaOH (pH 8.4). In the case of the soluble form of Hase I (without cyt*b*) titrations were carried both in the presence and absence of redox mediating agents. The mediators added in the protein solution were: methyl viologen, benzyl viologen, neutral red, phenosafranine, anthraquinone-2-sulfonate, anthraquinone-1,5-disulfonate, 2-hydroxy-1,4-naphthoquinone, potassium indigo tetrafulfonate, methylene blue, phenazine methosulfate and naphthoquinone. Their redox potentials and pH dependence have been extensively described elsewhere[30,31]. Their relative concentration with respect to the protein content was 1:3. Potentiometric titrations of the Hase I co-purified with the cyt*b* were carried out in the absence of any electron-transfer reagents to avoid inhibition of the quinone binding site of cyt*b*. In all solutions KCl was added to a final concentration of 150 mM. An equilibration time of 10 - 15 minutes was allowed prior recording the infrared spectra in this case, while in the presence of mediators the equilibration times were restricted to 3 minutes. The potentiometric titrations were fitted using the Nernst equation[32]:

$$E = E_m + \frac{RT}{nF} \ln\left( \frac{[Ox_1]}{[Red_1]} \right),$$

where $E_m$ it the standard reduction potential, R is the universal gas constant, F is the Faraday constant, n the number of electrons, T the temperature, $[Ox_1]$ the concentration of the oxidised species and $[Red_1]$ the concentration of the reduced species. All potentials referred in the present work are quoted with respect to the normal hydrogen electrode potential (NHE).

Cyclic voltammetry and chronoamperometry were carried out in a glovebox under an anaerobic atmosphere. Hase I was adsorbed on a rotating pyrolytic graphite edge electrode (PGE) as previously described[33]. The experiments were carried out in a buffer mixture of MES, CHES, TAPS, HEPES and sodium acetate (5mM each) and 0.1 M NaCl. All experiments described in the present work were carried out by Vincent Fourmond and Christophe Leger.

*Fourier transform infrared (FTIR) spectroscopy.* Infrared measurements were carried out on a Bruker IFS 66v/s FTIR spectrometer with 2 cm⁻¹ resolution. The detector was a photovoltaic mercury cadmium telluride (MCT) element. The software for data recording consisted of the OPUS package (Bruker Optics). Analysis and further processing was performed with MATLAB 7.0 (Mathworks). The measured intensity of the bands was divided by the enzyme concentration and the optical path length so obtain the apparent normalised absorbance (B, mM⁻¹ cm⁻¹).

## Results

The [NiFe] hydrogenase from the hyperthermophilic bacterium *A. aeolicus* has been obtained in two forms; as a hetero-dimeric enzyme consisting of the NiFe site and the iron-sulphur clusters (Hase I) and as a hetero-trimer including additionally the di-haem *b*-type cytochrome (Hase I-cyt*b*). The protein film voltammetry experiments were performed on the soluble Hase I, while the in-solution redox titrations were carried for both forms and at temperatures 4°C, 25°C and 40°C. Results were identical within error for all temperatures, thus only the findings at 25°C are presented. Potentiometric titrations of the Hase I-cyt*b* complex were carried out in the absence of any electron-transfer mediators to avoid inhibition of the quinone binding site of cyt*b*. For the soluble Hase I (without cyt*b*) measurements were performed both in the presence and the absence of any redox mediators. All processes were reversible and reproducible independent of the addition of electron mediating substances, leading to essentially identical results.

### *Electrochemistry of Hase I immobilized on a PGE*

Using cyclic voltammetry, the interconversion of Hase I between active and inactive states was examined. The related experiment is shown in Figure 1a. The potential of the electrode is scanned and the hydrogen oxidation activity is monitored as a current. Initially the enzyme is fully activated at -440 mV and then the potential is swept towards more positive values at which hydrogen activation decreases and the enzyme forms an inactive state. This inactivation is reversed by sweeping back towards more reducing potentials. The inflection point in the sigmoidal rise of the $H_2$ oxidation current corresponds to the so-called 'switch-potential' and is equal to +77 mV. At very low potentials no negative current could be observed showing that the rate of hydrogen evolution is much too slow compared to the one of hydrogen oxidation (no detectable $H_2$ production)[34].

In a subsequent experiment, the effect of $O_2$ on the $H_2$ oxidation activity was investigated (Figure 1b). This was performed by a chronoamperometric measurement at a fixed potential of +190 mV, indicated with a blue arrow in Figure 1a. Aliquots of saturated oxygen were injected in the solution. The current decreased, but did not drop to zero demonstrating that a partial activity is retained. After removal of the $O_2$ by flushing with $H_2$, activity was recovered.
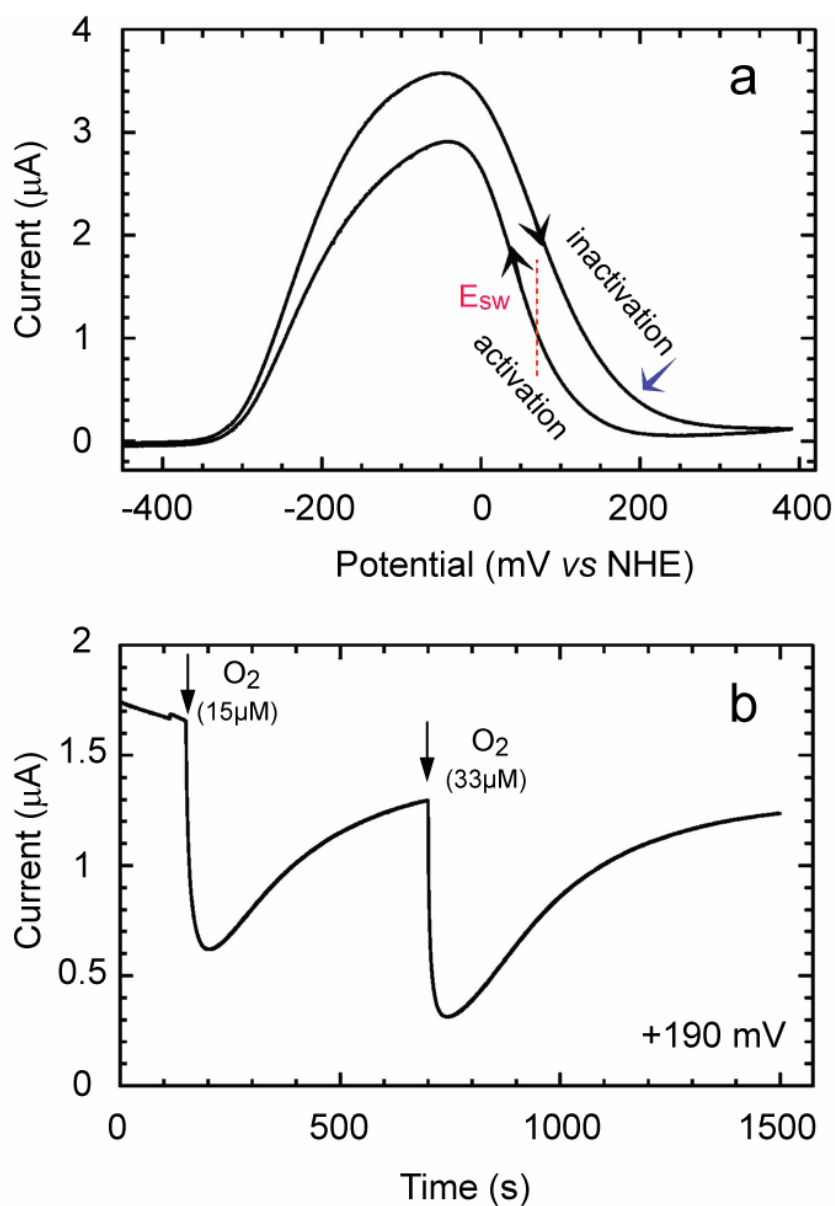
**Figure 1.** a) Cyclic voltammogram of Hase I film adsorbed on a rotating edge PGE recorded at a scan rate 0.3 mV s$^{-1}$, The conditions were 40 °C, pH 7.0, 10% H$_2$/ 90% N$_2$, 3000 rpm rotation rate, b) Experiment demonstrating the effect of addition of O$_2$ on the hydrogen oxidation current as a function of time at +190 mV; other conditions were: 40°C, 1 bar H$_2$, pH 7.

*Chapter 7*

***FTIR-electrochemistry in-solution***

**Oxidized inactive enzyme**

***Ni-B.*** Infrared spectroscopy detects the absorbance corresponding to the vibrations of the diatomic ligands bound to the active site, which appear in the spectra as bands at specific frequency positions. For the intrinsic ligands to Fe, bands in the region from 1970 to 1900 $cm^{-1}$ are associated with the CO stretching vibrations, while bands between 2105 and 2040 $cm^{-1}$ are related to the coupled $CN^-$ vibrations. Figure 2a shows the FTIR spectrum of the as isolated Hase I-cyt*b* complex from *A. aeolicus* at a resting potential of +224 mV at 25°C and pH 7.4 in the absence of any redox mediators. In this spectrum three main bands can be observed; one CO stretching vibration at 1939 $cm^{-1}$ and two $CN^-$ vibrations at 2081 and 2092 $cm^{-1}$. The coordination of the active site conformation with respect to standard hydrogenases is found to be preserved and is consistent with a $Fe(CN)_2CO$ moiety. On the basis of the EPR spectrum of the as purified enzyme and on previous studies on hydrogenases, this set of peaks corresponds to the Ni-B state[34,35] (see Table 1 and Appendix D). A band of low intensity at 2098 $cm^{-1}$ is also observed, but this is neither related to Ni-A nor to an extra $CN^-$ as will be discussed below. The absence of Ni-A and the presence only of Ni-B in the FTIR (and EPR)[10] corroborates the finding of a very fast activation for the *A. aeolicus* hydrogenase and indicates an electronic configuration of the active centre that is similar to the oxygen-sensitive hydrogenases.

**Enzyme activation in the electrochemical cell**

***Ni-SI<sub>a</sub>.*** The enzyme could be fully activated in the electrochemical cell at 25°C by applying a potential of -326 mV for 20 min. The protein solution was subsequently reoxidised at +100 mV. The obtained spectrum was identical to that of Figure 2a, excluding that the low intensity band at 2098 $cm^{-1}$ corresponds to any of the unready states (i.e. Ni-A, Ni-SU), since their anaerobic reoxidation is irreversible[20]. At a potential of -184 mV all the bands shifted towards lower frequencies (Figure 2b). The CO band is now centred at 1927 $cm^{-1}$ and the two coupled $CN^-$ are shifted to 2076 and 2087 $cm^{-1}$, respectively. Such shifts are consistent with a reduction of the Ni-B state to an EPR-silent ($Ni^{2+}$, $d^8$) species. According to the mechanistic scheme of the standard hydrogenases, this state should correspond to $(Ni-SI_r)_I$. However, by taking into account that the $CN^-$ stretching vibrations of a specific redox state are within 0-6 $cm^{-1}$ similar among [NiFe] enzymes from different organisms, the $CN^-$ bands in

Figure 2b more closely resemble the ones of the Ni-SIa[‡] state and not those of (Ni-SI$_r$)$_I$, indicating that in this process the latter is too transient to be resolved. Performing the experiment at 4°C in order to decelerate the kinetics of activation, no additional bands could be observed that could be associated with the (Ni-SI$_r$)$_I$ .
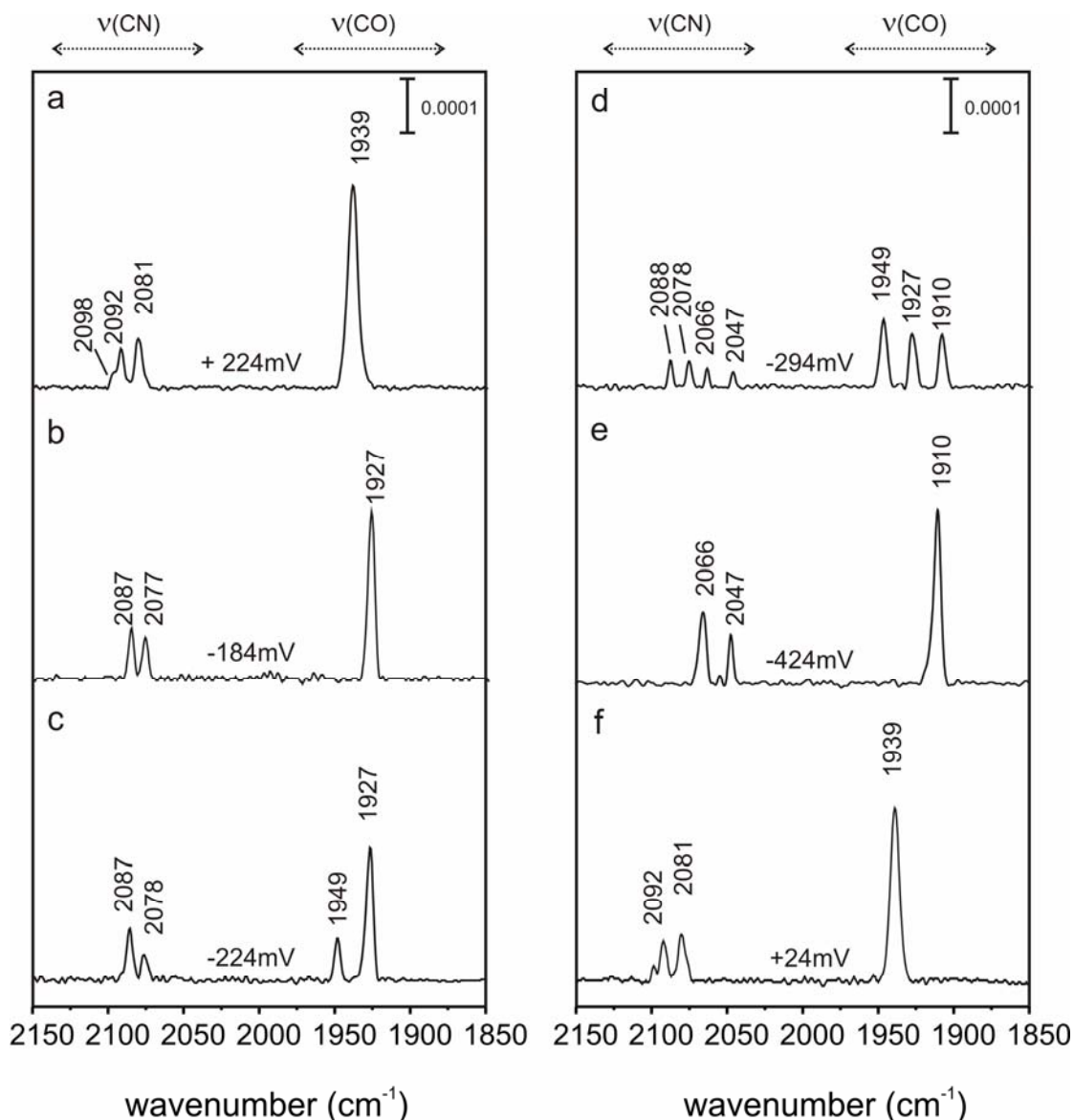


**Figure 2.** FTIR spectra of the Hase I-cyt*b* complex from *A. aeolicus* at 25°C, pH 7.4. (a) the as-isolated enzyme at the resting potential of +224 mV, (b) enzyme after full activation poised at -184 mV, (c) at -224 mV, (d) at -294 mV, (e) at -424 mV and (f) re-oxidised at +24 mV. The protein solution did not contain any electron mediating reagents.

---

[‡] The stretching vibrations corresponding to the Ni-SI$_a$ and the (Ni-SIr)$_{II}$ are identical. These two states cannot be distinguished by FTIR but by an activity measurement. At temperatures $\geq$ 25°C the loosely bound water ligand is easily liberated leading to Ni-SIa.

***Ni-C.*** Lowering the potential further to -224 mV led to the appearance of a redox intermediate with a CO vibration at 1949 cm$^{-1}$ and CN$^-$ bands very similar to the ones of Ni-SI$_a$ (Figure 2c, Table 1). Such a spectrum is consistent with the appearance of the catalytically active Ni-C state (EPR-active, S = ½, Ni$^{3+}$), which has been shown to carry a hydride ligand (H$^-$)[22] that can be photodissociated at temperatures lower than 170 K leading to Ni-L[36] (Figure 1). To examine experimentally whether this state corresponds to Ni-C, the Hase I-cyt*b* complex was reduced with H$_2$ and the sample was subsequently measured simultaneously at EPR (100 K) and FTIR (100 K). A rhombic signal with g-values 2.21, 2.15 and 2.01 confirmed the presence of Ni-C, which by illumination converted to a light-induced form (Ni-L2: with g-values 2.28, 2.12, and 2.05). Illumination of the sample in the FTIR resulted in the disappearance only of the

1949 cm$^{-1}$ at the same temperature, demonstrating that it can be uniquely assigned to the Ni-C state of the enzyme. The amount of Ni-C is almost maximal at a potential of -294 mV and corresponded to 35 - 40 % of the enzyme molecules (Figure 2d).

**Table 1.** Frequencies of the infrared stretching vibrations for the CO, CN$^-$ diatomic ligands of the NiFe hydrogenase from *Aquifex aeolicus* at 25°C. The error in the values is ± 1 cm$^{-1}$.

| State | $\bar{v}_{CO}(Fe)$ (cm$^{-1}$) | $\bar{v}_{CN^-}(Fe)_{asym}$ (cm$^{-1}$) | $\bar{v}_{CN^-}(Fe)_{sym}$ (cm$^{-1}$) |
|---|---|---|---|
| **Ni-B** | 1939 | 2081 | 2092 |
| **Ni-SIa** | 1927 | 2076 | 2087 |
| **Ni-C** | 1949 | 2078 | 2088 |
| **Ni-R** | 1910 | 2047 | 2066 |

***Ni-R.*** Ni-C is of very transient nature and converts at slightly more negative potentials to another state, described by one CO and two CN$^-$ stretching bands at 1910, 2047 and 2066 cm$^{-1}$, respectively (-424 mV, Figure 2e). This is the most reduced state of the enzyme as no spectral changes further take place by applying more negative

potentials. This intermediate is thus assigned to the Ni-R state (EPR-silent, $Ni^{2+}$). On the basis of the stretching vibrations, the observed Ni-R in Hase I is not the typical form (Ni-R1) found in mesophilic hydrogenases[35,37] (both anaerobic and oxygenic), but resembles more the Ni-R2 state (Appendix D).

**Re-oxidation in the electrochemical cell**

Re-oxidation of the enzyme at +24 mV resulted in the infrared spectrum shown in Figure 2f, which corresponds to the Ni-B state (see Table 1). The $CN^-$ band at 2098 $cm^{-1}$ is also present. This shows that this band is neither related to Ni-A nor to Ni-SU. However the related $CN^-$ or CO vibrations are not resolved presumably due to an overlap with the Ni-B state. This band therefore can either correspond to another state or to a slightly different conformation of Ni-B.

Electron paramagnetic resonance experiments have shown that at such positive potentials an additional (unknown) state is present in the spectra (Appendix D). This state is different from Ni-A and was identified by pulsed Q-band EPR, as it has different relaxation properties compared to Ni-B and the iron-sulphur clusters. It is not known so far, which state of the enzyme this signal represents and further experiments are needed to characterize it (Appendix D). However, it does not appear to have different activation kinetics (like Ni-A). This state could be related with the extra band present in the infrared spectra (Figures 2a, f).

**Potentiometric titration at pH 7.4 (Hase I-cyt*b*)**

Figure 4A shows the potentiometric titration for the Hase I-cyt*b* complex at pH 7.4, in which the redox transitions between different states are monitored via changes in the infrared spectra as a function of the applied potential. FTIR spectra were recorded with potential steps of 20 mV. The normalized absorption of all states was fitted to the Nernst equation with n = 1. Activation of the enzyme starting from the Ni-B state resulted in Ni-SIa, without the $(Ni-SI_r)_I$ state being a detectable intermediate. This redox transition corresponds to a one-electron process with an apparent midpoint potential of -105 mV. The Ni-SI$_a$/Ni-C couple has a value of -295 mV, while the midpoint potential for the Ni-C/Ni-R couple was estimated to be -300 mV. All processes were fully reversible and the error in the value determination was ± 10 mV.
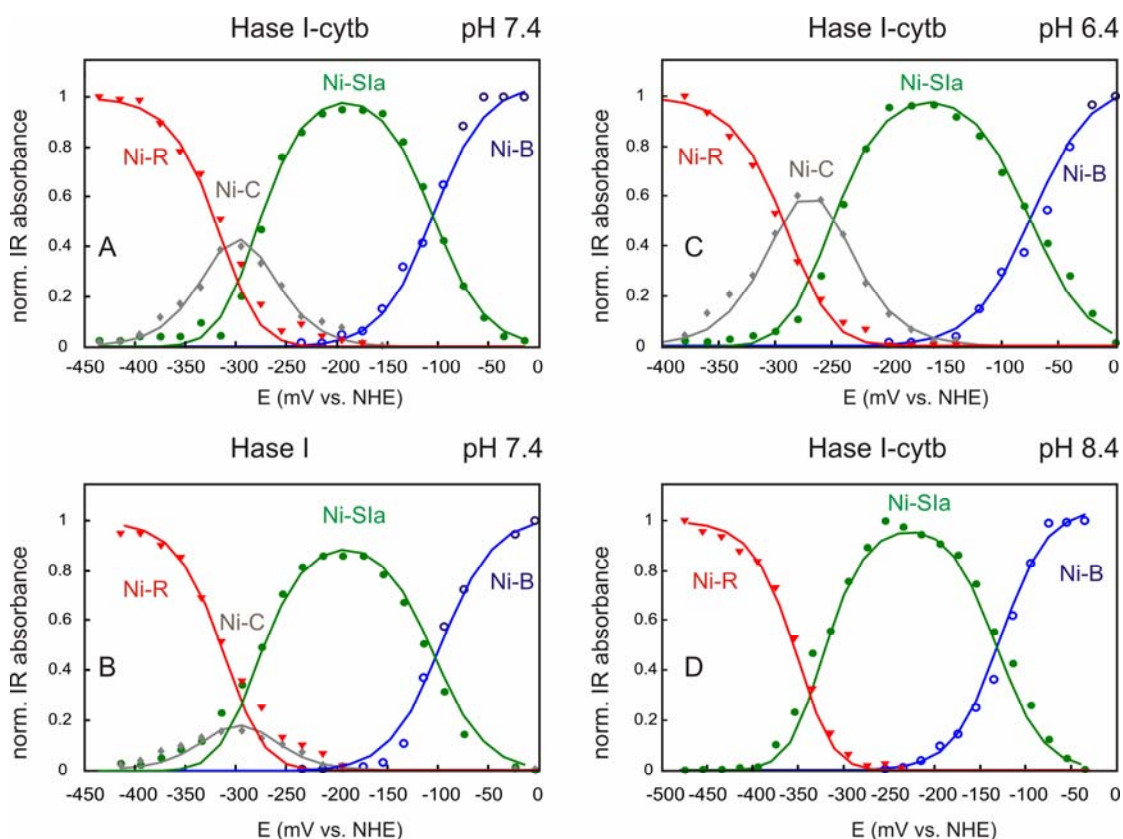
**Figure 3.** Potential dependent behaviour of the redox intermediates of the Hase I from *A. aeolicus* at three different pH values; A) 7.4 (with cyt*b*), B) 7.4 (without cyt*b*), C) 6.4 (with cyt*b*), and D) 8.4 (with cyt*b*). The temperature was 25°C and redox mediators were present in solution only for the case of Hase I without the cyt*b*.

**Potentiometric titration at pH 7.4 (Hase I)**

The potentiometric titration corresponding to the Hase I without the cyt*b* at pH 7.4 is presented in Figure 3B. Results were within the error identical to the ones obtained for the Hase I-cyt*b* enzyme (Table 2). The only difference is related to the Ni-SIa and the Ni-C state intermediate states that appear to be more transient. Ni-C appears in the same potential range as in the case of Hase I-cyt*b*, however its yield is notably smaller. This behaviour shows a smaller population of Ni-C during the transition from the more oxidised Ni-SIa state with a concomitant faster conversion to the Ni-R state. Such behaviour could be associated with the presence of the mediators in solution. From hereafter the notation Hase I(-cyt*b*) will be used to refer to both the dimeric and

trimeric enzymes, since results are within the error essentially identical for both complexes.

**Effect of pH on the redox processes (Hase I-cyt*b*)**

The potentiometric titrations of the Hase I-cyt*b* complex were carried out additionally for pH values 6.4 and 8.4, see Figures 3c and 3d, respectively. At pH 6.4 the yield of the Ni-C state was increased, in agreement with previous observations on the standard hydrogenases[20]. However, at a higher pH of 8.4, the Ni-C could not be detected as an intermediate in the spectra, which suggests that in a more basic environment this state becomes rapidly reduced to form Ni-R. The reduction potentials for all intermediates were pH-dependent demonstrating that the redox processes are coupled to proton transfer.

**Table 2.** Midpoint redox potentials for the intermediate redox states of the Hase I-cyt*b* from *A. aeolicus* at different pH values and comparison with those measured for Hase I at pH 7.4. The potentials are quoted vs the standard hydrogen electrode potential (SHE). The error is ± 10 mV.

| pH | Ni-B/Ni-SIa couple | Ni-SIa/Ni-C couple | Ni-C/Ni-R couple |
|---|---|---|---|
| **Hase I-cyt*b*** | | | |
| 6.4 | -73 | -264 | -270 |
| 7.4 | -105 | -295 | -300 |
| 8.4 | -128 | -340 | -340 |
| **Hase I** | | | |
| 7.4 | -105 | -295 | -297 |
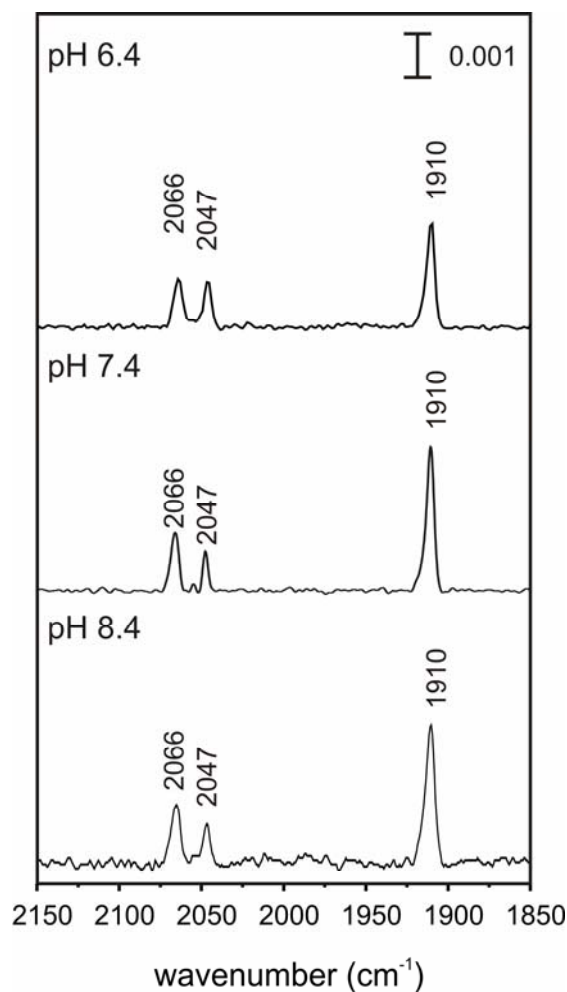
**Figure 4.** FTIR spectra of the most reduced Ni-R state of the Hase I-cyt*b* from
*A. aeolicus* at 25 °C. (a) pH 6.4 poised at -400 mV, (b) pH 7.4 poised at -444 mV and
(c) pH 8.4 poised at -486 mV. No additional Ni-R forms were found to be in an acid-
base equilibrium with this state in the pH range examined.

An additional result of these titrations was that only one Ni-R state can be
observed. This finding was unexpected, since Ni-R commonly exists in more than one
protonation state, depending on the pH of the protein solution[19,20]. Such a situation
however, does not apply for Ni-R in Hase I-cyt*b*. At all three pH values examined, no
additional bands associated with different forms of this most reduced state of the
enzyme were detected. This is clearly demonstrated in Figure 4.

## Discussion

Oxygen-tolerant enzymes are ideal candidates for biotechnological applications[8,38], since they maintain a considerable hydrogen oxidising ability under aerobic conditions. The Hase I-cyt*b* from *A. aeolicus* is a particularly exceptional complex, since it is highly thermostable and shows an increased resistivity towards oxygen[39,40]. This is exemplified in the chronoamperometry experiment, in which injection of molecular oxygen did not lead to a dramatic decrease in the activity, in contrast to standard hydrogenases that become completely inhibited[34,41]. The respective measurement was carried out by poising the enzyme at the very positive potential of +190 mV. Removal of the oxygen upon flushing with $H_2$, resulted in a fast recovery of the partially lost activity. This is rather remarkable considering that activity could be recovered at this high potential, without having to reduce the enzyme prior to reactivation. This situation is similar to the case of the membrane bound (MBH) hydrogenase from *Ralstonia eutropha*[7,42] but contrasts the behaviour of the oxygen-sensitive hydrogenases, for which reactivation at such positive potentials is essentially irreversible. In addition, the 'switch potential' at which the enzyme reactivates is markedly more positive than that of standard hydrogenases[41] and the overall activity of the enzyme takes place at more positive potentials.

It is thus compelling to elucidate the mechanism associated with the function of this enzyme and identify the underlying reasons for its intriguing properties. On these grounds, FTIR spectroscopy was employed to detect possible modifications in the [NiFe] centre, since the infrared stretching vibrations are remarkably sensitive to changes in the coordination and hydrogen bonding environment of the active site of hydrogenases[21]. Furthermore, combined with *in-situ* electrochemistry it is an important technique for constructing a scheme on the redox chemistry and properties of the hydrogenase enzyme.

The current study presents a systematic FTIR investigation of a [NiFe] hydrogenase from an extreme thermophilic organism. Our results demonstrate that the active site retains the typical iron coordination of one carbonyl and two cyanide ligands. This is consistent with recent observations on the MBH hydrogenase from *R. eutropha*[37], but not with those on the soluble $NAD^+$-reducing hydrogenase (SH) from the same organism, in which additional $CN^-$ were proposed for both nickel and

iron[27]. It can be concluded that no additional ligands present in the active site of the Hase I hydrogenase from *A. aeolicus* are related to the oxygen-tolerance

The FTIR spectrum of the as-isolated Hase I(-cyt*b*) showed absorption bands of an oxidised state, which on the basis of concomitant EPR[10] studies can be assigned to Ni-B. The g-values are slightly different with the larger deviation being observed for the $g_x$ component, while the stretching vibrations of the diatomic ligands were very similar to those of Ni-B present in oxygen-sensitive hydrogenases[35] (see Appendix D). This indicates a rather strong similarity of the structure of their active sites. X-ray crystallographic and EPR/ENDOR[15] studies on the *D. vulgaris* Miyazaki hydrogenase have detected a hydroxide ligand bridging the two metal ions in this state, rendering it inactive. Thus, Ni-B represents an inhibited form that is, however, quickly activated. We can thus suppose that such an oxygenic species coordinates also the [NiFe] site in *A. aeolicus*, suggesting that the latter has the affinity of binding an oxygen-based ligand. However, based on present experiments it cannot be elucidated whether this ligand originates from the solvent or from $O_2$. The absence of the Ni-A and Ni-SU states accounts for the very fast reactivation of the enzyme and indicates a different reaction of the [NiFe] site under oxidising conditions or with molecular oxygen, impeding formation of these intermediates.

One-electron reduction of Ni-B in the electrochemical cell led to the appearance of an EPR-silent state. On the basis of the observed stretching vibrations, the reduced species in Figure 2b is associated rather with Ni-SIa than with (Ni-SIr)$_I$. The possibility that it could correspond to (Ni-SIr)$_{II}$ should not be overlooked, since these two states are proposed to have identical infrared stretching vibrations[20]. However, at 25°C or higher the putative water ligand in (Ni-SIr)$_{II}$ can be easily liberated and transition to Ni-SIa is thermodynamically favoured[43,44]. Therefore we assign this state to Ni-SIa.

Reduction of Ni-B at lower temperatures (4°C), where the activation kinetics become markedly slower, had no effect on the spectra. A change of the pH of the solution also did not result in the appearance of (Ni-SIr)$_I$[20,45]. Presumably, the lifetime of the (Ni-SIr)$_I$ state is too short to enable its detection under the conditions of the current experiments. The redox potential for the Ni-B / Ni-SIa couple was determined to be -107 ± 5 mV. This value cannot be directly compared with the respective one for the oxygen sensitive enzymes, since in *A. aeolicus* the (Ni-SIr)$_I$ is absent. It is however, approximately 30-50 mV higher compared to the values reported for

*D. gigas*[19], *A. vinosum*[20] and *D. vulgaris*[45]. Hase I(-cyt*b*) is thus shown to convert to the active states at higher redox potentials. In addition, reactivation of Ni-B did not show a temperature dependent kinetic barrier, which is consistent with the inability to detect the (Ni-SIr)$_I$ state[35]. The fast reactivation from Ni-B, could be associated with a different interaction of the oxygenic ligand with the [NiFe] site in *A. aeolicus*. This is corroborated by the up-shifted g-values in the EPR spectrum of Ni-B[10], indicating a slightly different electronic structure of the spin carrying [NiFe] centre.

Further reduction of Ni-SIa was followed by the appearance of signals at higher frequencies, with the CO band centred at 1949 cm$^{-1}$ and the coupled CN pair at 2078 and 2088 cm$^{-1}$, respectively. This state corresponds to Ni-C and has CN bands close to those of Ni-SIa. The titrations at pH 7.4 exhibited a comparatively small yield of the Ni-C state, while at higher pH (8.4) it could not be discerned as a detectable intermediate. In all cases, the transition to Ni-R is observed to be rapid due to the fact that the midpoint potentials of Ni-R and Ni-C are comparatively close. This results in an underpopulated Ni-C state and indicates that the hydride in the Ni-C state of the *A. aeolicus* Hase I(-cyt*b*) is bound more weakly, thus increasing the reactivity of the complex. In support of the latter assumption, ENDOR and HYSCORE studies of Ni-C in *A. aeolicus* detected a hydride ligand that is more loosely bound[46], presumably due to an elongated or a more asymmetric positions of the hydride in the Ni-Fe bridge.

The midpoint potential for the appearance of the Ni-SIa /Ni-C couple is -283 ± 5 mV. This value is approximately 100 mV more positive with respect to the one observed in mesophilic anaerobic hydrogenases, showing a less energy demanding activation of dihydrogen. Experiments carried out on the dimeric Hase I (without cyt*b*) led to essentially identical results and showed that the presence of cyt*b* does not shift the redox potentials of the various intermediates, but stabilizes the Ni-C state.

At a potential of -444 mV all redox processes in the Hase I(-cyt*b*) complex are completed and the enzyme is found in the most reduced Ni-R state. There are no signals corresponding to Ni-C, which shows that at 25°C no equilibrium is formed between the substrate and the active states. *In vitro* and at room temperatures, Hase I is in an inactive state, working exclusively as a hydrogen oxidising enzyme. Ni-R in *A. aeolicus* is spectroscopically similar to the Ni-R2 and not to the typical Ni-R1 form of such states (Table 1). In other enzymes, Ni-R2 shows considerable intensity only at high pH values[19,20,45], suggesting that it corresponds to a more deprotonated form with

respect to Ni-R1. However, in Hase I, only one Ni-R could be detected and it was not in an acid base equilibrium with other states in the pH range examined (6.4-8.4). The midpoint potential for the Ni-C / Ni-R couple is -310 ±5 mV. Compared to mesophilic hydrogenases this value is about 100 mV more positive and again shows that the hydrogen oxidising ability in hyperthermophilic organisms is more efficiently 'tuned'.
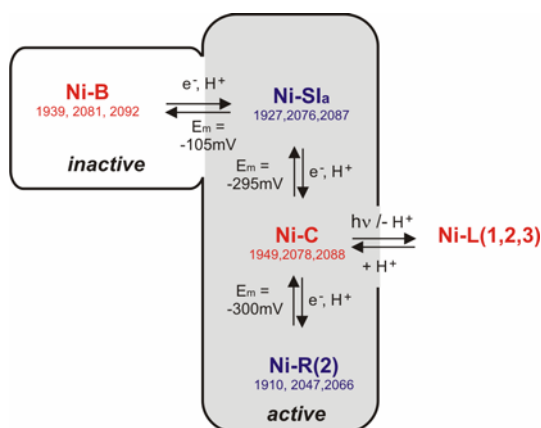


**Scheme 2.** Schematic overview of the proposed catalytic cycle for the Hase I (-cyt*b*) from the hyperthermophilic bacterium *A. aeolicus*. The paramagnetic states are denoted in red and the EPR-silent states in blue. The infrared stretching vibrations at 25 °C are also included. With grey the non-detectable transient states are illustrated. The midpoint potentials for these redox transitions are given for pH 7.4.

## Conclusions

The present study comprises the first systematic investigation on the redox processes involved in the redox chemistry of hyperthermophilic enzymes and in particular of the Hase I(-cyt*b*) from *A. aeolicus*. FTIR-electrochemistry in solution revealed a simple enzymatic mechanism comprising only four redox states; namely Ni-B, Ni-SI$_a$, Ni-C and Ni-R. The absence of the (Ni-SI$_r$)$_I$ state as a detectable intermediate suggests an instantaneous recovery from the oxygen inhibited Ni-B state.  Ni-C, which is mechanistically of central importance since it binds the substrate, is more unstable as an intermediate and quickly forms the most reduced Ni-R state. It is demonstrated that both oxygen and substrate carrying states have a more transient character, most likely originating from a weaker bonding interaction with exogenous ligands. The fewer redox intermediates and their notably more positive midpoint potentials, show that such enzymes perform under optimised conditions a less energy demanding activation of dihydrogen. Hydrogenases in hyperthermophilic bacteria such as *A. aeolicus* are ideally designed systems; the reactivity of their [NiFe] site is much higher than the one of their mesophilic counterparts leading to a more efficient enzymatic mechanism and possibly to the enhanced oxygen tolerance observed.

## References

1. Vignais, P. M. *Results Prob. Cell Differ.* **2008**, *45*, 223-252.

2. Vignais, P. M.; Billoud, B. *Chem. Rev.* **2007**, *107*, 4206-4272.

3. Volbeda, A.; Charon, M. H.; Piras, C.; Hatchikian, E. C.; Frey, M.; Fontecilla-Camps, J. C. *Nature* **1995**, *373* (6515), 580-587.

4. Nicolet, Y.; Lemon, B. J.; Fontecilla-Camps, J. C.; Peters, J. W. *Trends in Biochemical Sciences* **2000**, *25* (3), 138-143.

5. Shima, S.; Pilak, O.; Vogt, S.; Schick, M.; Stagni, M. S.; Meyer-Klaucke, W.; Warkentin, E.; Thauer, R. K.; Ermler, U. *Science* **2008**, *321* (5888), 572-575.

6. Guiral, M.; Tron, P.; Belle, V.; Aubert, C.; Leger, C.; Guigliarelli, B.; Giudici-Orticoni, M. T. *International Journal of Hydrogen Energy* **2006**, *31* (11), 1424-1431.

7. Ludwig, M.; Cracknell, J. A.; Vincent, K. A.; Armstrong, F. A.; Lenz, O. *J. Biol. Chem.* **2009,** *284* (1), 465-477.

8. Mertens, R.; Liese, A. *Curr. Opin. Biotechnol.* **2004**, *15* (4), 343-348.

9. Huber, R.; Wilharm, T.; Huber, D.; Trincone, A.; Burggraf, S.; Konig, H.; Rachel, R.; Rockinger, I.; Fricke, H.; Stetter, K. O. *Systematic and Applied Microbiology* **1992**, *15* (3), 340-351.

10. Brugna-Guiral, M.; Tron, P.; Nitschke, W.; Stetter, K. O.; Burlat, B.; Guigliarelli, B.; Bruschi, M.; Giudici-Orticoni, M. T. *Extremophiles* **2003**, *7* (2), 145-157.

11. Cammack, R.; Patil, D. S.; Hatchikian, E. C.; Fernandez, V. M. *Biochim. Biophys. Acta* **1987,** *912* (1), 98-109.

12. Albracht, S. P. J. *Biochim. Biophys. Acta-Bioenergetics* **1994**, *1188* (3), 167-204.

13. Fernandez, V. M.; Hatchikian, E. C.; Cammack, R. P. *Biochim. Biophys. Acta* **1985,** *832* (1), 69-79.

14. Lamle, S. E.; Albracht, S. P. J.; Armstrong, F. A. *J. Am.Chem. Soc.* **2004**, *126* (45), 14899-14909.

15. Lubitz, W.; Reijerse, E.; van Gastel, M. *Chem. Rev.* **2007**, *107*, 4331-4365

16. van Gastel, M.; Stein, M.; Brecht, M.; Schroder, O.; Lendzian, F.; Bittl, R.; Ogata, H.; Higuchi, Y.; Lubitz, W. *J. Biolog. Inorg. Chem.* **2006**, *11* (1), 41-51.

17. Ogata, H.; Hirota, S.; Nakahara, A.; Komori, H.; Shibata, N.; Kato, T.; Kano, K.; Higuchi, Y. *Structure* **2005**, *13* (11), 1635-1642.

18. Volbeda, A.; Martin, L.; Cavazza, C.; Matho, M.; Faber, B. W.; Roseboom, W.; Albracht, S. P. J.; Garcin, E.; Rousset, M.; Fontecilla-Camps, J. C. *J. Biolog. Inorg. Chem.* **2005**, *10* (3), 239-249.

19. De Lacey, A. L.; Hatchikian, E. C.; Volbeda, A.; Frey, M.; Fontecilla-Camps, J. C.; Fernandez, V. M. *J. Am. Chem. Soc.* **1997**, *119* (31), 7181-7189.

20. Bleijlevens, B.; van Broekhuizen, F. A.; de Lacey, A. L.; Roseboom, W.; Fernandez, V. M.; Albracht, S. P. J. *J. Biolog. Inorg. Chem.* **2004**, *9* (6), 743-752.

21. Pandelia, M.-E.; Ogata, H.; Currell, L. J.; Flores, M.; Lubitz, W. *J. Biol Inorg. Chem.* **2009,***14(8),* 1227.

22. Brecht, M.; van Gastel, M.; Buhrke, T.; Friedrich, B.; Lubitz, W. *J. Am Chem. Soc.* **2003**, *125* (43), 13075-13083.

23. Foerster, S.; van Gastel, M.; Brecht, M.; Lubitz, W. *J. Biolog. Inorg. Chem.* **2005**, *10* (1), 51-62.

24. Pershad, H. R.; Duff, J. L. C.; Heering, H. A.; Duin, E. C.; Albracht, S. P. J.; Armstrong, F. A. *Biochemistry* **1999**, *38* (28), 8992-8999.

25. Vincent, K. A.; Armstrong, F. A. *Inorg. Chem.* **2005**, *44* (4), 798-809.

26. Pierik, A. J.; Roseboom, W.; Happe, R. P.; Bagley, K. A.; Albracht, S. P. J. *J. Biolog. Chem.* **1999**, *274* (6), 3331-3337.

27. Happe, R. P.; Roseboom, W.; Egert, G.; Friedrich, C. G.; Massanz, C.; Friedrich, B.; Albracht, S. P. J. *FEBS Lett.* **2000**, *466* (2-3), 259-263.

28. Moss, D. A.; Leonhard, M.; Bauscher, M.; Mantele, W. *FEBS Lett.* **1991**, *283* (1), 33-36.

29. Baymann, F.; Moss, D. A.; Mantele, W. *Anal. Biochem.* **1991**, *199* (2), 269-274.

30. Fultz, M. L.; Durst, R. A. *Analytica Chimica Acta* **1982**, *140* (1), 1-18.

31. Prince, R. C.; Linkletter, S. J.; Dutton, P. L. *Biochim. Biophys. Acta* **1981**, *635* (1), 132-148.

32. Dutton, P. L. *Methods Enzymol* **1978**, *54*, 411-435.

33. Leger, C.; Jones, A. K.; Roseboom, W.; Albracht, S. P. J.; Armstrong, F. A. *Biochemistry* **2002,** *41* (52), 15736-15746.

34. Jones, A.K.; Lamle, S.E.; Pershad, H.R.; Vincent, K.A.; Albracht, S.P.J.; Armstrong, F.A.; *J. Am. Chem. Soc.* **2003**, 125, 8505-8514

35.  De Lacey, A. L.; Fernandez, V. M.; Rousset, M.; Cammack, R. *Chem. Rev.* **2007**, *107*, 4304-4330.

36.  Bagley, K. A.; Duin, E. C.; Roseboom, W.; Albracht, S. P. J.; Woodruff, W. H. *Biochemistry* **1995**, *34* (16), 5527-5535.

37.  Saggu, M.; Zebger, I.; Ludwig, M.; Lenz, O.; Friedrich, B.; Hildebrandt, P.; Lendzian, F. *J. Biolog. Chem.* **2009**, *284* (24), 16264-16276.

38.  Cammack, R.; Frey, M. *Hydrogen as a fuel;* Taylor and Francis: London, 2001.

39.  Giudici-Orticoni, M.; Guiral, M.; Tron, P.; Belle, V.; Aubert, C.; Leger, C.; Guigliarelli, B. *International Journal of Hydrogen Energy* **2006**, *vol.31, no.11*, 1424-1431.

40.  Jenney, F. E., Jr.; Adams, M. W. *Ann. N. Y. Acad. Sci.* **2008**, *1125*, 252-266.

41.  Leger, C.; Dementin, S.; Bertrand, P.; Rousset, M.; Guigliarelli, B. *Journal of the American Chemical Society* **2004**, *126* (38), 12162-12172.

42.  Vincent, K. A.; Cracknell, J. A.; Lenz, O.; Zebger, I.; Friedrich, B.; Armstrong, F. A. *Proc. Nat. Acad. Sci.* **2005**, *102* (47), 16951-16954.

43.  Kurkin, S.; George, S. J.; Thorneley, R. N. F.; Albracht, S. P. J. *Biochemistry* **2004**, *43* (21), 6820-6831.

44.  George, S. J.; Kurkin, S.; Thorneley, R. N. F.; Albracht, S. P. J. *Biochemistry* **2004,** *43* (21), 6808-6819.

45.  Fichtner, C.; Laurich, C.; Bothe, E.; Lubitz, W. *Biochemistry* **2006**, *45* (32), 9706-9716.

46.  Pandelia, M. E.; Tron-Infossi, P.; Giudici-Orticoni, M.-T.; Lubitz, W. *to be submitted* **2009** (see Chapter 10 of the present study)

# Chapter 8

## Hydrogenase I from the hyperthermophilic bacterium *Aquifex aeolicus*: CO inhibition studied by infrared spectroelectrochemistry and time-resolved FTIR at low temperatures
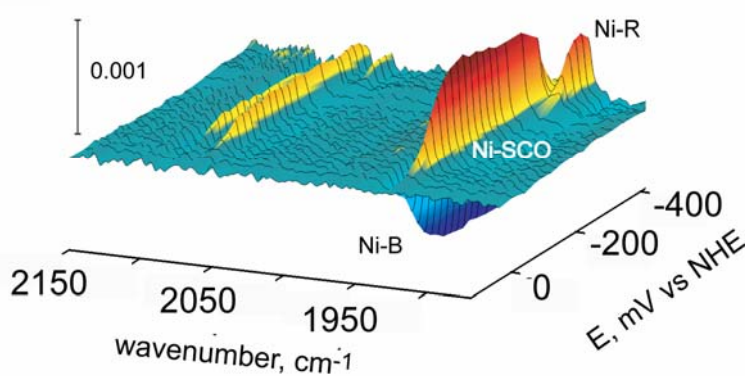


**Graphical Abstract.** Redox intermediates of Hase I from *A. aeolicus* in the presence of CO in a three dimensional representation as a function of the applied potential. The spectrum at +143 mV has been subtracted as a reference.

*Chapter 8*

# Hydrogenase I from the hyperthermophilic bacterium *Aquifex aeolicus*: CO inhibition studied by infrared spectroelectrochemistry and time-resolved FTIR at low temperatures[†]

Maria-Eirini Pandelia[*], Pascale Tron-Infossi[‡], Marie-Thérèse Giudici-Orticoni[‡], and Wolfgang Lubitz*

*Max-Planck-Institut für Bioanorganishe Chemie, Stiftstrasse 34-36, D45470, Mülheim*
[‡]*Laboratoire de Bioenergetique et Ingenierie des Proteines, IBSM-CNRS, 13402 Marseille*

## Abstract

The [NiFe] hydrogenase (Hase I) involved in the aerobic respiration mechanism of the hyperthermophilic bacterium *Aquifex aeolicus* shows increased oxygen tolerance, thermostability and it can form very stable films on pyrolytic graphite electrodes. These features are very appealing for its potential use for bio-applications in the framework of new alternative energy sources. Carbon monoxide is a competitive inhibitor for the function of oxygen-sensitive hydrogenases, such as those from sulphate reducing bacteria. On the other hand and on the basis of protein film voltammetry studies, oxygen tolerant hydrogenases, such as the one from *Aquifex aeolicus* and the membrane bound hydrogenase from *Ralstonia eutropha*, were insensitive towards CO inhibition. In the present study, these results are debated, since formation of a CO-adduct was observed under saturating carbon monoxide conditions. This provided a unique opportunity for investigating the affinity of the complex for CO binding and the reversibility of the processes involved by *in-situ* FTIR electrochemistry. In addition, low temperature photolysis of the extrinsic carbonyl was used to estimate the activation barrier for the rebinding of CO in the active site. The results can be directly compared to those reported for standard hydrogenases. The present findings are consistent with formation of a weak Ni-CO bond in the case of *Aquifex aeolicus* and are discussed on the basis of a different reactivity with inhibitors.

---

[†] *To be submitted* **2009**

## Introduction

Hydrogenases are metalloenzymes that couple oxidation of dihydrogen to the activity of redox related partners according to the elemental reaction[1]: $H_2 \rightleftharpoons 2H^+ + 2e^-$. They can be classified according to their metal ion content in three distinct classes; [NiFe], [FeFe] and iron-sulphur cluster-free hydrogenases (Hmd)[5], for which structural information has been obtained[2,3,4]. They are widespread in eukaryotic and prokaryotic microorganisms and are pivotal for their metabolic processes[6,7]. A subclass of these enzymes is found in microbes that thrive at extreme temperatures 80 °C or higher[7]. These are termed hyperthermophilic and one of their first bacterial representatives, *Aquifex (A. ) aeolicus*, is a micro-aerobic, obligate chemolithoautotrophic bacterium[8]. It is most commonly found in volcano submarine waters and grows optimally between 85 - 95 °C. Its complete genome has been sequenced[9] and encodes three distinct [NiFe] hydrogenases[10]. Among these enzymes, Hydrogenase I (Hase I) is membrane-bound and is involved in the respiration pathway with $O_2$ as the final electron acceptor[10,11]. It consists of two subunits. The large subunit (70 kDa) contains the heterobimetallic nickel-iron site, while the small subunit (40 kDa) contains the iron-sulphur centres that mediate the electron transfer between the [NiFe] site and the native electron acceptor, a di-haem cytochrome *b*. *In vitro*, it works preferably as an uptake hydrogenase.

Hase I is a particularly intriguing enzyme, due to its enhanced thermostability and oxygen tolerance[12-14]. It has been recently shown that at its physiological temperatures the oxygen inhibition rates are slow, allowing the enzyme to maintain a significant hydrogen oxidising ability under aerobic conditions[15]. At room temperatures it is in an inactive form that in the terms of standard hydrogenases can be associated with the readily activated Ni-B state ($Ni^{3+}$, paramagnetic S= 1/2)[10]. This species is known to carry a bridging hydroxide ($OH^-$)[16]. In contrast to oxygen-sensitive hydrogenases, no signals corresponding to the slowly reactivated Ni-A[17,18] state could be observed in the as isolated preparations of the enzyme. This has been shown by electron paramagnetic resonance (EPR)[10] and more recently Fourier transform infrared (FTIR) spectroscopy[14]. In addition, the latter showed that the $Fe(CN)_2CO$ coordination is preserved in Hase I, with the iron ($Fe^{2+}$) in a low spin and oxidation state [19].

One-electron reduction of Ni-B leads directly to the EPR-silent Ni-SIa state[14], without the inactive Ni-SI states as detectable intermediates[20]. Further reduction yields the active Ni-C state ($Ni^{3+}$, paramagnetic S=1/2). ENDOR and HYSCORE studies on the deuterated form of Ni-C have recently detected a hydride bound to the active site[21], consistent with previous studies on *Ralstonia (R.) eutropha*[22] and *Desulfovibrio* (*D.) vulgaris* Miyazaki F[23,24]. This hydride ligand is dissociated as a proton[25] upon illumination near cryogenic temperatures leaving the enzyme in the Ni-L state[24,26]. One electron reduction of Ni-C leads to the most reduced intermediate of the catalytic cycle termed Ni-R. Only one Ni-R state could be observed in a pH range between 6.4 and 8.4[14], in contrast to the three Ni-R forms reported for standard hydrogenases[27,28]. An overview of the redox processes in *A. aeolicus* Hase I is shown in Figure 1.
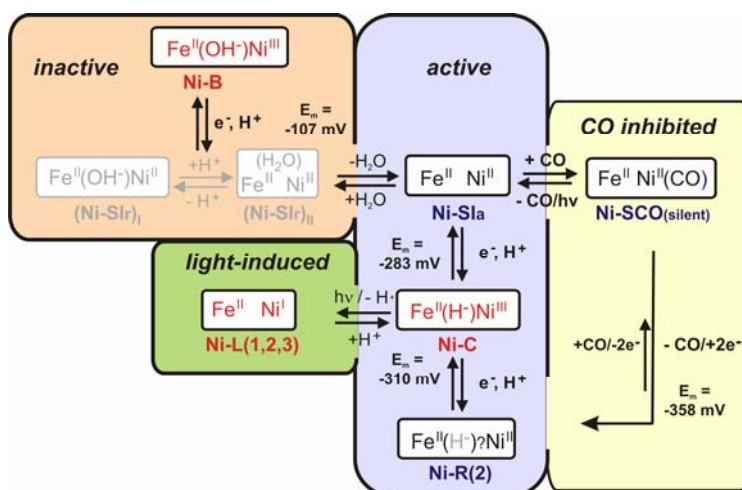


**Figure 1.** The proposed intermediate states of the Hase I from *A. aeolicus.* The paramagnetic states are given in red; the EPR-silent in black and the transient (non-detectable states) are indicated in grey. The reduction potentials for the transition between redox couples have been also included. The substrate ligand in Ni-R(2) is also shown in grey with questionmark, since it is most likely absent. The inactive, inactive, CO inhibited and light-induced intermediates are grouped into color-coded boxes.

It has been known for a long time that carbon monoxide inhibits the function of oxygen-sensitive hydrogenases[29]. Such an inhibition can be reversed if CO is removed from the protein solution or by illumination at cryogenic temperatures[30]. Infrared

spectroscopic studies showed that this exogenous carbonyl binds to the nickel ion[31], which was later corroborated by X-ray crystallographic experiments[32]. On the other hand, recent protein film voltammetry (PFV) studies have shown that the Hase I retains significant enzymatic activity in the presence of oxygen, whereas no inhibition by carbon monoxide could be observed[15]. Such a finding applies also for the oxygen tolerant membrane bound (MBH) hydrogenase from *R. eutropha*[33].

In the present work we demonstrated that it is possible to form a CO-adduct in Hase I of *A. aeolicus* under saturating CO conditions. This finding allows to spectroscopically study the CO inhibited state in such an enzyme, to identify its properties and compare results with the ones reported for standard hydrogenases[34,35]. For this purpose, *in-situ* infrared electrochemistry was carried out in the presence of carbon monoxide. Such an experiment allows the determination of the redox states that have the affinity for binding CO by combining a spectroscopic method (FTIR) with controlled potentiometric coulorimetry in solution[34,35]. Furthermore, on the basis of the light sensitivity of the CO-inhibited state formed[31,32], time-resolved low temperature measurements were performed to estimate the activation energy barrier for the ligand rebinding[36] and compare it to results obtained for *D. vulgaris*[35]. Such knowledge greatly contributes to understanding the reactivity of the Hase I from *A. aeolicus* with gaseous inhibitors such as carbon monoxide and may help in constructing a scheme for the enhanced oxygen tolerance of this enzyme.

*Chapter 8*

## Materials and Methods

*Protein purification.* Isolation and purification of the Hydrogenase I (Hase I) from *A. aeolicus* was carried out as previously described[10] in a 50 mM Tris-HCl buffer pH 7.0 in the presence of 5 -10 % glycerol and 0.01 % n-Dodecyl-β-D-maltoside (DDM).

*Electrochemical measurements.* Electrochemical measurements in solution were carried out in an Optically Transparent Thin-Layer Electrochemical (OTTLE) cell designed by Moss et al[37,38]. 25 µL of the protein-redox mediator solution were placed on a 8.5 µm thick gold (Au) mini-grid (70% transparent to infrared), which serves as the working electrode. A platinum (Pt) foil is used as the counter and a Ag/AgCl (1 M KCl) as the reference electrode. Calibration of the reference electrode prior to and after each measurement was performed by monitoring the reduction of methyl viologen (-448 mV, pH 7.0) with cyclic voltammetry. The temperature was regulated in the range between 4 and 40 ° C by water passing through the metallic body of the cell in a closed external circuit with a thermostat (LAUDA).

The pH of the protein solution was kept at pH 7.4 in a 25 mM Hepes-NaOH buffer for all measurements. The titrations were carried out in the presence of in total 11 redox mediating agents. These consist of: methylviologen, benzylviologen, neutral red, phenosafranine, anthraquinone-2-sulfonate, anthraquinone-1,5-disulfonate, 2-hydroxy-1,4-naphthoquinone, potassium indigo tetrafulfonate, methylene blue, phenazine methosulfate and naphthoquinone. Their redox potentials and pH dependence have been described elsewhere[39,40]. Additionally KCl was added as an electrolyte to a final concentration of 100 mM. The final concentration of the mediators in the solution was 83 µM and of the protein 180 µM.

An equilibration time of 3-5 minutes was allowed prior to recording the infrared spectra at each potential (steady state). The potentiometric titrations were fitted using the Nernst equation:

$$E = E_m + \frac{RT}{nF} \ln\left( \frac{[Ox_1]}{[Red_1]} \right),$$

where $E_m$ it the standard reduction potential, R is the universal gas constant, F is the Faraday constant, n the number of electrons, T the temperature, $[Ox_1]$ the concentration of the oxidised species and $[Red_1]$ the concentration of the reduced

species. All potentials referred to in the present work are quoted with respect to the normal hydrogen electrode potential (NHE).

*Fourier transform infrared (FTIR) spectroscopy.* Infrared measurements were carried out on a Bruker IFS 66v/s FTIR spectrometer with 2 cm$^{-1}$ resolution. The detector was a photovoltaic mercury cadmium telluride (MCT) element. Time resolved measurements at cryogenic temperatures were carried out in an Optistat CF cryostat with an ITC 503 temperature controller (Oxford Instruments). *In-situ* illumination for 5 minutes was performed with a slide projector (250 W halogen lamp, 24 V) equipped with an electronic shutter (Compor). The low temperature FTIR cell consists of two sapphire windows and the optical path-length is 80 μM. The software for data recording consisted of the OPUS package (Bruker Optics). Analysis and further processing was performed with home-built routines written in MATLAB 7.0 (Mathworks). The measured intensity of the bands was divided by the enzyme concentration and the optical path length in order to obtain the apparent normalised absorbance (B, mM$^{-1}$ cm$^{-1}$).

*Sample preparation and treatment with gases.* For the electrochemical measurements, the solution consisting of Hase I and mediators was degassed prior incubation for 30 min with carbon monoxide (N47, Air Liquide). The CO saturated solution was subsequently transferred into the OTTLE cell under 100% CO atmosphere in a glovebag.

For the low temperature measurements a 30 μL solution of 200 μM Hase I in 50 mM Hepes-NaOH (pH 7.4) was reduced with hydrogen gas (1.100 mbar, N50 Air Liquide) for 30 minutes at room temperature and was subsequently incubated for 20-30 min under 1.600 mbar CO (0°C). In contrast to standard hydrogenases (*e.g. D. vulgaris*), longer incubation times under CO saturating conditions are required for fully inhibiting the enzyme[‡]. The sample was transferred under anaerobic conditions in the FTIR cell and subsequently frozen in liquid nitrogen under dark conditions.

.

---

[‡] 5 min  under 1.6 bar CO for *D. vulgaris*[35], 20-30 min  1.6 bar CO for *A. aeolicus* at 0°C.

## Results

**Infrared electrochemistry in the presence of CO**

Figure 2a shows the FTIR spectrum of the as isolated Hase I in the presence of CO in the solution at the resting potential of +236 mV at 25 °C. Three bands can be observed in this spectrum, which are assigned to the stretching vibrations of the diatomic ligands coordinating the iron, one CO and two CN⁻. This spectrum corresponds to the inactive Ni-B state (see Table 1)[14]. The more intense band at 1939 cm⁻¹, is associated with the CO stretching vibration, while the two lower intensity bands at 2081 and 2092 cm⁻¹ correspond to the coupled CN⁻. Consistent with previous observations on the standard hydrogenases, the Ni-B state of Hase I is not inhibited by CO[34,35,41].

By applying a potential of -64 mV for 10 min, the FTIR spectrum in Figure 2b shows that the enzyme is now entirely clamped in a CO-inhibited state. This is corroborated by the appearance of a fourth band at 2066 cm⁻¹, which is assigned to the extrinsic CO bound to nickel. The bands corresponding to the intrinsic diatomic ligands to iron are shifted 2-4 cm⁻¹ with respect to the ones of Ni-SIa (Table 1), in agreement with previous findings on standard hydrogenases[34,35]. Formation of the CO-adduct (Ni-SCO, EPR-silent), indicates that the [NiFe] site of Hase I is accessible to CO and has the affinity to bind such an inhibitor.

Lowering further the potential no spectral changes occur until -274 mV. At more negative values, the Ni-SCO signals are being replaced by the most reduced state Ni-R. A form of electrochemical cleavage of CO takes place that is completed at -414 mV, in which all of the hydrogenase molecules are in the active Ni-R form (Figure 2c). The latter is described by a CO band at 1910 cm⁻¹ and a pair of cyanide bands at 2047, 2066 cm⁻¹. At these negative redox potentials Hase I has completely recovered from inhibition.

By slowly reoxidising the sample in the electrochemical cell, all the above spectral features are reproduced and at +143 mV the enzyme has returned to the Ni-B state (Figure 2d). This result was unforseen, since in all hydrogenases studied so far the Ni-SCO state is very resistant towards oxidation under these experimental conditions[34,35]. If reoxidation is performed at 15°C transition of the Ni-SCO to Ni-B appeared to be less favourable. At +143 mV and at 15°C only 40% of the molecules are in the Ni-B state and the rest in Ni-SCO (data not shown).
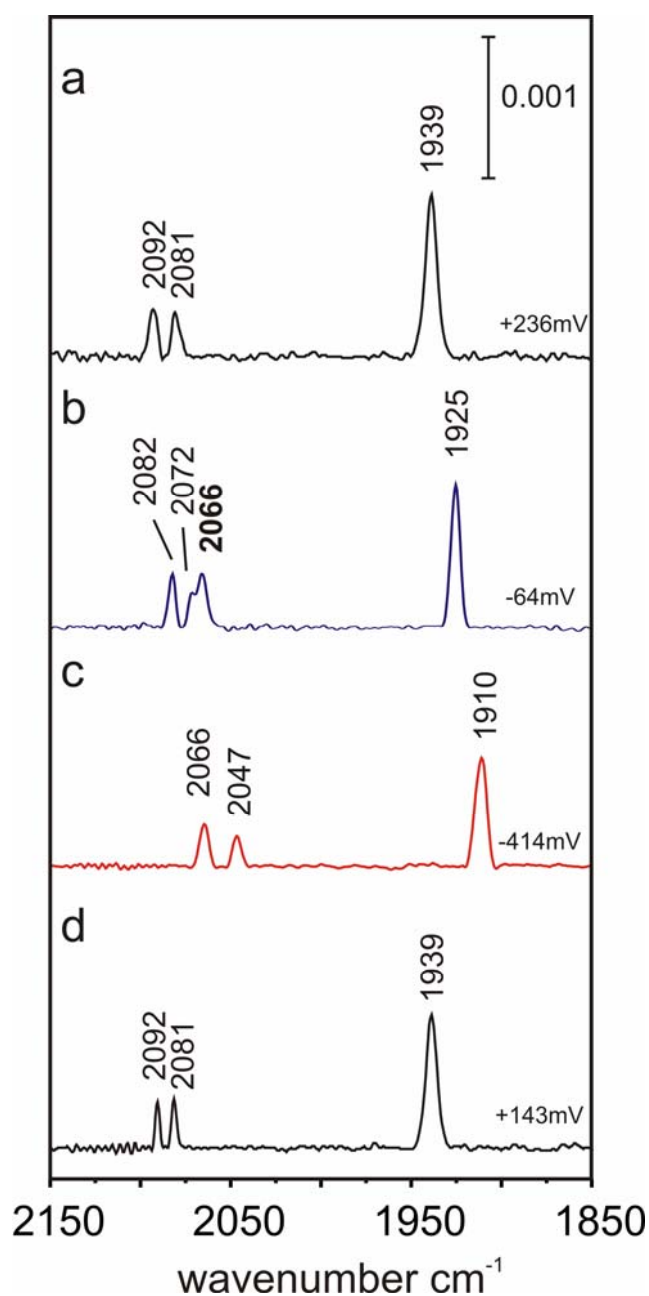
**Figure 2.** FTIR spectra of Hase I from *A. aeolicus* in the presence of CO at 25°C. a) At the resting potential +236 mV the as-isolated enzyme is in Ni-B, b) at -64 mV Ni-SCO has formed, as indicated by the fourth band at 2066 cm$^{-1}$ corresponding to the extrinsic CO c) at -414 mV the CO has been 'cleaved' and the enzyme is in Ni-R, d) reoxidation of the enzyme at +143 mV shows the Ni-B state. Each spectrum is an average of 1000 scans with 2cm$^{-1}$ resolution.

**Potentiometric titration in the presence of carbon monoxide**

The redox behaviour of all three states involved is depicted as a function of the redox poise in Figure 3a in a three dimensional representation. Shown are difference spectra, from which the infrared data at +143 mV has been subtracted. As the potential is lowered, the enzyme is being activated resulting in a decrease of Ni-B and the concomitant increase of the Ni-SCO state in a range between +100 and -100 mV. The protein remains in Ni-SCO and at values lower than -300 mV the Ni-R starts to form. At -414 mV all of the molecules are in the Ni-R active state.

Hase I at 25°C and depending on the potential, switches reversibly between the Ni-B and the Ni-SCO state. The titration of the Ni-B / Ni-SCO couple is shown in Figure 3b. The potential dependence of the intensity of the infrared bands corresponding to the Ni-B and Ni-SCO states is fitted by the Nernst equation corresponding to a one-electron process. A formal midpoint potential of $E_m$ = -9 ± 5 mV is obtained by taking the mean value of these two curves. At lower potentials CO can be 'cleaved' form the active site and the transition from Ni-SCO to active Ni-R takes place with a midpoint potential of -358 ± 5 mV (Figure 3c). This process can, however, be better described by a two-electron transfer. The Nernst fit for the one-electron transfer has been included with a dotted red line.

**Table 1.** FTIR stretching vibrations corresponding to the CO and CN$^-$ ligands of the Hase I from *A. aeolicus* for the observed intermediate states at 297 K and at 100 K (values in parenthesis). The error in the determination of the frequency bands is ± 1 cm$^{-1}$. The values for the Ni-B, Ni-C states are taken from [35].

| State | $\bar{v}_{CO}(Fe)$, cm$^{-1}$ | $\bar{v}_{CN^-}(Fe)_{asym}$, cm$^{-1}$ | $\bar{v}_{CN^-}(Fe)_{sym}$, cm$^{-1}$ | $\bar{v}_{CO}(Ni)$, cm$^{-1}$ |
|---|---|---|---|---|
| **Ni-B** | 1939 (1940) | 2081 (2083) | 2092 (2094) | - |
| **Ni-SI$_a$** | 1927 (1931) | 2077 (2079) | 2086 (2090) | - |
| **Ni-C** | 1949 (1952) | 2078 (2079) | 2088 (2093) | - |
| **Ni-R** | 1910 (1912) | 2047 (2047) | 2066 (2067) | - |
| **Ni-S$^{12}$CO** | 1925 (1927) | 2072 (2074) | 2082 (2086) | 2066 (2072) |
| **Ni-S$^{13}$CO** | (1926) | (2073) | (2085) | (2026) |
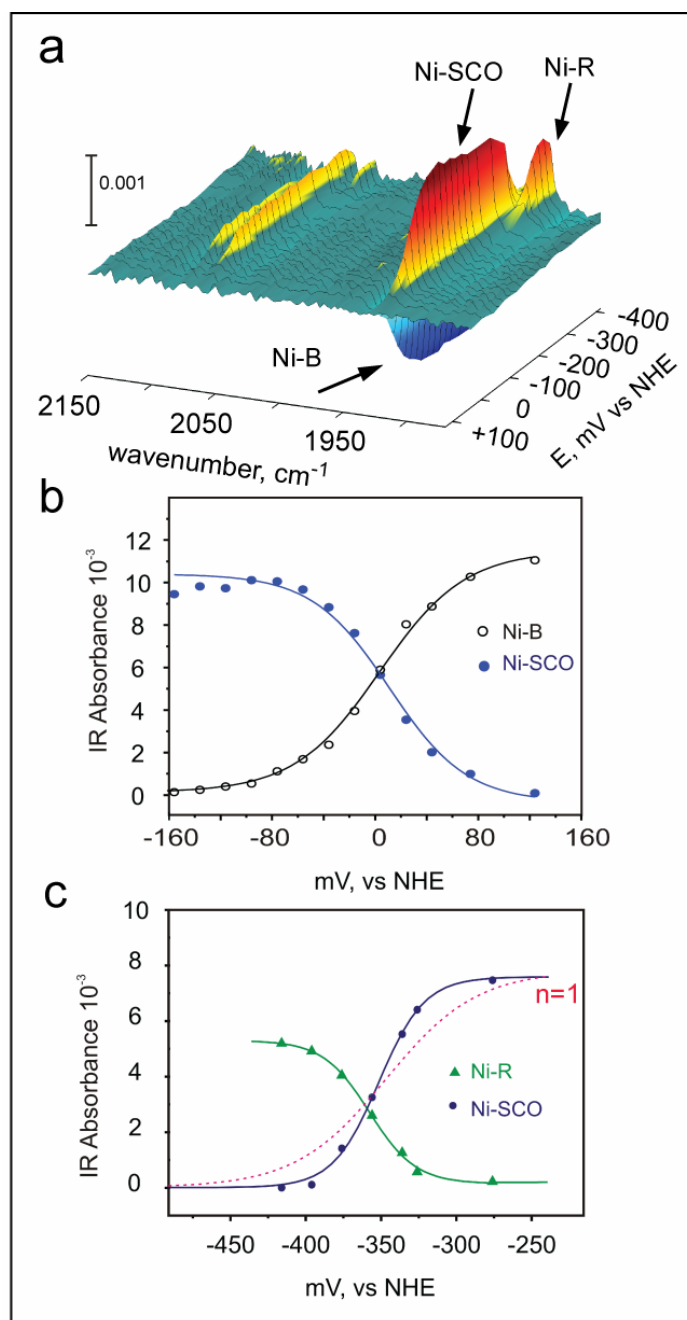
**Figure 3.** (a) Redox intermediates of Hase I from *A. aeolicus* in the presence of CO in a three dimensional representation as a function of the applied potential. (b) Potentiometric titration corresponding to the Ni-B/Ni-SCO couple at 25°C with apparent midpoint potential $E_m$ = -9 ± 5 mV. (c) Potentiometric titration of the Ni-SCO/Ni-R couple with a midpoint potential of -358 mV corresponding to a two-electron transfer. The Nernst fit for a one-electron transfer is plotted in red (dashed line). Experimental conditions: 25°C, IR resolution ± 1 cm$^{-1}$, potential step 20 mV.

**Low temperature FTIR and $^{13}$CO isotope labelling**

Figure 4a shows the FTIR spectrum of the CO inhibited state (Ni-SCO) in Hase I at 40 K. The infrared bands are now uniformly shifted by 0-4 cm$^{-1}$ with respect to room temperature measurements, due to the more restricted motion of the diatomic oscillators at low temperatures[42]. The band at 1927 cm$^{-1}$ is ascribed to the intrinsic to iron CO ligand and the two bands at 2074 and 2086 cm$^{-1}$ correspond to the two coupled CN$^{-}$ oscillators. The fourth band at 2072 cm$^{-1}$ is assigned to the extrinsically added carbon monoxide bound to nickel. Upon reaction of the active enzyme with isotope labelled $^{13}$CO, the band of the exogenous carbonyl is expected to shift, since stretching vibrations are mass-dependent properties.



**Figure 4.** (a) FTIR spectra of the Ni-SCO state of Hase I from *A. aeolicus* at 40 K in the dark. The extrinsic CO is centred at 2072 cm$^{-1}$ (b) $^{13}$CO isotope labelle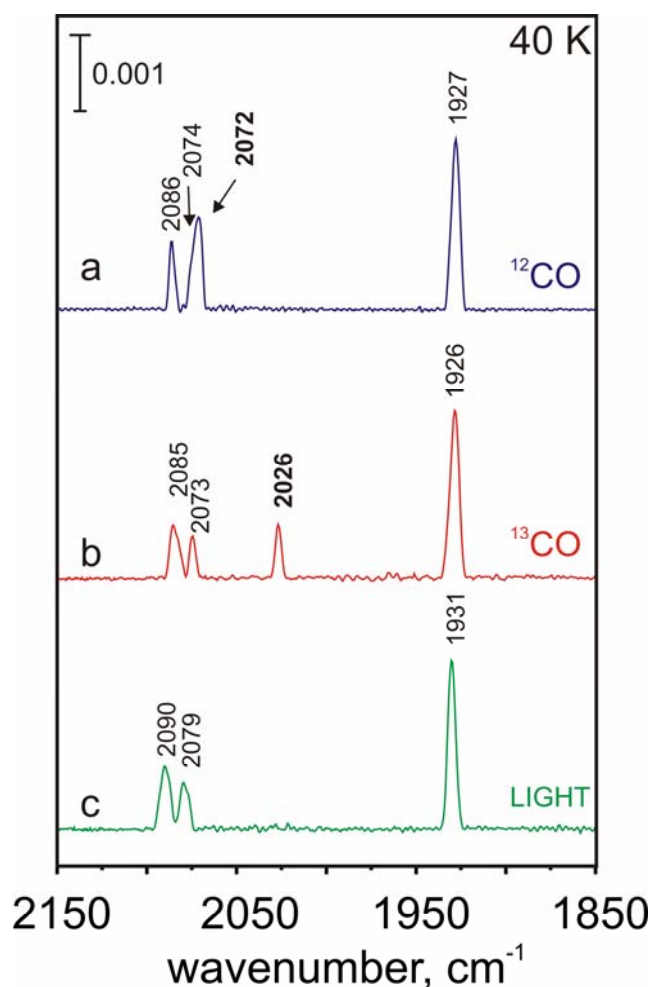d Ni-SCO state in the dark. The band corresponding to the exogenous CO is shifted to 2026 cm$^{-1}$. (c) Illuminated spectrum of the Ni-SCO state. The extrinsic CO is photodissociated and the enzyme is in the Ni-SI$_a$ state.

This is shown in the spectrum of the $^{13}CO$ inhibited Hase I at 40 K in the Figure 4b. The absorption band of the extrinsic CO is shifted by 46 cm$^{-1}$ towards lower frequencies and is centred now at 2026 cm$^{-1}$.

The Ni-SCO is light sensitive at cryogenic temperatures in agreement with earlier observations for the other known hydrogenases[31,32,35]. Illumination with white light at temperatures below 125 K leads to the disappearance of the bands at 2072 cm$^{-1}$ ($^{12}CO$) and 2026 cm$^{-1}$ ($^{13}CO$), respectively (Figure 4c). After the photolytic loss of the externally added CO, the light-induced state formed corresponds to Ni-SIa. The three bands of the intrinsic iron ligands are slightly shifted to higher frequencies with respect to the ones of the Ni-SCO, suggesting a slight decrease in the electron density at the iron atom.

**Kinetics of the CO rebinding in Ni-SI$_a$ and its activation energy barrier**

Conversion from Ni-SCO to Ni-SIa is reversible in the dark, involving dissociation of CO and its rebinding to the active site. In Figure 5a the time evolution of light-minus-dark difference spectra is shown in a three dimensional representation at 112.5 K. The first slice of the spectrum corresponds to t = 0, where the amount of Ni-SIa is maximal. At subsequent times the Ni-SCO state reappears, as rebinding of CO to the active site occurs. The recombination rate constants were measured in a range between 120 and 105 K and have a single-exponential character indicating a first-order reaction.

**Table 2.** Activation energies for the CO rebinding in the active site of the Hase I from *A. aeolicus*. The error in the calculated activation energies is 8 % and in the frequency factors one order of magnitude. Results for *D. vulgaris*[35] are included for comparison.

| State | $E_a$ (kJ mol$^{-1}$) | $A_0$ (s$^{-1}$) |
|---|---|---|
| *A. aeolicus* | | |
| (single exp) | 10.5 | 14 |
| | | |
| *D. vulgaris* | | |
| (slow bi-exp) | 8.8 | $2 \cdot 10^3$ |
| (fast bi-exp) | 8.0 | $4 \cdot 10^3$ |

The temperature dependence of the rate constants follows the empirical Arrhenius equation $k = A_0 \exp(-E_a/RT)$, where k is the rate constant in $s^{-1}$, $A_0$ is the frequency factor in $s^{-1}$ ( intercept at $1/T \rightarrow 0$), $E_a$ is the activation energy in kJ $mol^{-1}$, R is the universal gas constant 8.3144 J $K^{-1}$ $mol^{-1}$ and T the temperature in K. The activation barrier for the CO rebinding was estimated by analysing the kinetics of the disappearance of Ni-SIa and the recovery of Ni-SCO, which were the same within the experimental error (Figure 5b, Table 2). The inverse of the averaged rate constants (lifetimes) are given in Table 3. The activation barrier corresponds to $\sim$ 10.5 kJ $mol^{-1}$, which is smaller than that for *D. vulgaris*[35] as will be discussed in the following.
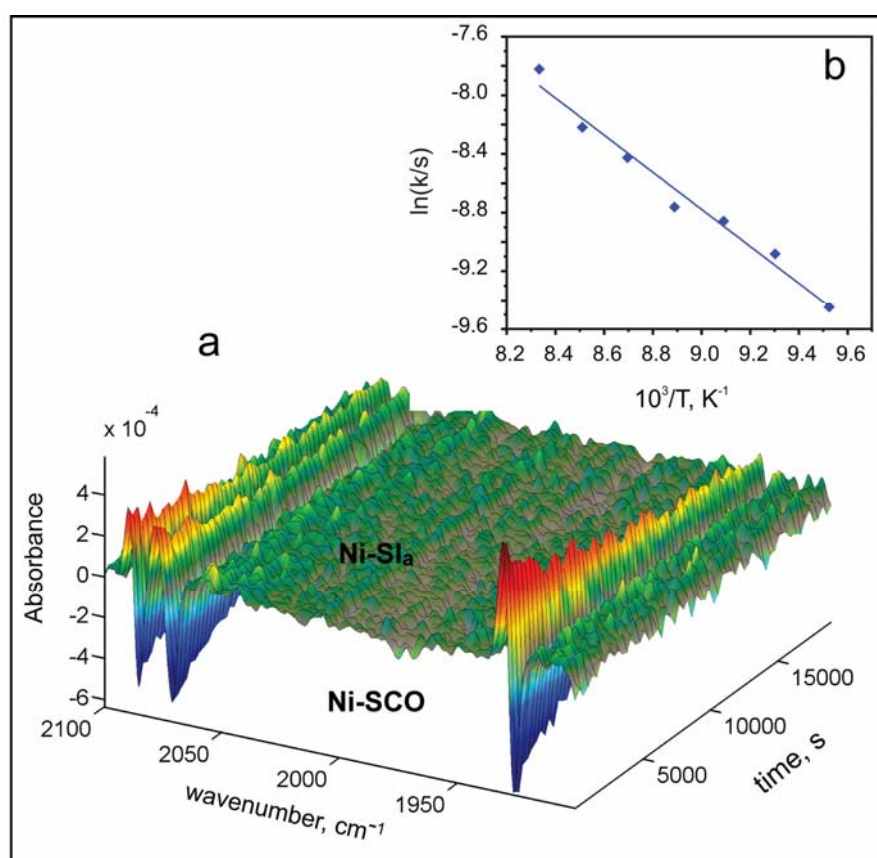


**Figure 5.** (a) A three dimensional representation of a light-minus-dark difference infrared spectrum at 112.5 K. The disappearance of the bands corresponding to the Ni-SIa state (light product) and the recovery of the Ni-SCO state (dark educt) during dark adaptation is shown as a function of time, (b) Temperature dependence of the recombination rate constants. The activation energy barrier is given by the slope of the linear fit (Arrhenius).

**Table 3.** Averaged lifetimes (inverse rate constants) obtained from analysing the back conversion kinetics corresponding to the decay of Ni-SI$_a$ and the recovery of Ni-SCO. The experimental error is ± 8 %.

| Temperature, K | mono-exponential time constants, s |
|---|---|
| 120.0 | 2495 |
| 117.5 | 3710 |
| 115.0 | 4560 |
| 112.5 | 6390 |
| 110.0 | 7040 |
| 107.5 | 8790 |
| 105.0 | 12700 |

## Discussion

The reactivity of Hase I from *A. aeolicus* with carbon monoxide was studied by a combination of *in-situ* infrared electrochemistry and low temperature FTIR spectroscopy.

The results can be summarized as follows:

i) The as-isolated enzyme in the presence of CO is in the Ni-B state. The latter is spectroscopically very similar to the one from mesophilic hydrogenases $(Ni^{3+})$[10] and thus we can speculate that it carries a hydroxide ligand[16] also bound to its active site, hindering binding of CO.

ii) Application of moderate negative potentials results in the activation of the enzyme by release of the oxygenic species and a first reduction of nickel to the 2+ oxidation state. Under these conditions, carbon monoxide can bind to the active centre and the CO inhibited state is formed. Poising the enzyme at -64 mV for 10 min was adequate to convert the enzyme entirely to the Ni-SCO state. This is in a remarkable contrast to previous observations on *D. fructosovorans*[34], where prior to the appearance of Ni-SCO the enzyme had to be activated for 210 min at -249 mV. The potential for the formation of the CO inhibited state in Hase I is approximately 200 mV more positive with respect to *D. fructosovorans* (-245 mV)[34] and *D. vulgaris* (-280 mV)[35], respectively. In addition, the reactivation kinetics are at least one order of magnitude faster. Taking into account that the Ni-SI$_a$ is the state that under physiological conditions binds CO, results demonstrate that Hase I is an exceptionally efficient catalyst compared to oxygen-sensitive hydrogenases.

iii) Formation of Ni-SCO shows that carbon monoxide has both access and affinity to bind at the active site of Hase I. The stretching vibration of the extrinsic CO at 25 °C in Hase I is centred at 2066 cm$^{-1}$, while in all hydrogenases studied so far (i.e. *A. vinosum, D. gigas, D. fructosovorans* and *D. vulgaris*)[28,35] it appears at 2055 - 2056 cm$^{-1}$. The 10 - 11 cm$^{-1}$ shift of this band towards higher frequencies in the case of the *A. aeolicus* is associated with a decrease in the extent of π-back donation from the nickel to the carbon atom and shows that CO binds weaker in Hase I[43].

iv) In the potential range between -100 mV and -300 mV the enzyme remains in the Ni-SCO state, but the signal intensity slightly decreases. No shifts of the bands of the Ni-SCO state were detected, whereas a shift in the case of *D. fructosovorans*[34] and *D.vulgaris*[35] was observed that was related to reduction of the proximal $[Fe_4S_4]$

cluster. This is in accordance with the EPR electrochemical titration, as in Hase I at this potential range the proximal cluster is already in the reduced $[Fe_4S_4]^{1+}$ state ($E_m$ = +87 mV)[44]. The extrinsic carbonyl can be electrochemically cleaved at potentials lower than -300 mV leading to the appearance of the most reduced Ni-R state. This effect has also been observed to a small or to larger extent in *D. fructosovorans*[34] and *D. vulgaris*[35], at however, considerably lower potentials (200 to 300 mV more negative). Transition from Ni-SCO to Ni-R in Hase I has an apparent midpoint potential of -358 mV and corresponds to a two-electron process. This is in contrast to the findings in *D. vulgaris*[35], where it could be described as a single-electron transfer. A transfer of the second electron to the iron-sulphur centres in the case of *A. aeolicus* is excluded, since at these potentials all clusters in Hase I are reduced. The midpoint potentials in Hase I corresponding to the Ni-C and Ni-R states are rather close to each other[14] compared to those measured in standard hydrogenases[28]. Based on this fact, it may be thus possible to discern a two-electron transfer in Hase I, whereas in *D. vulgaris* this may not be resolved[35]. Furthermore, the Ni-R state in Hase I is not the typical Ni-R observed at physiological pH for the mesophilic enzymes[28] and therefore its chemical composition may be also related with the observed two-electron transfer.

vi) The Ni-SCO state in the oxygen sensitive hydrogenases is extremely resistant towards electrochemical oxidation. Application of very positive redox potentials does not have an effect, as Ni-SCO persists[34,35]. The situation in the *A. aeolicus* enzyme is markedly different. Already, at a potential of -9 mV at 25 °C, the enzyme is a mixture of equivalent amounts of the Ni-SCO and Ni-B states. This shows that the externally added CO can be easily displaced upon oxidation and Ni-B can be formed most likely via insertion of an $OH^-$ ligand from the solvent (anaerobic inactivation). Both CO and oxygen inhibition are selectively tuned by changing the redox potential, indicating competitive processes of similar magnitude and a weaker interaction of the active site with the oxygen based ligand compared to standard enzymes. At lower temperatures (i.e. 15 °C) transition of the Ni-SCO to Ni-B is not so favourable. At +143 mV only 40 % of the molecules are in the Ni-B state and the rest remain in Ni-SCO (data not shown). The change in the pH solution is not so significant that it could account for such a difference at 15 °C (pKa of glutamate is 4.4 and of cysteine 8.28). It appears that at lower temperatures the energetic barrier for the transition to Ni-B (mechanism for insertion of the hydroxide ligand) becomes larger.

vii) The stretching vibration of the externally added CO at cryogenic temperatures is centred at 2072 cm$^{-1}$. $^{13}$CO labelling shifted the extrinsic CO band 46 cm$^{-1}$ towards lower frequencies to 2026 cm$^{-1}$, in agreement with the theoretically predicted value for a 'pure' CO vibration[45]. Thus, the CKFF (Cotton Kraihanzel force field)[45] approximation can be used to calculate the stretching parameters and make a qualitative inference of the force constants and the extent of metal to carbon π-back donation. A force constant k ($^{12}$CO)$_{aquifex}$ 1730 N/m  (k ($^{12}$CO)$_{vulgaris}$ = 1665 N/m) could be estimated[&]. The higher force constant in the case of Hase I shows a strengthening of the C-O bond and a concomitant weakening of the Ni-CO bond.

viii) Illumination with white light at cryogenic temperatures results in the photolytic loss of the extrinsic CO. A comparison between the activation barriers for the rebinding of CO to the [NiFe] active site showed that this is systematically larger for Hase I compared to oxygen sensitive enzymes (e.g. *D. vulgaris*)[35]. It is therefore energetically more difficult for the CO to rebind. In addition, the CO rebinding kinetics between *A. aeolicus* and *D. vulgaris* are notably different. A direct comparison cannot be made since the temperature range for the light induced processes in the two enzymes is different, but if we compare the kinetics at the higher temperature point where cleavage of CO occurs, the recombination kinetics of CO in *Aquifex* are 52 times slower. Upon lowering the temperature this difference becomes smaller (~17 times), but remains still an order of magnitude slower (see Appendix E). This is reflected in the frequency factors $A_0$ and suggests a smaller probability for a CO molecule to have the appropriate energy to rebind in Hase I, which might be explained by a possible steric hindrance or a fewer number of free CO molecules in the vicinity of the active site.

---

[&] The force constant of the CO bond is given by the equation k($^{12}$CO)=4.0383·10$^{-4}$·v$^2$. For the free CO the force constant is k = 1875 N/m.

## Conclusions

The present study demonstrates that it is possible to inhibit Hase I from *A. aeolicus* with carbon monoxide under extreme CO saturating conditions in the protein solution. The Ni-SCO state is formed with the CO coordinating the nickel atom. The comparatively high stretching vibration and large force constant of the exogenous carbonyl denotes that this ligand is bound only weakly to the active site of Hase I. A unprecedented finding was that the CO-adduct can be reversibly reduced and reoxidised to Ni-R and Ni-B, respectively, showing the versatility of this enzyme in switching between active and inactive forms in a comparatively small potential range. The energy barrier for the rebinding of CO is slightly larger compared to the oxygen-sensitive hydrogenase from *D. vulgaris*. In addition, the magnitude of the rebinding rate constants and concomitantly of the frequency factor $A_0$ are markedly different. The smaller $A_0$ may suggest that the amount of CO molecules in the vicinity of the active centre that are able to recombine are fewer in number or some steric hindrance occurs for the rebinding of CO. We conclude that the enhanced tolerance of this enzyme towards gaseous inhibitors and in particular carbon monoxide is a synergetic effect; i.e. it is a consequence of the different reactivity of the [NiFe] site ( redox potentials of the respective transitions), of the formation of a weaker Ni-CO bond and possibly of steric reasons that would reduce the probability of inhibition.

# References

1.  Vignais, P. M. *Cell Differ.* **2008**, 45, 223-252.

2.  Vignais, P. M.; Billoud, B. *Chem.Rev.* **2007**, 107, 4206-4272.

3.  Volbeda, A.; Charon, M. H.; Piras, C.; Hatchikian, E. C.; Frey, M.; Fontecilla-Camps, J. C. *Nature* **1995**, 373 (6515), 580-587.

4.  Nicolet, Y.; Lemon, B. J.; Fontecilla-Camps, J. C.; Peters, J. W. *Trends in Biochemical Sciences* **2000**, 25 (3), 138-143.

5.  Shima, S.; Pilak, O.; Vogt, S.; Schick, M.; Stagni, M. S.; Meyer-Klaucke, W.; Warkentin, E.; Thauer, R. K.; Ermler, U. *Science* **2008**, 321 (5888), 572-575.

6.  Dworkin, M.; Falkow, S.; Rosenberg, E.; Schleifer, K. H. The Prokaryotes; Ecophysiology and Biochemistry; 3rd ed.; Springer: **2007**; Vol. 2.

7.  Brock, T.; Madigan, T.; Martinko, J. M.; Parker, J. Biology of Microorganisms; 7th ed.; Prentice-Hall International: **1994**.

8.  Huber, R.; Wilharm, T.; Huber, D.; Trincone, A.; Burggraf, S.; Konig, H.; Rachel, R.; Rockinger, I.; Fricke, H.; Stetter, K. O. *Systematic and Applied Microbiology* **1992**, 15 (3), 340-351.

9.  Deckert, G.; Warren, P. V.; Gaasterland, T.; Young, W. G.; Lenox, A. L.; Graham, D. E.; Overbeek, R.; Snead, M. A.; Keller, M.; Aujay, M.; Huber, R.; Feldman, R. A.; Short, J. M.; Olsen, G. J.; Swanson, R. V. *Nature* **1998**, 392 (6674), 353-358.

10. Brugna-Guiral, M.; Tron, P.; Nitschke, W.; Stetter, K. O.; Burlat, B.; Guigliarelli, B.; Bruschi, M.; Giudici-Orticoni, M. T. *Extremophiles* **2003**, 7 (2), 145-157.

11. Guiral, M.; Prunetti, L.; Lignon, S.; Lebrun, R.; Moinier, D.; Giudici-Orticoni, M. T. *Journal of Proteome Research* **2009**, 8 (4), 1717-1730.

12. Guiral, M.; Tron, P.; Belle, V.; Aubert, C.; Leger, C.; Guigliarelli, B.; Giudici-Orticoni, M. T. *International Journal of Hydrogen Energy* **2006**, 31 (11), 1424-1431.

13. Luo, X.; Brugna, M.; Tron-Infossi, P.; Giudici-Orticoni, M. T.; Lojou, E. *J. Biol Inorg. Chem.* **2009** DOI: 10.1007/s00775-009-0572-y

14. Pandelia, M. E.; Tron-Infossi, P.; Fourmond, V.;Leger, C.; Giudici-Orticoni, M. -T.; Lubitz, W. to be submitted in *J. Biolog. Chem.* (see Chapter 7 of the present study)

15. Fourmond, V.; Leger, C. Unpublished observations

16. van Gastel, M.; Stein, M.; Brecht, M.; Schroder, O.; Lendzian, F.; Bittl, R.; Ogata, H.; Higuchi, Y.; Lubitz, W. *J. Biolog. Inorg.Chem.* **2006**, 11 (1), 41-51.

17. Lubitz, W.; Reijerse, E.; van Gastel, M. [NiFe] and [FeFe] hydrogenases studied by advanced magnetic resonance techniques. *Chem.Rev.* **2007**, 107, 4331-4365.

18. Lamle, S. E.; Albracht, S. P. J.; Armstrong, F. A. *J. Am. Chem. Soc.* **2004**, 126 (45), 14899-14909.

19. Pierik, A. J.; Roseboom, W.; Happe, R. P.; Bagley, K. A.; Albracht, S. P. J. *J. Biolog. Chem.* **1999**, 274 (6), 3331-3337.

20. De Lacey, A. L.; Hatchikian, E. C.; Volbeda, A.; Frey, M.; FontecillaCamps, J. C.; Fernandez, V. M. *J. Am. Chem. Soc.* **1997**, 119 (31), 7181-7189.

21. Pandelia, M. E.; Tron-Infossi, P.; Giudici-Orticoni, M. -T.; Lubitz, W. to be submitted **2009** (see Chapter 10 of the present study).

22. Brecht, M.; van Gastel, M.; Buhrke, T.; Friedrich, B.; Lubitz, W. *J. Am. Chem. Soc.* **2003,** 125 (43), 13075-13083.

23. Foerster, S.; van Gastel, M.; Brecht, M.; Lubitz, W. *J. Biolog. Inorg. Chem.* **2005,** 10 (1), 51-62.

24. Foerster, S.; Stein, M.; Brecht, M.; Ogata, H.; Higuchi, Y.; Lubitz, W. *J. Am. Chem. Soc.* **2003**, 125 (1), 83-93.

25. Stein, M.; van Lenthe, E.; Baerends, E. J.; Lubitz, W. *J. Am. Chem. Soc.* **2001,** 123 (24), 5839-5840.

26. Albracht, S. P. J. Nickel Hydrogenases - in Search of the Active-Site. *Biochim. Biophys. Acta-Bioenergetics* **1994**, 1188 (3), 167-204.

27. Fichtner, C.; Laurich, C.; Bothe, E.; Lubitz, W. *Biochemistry* **2006**, 45 (32), 9706-9716.

28. De Lacey, A. L.; Fernandez, V. M.; Rousset, M.; Cammack, R. *Chem. Rev.* **2007**, 107, 4304-4330.

29. Hoberman, H.D; Rittenberg, D. *J. Biolog. Chem.* **1943**, 147, 211.

30. van der Zwaan, J. W.; Albracht, S. P. J.; Fontijn, R. D.; Slater, E. C. *FEBS Lett.* **1985**, 179 (2), 271-277.

31. Bagley, K. A.; Vangarderen, C. J.; Chen, M.; Duin, E. C.; Albracht, S. P. J.; Woodruff, W. H. *Biochemistry* **1994**, 33 (31), 9229-9236.

32. Ogata, H.; Mizoguchi, Y.; Mizuno, N.; Miki, K.; Adachi, S.; Yasuoka, N.; Yagi, T.; Yamauchi, O.; Hirota, S.; Higuchi, Y. *J. Am. Chem. Soc.* **2002**, 124, 11628-11635.

33. Vincent, K. A.; Cracknell, J. A.; Lenz, O.; Zebger, I.; Friedrich, B.; Armstrong, F. A. *Proc. Nat. Acad. Sci.* **2005**, 102 (47), 16951-16954.

34. De Lacey, A. L.; Stadler, C.; Fernandez, V. M.; Hatchikian, E. C.; Fan, H. J.; Li, S. H.; Hall, M. B. *J. Biolog. Inorg. Chem.* **2002,** 7 (3), 318-326.

35. Pandelia, M. E. ; Ogata, H.; Currell, L. J. ; Flores, M.; Lubitz, W. *Biochim. Biophys. Acta - Bioenergetics* **2009**, doi:10.1016/j.bbabio.2009.11.002.

36. Ansari, A.; Berendzen, J.; Braunstein, D.; Cowen, B. R.; Frauenfelder, H.; Hong, M. K.; Iben, I. E. T.; Johnson, J. B.; Ormos, P.; Sauke, T. B.; Scholl, R.; Schulte, A.; Steinbach, P. J.; Vittitow, J.; Young, R. D. Rebinding and relaxation in the myoglobin pocket. *Biophysical Chemistry* **1987**, 26 (2-3), 337-355.

37. Moss, D. A.; Leonhard, M.; Bauscher, M.; Mantele, W. *FEBS Lett.* **1991**, 283 (1), 33-36.

38. Baymann, F.; Moss, D. A.; Mantele, W. *Anal. Biochem.* **1991**, 199 (2), 269-274.

39. Fultz, M. L.; Durst, R. A. *Analytica Chimica Acta* **1982**, 140 (1), 1-18.

40. Prince, R. C.; Linkletter, S. J.; Dutton, P. L. *Biochim. Biophys. Acta* **1981**, 635 (1), 132-148.

41. George, S. J.; Kurkin, S.; Thorneley, R. N. F.; Albracht, S. P. J. *Biochemistry* **2004**, 43 (21), 6808-6819.

42. Nyquist, R. A. *Appl. Spectrosc.* **1986**, 40 (1), 79-85.

43. Nakamoto, K. Infrared and Raman Spectra of Inorganic and Coordination Compounds; 5th ed.; John Wiley & Sons, Inc: **1997**; Vol. B.

44. Pandelia, M. E.; Nitschke, W.;Tron-Infossi, P.; Giudici-Orticoni, M. -T.; Lubitz, W. to be submitted **2009** (see Chapter 9 of the present study)

45. Braterman, P. S. Metal carbonyl spectra; Academic Press Inc: London, **1975**.

# Chapter 9

**Electron transfer and redox properties of the FeS clusters in the Hydrogenase I from the hyperthermophilic bacterium *Aquifex aeolicus*: A model for oxygen tolerance**
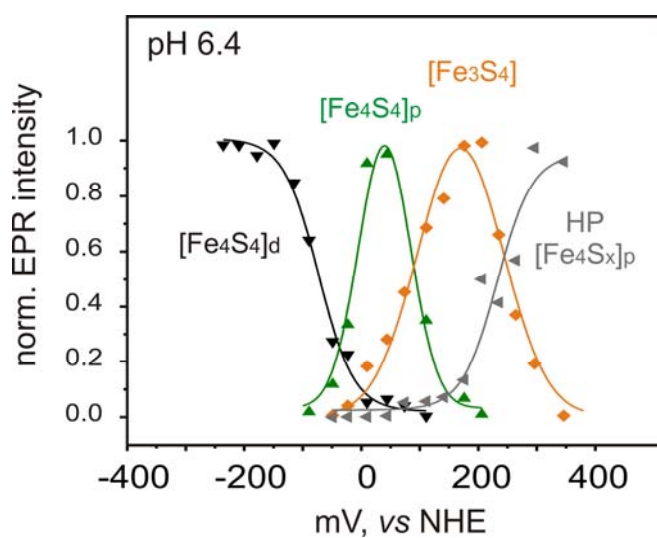


**Graphical Abstract.** EPR redox titration of the iron-sulphur centres in the Hase I from *Aquifex aeolicus* at pH 6.4. Four distinct one-electron processes were observed and fitted by the Nernst equation.

*Chapter 9*

# Electron transfer and redox properties of the FeS clusters in the Hydrogenase I from the hyperthermophilic bacterium *Aquifex aeolicus*: A model for oxygen tolerance[†]

Maria-Eirini Pandelia*, Wolfgang Nitschke‡, Pascale Tron-Infossi‡,
Marie-Thérèse Giudici-Orticoni‡, and Wolfgang Lubitz*

*Max-Planck-Institut für Bioanorganishe Chemie, Stiftstrasse 34-36, D45470, Mülheim a.d. Ruhr*
‡*Laboratoire de Bioenergetique et Ingenierie des Proteines, IBSM-CNRS, 13402 Marseille France*

## Abstract

Iron-sulphur clusters are essential electron transfer cofactors in metalloenzymes such as hydrogenases. In the present work, the nature and properties of these versatile electron-carriers are studied in the thermostable and oxygen tolerant [NiFe] Hydrogenase I from the hyperthermophile *Aquifex aeolicus*. Amino acid sequence analysis and comparison with standard hydrogenases showed a conserved binding motif for three iron-sulphur clusters. However, electron paramagnetic resonance spectra exhibited more complex and divergent signals reminiscent of additional paramagnetic centres. Redox titrations reveal the presence of one $[Fe_3S_4]^{1+/0}$ and two $[Fe_4S_4]^{2+/1+}$ clusters that have significantly more positive reduction potentials with respect to the ones occurring in typical hydrogenases. An additional high potential (HP) species was discerned that magnetically interacts with both the bimetallic nickel-iron site and the $[Fe_3S_4]$. On the basis of a non-typical $CXCCX_{94}CX_4CX_{28}C$ ligation of the iron-sulphur centre proximal to the [NiFe] site, we attribute the occurence of this HP centre to the super-oxidised form of the proximal cluster, postulating a $[Fe_4S_4]^{3+}$ moiety. The transition is induced by the presence of the two additional cysteinyl residues that can be potentially involved in its coordination or alternatively in the formation of a disulfide bridge. Furthermore, the reduction potentials of the proximal and distal iron-sulphur clusters were found to be pH dependent in a range between pH 6.4 and 8.3. The implications of the present findings on the catalytic mechanism of Hydrogenase I and its interaction with its physiological redox partners are discussed particularly a possible role of the HP species.

---

[†] *to be submitted* **2009**

## Introduction

Hydrogenases are metalloproteins occurring in the metabolic pathway of a wide variety of microbial organisms. They catalyse the reversible oxidation of dihydrogen according to the elemental reaction[1]: $H_2 \rightleftharpoons 2H^+ + 2e^-$. On the basis of the metal ion content of their active site, they can be classified into [NiFe], [FeFe] and [Fe]-only hydrogenases[2-4]. The growing interest in alternative sources of energy has focused scientific research to understanding and engineering these enzymes for applications such as biofuel cells[5]. One of the major limitations towards this direction, however, is the strict requirement for anaerobicity. Recently, the discovery of hydrogenases that can retain catalytic activity in oxygenic environments opened a new possibility for their extensive utilization[6,7]. A characterization of such enzymes is crucial for determining the basis for the increased oxygen resistance and the possible implications for improving standard hydrogenases.

*Aquifex aeolicus* is an extreme thermophilic, chemolithoautotrophic bacterium with optimum growth temperature of 85 °C[8]. It harbours three distinct [NiFe] hydrogenases, among which Hydrogenase I (Hase I) is located in the aerobic respiration pathway and is attached to the membrane by a di-haem cytochrome *b* [9]. Biochemical investigations have shown that it consists of two subunits; a large subunit that contains the hetero-bimetallic nickel-iron site and a small subunit that contains the electron relay centres[9], namely iron-sulphur clusters[10]. Based on its physicochemical properties and protein film voltammetry studies, this enzyme exhibits enhanced thermostability and oxygen tolerance with respect to its mesophilic counterparts[7,11].

Although the structures of hydrogenases from mesophiles are well characterized, such information is still lacking for hyperthermophilic organisms. A comparison between the sequence of Hase I from *A. aeolicus*[9] and the oxygen-sensitive hydrogenase from *Desulfovibrio* (*D.) vulgaris* Miyazaki F[12] demonstrates that the four cysteinyl residues coordinating the [NiFe] site are conserved. These are located in pairs in the N- and C-terminus of the large subunit in the canonical positions, while their surrounding is also well-preserved. Electron paramagnetic resonance (EPR) studies have shown that the spectrum of the as-isolated Hase I consists of characteristic nickel signals for the oxidised enzyme in the Ni-B state[9]. This suggests a similar electronic structure and molecular symmetry of the spin-

carrying [NiFe] centre between *A. aeolicus* and standard hydrogenases[13]. Intriguingly, the slowly activated Ni-A[14,15] state was not detected in any of the enzyme preparations. Reduction with dihydrogen resulted in the formation of the hydride carrying Ni-C state[16], which upon illumination at cryogenic temperatures converts to the Ni-L state(s)[17,18].

Dihydrogen oxidation takes place at the [NiFe] site, while the products of this reaction (e.g. $H^+$, $e^-$) exit the active site via specific pathways[2,19]. The transfer of electrons to the redox partners occurs by means of a chain of iron sulphur centres. Up to present, this electron transfer pathway in standard [NiFe] hydrogenases is known to consist of one [$Fe_3S_4$] placed in-between two low potential [$Fe_4S_4$] clusters [10,20-22] (Figure 1), while in the subclass of the [NiFeSe] hydrogenases all three clusters are of the [$Fe_4S_4$] type[23]. The [$Fe_3S_4$] $^{+1/0}$ cluster in its oxidised form is low spin paramagnetic (S=1/2) and becomes high spin (S=2) by one-electron reduction. The low potential [$Fe_4S_4$] $^{+2/+1}$ in its oxidised form is diamagnetic (S=0) and becomes paramagnetic (S=1/2) by one-electron reduction to the [$Fe_4S_4$]$^{1+}$ state [24].



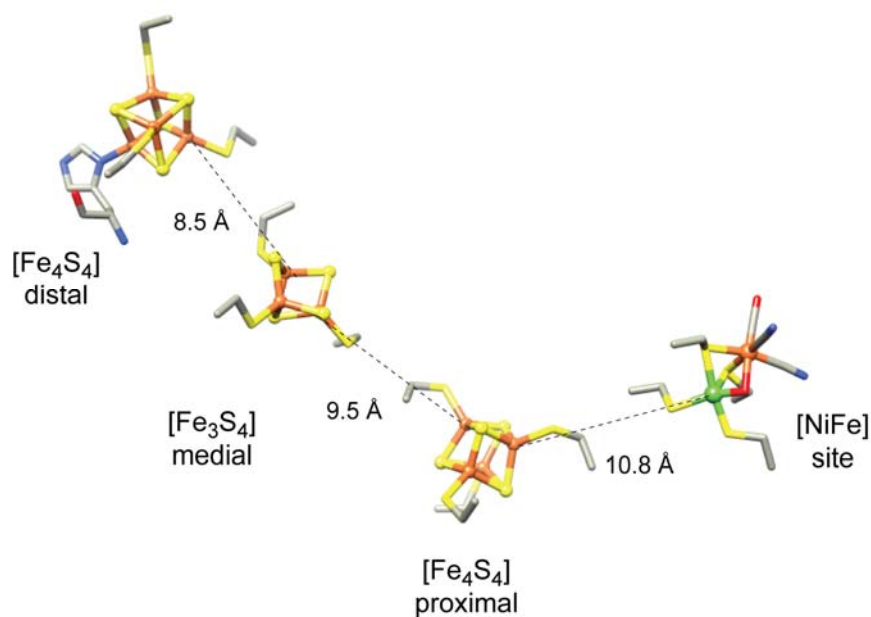**Figure 1.** Structure and distances between the [NiFe] site and the iron-sulphur centres in the *Desulfovibrio vulgaris* Miyazaki F hydrogenase (1WUJ pdb entry).

In the sequence of the Hase I small subunit, the ten cysteines that bind the three iron-sulphur centres in known hydrogenases are well conserved, indicating the presence of two [$Fe_4S_4$] and one [$Fe_3S_4$] clusters also in Hase I, though the EPR

signals of the FeS centres in the latter are more complex [9]. Similarly, the distal cluster is found to be ligated to the protein backbone by three cysteinyl residues and one histidine. The iron-sulphur centre proximal to the active site, however, has an atypical sequence motif $CXCCX_{94}CX_4CX_{28}C$. The two extra cysteines can potentially participate in its coordination affecting its electronic and redox properties.

In view of the thermostability and the increased oxygen tolerance exhibited by thermophilic and extreme thermophilic enzymes, a complete characterization of their redox components is quintessential. Recent Fourier transform infrared (FTIR) spectro-electrochemical investigations have demonstrated reduction potentials for the [NiFe] site approximately 100 mV more positive than the ones found in standard hydrogenases[25,26]. In the present work the electron transfer chain in Hase I is investigated in order to examine the type and redox properties of the constituent iron-sulphur clusters. Their reduction potentials and possible pH dependence will help elucidate the energy coupled processes between Hydrogenase I and its related redox partners (i.e. cyt *b*).

*Chapter 9*

## Materials and Methods

*Purification and growth.* The hyperthermophilic bacterium *A. aeolicus* was grown at 85°C in two-litre bottles under a $CO_2/H_2/O_2$ atmosphere. Hydrogenase I was purified at room temperature under semi-anaerobic conditions in a 50 mM Tris-HCl buffer pH 7.0, in the presence of 5-10 % glycerol and 0.01 % n-dodecyl-β-D-maltoside (DDM) as previously described[9].

*Determination of redox potentials.* Redox potentials were determined by EPR potentiometric titrations using a Bruker ESP-300 cw X-band spectrometer equipped with an Oxford Instruments helium flow cryostat and an ITC 503 temperature controller. The titration cell used is similar to the one described by Dutton[27]. The protein solution was kept under anaerobic conditions during the titration by flushing with hydrated argon gas, which was prior passed through an Oxisorb cartridge to remove residual traces of oxygen. The titration was carried out by adjusting the potential with substoichiometric amounts of solutions of sodium dithionite ($Na_2S_2O_4$) and potassium ferricyanide ($K_3[Fe(CN)_6]$). The temperature was maintained at 15 ° C by cold water passing through the glassy body of the cell in a closed external circuit with a thermostat (LAUDA). The potentials were measured with a pH/redox meter (GPHR 1400, Greisinger) using a combination Pt/Ag/AgCl micro-electrode (3M KCl, Mettler Toledo) and are quoted relative to the normal standard hydrogen electrode. The electrode was calibrated with a saturated quinhydrone solution at pH 7.4 (1M Hepes buffer) based on the formula: $E = E_{st.qh} -0.1984(273.16+T)pH$, where $E_{st.qh}$ is the measured potential of the saturated quinhydrone solution in mV and T the temperature in K. For the titration at pH 7.4 the buffering solution was 50 mM Hepes-NaOH and the following redox mediators were present at a final concentration of 100 μM, with the exception of phenazine methosulfate which was in a final concentration of 50 μM: 1,2-naphthoquinone (+145 mV), phenazine methosulfate (+90 mV), phenazine ethosulfate (+55 mV), methylene blue (+11 mV), indigo tetrasulfonate (-46 mV), 2- hydroxyl-1,4 naphthoquinone (-137 mV), anthraquinone-1,5-disulfonate (-170mV), phenosafranine (-252 mV), safranine T (-290 mV), benzyl viologen (-345mV) [Ref]. 5% of glycerol was added to the final redox solution to assist in dissolving of the redox mediators. For the pH dependent redox titrations buffering solutions of 100 mM MES-NaOH (pH 6.4) and 100 mM Tricine-NaOH (pH 8.3) were

used. A modified mediator mixture was used consisting of: 1,2-napthoquinone-4-sulfonic acid, phenazine methosulfate, phenazine ethosulfate, methylene blue, vitamin K3, 2,3-dihydroxy-5-methyl-benzoquinone, 2-hydroxyl-1,4 naphthoquinone, anthraquinone-1,5-disulfonate, phenosafranine, safranine T, benzyl viologen. The dependence of the reduction potentials of these electron reagents are described elsewhere[28,29]. The error in the determination of the oxidation-reduction potentials is $\pm$ 20 mV.

*Samples.* 300 µL samples of 12 µM protein concentration were loaded in calibrated EPR X-band tubes under a stream of argon gas and rapidly frozen in a cold liquid ethanol-nitrogen mixture.

**Results**

The cw EPR spectrum of the as purified hydrogenase from *A. aeolicus* exhibits complex spectral features in the region where an almost isotropic signal at g ~ 2.02 from an oxidised medial $[Fe_3S_4]^{+1}$ is observed in standard hydrogenases (Figure 2a)[21,22,30,31]. In the spectrum from *A. aeolicus* in addition to the $[Fe_3S_4]^{+1}$ (g = 2.019), four other components almost symmetrically positioned around the latter can be discerned with apparent g-values: 2.104 (~13.5 mT), 2.065 (~7.9 mT), 1.97 (~8.3 mT) and 1.94 (shoulder, ~ 13.4 mT). The values in parentheses denote the distance in field units from the g = 2.02 signal. Moreover, other spectral components are present at 2.078 (shoulder), 2.046, 2.005 and 1.86. EPR quantification of these signals using a $Cu^{2+}$-EDTA standard showed that the integrated area of the latter corresponds to $1.9 \pm 0.4$ spins/mol, demonstrating the presence of two paramagnetic centres. The same sample recorded at Q-band frequencies verified that this is an 'interaction' spectrum of two magnetically coupled paramagnetic species[32], since the lines are not at the same effective g- values (Figure 2b). The multiline pattern of the X- and Q-band spectra indicates an anisotropic spin-spin interaction between two paramagnetic centres; for a qualitative analysis of these signals however, knowledge of the identity of the involved species and further simulation are required. The temperature dependence between 10 and 55 K demonstrated similar relaxation properties for all the related components of the complex spectrum (Figure 2c). Above 60 K the iron-sulphur clusters were broadened beyond detection limits.

To unambiguously assign the signals corresponding to the iron-sulphur clusters of the *A. aeolicus* hydrogenase, a redox titration of these centres was carried out. In addition, redox changes related to the [NiFe] active site could also be followed, by monitoring the nickel signals in the low field region at g > 2.10 [33]. Figure 3 shows a stack plot of the potentiometric titration, where the respective EPR spectra at 15 K are plotted as a function of the redox potential. The intensity of the radical signal around g = 2.0 arising from the mediators in solution has been 'cut' for better illustrating the evolution of each paramagnetic species. In the following, results are presented in groups starting from the most oxidised enzyme and going to the more reducing potentials. Table 1 collects the effective g-values of all detectable species, according to the initial working hypothesis that similar to the standard hydrogenases three iron-sulphur cofactors are present and taking into account that the cysteinyl-rich

ligation of one of the clusters may affect its electronic properties, yielding the complex signals observed.  For each group Figure 3 can be referred to, as it collects all EPR-detectable changes in the range examined.
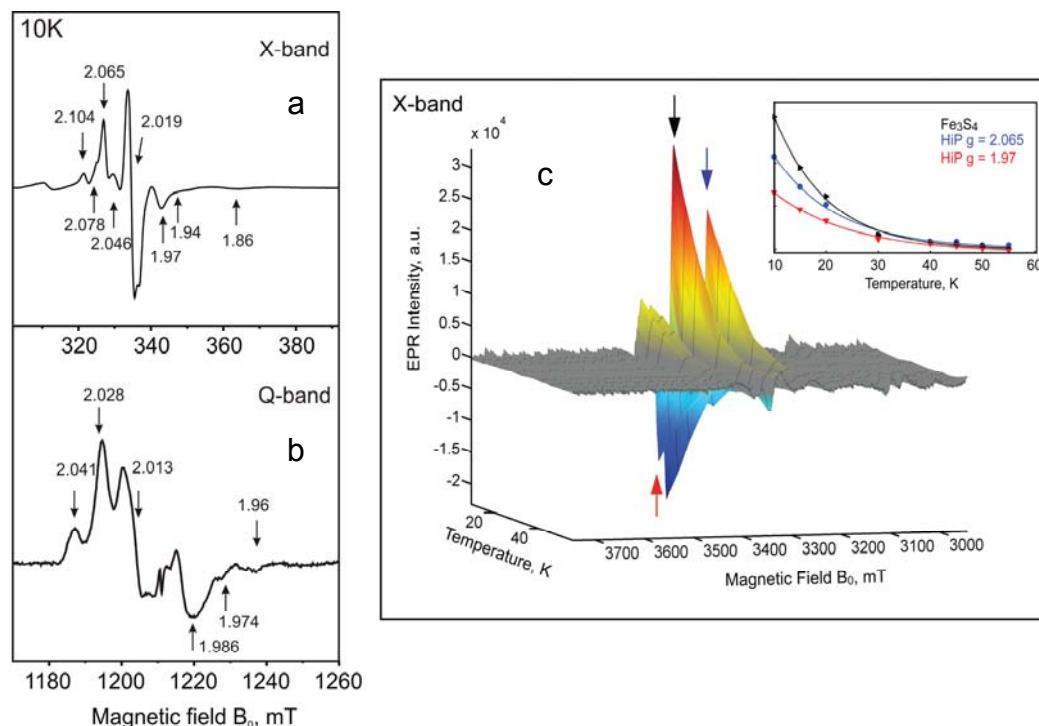


**Figure 2**. cw EPR spectra of the 'as-isolated' Hase I from *A. aeolicus* at 10 K (a) at X-band and (b) at Q-band. (c) Temperature dependence of the complex signal from the iron-sulphur centres between 10 and 55 K at X-band. Experimental: modulation amplitude 1 mT, microwave power 0.05mW, microwave frequency 9.4147 GHz (X-band) and 34.015 GHz (Q-band).
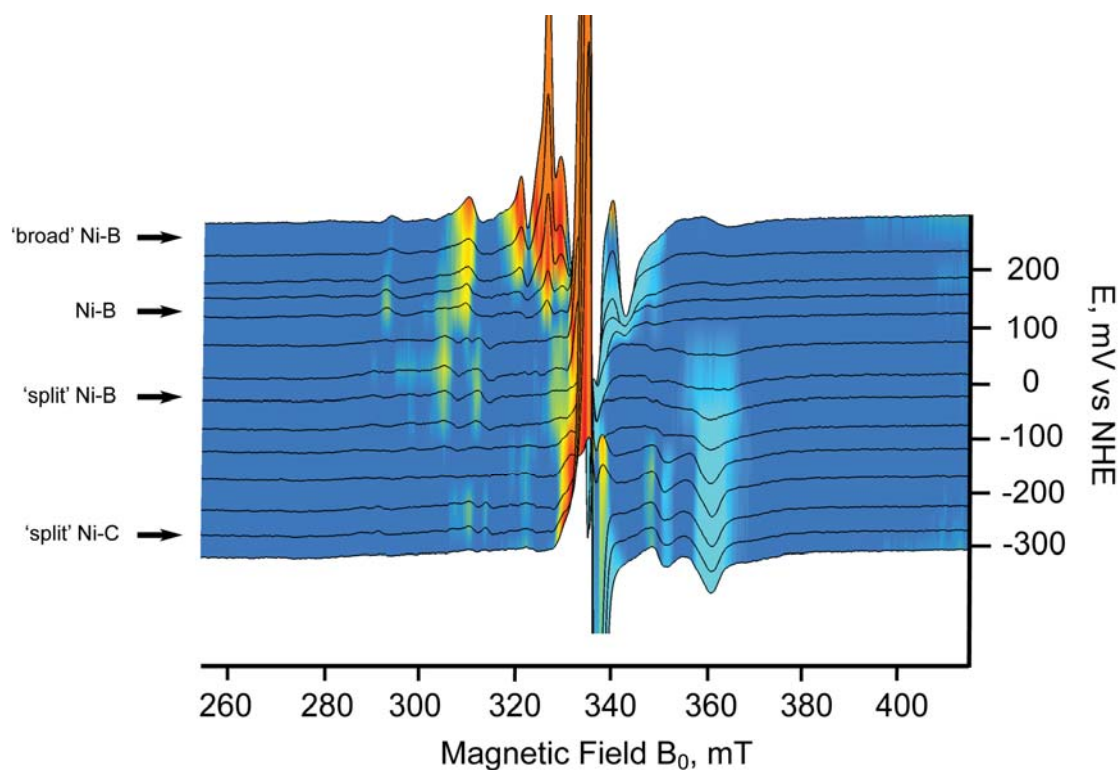
**Figure 3.** Stack plot of the potentiometric titration at pH 7.4 in the presence of redox mediators. Experimental: microwave frequency 9.4326 GHz, modulation amplitude 1 mT, microwave power 2.0 mW, temperature 15 K. The arrows indicate the potential regions in which the nickel signals are different.

**Table 1.** Effective g-values of the iron-sulphur paramagnetic species present in the potential range examined based on the working scheme for three iron-sulphur centres in *Aquifex*. The role of the proximal cluster and the switching between three possible redox states will be discussed. The clusters are denoted according to their position with respect to the [NiFe] site as P (proximal), M (medial) and D (distal). The spin states are included in parenthesis.

| Paramagnetic Species | Effective g-values |
|---|---|
| $P^{3+}(S=1/2)$ - $M^{1+}(S=1/2)$ | 2.104, 2.078, 2.065, 2.046, 2.005, 1.97, 1.86 |
| $M^{1+}(S=1/2)$ | 2.019 |
| $P^{1+}(S=1/2)$ - $M^{0}(S=2)$ | 2.05, 1.94, 1.89, 1.86 |
| $P^{1+}(S=1/2)$ - $M^{0}(S=2)$ –$D^{1+}(S=1/2)$ | 2.034, 1.98, 1.925, 1.87, 1.82 |

**Group I: ([Fe₃S₄] and the unknown interaction signal)**

Group I contains all the EPR-detectable iron-sulphur centres that are typically seen in samples of the as purified enzyme (Figure 2a). The EPR intensity of the all these redox components was plotted against the ambient redox potential (Figure 4A). All processes are fitted to curves calculated from the Nernst equation corresponding to a single electron transition. The $[Fe_3S_4]^{+1}$ cluster (g ~2.02) has maximal intensity around +170 mV. Extrapolation of the fit to more positive values converged to a midpoint potential for the disappearance of this signal of $E_m$ = +251 (±25) mV. The error in the determination of the latter is quite large, since not enough data points were available. The midpoint potential for the one-electron reduction to $[Fe_3S_4]^0$ was found to be +68 mV.

At very positive redox potentials, the disappearance of the $[Fe_3S_4]^{1+}$ signal coincides with the increase in intensity of the complex interaction signal and vice versa. The redox behaviour of the strong 'satellite'-like signals symmetrical to the signal at g ~ 2.02 and with apparent values g = 2.065 (blue circles) and g = 1.97 (black circles) is included in Figure 4A. A midpoint potential of +232 mV was estimated and thus the species interacting with the $[Fe_3S_4]^{1+}$ will be denoted in the following as HP (High Potential). All additional components of lower intensity titrate with the same $E_m$ suggesting that they are related to the same paramagnetic centre (HP). This is demonstrated in Figure 4B, in which all detectable components have been plotted.

At the same potential range (Figure 3), the [NiFe] site is found in the oxidised Ni-B state ($g_x$ = 2.29, $g_y$ = 2.16, $g_z$ = 2.01). Decreasing the potential down to +70 mV led to a small but consistent shift of the $g_x$ component to g =2.30, while the $g_y$ component became sharper and less intense. These changes suggest that the unknown HP species that is spin-spin coupled to the $[Fe_3S_4]^{1+}$ cluster interacts also magnetically with the spin carrying [NiFe] site. This is evidenced by the fact that one-electron reduction of the HP (disappearance) affected the spectrum of Ni-B.

**Group II (Proximal [Fe₄S₄] cluster and the Ni-B state)**

At +12 mV the majority of the $[Fe_3S_4]^{+1}$ clusters is reduced and a spectrum with features at 2.05, 1.94, 1.89 and 1.86 is observed. The appearance of this composite spectrum, whose apparent g-values resemble the ones reported for low potential

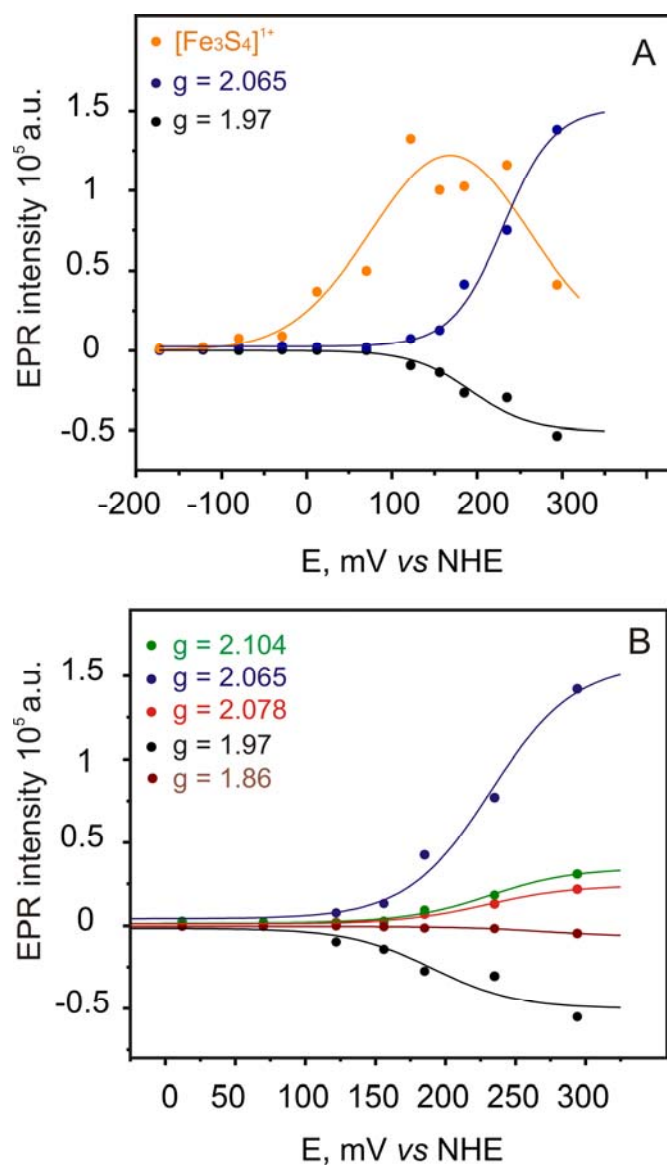**Figure 4.** A) Potentiometric titrations of the EPR signals corresponding to the $[Fe_3S_4]^{1+}$ cluster and to the larger intensity components of the HP species with effective g =2.065, 1.97. B) Titrations of the lower intensity components of the HP signal. The Nernst curves correspond to a one-electron process with a midpoint potential of +232 mV, by considering the apparent midpoint of all the plots.

$[Fe_4S_4]^{1+}$ ferredoxins, coincides with the formation of a 'split' Ni-B signal. This 'split' EPR signal is reminiscent of a magnetic interaction of the [NiFe] site with another paramagnetic centre in a permitted range[34]. At increasing temperatures (i.e. 70 K), the true g-spectrum of the Ni-B state ($g_x = 2.30$, $g_y = 2.17$, $g_z = 2.01$) is recovered, since the magnetic interaction is averaged out due to faster relaxation rates of the other species coupled to Ni-B. The related spectra are shown in Figure 5(A, B). The signal at g =2.004 is presumably related to one of the in solution redox mediators, the g = 2.08 signal comes from the cavity background, while the residual signals could not be assigned.

In standard hydrogenases, reduction of the FeS cluster proximal to the [NiFe] site, manifests itself in a splitting of the nickel signals and has been previously characterized to result from exchange and dipole-dipole interactions[35]. Based on this approach and assuming a first order effect of the exchange interaction (i.e. $|2J| \ll \Delta g \cdot \beta \cdot B$), the isotropic exchange coupling constant J can be estimated[35] from the splitting in the $g_x$ and $g_y$ components of the Ni-B signal. This assumption is based on the observation that these signals are of comparable amplitude and split into two components symmetrically positioned with respect to $g_x$ and $g_y$. Considering the splitting of the $g_y$ component of 6.52 mT, the magnitude of the isotropic exchange is calculated to be $34 \times 10^{-4}$ cm$^{-1}$. This value is in the range for a spin-spin interaction expected for a coupling of the proximal iron-sulphur centre with the nickel-iron site[35].

Figure 5C shows as a function of the redox potential the co-appearance of the g=1.94 component corresponding to the $[Fe_4S_4]^{1+}$ cluster and of the 'split' Ni-B signals. The averaged midpoint potential taking into account the intensities of the apparent values $g_x$ and $g_y$ for the appearance of the 'split' Ni-B signal is +95 mV and for the appearance of the $[Fe_4S_4]$ signal at $g_y = 1.94$ is +87 mV. Similar values were obtained by following the other components of the cluster. The development of a 'split' Ni-B spectrum that coincides with the reduction of a $[Fe_4S_4]$ cluster indicates that this is located in a distance shorter than 15 Å from the [NiFe] site. Therefore, this iron-sulphur centre is considered to be in the proximal position to the [NiFe] site (Figure 1)[34,36].
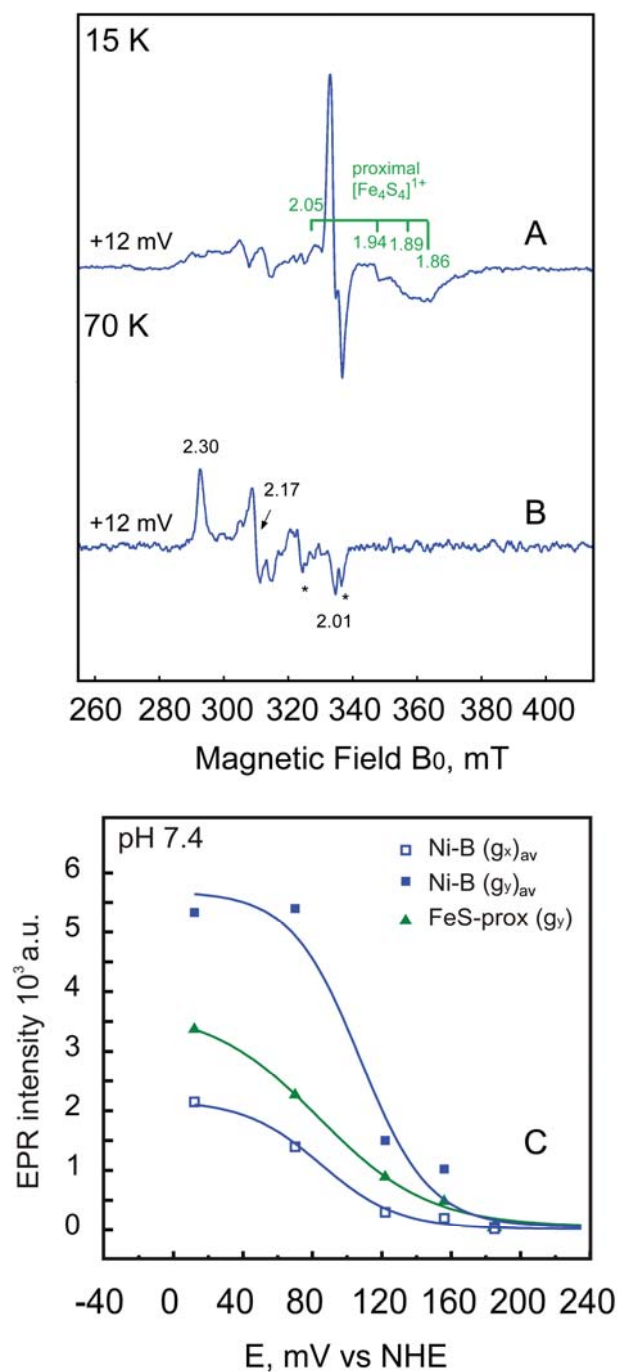
**Figure 5.** cw EPR spectra of the Hase I from *A. aeolicus* at a potential of +12 mV recorded A) at 15 K and B) at 70 K. C) Potentiometric titration for the appearance of the 'split' Ni-B signal (both 'effective' $g_x$, $g_y$ components) and of the signal corresponding to the low potential proximal [Fe$_4$S$_4$] cluster (g = 1.94). Experimental: microwave frequency 9.4326 GHz, microwave modulation amplitude 1 mT , power 2.0 mW and 20.0 mW for A) and B), respectively.

**Group III (2 x [Fe$_4$S$_4$] clusters, Ni-B, Ni-C)**

At potentials as low as -29 mV, the spectral features assigned to the proximal [Fe$_4$S$_4$]$^{1+}$ cluster start to decrease in intensity and more composite signals concomitantly appear (Figure 3). This shows the reduction of another species, which is assigned to the distal [Fe$_4$S$_4$] cluster. Decreasing the potential further to -173 mV, leads to the complete disappearance of the signal of Ni-B and the proximal [Fe$_4$S$_4$]$^{1+}$ cluster, while a spectrum with effective g-values: 2.034, 1.98, 1.92, 1.87 and 1.82, has fully developed (Figure 6A). On the basis of homology model structures of Hase I, the distance between the proximal and the distal clusters is found similar to the one in standard hydrogenases (Figure 1), which is too large for these two species to exhibit magnetically coupled EPR spectra. Therefore, the complex signals are attributed to an interaction spectrum of the two reduced [Fe$_4$S$_4$]$^{1+}$ clusters mediated by the high spin [Fe$_3$S$_4$]$^0$ cluster (S = 2).

A potentiometric titration for the disappearance of the 'split Ni-B', the proximal [Fe$_4$S$_4$] and of the concomitant appearance of the magnetically coupled 2x[Fe$_4$S$_4$]$^{1+}$/ [Fe$_4$S$_4$]$^0$ clusters is shown in Figure 6b. The reduction of Ni-B is characterized by an apparent midpoint potential of -96 mV, in good agreement with results obtained from an infrared electrochemical study for this state ($E_m$ = -105 ± 5 mV) [25] The appearance of the complex spectrum was titrated by following the components at g = 1.92 (red triangles) and g = 1.87 (cyan triangles). A midpoint potential of -78 mV was obtained by fitting the data to one-electron Nernst curves and is assigned to the reduction of the distal cluster.

At -228 mV the 'split' signal of the active Ni-C appears with features at $g_x$ = 2.22, 2.19, $g_y$ = 2.16, 2.14 (Figure 3). The $g_z$ component could not be resolved, as it is masked by the presence of the iron-sulphur clusters. The samples were frozen in the dark, which however could not prevent the formation of a light-sensitive state (Ni-L1)[37] in a fraction of the sample. This is visible in the spectra with apparent g-values at $g_x$ = 2.34, 2.32, $g_y$ = 2.16, 2.14. At - 310 mV the Ni-C and Ni-L1 signals have significantly decreased in intensity, showing the further reduction of Ni-C to the EPR-silent Ni-R state[26]. The splitting of the $g_y$ component is ~ 3.1 mT, from which an isotropic exchange coupling constant of 16x10$^{-4}$ cm$^{-1}$ was estimated. This is one third of the related spin-spin interaction observed in the bacterial hydrogenases from sulphate reducing anaerobes[35]. Reduction of Ni-B, appearance of Ni-C and its further reduction did not result in any detectable changes in the composite signals of the

clusters, showing that the nickel signals are not related to the multiline pattern in the iron-sulphur cluster region.

**Groups I, II, III; An overview**

Figure 7 collects selected spectra, in which the main redox events are maximal. At +294 mV the oxidised $[Fe_3S_4]^{1+}$ has decreased in intensity with concomitant increase of an interaction spectrum - oxidation of a HP species. At +156 mV only a small fraction of this interaction signal remains. The Ni-B signal is now of lower intensity and the $g_x$ component shows a consistent shift from 2.29 to 2.30. At +70 mV the Ni-B signal begins to 'split'. Such a spin-spin coupling is correlated with the appearance of features assigned to a reduced $[Fe_4S_4]^{1+}$ in the proximal position to the [NiFe] site with g- values at 2.05, 1.94, 1.89, and 1.86, respectively. At -29 mV the main features at g = 2.034, 1.92, 1.86 and concomitant disappearance of the proximal $[Fe_4S_4]$ cluster signals correlate with the onset for the reduction of the distal $[Fe_4S_4]$ cluster. At -173 mV the Ni-B state is completely reduced and the magnetically coupled signals of the three reduced iron-sulphur clusters are of maximal intensity.
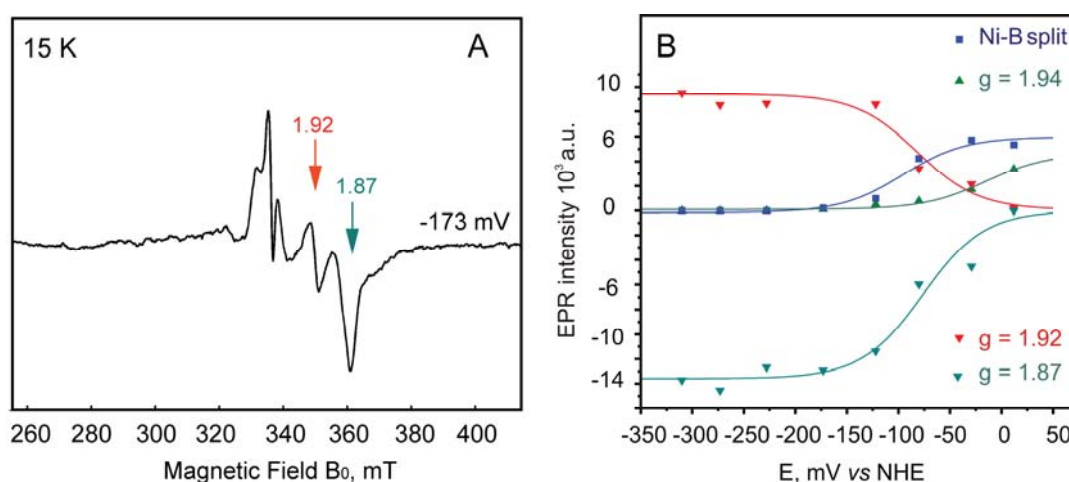


**Figure 6.** A) cw EPR spectrum of Hase I at -173 mV and 15 K. The composite signal corresponds to the three reduced clusters that are magnetically coupled. B) Potentiometric titration of the signals corresponding to the 'split' Ni-B (blue squares), the proximal $[Fe_4S_4]^{1+}$ cluster (green triangles) and the coupled iron-sulphur cluster spectrum with g = 1.92 (red triangles) and g = 1.87 (cyan triangles). The processes follow the Nernst equation with a midpoint potential of -96 mV for the disappearance of the Ni-B state and -78 mV for the reduction of the distal $[Fe_4S_4]$. Experimental: microwave frequency 9.4326 GHz, modulation amplitude 1 mT, mw power 2.0 mW

**Figure 7.** Selected cw EPR spectra of the redox titration for the paramagnetic centres in Hase I at pH 7.4. For a detailed description see text. Experimental: microwave frequency 9.4326 GHz, microwave modulation amplitude 1 mT, power 2.0 mW, temperature 15 K.
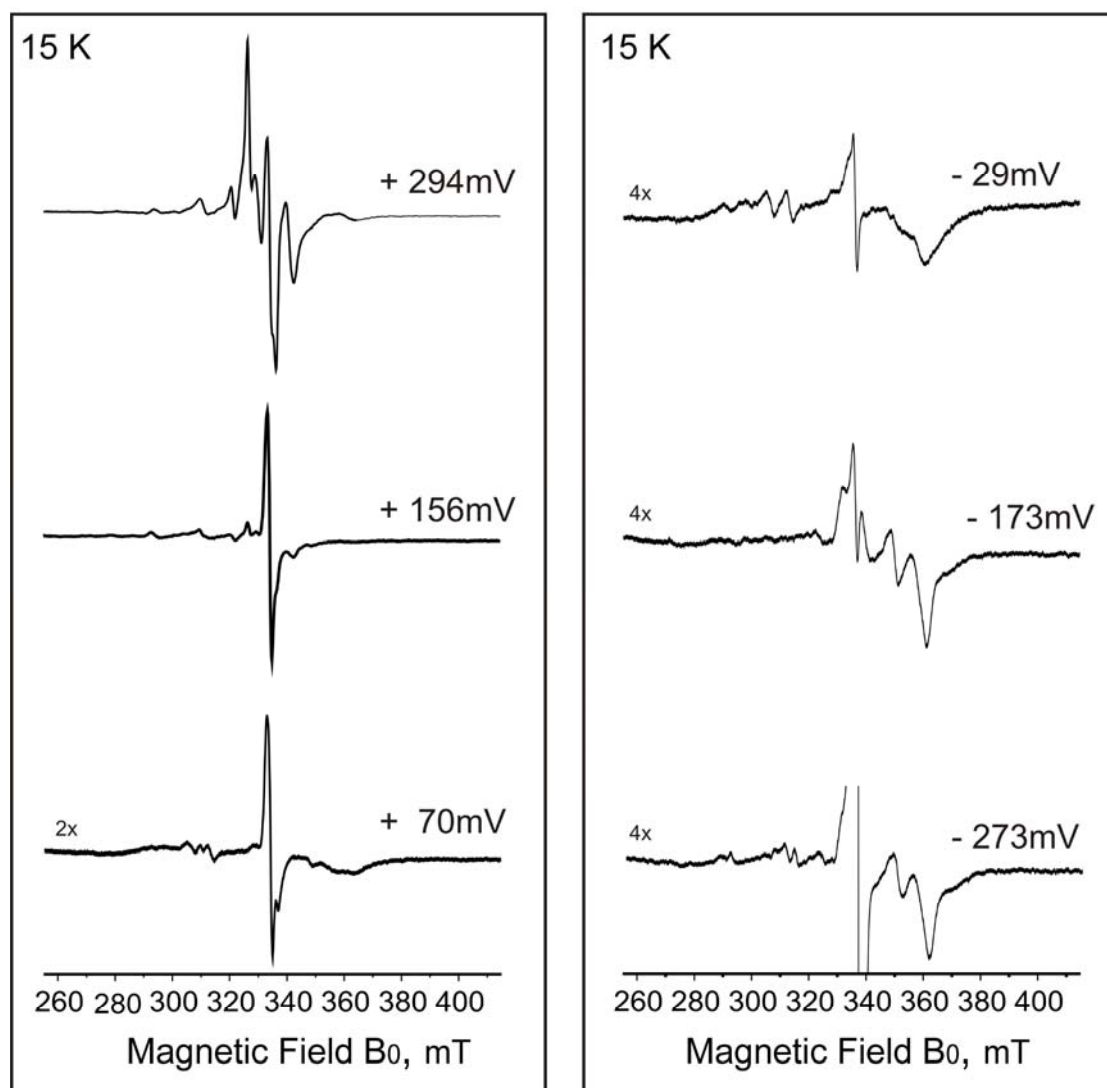
At -273 mV the 'split' Ni-C/Ni-L1 signals are observed in the spectra. The signal of the mediators at g = 2.005 is of very high intensity due to reduction of benzyl viologen and was 'cut' to better illustrate all the signals. All the midpoint potentials of the related redox centres at pH 7.4 are collected in Table 2.

**pH dependence of the reduction potentials**

**i) distal [Fe$_4$S$_4$]$^{2+/1+}$**

According to the conserved sequence motif HX$_2$C(X$_{24}$) CX$_5$C, the distal Fe$_4$S$_4$ cluster in the Hase I from *A. aeolicus* is coordinated by three cysteines and one histidine similar to standard hydrogenases. The midpoint potential for the reduction of this cluster exhibits a pH dependence (Figure 8). This dependence could be fitted by taking into account the Henderson–Hasselbalch relation and using the equation[38]:

$$E_m = E_m(lowpH) + \frac{R \cdot T}{n \cdot F} \log\left[\frac{1+10^{(pKred-pH)}}{1+10^{(pKox-pH)}}\right] ,$$

where $E_m$ are the experimentally obtained midpoint potentials at each respective pH, $E_m(lowpH)$ is the first formal midpoint potential for the protonation of the related amino acid , R is the universal gas constant ( 8.3145 JK$^{-1}$mol$^{-1}$), F the Faraday constant (96485 Cmol$^{-1}$), n the number of electrons and T the temperature (K).



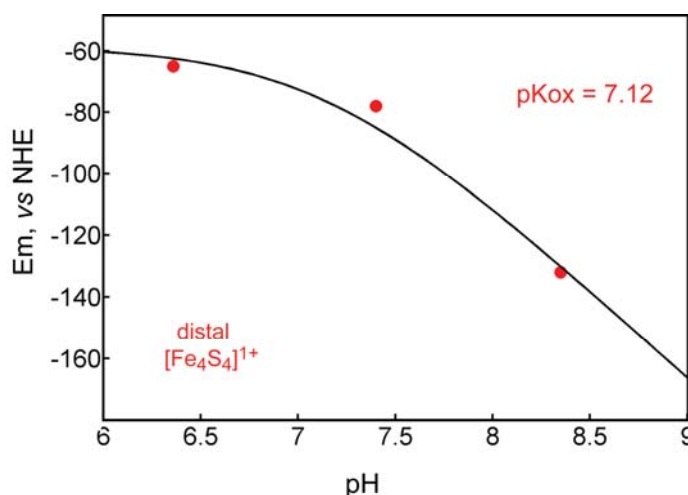**Figure 8.** pH dependence of the distal [Fe$_4$S$_4$] cluster in Hase I from *A. aeolicus*. A p$K_{a(ox)}$ of 7.1 was calculated that is attributed to the protonation of the imidazole side chain of the ligating histidine.

The pH dependence of the reduction potential of the distal $[Fe_4S_4]$ cluster is substantial and reaches 54 mV/pH for pH greater than 7.4, which is close to the theoretically predicted (57mV/pH at 15°C). Such dependence is likely to be correlated to a protonation of the ligating His187 (*A. aeolicus* numbering).

**Table 2**: Midpoint potentials ($E_m$) for the paramagnetic species in *A. aeolicus* Hydrogenase I, as obtained by the EPR redox titration in the presence of redox mediators at pH 6.4, 7.4 and 8.3, respectively. The error in the determination of the values is ± 20 mV.

| pH | 6.4 | 7.4 | 8.3 |
|---|---|---|---|
| **Species** | $E_m$, mV | $E_m$, mV | $E_m$, mV |
| High Potential species (HP) | +232 | +232 | nd |
| $[Fe_3S_4]^{1+/0}$ | +78 | +68 | +66 |
| $[Fe_4S_4]^{2+/1+}$ proximal | +98 | +87 | +30 |
| $[Fe_4S_4]^{2+/1+}$ distal | -65 | -78 | -132 |
| Ni-B split (appear) | +107 | +95 | +23 |
| Ni-B split (disappear) | -67 | -96 | -140 |

**ii) medial [Fe₃S₄]cluster**

The midpoint potential of the $[Fe_3S_4]$ cluster exhibited a minor dependence in the examined pH range, accounting for 2 to 10 mV/pH, a value that lies within the experimental error of the measurements. In the range examined, its $E_m$ is essentially pH independent.

**iii) proximal [Fe₄S₄]$^{2+/1+}$**

The appearance of the 'split' Ni-B signal and the reduction of the proximal $[Fe_4S_4]$ are described by very similar redox potentials. These exhibited a pH dependence which varied between 54 to 60 mV/ pH for pH values greater than pH 7.4, indicating that

one-electron reduction is associated with a proton transfer to a group that is a direct ligand of the cluster. A $pK_{a(ox)}$ value of approximately 7 was obtained for the protonated group. This value is within experimental error essentially identical for both the 'split' Ni-B signal and for the proximal iron-sulphur centre (Figure 9).

**iv) The HP signal and its relation to the proximal [Fe$_4$S$_4$] cluster**

At +346 mV and pH 6.4 the EPR spectrum in Figure 10A shows signals resulting from the spin-spin interaction of the $[Fe_3S_4]^{1+}$ cluster with a HP species. In addition, broadening and shifts are detected for the g-values of the Ni-B components. Raising the temperature to 70 K led to the disappearance of the nickel signals, showing that the relaxation behaviour of the latter has changed. The HP centre therefore magnetically interacts both with the $[Fe_3S_4]^{1+}$ cluster and the nickel-iron site.

At +44 mV, the complex signal is absent and a reduced $[Fe_4S_4]^{1+}$ centre with g-values 2.05, 1.94 and 1.87 has appeared (Figure 10B). The $g_x$ component of this cluster at pH of 7.4 is a 'doublet', while at pH 6.4 only a broad feature can be discerned ($\sim g_x = 1.87$). The broadening in the $g_x$ component of the proximal $[Fe_4S_4]^{1+}$ cluster might either reflect a magnetic coupling with the $[Fe_3S_4]$ cluster or alternatively two different conformations[39].
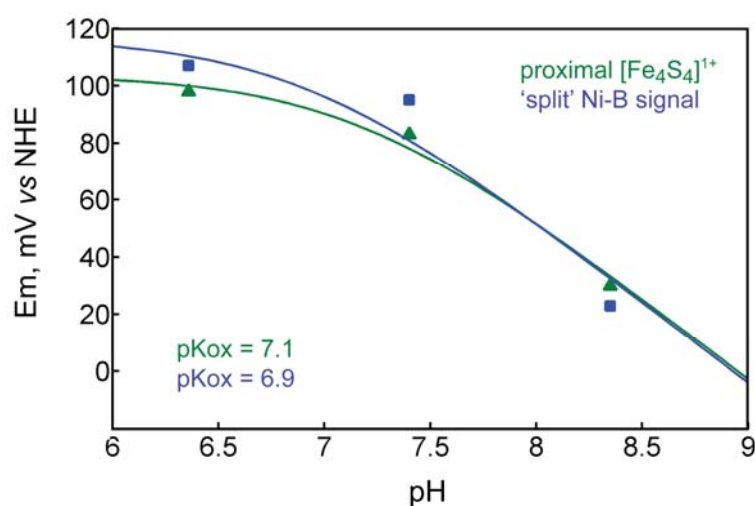


**Figure 9.** pH dependence of the proximal [Fe$_4$S$_4$] cluster in Hase I from *A. aeolicus*. A $pK_{a(ox)}$ of 7.0 was estimated for both the appearance of the 'split' Ni-B signal and the reduction of this cluster.
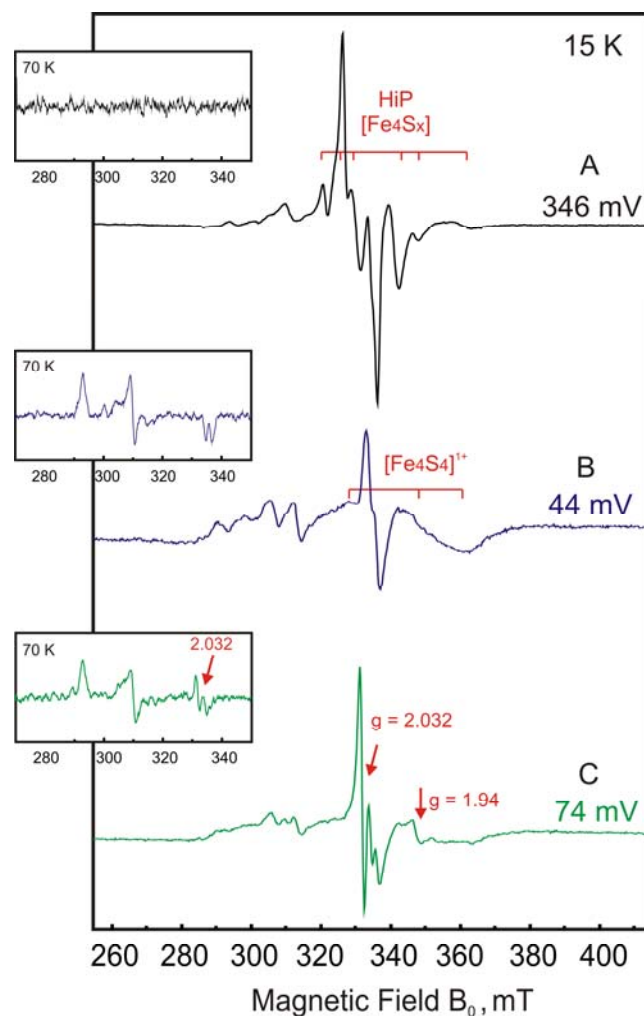
**Figure 10.** cw EPR spectra of the Hase I at pH 6.4 poised at a) +346 mV, b) +44 mV and c) +74 mV. Experimental: microwave frequency 9.4326 GHz, microwave modulation amplitude 1 mT, power 2.0 mW, temperature 15 K.

The Ni-B signal is 'split' and the $[Fe_3S_4]$ cluster has decreased in intensity as a result of its partial reduction. At higher temperatures (70 K), the Ni-B signal regains its rhombic 'unsplit' form, as the interacting $[Fe_4S_4]$ cluster at these temperatures has broadened beyond detection due to faster relaxation.

At the potentials of +346 and +44 mV, both Ni-B and the $[Fe_3S_4]^{1+}$ appear to be spin-spin coupled to another paramagnetic centre; however, the type of interaction is markedly different. At +44mV this centre is clearly identified as a $[Fe_4S_4]$ in the position proximal to the [NiFe] site (Figure 1), while at +346 mV it cannot be spectroscopically characterized. Since it interacts with the bimetallic site and the $[Fe_3S_4]^{1+}$ cluster, it should be localised between these two species in the vicinity

of the [NiFe] centre[34,35]. These results can be interpreted considering that the proximal iron-sulphur cluster is responsible for the spectral features at both potentials.

The redox processes were examined in both forward and backward titrations to ascertain their reversibility and the integrity of the potential-dependent changes. The forward titration (towards negative potentials) is carried out in approximately 60 mV steps staring from +296 mV to -49 mV, while the backward titration (towards positive potentials) is performed in approximately 60 mV steps from -12 mV to +346 mV. Therefore an EPR spectrum is taken every 30 mV and every reversible process can be then described by the Nernst equation. At pH 6.4 however, not all spectral components followed a Nernst behaviour. This is shown in Figure 11, where for example in some of the traces a radical like signal appeared.
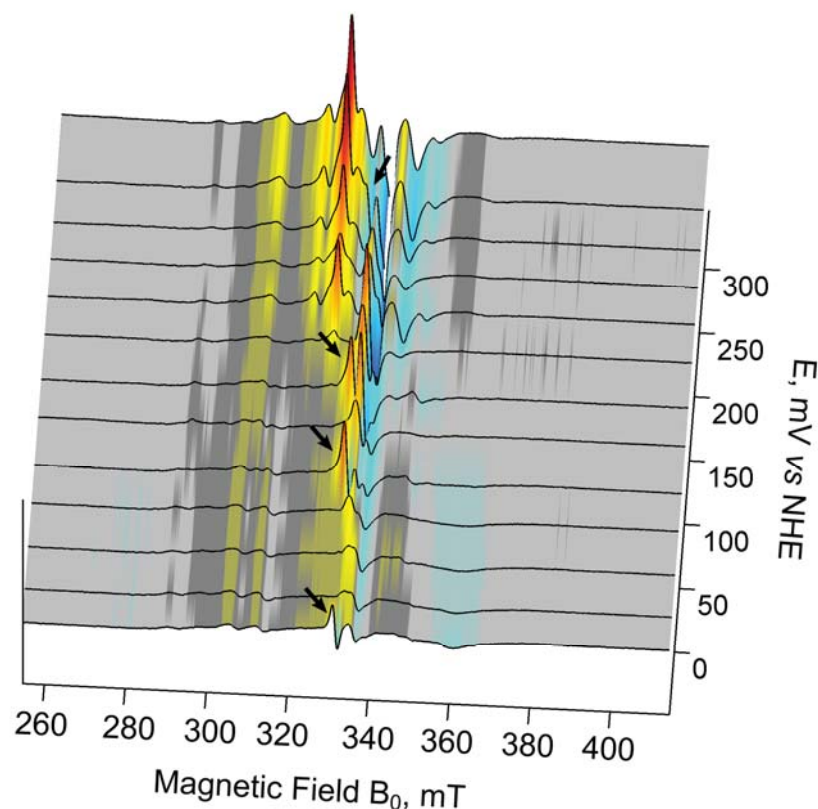


**Figure 11.** A stack plot of the potentiometric titration of Hase I at pH 6.4 at potentials higher than -49 mV. Consecutive traces in the stack plot represent forward and backward titrations. All processes are fully reversible apart from the appearance of a radical-like signal. The out-of-Nernst equilibrium behaviour of the latter is indicated with black arrows.

At +74 mV signals with apparent g-values of 2.032 and 1.94 were observed. The 2.032 signal could be detected at high temperatures (70-80 K), indicating a 'radical-like' species rather than an iron-sulphur cluster. The time scale between each point of the titration was estimated between one and two hours. Only after such long waiting times and at potentials equal to or below -49 mV was this signal reproducibly generated, showing a slow formation of a species that is not in redox equilibrium. It should be noted that this signal was present only at pH 6.4, while at higher pH values it was not possible to detect. This out-of equilibrium behaviour for the g = 2.032 feature is illustrated in Figure 11 and is highlighted by arrows.

**Discussion**

The characterization of the redox centres participating in energy transfer processes is a critical step in building a mechanistic scheme for the Hase I from *A. aeolicus*. Several advantages contribute to a precise description of these centres in this intriguing system. The enzyme could be repeatedly titrated under various pH conditions without signs of significant degradation over a time period of one week. In addition, at 15 °C, Hase I works *in vitro* exclusively as an uptake hydrogenase[11]. The turnover of the enzyme (hydrogen evolution) is therefore excluded at fairly negative potentials and all processes under study are in redox equilibrium, contrary to known hydrogenases from anaerobic and oxygenic microbes. The similarities of *A. aeolicus* hydrogenase with its mesophilic counterparts relates to the type of the electron relaying clusters, while the redox potentials and their chemical properties are to a large degree atypical and reminiscent of other complexes.

In total, four distinct one-electron transitions could be identified for the iron-sulphur centres. These were associated with the reduction of a HP species, of a $[Fe_3S_4]$ and two $[Fe_4S_4]$ clusters (distal/proximal). The discussion is divided accordingly, covering each centre separately; Table 3 collects the reduction potentials found for *A. aeolicus* and hydrogenases derived from other organisms.

*i)* A $[Fe_3S_4]^{1+/0}$ cluster was found with a reduction potential of +68 mV. This value is between 80 and 140 mV more positive than those reported for the medial $[Fe_3S_4]^{1+/0}$ cluster in *Desulfovibrio gigas* and *Allochromatium vinosum* hydrogenases[10,21,22]. On the other hand, elevated values similar to those in *A. aeolicus* were found for the membrane bound oxygen tolerant hydrogenase from *R. eutropha*[40]. The midpoint reduction potentials have been shown to exhibit a linear dependence on temperature (-1.2 to -1.5 mV/°C)[41]. This would mean that at *in vivo* physiological temperatures (85 °C) the potential of the $[Fe_3S_4]^{1+/0}$ cluster will be 60 to 90 mV more negative compared to the one measured in the present work. However, the $E_m$ obtained from titrations carried out in EPR (cryogenic temperatures-frozen solutions) correspond to extrapolated values at 0 °C and are comparable for the different organisms[41] (Table 3). Considering that the physiological temperatures for the mesophiles are near 37 °C and correcting for the temperature offset in the potentials, the $E_m$ for the

$[Fe_3S_4]^{+1}$ in the case of *A. aeolicus* is still of more positive value than in standard hydrogenases.

The redox potentials of the iron-sulphur centres are largely governed by their local environment; the direct and second sphere amino-acid coordination, the presence of polar groups and those capable of forming hydrogen bonds as well as exposure to solvent[42,43]. For the $[Fe_3S_4]$ cluster in *A. aeolicus* in the adjacent amino-acids of the cysteinyl residues, the presence of the non-conserved serine is found. Such groups can form strong hydrogen bonds and are thus capable of modulating the redox potential of the cluster, leading to the increased midpoint potential observed. In addition, in the homology model structure, the presence of a non-conserved histidine (His239, *A. aeolicus* numbering) belonging to the protein fold of the large subunit comes in great proximity to the cluster (< 5Å), which could also have an influence in shifting the potential to more positive values.

In the pH range between 6.4 and 8.3, the midpoint potential for the $[Fe_3S_4]$ was found to be independent of the proton concentration. On the other hand, in ferredoxins such as the one from *Azotobacter vinelandii*, the $[Fe_3S_4]$ is fairly pH dependent[44]. However, no such effect is observed for the $[Fe_3S_4]$ from *A. aeolicus*, excluding the protonation of one of its direct ligating groups. This is in agreement with previous observations for this centre in oxygen-sensitive hydrogenases[45].

*ii)* An EPR signal typical for a reduced low potential $[Fe_4S_4]^{1+}$ ferredoxin was present in the spectra and was found to have a midpoint potential of +87 mV. This value is between 300 and 440 mV more positive than the one found in the ferredoxin type of clusters in the hydrogenases from *Desulfovibrio* and *Allochromatium* species[21,31,45]. Such a high potential value however, is not entirely atypical for $[Fe_4S_4]^{2+/1+}$ clusters. In the MBH hydrogenase from *R. eutropha*, the reduction potential for this cluster was likewise positive[40], while in the nitrate reductase from *E. coli,* both $[Fe_3S_4]$ and $[Fe_4S_4]$ clusters have comparable reduction potentials with those in *A. aeolicus*[39]. The $g_x$ component of the $[Fe_4S_4]^{1+}$ appears split into a 'doublet' in both cases (*A. aeolicus* hydrogenase, *E. coli* nitrate reductase), a fact that was attributed to different cluster conformations for the latter [39]. In Hase I, however, such a 'splitting' most likely originates from a spin-spin interaction between this $[Fe_4S_4]^{1+}$ and a second paramagnet (i.e. the $[Fe_3S_4]^0$ cluster or even the [NiFe] site). The changes in the linewidth broadness or complexity of this component at the various pH

values examined in this work may be associated with the different pH dependence of these centres, which determines the extent of their EPR-detectable interaction.

The appearance of a 'split' Ni-B signal coincides with the reduction of this $[Fe_4S_4]$ cluster indicating a magnetic coupling between these two centres. Based on the structure of standard hydrogenases and the homology model of *A. aeolicus*, this cluster, is the only species that can magnetically interact with the [NiFe] site, resulting in a 'split' signal. We conclude that this is the cluster in the position proximal to the [NiFe] site. The isotropic exchange coupling constant between these two centres is $34 \times 10^{-4}$ cm$^{-1}$, which agrees in magnitude with the case of *D. gigas* in the reduced enzyme ($40 \times 10^{-4}$ cm$^{-1}$) [35] and with the 'split' oxidised state in *Acidithiobacillus (A.) ferrooxidans* ($54 \times 10^{-4}$ cm$^{-1}$) [46]. The smaller spin-spin interaction in *A. aeolicus* is presumably related to the modified coordination of this cluster by two extra cysteines and /or a different interaction between the metal cofactors.

The reduction potentials of the iron-sulphur clusters are greatly affected by the polypeptide chain and it is likely that the presence of two additional cysteinyl residues in the protein fold of the proximal $[Fe_4S_4]$ is to a large extent responsible for the very positive $E_m$ [42]. The latter is found to be pH dependent. For pH values greater than 7.4 it approaches a dependence of 57 mV/pH indicative of an oxidation state dependent on the binding of a proton. The proton association constant inferred for the oxidised form of the cluster was between 6.9 and 7.1 for the $[Fe_4S_4]$–H$^+$.

By means of the PKORKA method[47], the p$K_a$ values of titratable groups in proteins can be predicted by taking into account effects of hydrogen bonding and structural changes imposed by protein-ligand interactions. Although such methods are approximate and often the explicit solution of the Poisson-Boltzmann equation is needed, they can reproduce p$K_a$ values with sufficient precision. In the case of *A. aeolicus* a crystal structure is not available and thus a model was used as an input containing the FeS centres . The sequence motif of the proximal cluster is $CXCCX_{94}CX_4CX_{28}C$ and the respective model is shown in Figure 12. For three of the conserved cysteines (Cys20, Cys115, Cys149), which are expected to ligate the iron-sulphur centre, p$K_a$ values greater than 12 were found. The conserved Cys17, also expected to ligate the cluster was attributed a p$K_a$ of 7.4. The two extra cysteines in the amino acid sequence (Cys19, Cys120) have p$K_a$ values of 9.1 and 6.2, respectively. These predictions are consistent with the p$K_a$ value obtained (6.9-7.1) and support a protonation of one of the coordinating sulfides. Such a pH dependence

is rather intriguing for a 'buried' FeS cluster in the vicinity of the [NiFe] active site. These extra cysteinyl residues should therefore participate in redox-dependent processes and may be potentially involved in modulating the structural properties of this cluster[48].

*iii)* A second $[Fe_4S_4]^{2+/1+}$ with a reduction potential of -78 mV was obtained by titrating the disappearance of the signal corresponding to the proximal $[Fe_4S_4]$ and the concomitant  appearance of a complex spectrum. All features are clearly resolved, contrary to standard hydrogenases, where the spectrum of the reduced clusters is broad and featureless[21,31,35]. This indicates that the magnetic interaction between these clusters in *A. aeolicus* does not have such a drastic effect on the relaxation and magnetic properties of the individual species. These distinct spectral features in the case of Hase I enabled the unambiguous assignment of the redox potentials corresponding to each of the $[Fe_4S_4]$ clusters.

This second $[Fe_4S_4]$ is assigned to the distal cluster, which, similar to hydrogenases from oxygen-sensitive enzymes, is bound to the polypeptide backbone by three cysteines and one histidine[2,49]. The midpoint potential for the reduction of the distal cluster exhibited a pH dependence and for the protonated form of this centre a $pK_{a(ox)}$ value of 7.1 was inferred. The theoretical calculations with PKORKA attributed a $pK_{a(ox)}$ of 6.5 to the histidine ligand of this cluster, in close agreement with the value obtained in our experiments. The observation that the oxidised state of the distal cluster binds a proton can be understood in terms of the position of this histidine group in the protein environment. This histidine is located close to the surface and the physiologically binding of the cyt*b* may affect the redox properties of this cluster, i.e. by a protonation of the $N^\delta$ nitrogen of the imidazole side-chain. The pH dependence of 60 mV/pH determined previously also for the *D. vulgaris* hydrogenase[31], emphasizes the important role of this histidine residue in the metal cofactor interactions between hydrogenases and their redox partners[50].

The midpoint potentials of both $[Fe_4S_4]$ clusters are substantially more positive compared to low potential iron-sulphur centres in bacterial ferredoxins [51]. The determining factors for the high $E_m$ are located in the electrostatic interactions with the surrounding protein matrix, the number of charged residues and the solvent accessibility. A recent electrochemical study on the *A. aeolicus* Hase I in conjunction with the present results demonstrated that the midpoint potentials of the [NiFe] site

are more negative than those of the clusters (Figure 13). The $E_m$ of the most reduced [NiFe] complex is close to the potential for proton reduction (-414 mV, pH 7.0). This is expected for an optimal electron shuttle between hydrogenase and the substrate.

The directionality of the electron transfer is determined by the redox potentials of the involved cofactors. Electron transfer takes place from the more negatively charged nickel-iron site to the iron-sulphur centres that have more positive redox potentials. The reversibility of this reaction is dictated by the extent of overlap of the redox potentials between these centres. The lack of an overlap in the reduction potentials measured for the [NiFe] site and the iron-sulphur clusters in the case of *A. aeolicus*, hinders a reversible electron transfer to the [NiFe] and can account for the explicit function of Hase I as an uptake hydrogenase[52].

**Table 3.** Collection of the midpoint potentials estimated by EPR redox titrations for the iron-sulphur clusters in [NiFe] hydrogenases from *A. aeolicus*, *Desulfovibrio gigas*, *Desulfovibrio vulgaris,* MBH from *R. eutropha* (H16, CH34 strains) and *A. vinosum*.

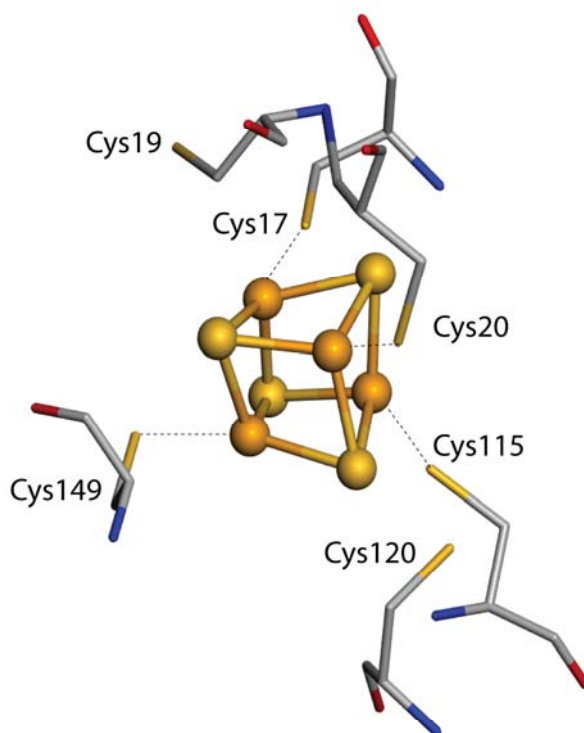| Redox centre | Midpoint potential, mV *vs* NHE | | | | |
|:---:|:---:|:---:|:---:|:---:|:---:|
| | *A. aeolicus* | *D. gigas*[22] | *D. vulgaris*[30] | *R.eutropha H16/ R. eutropha CH34*[40] | *A. vinosum*[40] |
| HP | +232 | nd | nd | +160/+240 | nd |
| $[Fe_3S_4]^{1+/0}$ | +68 | -35, -70 | -70 | +25/+100 | -10 |
| $[Fe_4S_4]^{2+/1+}$ Proximal | +87 | -350 | -350 | -60/+50 | nd |
| $[Fe_4S_4]^{2+/1+}$ Distal | -78 | -350 | -350 | -180/-80 | nd |

**Figure 12.** Homology modelled structure of the cysteinyl ligation of the proximal cluster in Hase I from *Aquifex aeolicus* the based on the 1WUJ template (*D. vulgaris*) generated with the Ps$^2$ server for protein structure prediction.

*iv)* To completely characterize the redox events and the centres implicated in the electron-transfer pathway of Hase I, the presence and role of the HP species remains to be clarified. This centre has a reduction potential of +232 mV that is essentially independent of pH in the range examined. The observation that it interacts magnetically both with the [NiFe] site and the oxidised [Fe$_3$S$_4$] cluster, leads to the conclusion that it is situated in-between these two centres. Dipole-dipole and spin exchange interactions in related 'coupled' systems are consistent with a distance between them below 15 Å. This interaction determines an upper limit in the distance between the unpaired spin distributions of the two centres, which shows that the HP species has to be located in the position expected for the proximal cubane [Fe$_4$S$_4$] in standard hydrogenases.

At first sight, these results appear contradictory, since the one-electron reduction of the centre assigned to the proximal cluster was found to appear in the spectra with a midpoint potential of +87 mV. Furthermore, the magnitude of the isotropic exchange between this [Fe$_4$S$_4$]$^{2+/1+}$ and the [NiFe] site is in agreement with

the one measured in oxygen-sensitive hydrogenases. It is evident from the above that both the HP and the $[Fe_4S_4]^{2+/1+}$ centre are associated with the cluster in the proximal to the [NiFe] site position (Figures 1, 13). This interpretation thus raises the question how an iron-sulphur centre can be associated with the observed transfer of two electrons, indicating that it switches between an oxidised and a super-reduced state (i.e. $[Fe_4S_4]^{3+/2+/1+}$).

The titration showed that the $E_m$ for the proximal $[Fe_4S_4]^{2+/1+}$ is pH dependent and the $pK_{a(ox)}$ could be attributed to one of the coordinating sulfides. This suggests the versatility of these groups and their potential participation in redox-related changes of the cluster. The homology model in Figure 12 shows that six cysteinyl residues in total are in principle capable to ligate this cluster. These cysteinyls can modulate the electronic properties by either formation of a disulfide bridge or another type of interaction, which would alter the coordination number of the cluster[53,54].

A possible disulfide formation will draw charge away from the iron that will become more ferric ($Fe^{3+}$), leading formally to a high potential cluster with three $Fe^{3+}$ and one in $Fe^{2+}$. The presence of the second extra cysteine may either be important for the stability of the induced HP cluster or participate also in a disulfide bridge. Such a scenario would account for the out-of-equilibrium radical-like signals observed at pH 6.4, which in the case of a disulfide generation would favour the protonated (open) form. These signals did not follow the Nernst equation and are consistent with the slow formation of a sulphur based radical involved in this transition. In support of this hypothesis incubation of this complex signal related to the HP (Figure 2) in the case of the MBH from *R. eutropha* with β-mercaptoethanol[55], known to 'cleave' disulfide bonds, led to its disappearance. Though for such a disulfide formation a pH dependence of 120 mV/pH would be expected, this was not observed in our experiments. However, it cannot be excluded since the disulfide might not be solvent accessible or the pH range is not appropriate. A proposed disulfide would be in line with recent observations that creation of such entities can react as switches against oxidative stress and protect the enzyme from reactive oxygen species[53]. Such a possibility could also apply for *A. aeolicus* and thus account for its increased oxygen tolerance.

We therefore propose that the presence of these additional cysteines may be related to the formation of disulfide bonds able to change the co-ordination of the cluster and therefore its electronic properties. In the as-isolated enzyme such a

disulfide bond would be present (between Cys115 and Cys120) or (Cys17 and Cys19) or both and would alter the electronic configuration of the cluster so that it behaves like a high potential $Fe_4S_4$ that is paramagnetic and can therefore be seen in the spectra. Slight reduction leads to the disappearance of this signal as the disulfide bonds are broken and the cluster attains its normal coordination/geometry. Further reduction to +78mV leads to the appearance of the typical proximal $[Fe_4S_4]^{2+/1+}$ cluster.

Another possibility would be that the presence of the two additional thiols can alter the cluster geometry and symmetry by imposing structural changes. It has been found that the differences in the redox potentials between $[Fe_4S_4]^{3+/2+}$ and $[Fe_4S_4]^{2+/1+}$ are localised in the $C_\beta$-S-Fe-S dihedral angles and in the number of the hydrogen bonds available[42,56]. Cys17 is surrounded by hydrophilic residues such as glycine, glutamate and threonine, which might indicate a possible exposure to the solvent and may be associated with the low $pK_a$ value found in the pH dependent titrations.
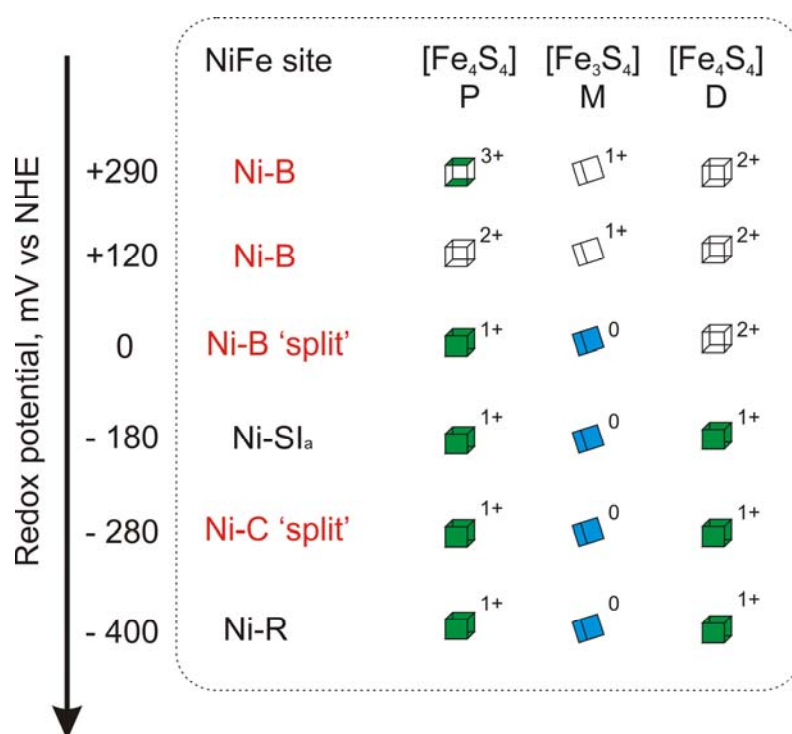


**Figure 13.** Schematic overview of the redox centres in the Hase I from *A. aeolicus* based on their midpoint reduction potentials as obtained by EPR and FTIR.

In the present study, the proximal [Fe$_4$S$_4$] cubane is suggested to shuttle reversibly through three different oxidation states in a very small potential range. The molecular mechanism is not clear, so several schemes can be proposed as described above. Up to date, however, attempts to over-oxidise an [Fe$_4$S$_4$] $^{1+}$ resulted in loss of an iron, whereas super-reduction of [Fe$_4$S$_4$] $^{3+}$ is possible but the potential range between the [Fe$_4$S$_4$] $^{3+}$ and the [Fe$_4$S$_4$] $^{1+}$ spans more than 1000 mV[57]. The unusual case of *A. aeolicus* suggests that the presence of these two extra electron-rich sulfides in the protein fold of the cluster may increase its redox versatility. It appears that the formation of a high potential cluster may serve to protect the active site against reactive oxygen species as well as oxidative inactivation. To ascertain these structural properties further experiments are required (e.g. Mössbauer, X-ray crystallographic studies).

In summary, the electron transfer pathway in the oxygen-tolerant Hase I from *A. aeolicus* consists of three iron-sulphur centres similar to standard hydrogenases. Four single electron transitions were discerned, two of which were pH dependent in a range between 6.4 and 8.3. The midpoint potentials measured were significantly higher than those in oxygen sensitive enzymes but in the range of the values reported for other oxygen tolerant enzymes. This is associated with differences in the surrounding protein matrix and electrostatic effects such as hydrogen bonding interactions. The presence of two additional cysteines in the protein fold of the proximal cubane cluster results in its possible function both as a high and low potential [Fe$_4$S$_4$] cluster. This is rather unusual and needs to be further structurally characterized, since it is most likely related to a protection mechanism against oxygen.

# References

1. Vignais, P. M.; Billoud, B. *Chem. Rev.* **2007**, *107*, 4206.

2. Volbeda, A.; Charon, M. H.; Piras, C.; Hatchikian, E. C.; Frey, M.; Fontecilla-Camps, J. C. *Nature* **1995**, *373* (6515), 580.

3. Nicolet, Y.; Lemon, B. J.; Fontecilla-Camps, J. C.; Peters, J. W. *Trends in Biochemical Sciences* **2000**, *25* (3), 138.

4. Shima, S.; Thauer, R. K. *Chem. Rec.* **2007,** *7* (1), 37.

5. Mertens, R.; Liese, *Curr. Opin. Biotechnol.* **2004**, *15* (4), 343.

6. Cracknell, J. A.; Vincent, K. A.; Ludwig, M.; Lenz, O.; Friedrich, B.; Armstrong, F. A. *J. Am. Chem. Soc.* **2008**, *130*, 424.

7. Luo, X.; Brugna, M.; Tron-Infossi, P.; Giudici-Orticoni, M. T.; Lojou, E. *J. Biolog. Inorg. Chem.* **2009** DOI: 10.1007/s00775-009-0572-y

8. Deckert, G.; Warren, P. V.; Gaasterland, T.; Young, W. G.; Lenox, A. L.; Graham, D. E.; Overbeek, R.; Snead, M. A.; Keller, M.; Aujay, M.; Huber, R.; Feldman, R. A.; Short, J. M.; Olsen, G. J.; Swanson, R. V. *Nature* **1998**, *392* (6674), 353

9. Brugna-Guiral, M.; Tron, P.; Nitschke, W.; Stetter, K. O.; Burlat, B.; Guigliarelli, B.; Bruschi, M.; Giudici-Orticoni, M. T. *Extremophiles* **2003**, *7* (2), 145

10. Cammack, R.; Patil, D. S.; Hatchikian, E. C.; Fernandez, V. M. *Biochim. Biophys, Acta* **1987**, *912* (1), 98

11. Guiral, M.; Tron, P.; Belle, V.; Aubert, C.; Leger, C.; Guigliarelli, B.; Giudici-Orticoni, M. T. *Intern. J. Hydrogen Energy* **2006**, *31* (11), 1424

12. Ogata, H.; Hirota, S.; Nakahara, A.; Komori, H.; Shibata, N.; Kato, T.; Kano, K.; Higuchi, Y. *Structure* **2005**, *13* (11), 1635

13. Lubitz, W.; Reijerse, E.; van Gastel, M. *Chem. Rev.* **2007**, *107*, 4331

14. Fernandez, V. M.; Hatchikian, E. C.; Cammack, R. *Biochim. Biophys. Acta* **1985**, *832* (1), 69

15. Lamle, S. E.; Albracht, S. P. J.; Armstrong, F. A. *J. Am. Chem. Soc.* **2005**, *127* (18), 6595

16. Brecht, M.; van Gastel, M.; Buhrke, T.; Friedrich, B.; Lubitz, W. *J. Am. Chem. Soc.* **2003**, *125* (43), 13075

17. Van der Zwaan, J. W.; Albracht, S. P. J.; Fontijn, R. D.; Slater, E. C. *FEBS Lett.* **1985**, *179* (2), 271

18. Kellers, P.; Pandelia, M.E.; Currell, L. J.; Görner, H.; Lubitz, W. *Phys. Chem. Chem. Phys*. **2009**, DOI: 10.1039/b913635e

19. Dementin, S.; Burlat, B.; De Lacey, A. L.; Pardo, A.; Dryanczyk-Perrier, G.; Guigliarelli, B.; Fernandez, V. M.; Rousset, M. *J. Biolog. Chem.* **2004**, *279* (11), 10508

20. Huynh, B. H.; Patil, D. S.; Moura, I.; Teixeira, M.; Moura, J. J. G.; Der Vartanian, D. V.; Czechowski, M. H.; Prickril, B. C.; Peck, H. D.; LeGall, J. *J. Biolog. Chem.* **1987**, *262* (2), 795-800.

21. Coremans, J. M. C. C.; Van der Zwaan, J. W.; Albracht, S. P. J. *Biochim. Biophys. Acta* **1992,** *1119* (2), 157

22. Teixeira, M.; Moura, I.; Xavier, A. V.; Huynh, B. H.; Der Vartanian, D. V.; Peck, H. D.; LeGall, J.; Moura, J. J. G. *J. Biolog. Chem.* **1985**, *260* (15), 8942

23. Garcin, E.; Vernede, X.; Hatchikian, E.C., Volbeda, A.; Frey, M.; Fontecilla-Camps J.C. *Structure* **1999**, *7*(5), 557

24. Sweeney, W. V.; Rabinowitz, J. C. *Ann. Rev. Biochem.* **1980**, *49*, 139

25. Pandelia, M. E.; Tron-Infossi, P.; Fourmond, V.;Leger, C.; Giudici-Orticoni, M. -T.; Lubitz, W. to be submitted in *J. Biolog. Chem.* **2009** (see Chapter 7 of the thesis)

26. De Lacey, A. L.; Fernandez, V. M.; Rousset, M.; Cammack, R. *Chem. Rev.* **2007**, *107*, 4304

27. Dutton, P. L. *Methods Enzymol.* **1978,** *54*, 411

28. Prince, R. C.; Linkletter, S. J. G.; Dutton, P. L. *Biochim. Biophys. Acta* **1981**, *635* (1), 132

29. Wardman, P. *Journal of Physical and Chemical Reference Data* **1989**, *18* (4), 1637-1755.

30. Fernandez, V. M.; Hatchikian, E. C.; Patil, D. S.; Cammack, R. *Biochim. Biophys. Acta* **1986,** *883* (1), 145

31. Asso, M.; Guigliarelli, B.; Yagi, T.; Bertrand, P. *Biochim. Biophys. Acta* **1992**, *1122* (1), 50

32. Surerus, K. K.; Chen, M.; Van der Zwaan, J. W.; Rusnak, F. M.; Kolk, M.; Duin, E. C.; Albracht, S. P. J.; Munck, E. *Biochemistry* **1994**, *33* (16), 4980

33. Cammack, R.; Patil, D.; Aguirre, R.; Hatchikian, E. C. *FEBS Lett.* **1982**, *142* (2), 289

34. Coffman, R. E.; Buettner, G. R. *J. Phys. Chem.* **1979**, *83* (18), 2392

35. Guigliarelli, B.; More, C.; Fournel, A.; Asso, M.; Hatchikian, E. C.; Williams, R.; Cammack, R.; Bertrand, P. *Biochemistry* **1995**, *34* (14), 4781-4790.

36. Elsasser, C.; Brecht, M.; Bittl, R. *J. Am. Chem. Soc.* **2002**, *124* (42), 12606-12611.

37. Pandelia, M. E.; Tron-Infossi, P.; Giudici-Orticoni, M.-T.; Lubitz, W. *to be submitted* **2009** (see Chapter 10 of the thesis)

38. De Lacey, A. L.; Fernandez, V. M. pH-dependent redox behaviour of asymmetric viologens. *Journal of Electroanalytical Chemistry* **1995**, *399* (1-2), 163

39. Guigliarelli, B.; Asso, M.; More, C.; Augier, V.; Blasco, F.; Pommier, J.; Giordano, G.; Bertrand, P. *Eur. J. Biochem.* **1992**, *207* (1), 61

40. Knuttel, K.; Schneider, K.; Erkens, A.; Plass, W.; Muller, A.; Bill, E.; Trautwein, A. X. *Bulletin of the Polish Academy of Sciences-Chemistry* **1994**, *42* (4), 495

41. Hagedoorn, P. L.; Driessen, M. C. P. F.; van den Bosch, M.; Landa, I.; Hagen, W. R. *FEBS Lett.* **1998**, *440* (3), 311

42. Capozzi, F.; Ciurli, S.; Luchinat, C. *Metal Sites in Proteins and Models* **1998**, *90*, 127

43. Sweeney, W. V.; Magliozzo, R. S. *Biopolymers* **1980**, *19* (11), 2133

44. Magliozzo, R. S.; Mcintosh, B. A.; Sweeney, W. V. *J. Biolog. Chem.* **1982,** *257* (7), 3506

45. Roberts, L. M.; Lindahl, P. A. *J. Am. Chem. Soc.* **1995**, *117* (9), 2565

46. Schröder, O.; Bleijlevens, B.; de Jongh, T. E.; Chen, Z.; Li, J.; Fischer, J.; Forster, J.; Friedrich, C. G.; Bagley, K. A.; Albracht, S. P. J.; Lubitz, W. *J. Biolog. Inorg. Chem.* **2007,** *12* (2), 212

47. Bas, D. C.; Rogers, D. M.; Jensen, J. H. *Proteins* **2008,** *73* (3), 765

48. Sainz, G.; Jakoncic, J.; Sieker, L. C.; Stojanoff, V.; Sanishvili, N.; Asso, M.; Bertrand, P.; Armengaud, J.; Jouanneau, Y. *J. Biolog. Inorg. Chem.* **2006**, *11* (2), 235

49. Dementin, S.; Belle, V.; Bertrand, P.; Guigliarelli, B.; dryanczyk-Perrier, G.; de Lacey, A. L.; Fernandez, V. M.; Rousset, M.; Leger, C. *J. Am. Chem. Soc.* **2006**, *128* (15), 5209

50. Yahata, N.; Saitoh, T.; Takayama, Y.; Ozawa, K.; Ogata, H.; Higuchi, Y.; Akutsu, H. *Biochemistry* **2006**, *45* (6), 1653

51. Roberts, L. M.; Lindahl, P. A. *Biochemistry* **1994**, *33* (47), 14339

52. Adams, M. W. W. *J. Biolog. Chem.* **1987**, *262* (31), 15054

53. Vita, N.; Hatchikian, E. C.; Nouailler, M.; Dolla, A.; Pieulle, L. *Biochemistry* **2008**, *47* (3), 957

54. Dai, S. D.; Johansson, K.; Miginiac-Maslow, M.; Schurmann, P.; Eklund, H. *Photosynthesis Research* **2004**, *79* (3), 233

55. Saggu, M.; Zebger, I.; Ludwig, M.; Lenz, O.; Friedrich, B.; Hildebrandt, P.; Lendzian, F. *J. Biolog. Chem.* **2009**, *284* (24), 16264

56. Heering, H. A.; Bulsink, Y. B. M.; Hagen, W. R.; Meyer, T. E. *Biochemistry* **1995**, *34* (45), 14675

57. Heering, H. A.; Bulsink, Y. B. M.; Hagen, W. R.; Meyer, T. E. *Eur. J. Biochem.* **1995**, *232* (3), 811

# Chapter 10

## Hydrogenase I from the hyperthermophilic bacterium *Aquifex aeolicus*:

## Detection of a loosely bound hydride ligand in the Ni-C state.

## A HYSCORE and ENDOR study at X- and Q-band frequencies
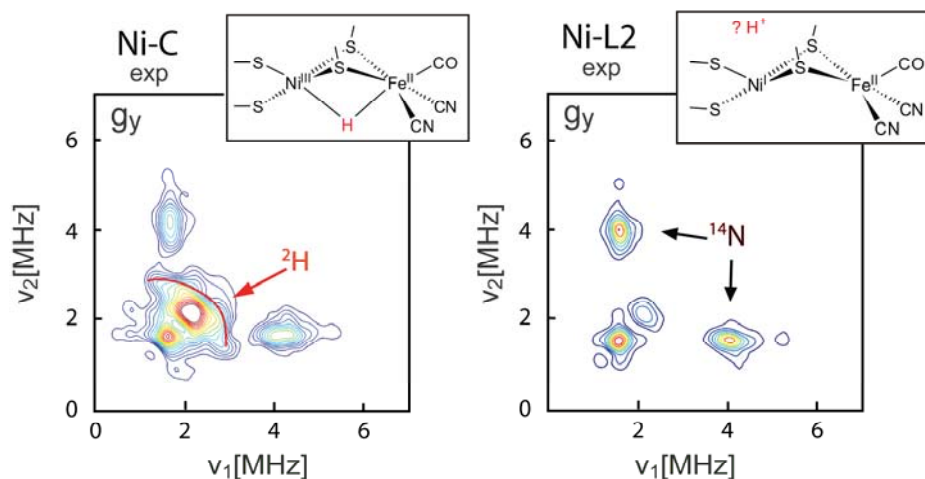


**Graphical abstract.** X-band HYSCORE of Ni-C prepared in $D_2O(D_2)$ at the $g_y$ orientation (left) and of the Ni-L2 (illuminated sample) at the same field position. Illumination of Ni-C to Ni-L2 at 7 K leads to disappearance of the $^2H$ ridges corresponding to the deuterated form of the hydride ligand. The schematic structures illustrating the related reaction are included as inserts.

*Chapter 10*

# Hydrogenase I from the hyperthermophilic bacterium Aquifex aeolicus: Detection of a loosely bound hydride ligand in the Ni-C state. A HYSCORE and ENDOR study at X- and Q-band frequencies†

Maria-Eirini Pandelia*, Pascale Tron-Infossi‡, Marie-Thérèse Giudici-Orticoni‡, and Wolfgang Lubitz*

*Max-Planck-Institut für Bioanorganishe Chemie, Stiftstrasse 34-36, D45470, Mülheim a.d. Ruhr*
‡*Laboratoire de Bioenergetique et Ingenierie des Proteines, IBSM-CNRS, 13402 Marseille France*

## Abstract

The [NiFe] hydrogenase (Hase) I from the extreme thermophilic bacterium *Aquifex aeolicus* exhibits increased oxygen tolerance and thermostability, properties that make it an important candidate for future bio-technological applications. The catalytic cycle of this enzyme is centered on the Ni-C state, shown in hydrogenases from other organisms to carry a hydride ligand originating from the heterolytic splitting of dihydrogen. The EPR spectrum of the Ni-C state in *A. aeolicus* indicates a similar electronic structure with respect to standard and regulatory hydrogenases. By means of X-band HYSCORE in (H/D) exchanged samples, a light-sensitive hydride species was shown to be present. In addition, Mims ENDOR spectroscopy showed two exchangeable protons; one is clearly correlated with the bridging hydride. It is concluded that in Ni-C of the Hase I from *A. aeolicus* the hydride ligation is conserved, similarly to known anaerobic and oxygenic hydrogenases. A notable difference, however, is the comparatively smaller hyperfine interaction, which indicates a slightly different position and a weaker binding of the bridging hydride in the active site, in agreement with the more transient nature of Ni-C in *A. aeolicus* (i.e. its higher reactivity).

---

† *To be submitted as a communication* **2009**

The constantly growing interest in the usage of alternative sources of energy has brought hydrogenases into the proscenium of bio-scientific research. Hydrogenases are metalloenzymes that perform the reversible oxidation of dihydrogen[1]: $H_2 \rightleftharpoons 2H^+ + 2e^-$ and understanding of their mechanism is crucial for improving their performance and for synthesizing biomimetic catalytic systems. A distinct subclass of these enzymes is found in hyperthermophilic microorganisms growing at extreme temperatures of 80°C or higher[2]. In their majority, they contain a [NiFe] center in their active site[3]. Although they share many biological similarities with their respective mesophilic counterparts, they have been shown to partially maintain catalytic activity under aerobic conditions[4]. The enhanced thermostability and oxygen tolerance, makes them particularly suitable for biotechnological applications as in biofuel cells and biohydrogen production[5, 6].
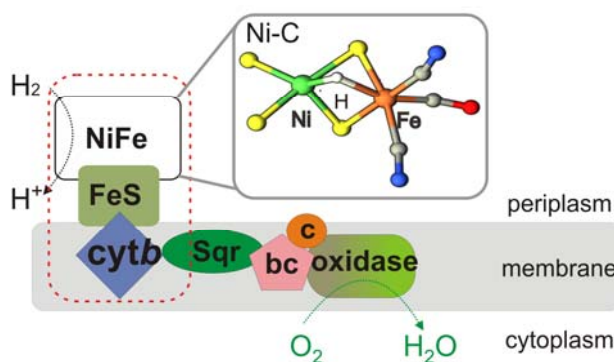


**Figure 1.** Hydrogenase I-cyt*b* complex and its redox partners[14] in the energetic pathway coupling dihydrogen oxidation to oxygen reduction in *A. aeolicus*. In the insert the suggested structure of the active site of Ni-C is shown, based on the structure of standard hydrogenases.

*Aquifex (A.) aeolicus* is a hyperthermophilic hydrogen-oxidizing bacterium with an optimal growth temperature of 85°C[7]. Its metabolic pathway consists of three hydrogenases, among which hydrogenase I (Figure 1) is part of a mechanism associated with the final reduction of oxygen to water[8]. Hydrogenase (Hase) I alone or co-purified with its native electron acceptor cytochrome *b* shows increased oxygen tolerance[9]. It has been shown that at its physiological temperatures considerable hydrogen activation takes

place under atmospheric conditions[10] while at 25°C inhibition by oxygen is very slow and reactivation has remarkably fast kinetics[9]. Electron paramagnetic resonance (EPR) and protein-film voltammetry (PFV) studies have shown that the as purified enzyme consists only of the readily activated Ni-B state[10,11], which is spectroscopically similar to the one present in anaerobic and oxygenic hydrogenases[12,13].

For [NiFe] hydrogenases from hyperthermophilic bacteria such as *A. aeolicus* a crystal structure is not yet available. Recent Fourier transform infrared (FTIR) studies[15] have shown that the active site coordination is similar to that of standard hydrogenases with a conserved $Fe(CN)_2CO$ moiety[16,17a]. In addition, FTIR-electrochemistry in solution revealed a simple enzymatic mechanism comprising only four detectable redox states; namely Ni-B, Ni-SI$_a$, Ni-C and Ni-R[15,18]. All redox processes took place at more positive potentials (~ 100 mV) with respect to known standard hydrogenases. Ni-C was found to be a more transient intermediate, since reduction to Ni-R takes place at comparatively close redox potentials to that of Ni-SI$_a$ to Ni-C.

In all hydrogenases studied so far, only Ni-C has been shown to have the substrate bound in its active site[19], emphasizing its primary role in the catalytic function of these enzymes. Hence, it is compelling to characterize the electronic properties of this state in *A. aeolicus* as this would contribute to elucidating the enzymatic function in oxygen-tolerant enzymes. For this purpose, electron-nuclear double resonance (ENDOR) and hyperfine sublevel correlation (HYSCORE) spectroscopies can be employed, as these methods are sensitive to hyperfine interactions of nuclei such as $^1$H. Protons that are related to the hydrogen oxidation process can further be exchanged with $^2$H allowing a unique identification[19,20,21,22]. Such a study has however several drawbacks. Due to its transient nature, Ni-C cannot be obtained in sufficiently high concentrations, accounting for only 0.2-0.4 spins/mol in samples of ~ 250 µM. This results in quite low signal-to-noise ratio. In addition, the magnetic coupling between the [NiFe] site and the reduced proximal iron-sulphur cluster leads to line broadening/splitting and has thus to be avoided. Furthermore, contribution from signals corresponding to $^{14}$N nuclei complicates the HYSCORE spectra.
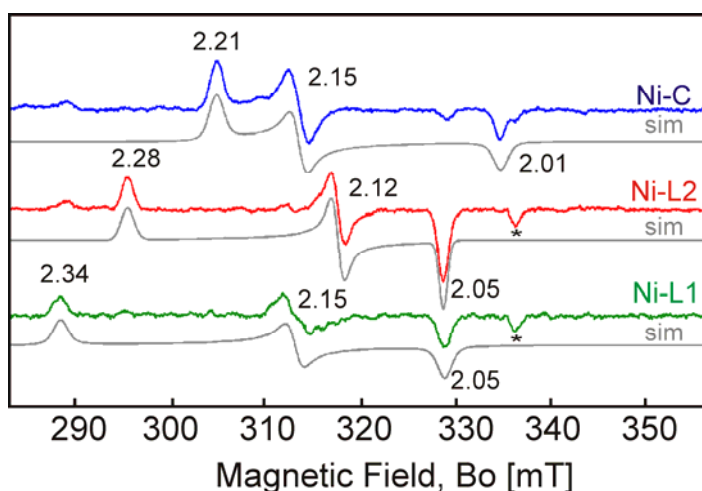
**Figure 2.** cw EPR spectra of the Hase I-cyt*b* complex in the Ni-C state at 100 K (blue). After illumination at 100 K in Ni-L2 (red) and at 170 K in Ni-L1 (green). Experimental: Frequency 9.432 GHz, modulation amplitude 1 mT, microwave power 10 mW, accumulation time 1 hour.

In the present work, Ni-C was initially characterized by cw EPR, later by HYSCORE in protonated and deuterated samples and finally results from $^2$H ENDOR were used to simulate the respective HYSCORE spectra.

Reduction of Hase I with dihydrogen results in the formation of a paramagnetic state with principal g-values $g_x = 2.21$, $g_y = 2.15$ and $g_z = 2.01$ (Figure 2), which resembles the Ni-C from mesophilic hydrogenases (see Appendix G). This state is associated with a formally trivalent $Ni^{3+}$ species with the unpaired electron in a $d_z^2$ orbital[23]. The $g_x$, $g_y$ values are slightly up-shifted indicating a somewhat different electronic structure. Heterolytic splitting of dihydrogen results in the formation of a bridging hydride in the active site of Ni-C, as illustrated in the insert of Figure 1, which is light sensitive. Illumination at low temperatures converts Ni-C to the Ni-L state(s) with dissociation of the hydride as a proton[21,24], leaving the nickel ion in a formal $Ni^{1+}$ state[23]. This is shown also for the Ni-C state in *A. aeolicus* by formation of two light-induced states Ni-L1 and Ni-L2 after illumination at 170 K and 100 K, respectively. Unlike to standard hydrogenases however, Ni-L1 could be observed also at $\leq$ 100 K even in the absence of light[17b]. The lowering of the temperature was adequate to overcome the barrier

for dissociation of the hydride, suggesting that this ligand is more weakly bound in Ni-C from *A. aeolicus* than in other standard hydrogenases.

Further, the Ni-C state was prepared in $D_2O$ based Tris buffer, by reducing the enzyme with $D_2$. The HYSCORE spectra of the Ni-C state at the canonical orientations $g_x$ and $g_y$ are shown in Figure 3A. In these spectra, correlations between nuclear frequencies of different electronic manifolds corresponding to $^{14}N$ and $^{2}H$ nuclei were present. The $^{14}N$ signals are typical for a nitrogen nucleus in the so-called cancellation condition[25], where only the 'pure' quadrupole frequencies ($v_0$, $v_-$, $v_+$) are observed. In *D. vulgaris* it was explicitly demonstrated that they belong to the $N_\varepsilon$ nitrogen of the histidine residue that is hydrogen bonded to the apical bridging thiol[26]. On the basis of HYSCORE and ESEEM[17c] in both protonated and deuterated samples a quadrupole coupling constant $(e^2qQ)/h = (1.89 \pm 0.05)$ MHz and an asymmetry parameter $\eta = 0.39$ were obtained, in excellent agreement with the values reported for Ni-C in mesophilic hydrogenases[27]. The simulated spectra are shown in Figure 3B. The results demonstrate that the environment of this histidine in *A. aeolicus* is largely preserved with respect to the one in standard hydrogenases, suggesting an analogous coordination and interaction of the imidazole ring with the active site. No differences in the $^{14}N$ quadrupolar values were detected between Ni-C samples prepared either with $H_2$ ($H_2O$) or $D_2$ ($D_2O$).

In addition, in the HYSCORE spectra in Figure 3A a ridge centered at the $^{2}H$ Larmor frequency is also observed, showing the presence of at least one (H/D) exchangeable proton in the [NiFe] site of Ni-C. The simulation parameters will be discussed below and are shown in Figure 3C. The $g_z$ orientation is not presented since at this field position contributions from exchangeable protons occur, originating from the iron-sulphur centers.

Illumination at 7 K converted the Ni-C signal to Ni-L2. The HYSCORE spectrum recorded at the $g_y$ (323.6 mT) position shows that the ridges associated with the exchangeable proton in Ni-C are absent. Instead only a small isotropic signal centered at the $^{2}H$ Larmor frequency of 2.11 MHz is observed (Figure 3D). Similar results were found for the other orientations. The $^{2}H$ ridges can be thus associated with the deuterated form of the hydride ligand present in the Ni-C state of the *A. aeolicus* hydrogenase, which is dissociated upon illumination[19], as was exhibited in the cw EPR (Figure 2).
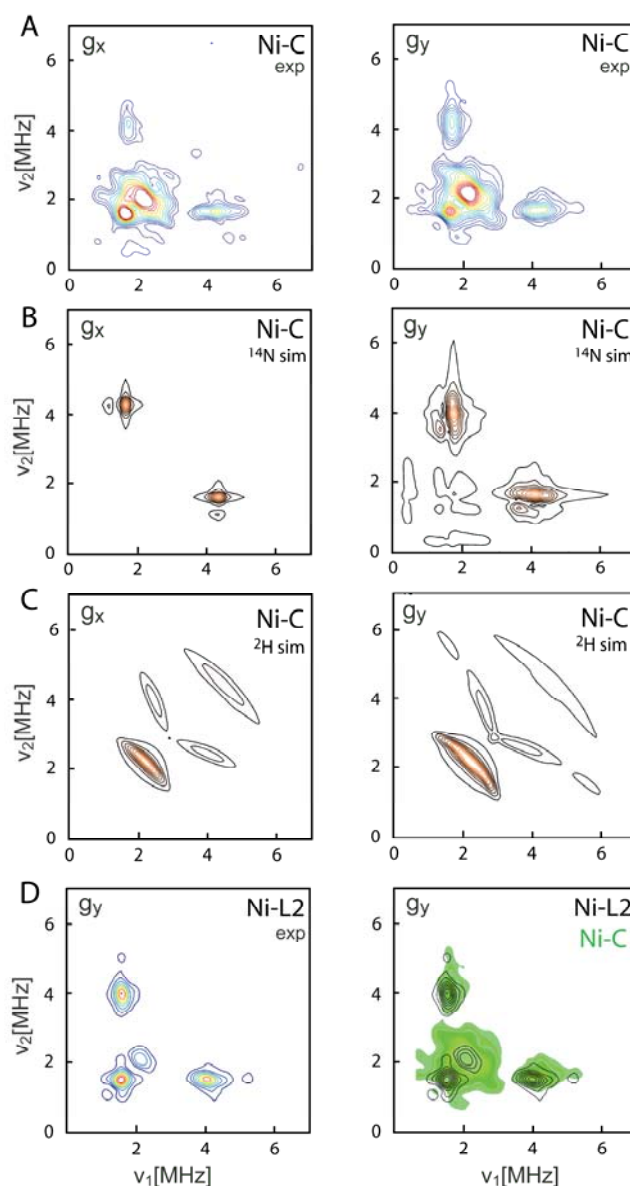
**Figure 3.** (A) X-band HYSCORE of Ni-C prepared in $D_2O(D_2)$ at $g_x$, $g_y$ orientations. (B, C) Simulated spectra of the $^{14}N$ and $^2H$ signals, respectively. The simulated $^2H$ parameters were obtained from the ENDOR experiments described below. The double quantum ridges of the $^2H$ in the simulation were not observed in the experiment, due to a "peak-suppression effect" and a small intensity of the Ni-C signal. (D) Illumination of Ni-C leads to disappearance of the $^2H$ ridges corresponding to the deuterated form of the hydride ligand, illustrated by superposition of the two spectra (D, right). Experimental: $\pi/2 = 8ns$, $\tau = 120$ ns, mw frequency 9.7266 GHz, T = 7 K, accumulation time 12-24 hours.

However, the restricted orientation selection of these measurements, the weak $^2$H ridges and the additional $^{14}$N signals make a unique assignment of this coupling difficult.

Therefore, a $^2$H Mims ENDOR study at Q-band was carried out to identify and characterize the (H/D) exchangeable protons bound to Ni-C. At Q-band frequencies the nuclear frequencies of $^{14}$N and $^2$H are well separated. Mims ENDOR was chosen as this technique can resolve small hyperfine interactions of local $^2$H nuclei[21]. The fraction of the molecules with the proximal clusters reduced was small and thus a broadening but no splitting of the nickel signals due to the magnetic interaction with the FeS cluster was observed in the 2-pulse ESE detected EPR spectrum (see Appendix G). Hence, a good orientation selection could be achieved. The ENDOR spectra were recorded for field positions between near $g_x$ (1106.1 mT) and the lowest g-value (g = 2.10), at which contributions from the iron-sulphur centers are negligible. These are collected in Figure 4.

In these spectra only signals related to exchangeable protons in the local surrounding of the spin carrying [NiFe] site in the Ni-C state are present[22]. Two hyperfine couplings were determined corresponding to two distinct deuterons; D(1) and D(2). The coupling of D(1) is relatively large and anisotropic with principal components $A_{x,y,z}$ = (-1.0, 2.0, -1.9) ± 0.15 MHz. The simulation for D(1) is depicted in Figure 4 (red line). Using these parameters, the $^2$H ridges in the HYSCORE spectra could be well simulated (Figure 3C).

The isotropic part is of the A-tensor small; (-0.30 ± 0.15) MHz, which is in line with a rather remote ligand of nickel in the equatorial plane of the $d_z^2$ orbital. This coupling can be thus assigned to the deuterated hydride (D$^-$) in Ni-C of *A. aeolicus*. However, the magnitude of the dipolar and isotropic components are significantly smaller compared to the ones found in *D. vulgaris*[19]. This suggests a larger bonding distance and a weaker interaction of the hydride with the active site of Ni-C in the case of *A. aeolicus*. The second coupling D(2) is rather small and isotropic ≤ 0.5 MHz (green simulation, Figure 4). A similar signal was reported for Ni-C[22] in *D. gigas* , where it was associated with a D$_2$O molecule. At present, no definitive assignment for this coupling is feasible for *A. aeolicus*.
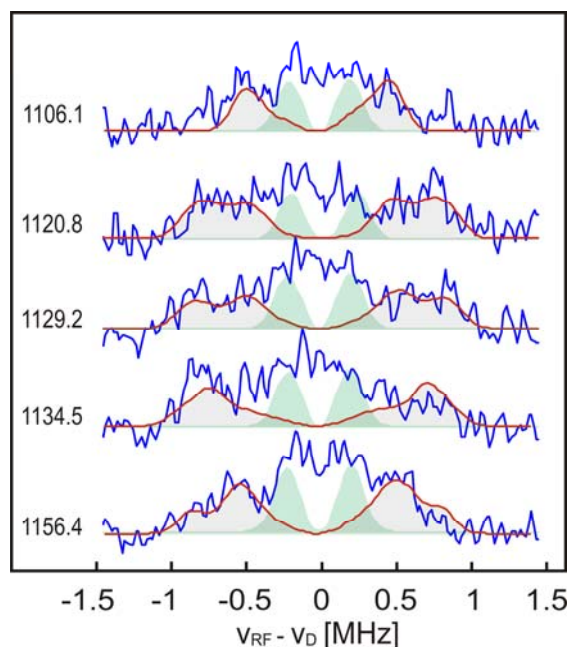
**Figure 4.** $^2$H Mims ENDOR spectra. The simulation of the coupling corresponding to the deuteride ligand D(1) is shown in red and of the second coupling D(2) in green (shaded). Experimental: $\pi/2$ = 36ns, rf =35$\mu$s, frequency = 33.999 GHz, T =7 K. Each spectrum was averaged between 48-72 hours and recorded in the stochastic mode on a Bruker ELEXSYS E580 with a homebuilt ENDOR resonator[29]. A low-pass filter (Trilithic) was used to cut off the $^1$H harmonics.

The magnitude of the D(1) coupling can be quite accurately determined but the uncertainty in its orientation is rather large, since the spectral overlap with the signal from the FeS clusters resulted in a restricted field dependent study.

On the basis of the Ni-C EPR spectrum from *D. vulgaris*, for which the g-tensor orientation in the crystallographic axes has been determined[28], the molecular symmetry of the [NiFe] site in the Ni-C from *A. aeolicus* is suggested to be similar to that of oxygen sensitive hydrogenases. A light sensitive hydride ligand is found to coordinate the active site of Ni-C that is, however, more loosely bound than that in the *D. vulgaris* species. The smaller hyperfine interaction could be associated with an increased bond distance between the nickel and the hydride and most likely with a more asymmetric bridging situation. The weaker binding of the hydride, as reflected also in its partial dissociation

even in the absence of illumination and in the more transient nature of Ni-C, is proposed to be related to the higher reactivity of the complex[30] and the more efficient catalytic process in the *A. aeolicus* enzyme.

## Experimental

The Hase I-cyt*b* complex from *A. aeolicus* was purified as previously described[8]. Reduction with $H_2$ (N27, Air Liquide) and $D_2$ (N27, Air Liquide) was performed in $H_2O$ and $D_2O$ (99, 9 %, Deutero GmbH) Tris buffers, respectively.

## Acknowledgment

## References and Notes

1. Vignais, P. M.; Billoud, B. *Chem. Rev.*, **2007**, *107*, 4206.

2. Jenney, F. E.; Adams, M. W. *Ann. N. Y. Acad. Sci.,* **2008**, *1125,* 252.

3. Volbeda, A.; Charon, M. H.; Piras, C.; Hatchikian, E. C.; Frey, M.; Fontecilla-Camps, J. C. *Nature*, **1995**, *373*, 580.

4. Jed, O.; Ely, Roger, L. *Crit. Rev. Microbiol.*, **2008**, *34(3-4)*, 117.

5. Chou, C.-J.; Jenney, F. E.; Adams, M. W.; Kelly, R. *Metab. Eng.*, **2008**, *10*, 394.

6. Luo, X.; Brugna, M.; Tron-Infossi, P.; Giudici-Orticoni, M. T.; Lojou, E. *J. Biolog. Inorg. Chem.* **2009** DOI: 10.1007/s00775-009-0572-y.

7. Deckert, G.; *Nature*, **1998**, *392*, 353.

8. Guiral, M.; Tron, P.; Aubert, C.; Gloter A.; Iobbi-Nivol C.; Giudici-Orticoni, M. T. *J Biolog. Chem.,* **2005**, *51*, 42004.

9. Guiral, M.; Tron, P.; Belle, V.; Aubert, C.; Leger, C.; Guigliarelli, B.; Giudici-Orticoni, M. T., *Intern. Hydrogen Energy* **2006**, *31 (11)*, 1424.

10. Protein-film voltammetry experiments, carried out in collaboration with Fourmond, V. and Leger. C., have shown that the Hydrogenase I from *A. aeolicus* shows enhanced resistance towards $O_2$ inhibition.

11. Brugna-Guiral, M.; Tron, P.; Nitschke, W.; Stetter, K. O.; Burlat, B.; Guigliarelli, B.; Bruschi, M.; Giudici-Orticoni, M. T. *Extremophiles* **2003**, *7 (2)*, 145.

12. Lubitz, W.; Reijerse, E.; van Gastel, M. *Chem. Rev.*, **2007**, *107*, 4331.

13. Vincent, K. A.; Parkin, A.; Armstrong, F. *Chem. Rev.*, **2007**, *107*, 4366.

14. Abbreviations used: Sqr stands for Sulfide Quinone Reductase, bc for ubiquinol cytochrome c oxidoreductase, c stands for cytochrome c.

15. Pandelia, M. E.; Tron-Infossi, P.; Fourmond, V.; Leger, C.; Giudici-Orticoni, M. T; Lubitz W. *to be submitted* **2009** (Chapter 7 of the present study).

16. De Lacey, A. L.; Fernandez, V. M.; Rousset, M.; Cammack, R. *Chem. Rev.* **2007**, *107*, 4304.

17. Appendix G; S3) FTIR spectra of Ni-C/Ni-L states, S4) cw EPR spectrum of Ni-C/Ni-L2, S5) ^{14}N ESEEM spectra

18. See Appendix G or references 12,13 for a complete scheme on the enzymatic mechanism of anaerobic hydrogenases.

19. Brecht, M.; van Gastel, M.; Buhrke, T.; Friedrich, B.; Lubitz, W. *J. Am. Chem. Soc,* **2003**, *125 (43)*, 13075.

20. Foerster, S.; van Gastel, M.; Brecht, M.; Lubitz, W. *J. Biolog. Inorg. Chem.* **2005**, *10 (1)*, 51.

21. Whitehead, J. P.; Gurbiel, R. J.; Bagyinka, C.; Hoffman, B. M.; Maroney, M. J. *J. Am. Chem. Soc.* **1993**, *115 (13)*, 5629.

22. Fan, C. L.; Teixeira, M.; Moura, J.; Moura, I.; Huynh, B. H.; LeGall, J.; Peck, H. D.; Hoffman, B. M. *J. Am. Chem. Soc.* **1991**, *113 (1)*, 20-24.

23. Stein, M.; Lubitz, W. *J. Inorg. Biochem.* **2001**, *86 (1)*, 442.

24. van der Zwaan, J. W.; Albracht, S. P. J.; Fontijn, R. D.; Slater, E. C. *FEBS Lett.* **1985**, *179 (2)*, 271.

25. Flanagan, H. L.; Singel, D. J. *J. Chem. Phys.* **1987**, *87 (10)*, 5606.

26. Agrawal, A. G.; van Gastel M.; Gartner, W.; Lubitz, W. *J. Phys. Chem. B* **2006**, *110 (15)*, 8142.

27. Chapman, A.; Cammack, R.; Hatchikian, C. E.; McCracken, J.; Peisach, J. *FEBS Lett.* **1988**, 242 (1), 134-138.

28. Foerster, S.; Stein, M.; Brecht, M.; Ogata, H.; Higuchi, Y.; Lubitz, W. *J. Am. Chem. Soc.* **2003**, *125 (1)*, 83-93.

29. Niklas, J.; Boris, E.; Antonkine M. L.; Sinnecker, S.;Pandelia, M. E.; Lubitz, W. *J. Phys. Chem. B*, **2009**, *113*, 10367.

30. Rakowski DuBois, M.; Dubois, D. L. *Chem. Soc. Rev.* **2009**, *38(1)*, 62.

# Chapter 11

## Summary and Conclusion

The present study consists of two parts; the first part deals with specific but so far unresolved mechanistic aspects of the well-characterized [NiFe] hydrogenase from the sulphate reducing bacterium *Desulfovibrio vulgaris* Miyazaki F. It aspires to obtain a more concise and complete knowledge of the function of this enzyme on the basis of a number of specifically designed spectroscopic experiments using EPR, FTIR and electrochemical techniques. In the second part, the so far insufficiently characterised [NiFe] hydrogenase (Hase I) from the extreme thermophile *Aquifex aeolicus* is thoroughly investigated in order to build a mechanism for the function of this enzyme and to understand the reactivity with the substrate $H_2$ as well as with inhibitors. Of particular importance is here the investigation of the oxygen tolerance of this species. The functional principles and the unique properties of the *A. aeolicus* hydrogenase are compared with the ones of oxygen sensitive hydrogenases, such as *D. vulgaris*.

The various redox states implicated in the catalytic cycle of the *D. vulgaris* hydrogenase were dynamically monitored by a combination of electrochemical and spectroscopic approaches. This demonstrated that in-solution equilibrium electrochemistry delivers results essentially identical to those of dynamic electrochemistry, where the enzyme is directly adsorbed on an electrode. In addition, the unready state Ni-A and its one-electron reduced state Ni-SU were re-investigated and a previous discrepancy in the Ni-SU infrared characteristics between *Desulfovibrio vulgaris* and other standard hydrogenases was resolved. Furthermore, the midpoint reduction potential of the Ni-A/ Ni-SU couple was estimated, which is in excellent agreement with the value obtained from EPR titrations for the reduction potential of Ni-A.

Infrared spectroelectrochemistry was in addition employed to examine the affinity of the enzyme for binding carbon monoxide. Similarly to *D. fructosovorans*, two EPR silent CO-adducts were observed to be formed when the active Ni-SI binds CO. Their one-electron difference is ascribed to the reduction of the proximal iron-sulphur cluster. Contrary to previous conclusions, the inactive (Ni-SI$_r$)$_I$ is not inhibited by carbon monoxide neither the active Ni-C state, while at very negative potentials

## *Summary and Conclusions*

electrochemical cleavage of the CO takes place and the enzyme performs a transition to the active Ni-R state. It was not possible to electrochemically oxidise the CO inhibited enzyme, showing that carbon monoxide inhibition cannot be reversed under these conditions. However, a partial transition to the oxidised Ni-B could be achieved by lowering the temperature and applying very positive potentials at the Ni-R redox level. The small fraction of Ni-B obtained was not an equilibrium state.

At cryogenic temperatures CO is photodissociated from the active site and the light-induced state is the active Ni-SI$_a$, in agreement with the electrochemical measurements at room temperature. For the first time, the kinetics for the reversible rebinding of the CO molecule in the dark were studied by rapid scan FTIR, enabling the determination of the activation barrier for such a process. Comparison with existing data for other proteins, in particular myoglobin, shows comparable activation energies, underlining their significance for reversible binding at cofactor sites with divalent metal ions.

The paramagnetic Ni-CO state was formed from the Ni-L state (Ni$^{1+}$) by dark adaptation of Ni-L in the presence of CO. The EPR spectrum was essentially identical to the one reported for *Allochromatium vinosum*. Integrating the results obtained for both EPR-silent and EPR-active CO-adducts the appropriate conditions for binding CO were determined to be: i) a high spin four coordinated Ni$^{2+}$ for the creation of the Ni-SCO states and ii) a monovalent four coordinated nickel for the creation of the paramagnetic Ni-CO state. This demonstrates that all states with a trivalent (Ni$^{3+}$) and a bridging ligand are inlikely to bind CO.

The study of *D. vulgaris* was subsequently focused on the not so well characterised (Ni-SI$_r$)$_I$ state. This was achieved by taking advantage of the light sensitivity exhibited at near cryogenic temperatures and formation of a novel light-induced intermediate denoted as Ni-SL. On this basis, solid experimental evidence was obtained that the hydroxide ligand coordinating Ni-B is still present in (Ni-SI$_r$)$_I$ and hinders catalytic function. Upon illumination, the hydroxyl group is displaced towards the side of the nickel ion, leading to formation of a putative hydrogen bond with a conserved arginine residue (Arg479, *D. vulgaris* numbering). This was confirmed by deuterium isotope labelling and following the back conversion kinetics from the Ni-SL to (Ni-SI$_r$)$_I$ state. The activation barrier was estimated to be 19 kJ mol$^{-1}$, which is in the range of related hydrogen bond energies. The measured λ-dependence of the photo-induced transition demonstrated that it involves a nickel

centred electronic transition with concomitant rearrangement of the hydroxyl ligand (displacement or dissociation).

At temperatures equal to or lower than 40 K the position and magnitude of the cyanide FTIR bands corresponding to Ni-SL were dependent on the wavelength of the incident light, while no changes were observed for the CO stretching vibration. The selective impact on the cyanide bands is presumably associated with a perturbation of the hydrogen bonding network between these ligands and nearby amino acid residues. This is proposed to be induced by an isomerisation of the C-N bond to N-C leading to an effective disruption of the existing hydrogen bonds.

Light-induced phenomena are related to electronic and structural changes of the photosensitive [NiFe] complex. So far, we studied the properties of the light-sensitive states Ni-SCO and (Ni-SI$_r$)$_l$. The last part of the *D.vulgaris* enzyme investigation is focused on the light sensitivity of the catalytically active Ni-C state and the nature of this transition, where dissociation of the hydride ligand bridging the bimetallic site occurs. Isotope exchange of the hydride ligand with deuteride led to a significant effect on the rebinding rate constants, being 5-7 times slower. This result showed that the rebinding of the hydride as a proton is the rate limiting step of the reaction. The activation barrier was determined with high accuracy and the Arrhenius pre-exponential factor is in the range predicted for proton rebinding. Extrapolation of the results to room temperature concluded that the lifetime of the Ni-L state at 297 K is 57 μs.

The complexity of the mechanism in *D. vulgaris* reflects the difficulties in understanding the function of such enzymes and in designing an optimised system for dihydrogen oxidation or production. The obtained knowledge will be used as a basis to exemplify and identify the grounds for the increased oxygen tolerance of other enzymes and in particular of the Hase I from the hyperthermophilic bacterium *Aquifex aeolicus*.

A first approach towards unravelling the properties of the *Aquifex aeolicus* enzyme was to identify the intermediates in the activation and catalytic mechanism. The method of choice was FTIR spectroscopy integrated with *in-situ* controlled potentiometry, since all possible intermediates are infrared accessible. A total number of four detectable redox states could be defined in contrast to oxygen-sensitive hydrogenases. The remarkable redox chemistry of Hase I compared to standard enzymes can be summarized in the following points:

## Summary and Conclusions

i) No Ni-A state was present in the as isolated enzyme.

ii) No inactive Ni-SI states could be resolved indicating a fast activation mechanism.

iii) Ni-C was observed to be more transient, since there is a large overlap between its midpoint potential and the transition to the more reduced Ni-R state.

iv) Only one Ni-R state was present, which is atypical at physiological pH (6-7) for mesophilic hydrogenases.

v) No turnover of the enzyme occurs under very reducing conditions, since Ni-C did not appear at potentials below -410 mV, showing that the equilibrium reaction

Ni-C + H$_2$ $\rightleftharpoons$ Ni-R does not take place.

vi) The FTIR frequencies of the respective redox states bear great resemblance with those corresponding to mesophilic hydrogenases, showing similar coordination and structural properties.

vii) The reduction potentials for the active states of the enzyme are approximately 100 mV more positive, revealing that Hase I is a very efficient catalyst.

The electrochemical study in solution was combined with protein film voltammetry in order to obtain an overall picture of the enzymatic activity and probe the sensitivity of this enzyme towards dioxygen. The reactivation of Hase I takes place at very positive potentials with the switch potential parameter being approximately 200 mV more positive compared to oxygen-sensitive hydrogenases and 70 mV more positive with respect to the membrane bound (MBH) enzyme from *R. eutropha*. This shows a less energy demanding reactivation for the Hase I from *Aquifex aeolicus*. Injection of dioxygen at very positive potentials (e.g. +190 mV) led to a decrease of the remaining hydrogen oxidation activity, but not to complete inactivation. When flushing the oxygen away, the activity is regained similarly to the MBH from *R. eutropha*, but unlike the oxygen-sensitive hydrogenases, for which inactivation under such oxidising conditions is essentially irreversible. In addition, Hase I formed very stable films on the electrode, which is of great advantage for its future biotechnological applications.

After having determined the possible redox intermediates, the response of the enzyme towards carbon monoxide inhibition was studied. We found that it is possible to inhibit the active Hase I with CO under strong saturating conditions. Formation of a CO-adduct demonstrates that CO can access the active centre and bind to nickel. The IR spectroelectrochemical findings compared to oxygen sensitive hydrogenases are summarized as following:

i) A Ni-CO bond can be formed. The FTIR frequency of the externally added carbonyl is at least 10 cm$^{-1}$ higher demonstrating a weaker binding (lesser back-donation from the metal d-orbital to the molecular orbital of CO).

ii) Activation of the enzyme in the presence of CO takes place at more positive potentials; approximately 200-280 mV. In addition, CO inhibition can be completely reversed upon mild reduction.

iii) CO inhibition can be completely reversed by oxidation presumably leading to Ni-SI$_a$, in which the oxygenic species can bind and yield Ni-B. The enzyme can be easily tuned between CO inhibited and oxidised forms within a small potential range.

These results show that the active site of Hase I is accessible to carbon monoxide and thus rule out the possibility of a narrow gas channel as the basis of oxygen-tolerance. This is further supported by the presence of the conserved amino acids valine and leucine in the entrance to the active site, similarly to oxygen-sensitive enzymes.

To further address the matter of carbon monoxide inhibition, experiments were carried out near cryogenic temperatures, where photodissociation of the extrinsic CO ligand occurs. The study of the kinetics for the CO rebinding can be directly correlated with the results obtained for the *D. vulgaris* hydrogenase. The activation barrier for the rebinding of CO in Hase I is larger (8-25%) than that in *D. vulgaris*. However, the most distinctive difference was found for the pre-exponential factor A$_0$ that is two orders of magnitude smaller in Hase I as compared to *D. vulgaris*. This shows a smaller probability of the carbon monoxide molecule to reassociate with the active centre. The reactivity of the Hase I with carbon monoxide is impaired due to a combined attenuated CO bonding situation and possible steric reasons that may be associated with a smaller number of inhibitor molecules near the active site.

The iron-sulphur clusters are important cofactors and are responsible for the electron transfer to the physiological acceptors. Results from amino acid sequence comparisons support the existence of three iron-sulphur centres in the case of Hase I, as has been observed for the standard hydrogenases. However, the EPR signals of these centres in Hase I are more complex and reminiscent of interactions between paramagnetic species that are absent in oxygen-sensitive hydrogenases. A similar observation holds for the membrane bound enzyme from *R. eutropha* and suggests that the increased oxygen tolerance observed both in the latter and in Hase I may be related to a modification of the electron-transfer relay centres.

*Summary and Conclusions*

The approach towards understanding these differences was to perform an EPR potentiometric titration and to assign the signals observed, which would in turn help to identify the redox processes and the type of clusters involved. A synopsis of the results obtained as well as differences to oxygen-sensitive hydrogenases is given below:

i) A medial $[Fe_3S_4]$ cluster was found with a midpoint reduction potential approximately 100 mV more positive, which was essentially pH-independent in a pH range between 6.4 and 8.3. The presence of a non-conserved serine residue, capable of hydrogen bonding is likely to be related to the higher midpoint potential values.

ii) On the basis of the amino acid sequence, a distal $[Fe_4S_4]$ cubane type cluster that is bound to the polypeptide backbone by three cysteinyls and one histidine was found. Its reduction potential is more positive, approximately by 300 mV than that in standard hydrogenases. It exhibits a 60 mV/pH unit dependence for pH greater than 7.4. A $pK_a$ of 7 was obtained that is in accordance with the one theoretically predicted for a solvent exposed nitrogen of the imidazole ring for the case of Hase I.

iii) The presence of a proximal $[Fe_4S_4]$ cluster is shown both by four conserved cysteinyl residues in its amino acid sequence motif as well as by the appearance of a 'splitting' in the nickel signals. reminiscent of a magnetic spin-spin interaction with a paramagnetic species in the vicinity of the latter (< 15 Angstroms). The magnitude of this interaction is in the range expected in related oxygen-sensitive systems such as the hydrogenases from *D. gigas* and *A. ferrooxidans*. The midpoint reduction potential is +87 mV, which is approximately 400 mV more positive than the one found in standard hydrogenases. It has a 60 mV/pH dependence for pH values greater than pH 7.4, showing that the electron transfer is coupled to binding of a proton species to one of the ligating cysteinyls.

iv) The midpoint potentials of the so far discussed iron-sulphur clusters are all more positive compared to oxygen sensitive complexes. Such positive values are also observed for the membrane bound hydrogenase from *R. eutropha* and in particular with the CH34 strain. On the basis that both *A. aeolicus* and *R. eutropha* are obligatory (micro)aerophilic, such a result can be related with an evolutionary upshift in the redox potentials to cope with the increased concentrations of dioxygen, which in the case of Hase I is the final electron acceptor.

v) All titrations are consistent with redox processes involving in total four electrons. This holds also for the membrane bound hydrogenase from *R. eutropha* (H16 and

CH34 strains). Both in Hase I and in *R. eutropha* three iron-sulphur centres could be clearly assigned; one $[Fe_3S_4]^{1+/0}$ and two low potential $[Fe_4S_4]^{2+/1+}$, similar to oxygen sensitive hydrogenases. However, an additional electron process was found, related to redox species that in the case of *A. aeolicus* has a reduction potential of +232 mV. The latter is denoted as HP (High Potential) iron-sulphur centre. The question thus arising is to what kind of paramagnetic species this transition corresponds to. On the basis of its magnetic interaction with both the [NiFe] site and the medial $[Fe_3S_4]$ cluster, it is concluded that the HP species is situated in between these two centres. Therefore the only possible assignment is that this HP centre is related to the $[Fe_4S_4]$ cluster proximal to the [NiFe] site.

Homology modelled structures of the Hase I reveal the presence of two additional cysteinyl residues in the protein fold of the proximal $[Fe_4S_4]$ cluster, that are not present in standard hydrogenases. Such a modification in the ligand surrounding of the proximal cluster is also observed for the membrane bound hydrogenase from *R. eutropha,* which in addition exhibits the same interaction signals in EPR, which are assigned to the HP species. Furthermore in our titrations at low pH, the appearance of an out-of-equilibrium radical signal was observed, which is likely to be associated with these extra cysteinyl residues by a formation of a sulphur based radical species.

There are three possible oxidation states for electron transfer cubanes in proteins; $[Fe_4S_4]^{3+}(S=1/2)$, $[Fe_4S_4]^{2+}(S=0)$, $[Fe_4S_4]^{1+}(S=1/2)$. The $[Fe_4S_4]^{2+/1+}$ couple for the oxido-reduction of the proximal cluster was found to be equal to +87 mV. However at more positive potentials (> +150 mV), this cluster becomes again paramagnetic, indicating a formal super-oxidation to a $[Fe_4S_4]^{3+}$ species (HP). We propose that the additional cysteinyl residues could be involved in the coordination of the cluster and the structural changes imposed could alter its electronic properties. This could take place either via formation of disulfide bonds or by changing the coordination sphere of the $[Fe_4S_4]$ cluster. This HP species plays an important role in the oxygen tolerance of the enzyme. For disulfides, there are several examples that these act like switches protecting the enzymes from oxidative stress. However, even if a disulfide is not formed, the very positive redox potential of this cluster can prevent the fast inactivation (oxidation) of the [NiFe] site and makes it a very poor electron donor for the dioxygen precluding the formation of reactive oxygen species.

*Summary and Conclusions*

The redox titrations carried out on Hase I from *A. aeolicus* both by FTIR and EPR, revealed redox centres with much more positive redox potentials as those found for standard hydrogenases. The presence of the HP species in Hase I is proposed to significantly contribute to the oxygen tolerance of the enzyme. On the other hand, the upshift in the midpoint potentials of the three conserved iron-sulphur clusters and of the [NiFe] intermediates in Hase I, can be explained by considering the related energy providing metabolic processes associated with these hydrogenases. In the case of sulphate reducing bacteria, dihydrogen oxidation (-414 mV) has to be coupled to the reduction of sulphate to sulphide (~ -200 mV). However, in *A. aeolicus* the dihydrogen oxidation performed by Hase I is coupled to the oxygen reduction to water (+800 mV). It is evident that the electron transfer pathway related to each enzyme is adjusted to the midpoint potential for the reduction of the final electron acceptor, so that optimum electron transfer can occur.

In addition to examining the redox properties and establishing relationships with potent inhibitors, the last chapter of the present study has been focused on the catalytically relevant interaction of the Hase I with $H_2$. For this purpose the Ni-C state was studied, which is the only intermediate that has been experimentally shown to bind the substrate in the form of a hydride. By its selective isotope exchange to deuteride and on the basis of its light sensitivity, the properties of the Ni-C were investigated. It was found that even in the absence of external illumination, the hydride ligand could be to a certain extent dissociated, showing that it can be easier detached from the active site. $^2$H ENDOR and HYSCORE experiments revealed a smaller hyperfine coupling as compared to *D. vulgaris*, which indicates an elongated and weaker Ni-H bond. These results show that not only the inhibitors but also the substrate binds weakly to the [NiFe] site, which could be related to the increased reactivity of the complex. This is most likely associated with a slightly different electronic configuration as for example exhibited in the small shifts of the g-tensor values for Ni-C in Hase I.

The current work on [NiFe] hydrogenases that are either strictly anaerobic or oxygen tolerant shows that the mechanistic aspects between these species are to a large degree similar. Resistance against oxygen is proposed not to be a localised property associated with a specific singularity in the active site but is found to be a synergetic effect. For the Hase I the reactivity of the [NiFe] active site both with inhibitors as well as with the substrate results in a more efficient catalysis and an

enhanced protection of the enzyme against inhibition. This is related to the redox potentials of all the redox centres that are more difficult to oxidise with respect to the low potential centres found in standard hydrogenases. The additional presence of an HP centre proximal to the [NiFe] site, contributes significantly to protecting the active site against oxidative inactivation. Combining the present results, we can now address the question why Hase I is activated by simply raising the temperature to 85°C; the solubility of the oxygen at this temperature decreases, leading to a lower redox potential in the protein solution. In addition, the Tris based buffer usually used is strongly pH dependent and at such temperatures this leads to a significant lower pH. The midpoint potential for the reactivation of the [NiFe] site becomes even more positive as a result of lowering the pH, effectively leading to an enzyme that is capable of hydrogen oxidation under atmospheric conditions.

It is concluded that the high stability of Hase I from *A. aeolicus*, its unique catalytic properties that are less-energy demanding and the tolerance against inhibitors makes it an ideal candidate for biotechnological applications and a model enzyme for further studies and potential bio-engineering.

*Summary and Conclusions*

# Nomenclature

Different nomenclature of the redox states of the [NiFe] hydrogenases used in the literature.

**Inactive states:**

Ni-B or $Ni_r$-B   (EPR-active, $Ni^{3+}$)

$(Ni\text{-}SI_r)_I$ or $(Ni_r\text{-}S)_I$  (EPR-silent, $Ni^{2+}$)

$(Ni\text{-}SI_r)_{II}$ or $(Ni_r\text{-}S)_{II}$  (EPR-silent, $Ni^{2+}$)

Ni-A or $Ni_u$-A  (EPR-active, $Ni^{3+}$)

Ni-SU or $Ni_u$-S (EPR-silent, $Ni^{2+}$)

**Active states:**

Ni-$SI_a$ or $Ni_a$-S  (EPR-silent, $Ni^{2+}$)

Ni-C or $Ni_a$-C (EPR-active, $Ni^{3+}$)

Ni-R(1) or $Ni_a$-SR (EPR-silent, $Ni^{2+}$)

Ni-R(2) or $Ni_a$-SR′ (EPR-silent, $Ni^{2+}$)

Ni-R(3) or $Ni_a$-SR′′ (EPR-silent, $Ni^{2+}$)

**Light induced states:**

Ni-L(1,2,3, etc.) (EPR-active, $Ni^{1+}$)

Ni-SL (EPR-silent, $Ni^{2+}$)

**CO inhibited states:**

Ni-SCO (EPR-silent, $Ni^{2+}$)

Ni-$SCO_{red}$ (EPR-silent, $Ni^{2+}$)

Ni-CO (EPR-active, $Ni^{1+}$)

*Nomenclature*

# Appendix A

Supporting Information: Spectroelectrochemical study of [NiFe] hydrogenase from *Desulfovibrio vulgaris* Miyazaki F in solution and immobilized on biocompatible gold surfaces

**Figure S1.** cw EPR spectrum of the *Dv*MF hydrogenase recorded at 80 K, modulation amplitude: 10 G, microwave Frequency: 9.280 GHz, microwave power: 10 mW. A radical like contamination at g~2 is shown with an asterisk (*)
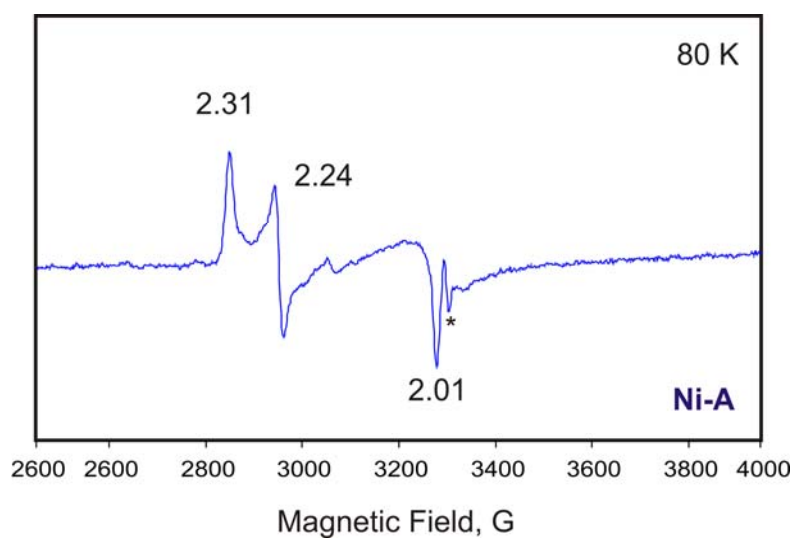
**Figure S2.** Orientation of the molecular dipole moment in *Dv*MF (left) and a structural model of *Dv*MF attached to a SAM-coated Au surface (right)
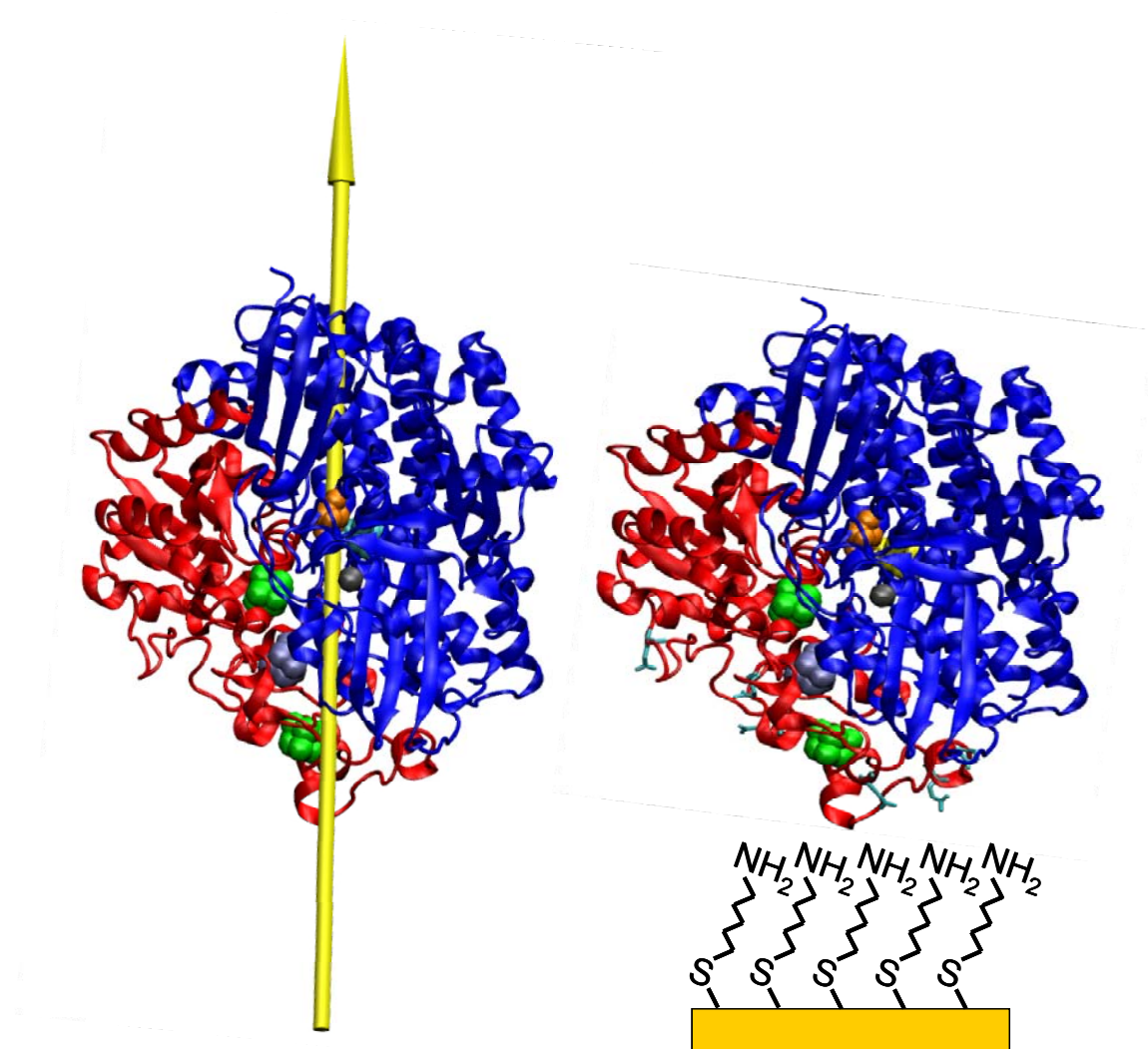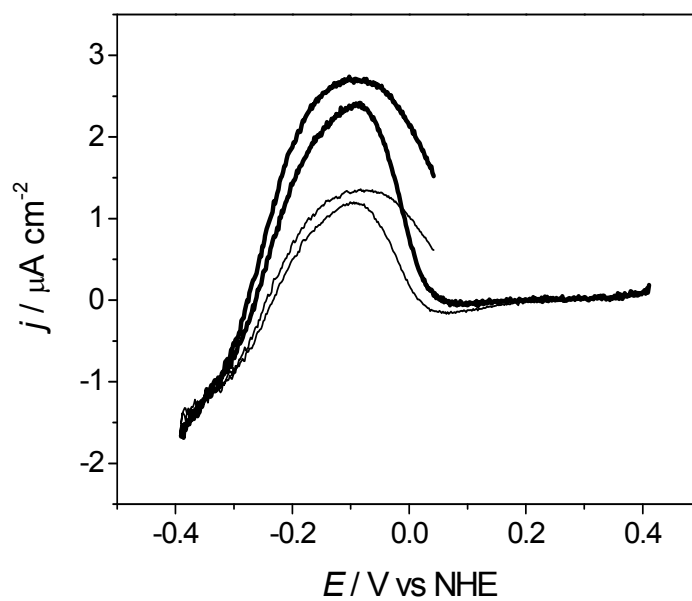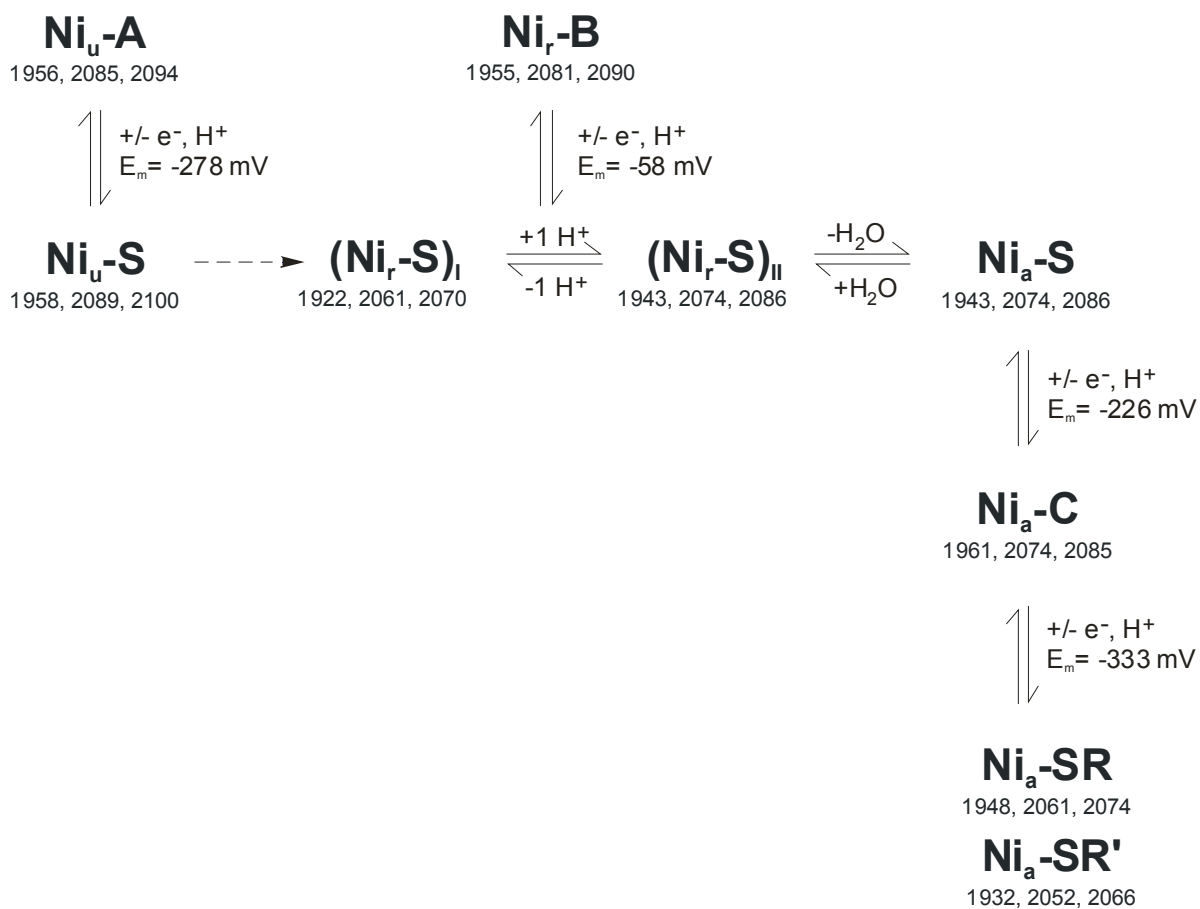
**Figure S3.** CV plot before (dark trace) and after (light trace) exposing the electrode to 1.0 M KCl solution for 10 minutes. Remarkably, the CV signal obtained under $H_2$ atmosphere indicates that the immobilized enzyme is still active.

**Scheme S1.** Overview on the Redox states found in *Dv*MF. All potentials are measured at pH 5.5, except for $Ni_u$-A to $Ni_u$-S (pH 8.2).

**$Ni_u$-A**
1956, 2085, 2094

**$Ni_r$-B**
1955, 2081, 2090

+/- e⁻, H⁺
$E_m$= -278 mV

+/- e⁻, H⁺
$E_m$= -58 mV

**$Ni_u$-S**
1958, 2089, 2100

**($Ni_r$-S)$_I$**
1922, 2061, 2070

+1 H⁺
-1 H⁺

**($Ni_r$-S)$_{II}$**
1943, 2074, 2086

-H₂O
+H₂O

**$Ni_a$-S**
1943, 2074, 2086

+/- e⁻, H⁺
$E_m$= -226 mV

**$Ni_a$-C**
1961, 2074, 2085

+/- e⁻, H⁺
$E_m$= -333 mV

**$Ni_a$-SR**
1948, 2061, 2074

**$Ni_a$-SR'**
1932, 2052, 2066

## Appendix B
Supporting information: Inhibition of the [NiFe] Hydrogenase from *Desulfovibrio vulgaris* Miyazaki F by Carbon Monoxide: An FTIR and EPR Spectroscopic Study

**Figure S1.** The FTIR spectrum of the aerobically isolated NiFe hydrogenase at + 229 mV (vs NHE) saturated without CO (red) and with CO under a 100 % CO atmosphere (green). Temperature: 25 °C. The FTIR spectra in the case of the aerobically purified hydrogenase with or without carbon monoxide in the solution were identical, showing the CO does not bind to the inactive enzyme.

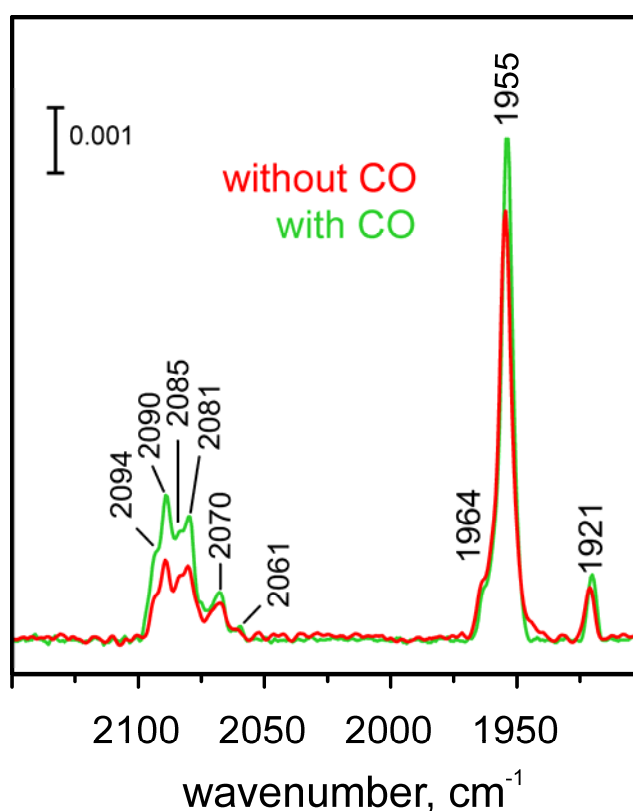**Figure S2.** The FTIR spectra of the CO saturated hydrogenase from *D. vulgaris* Miyazaki F, after having fully reduced the enzyme at -739 mV and then apply a potential of +229 mV, (Fig. 3e) (a) at 25 °C and (b) at 4 °C, in which a significant amount of Ni-B has been obtained. It appears that at lower temperatures insertion of the oxygenic species in the active site can compete with the binding of CO.
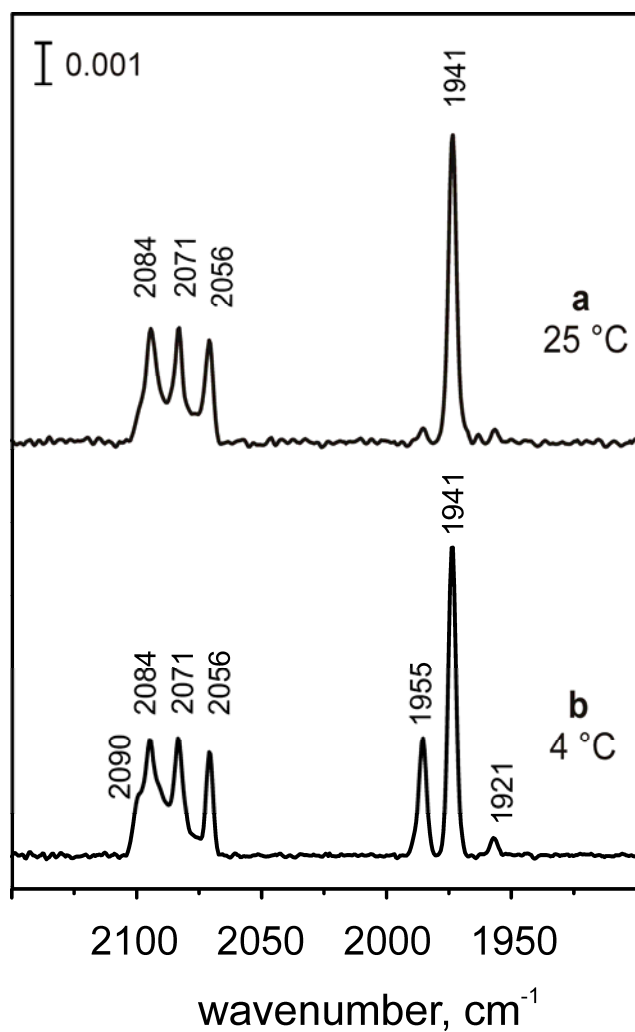
# Appendix C

## Supporting Information: Probing Intermediates in the Activation Cycle of [NiFe] Hydrogenase by Infrared Spectroscopy: The Ni-SI$_r$ State and its Light Sensitivity

**Figure S1**. Temperature dependence (90 K ≤ T ≤ 110 K) of the back conversion rate constants corresponding to Ni-SIr and Ni-SI$_{1961}$ states (Arrhenius plot).
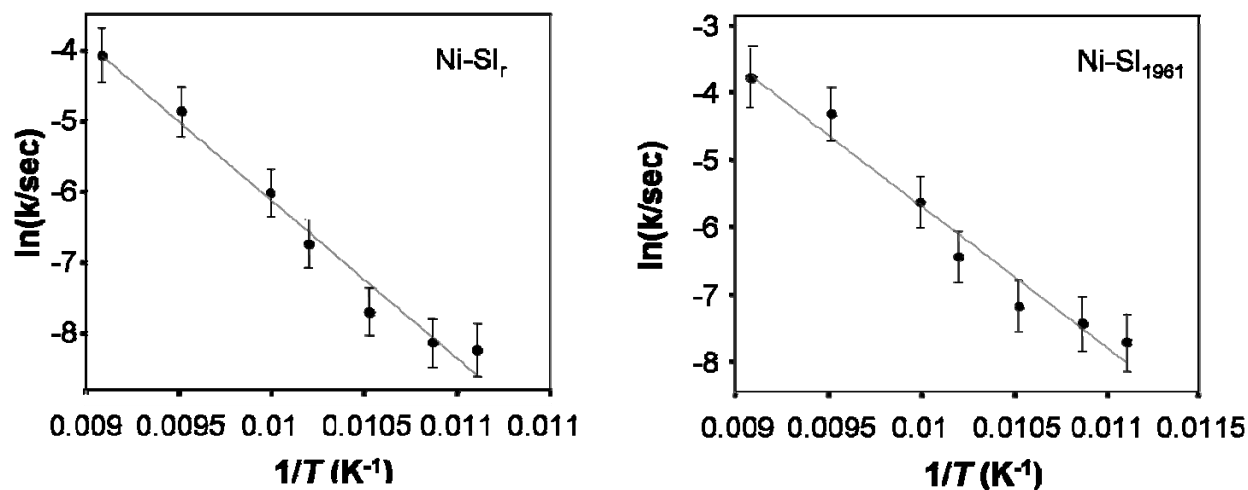


**Figure S2.** Time dependence of the disappearance of the CO absorption band associated with Ni-SL for both protonated (light blue) and deuterated forms (black) of the samples at 95 K. The difference in the rates exhibited was found to be small but reproducible.
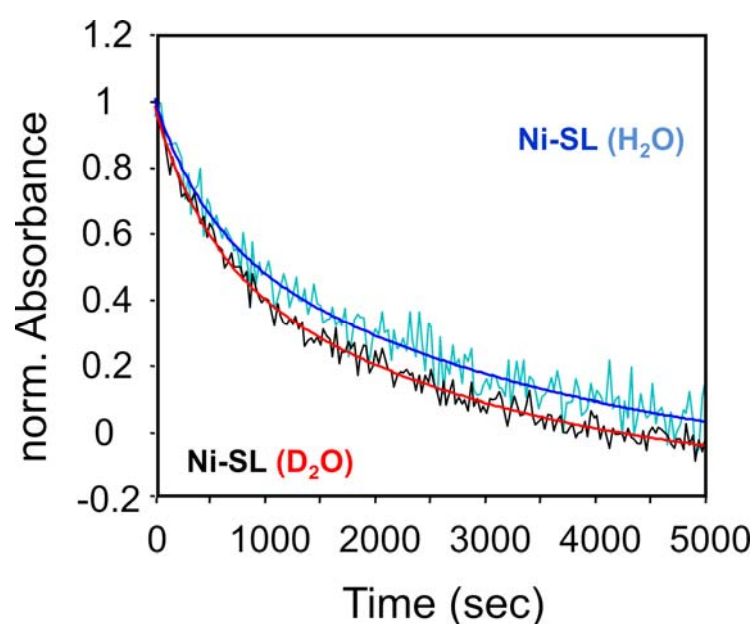
**Table S1**. Time constants obtained in the H$_2$O samples

| Temperature (K) | Ni-SIr [H$_2$O] $t_{rec}$ (s) | Ni-SI$_{1961}$ [H$_2$O] $t_{rec}$ (s) | Ni-SL [H$_2$O] $t_{rec}$ (s) |
|---|---|---|---|
| 110 | 58.4 ± 9.2 | 44.0 ± 5.6 | 51.2 ± 3.2 |
| 105 | 113.1 ± 13.6 | 75.6 ± 8.8 | 106.3 ± 5.2 |
| 100 | 408.9 ± 48.8 | 279.3 ± 31.1 | 334.6 ± 17.1 |
| 98 | 838.5 ± 66.1 | 631.2 ± 64.72 | 719.6 ± 26.0 |
| 95 | 2202.6 ± 164.9 | 1304.7 ± 108.51 | 1394.1 ± 39.8 |
| 92 | 3396.3 ± 300.0 | 1694.4 ± 200.0 | 2485.9 ± 180 |
| 90 | 3777.0 ± 416.0 | 2246.3 ± 295.14 | 3719.6 ± 238.3 |

**Table S2.** Time constants obtained in the deuterated samples.

| Temperature (K) | Ni-SIr [D$_2$O] $t_{rec}$ (s) | Ni-SI$_{1961}$ [D$_2$O] $t_{rec}$ (s) | Ni-SL[D$_2$O] $t_{rec}$ (s) |
|---|---|---|---|
| 110 | 44.0 ± 6.6 | 33.5 ± 7.0 | 38.0 ± 3.4 |
| 105 | 114.2 ± 13.6 | 79.0 ± 15.9 | 97.8 ± 7.5 |
| 100 | 394.7 ± 20.9 | 237.4 ± 21.9 | 341.2 ± 11.8 |
| 98 | 579.6 ± 23.5 | 380.3 ± 36.6 | 603.9 ± 17.4 |
| 95 | 1759.4 ± 57.2 | 992.7 ± 82.7 | 1643.5 ± 43.9 |
| 92 | 2859.3 ± 133.9 | 1316.4 ± 128.7 | 2681.5 ± 93.7 |
| 90 | 4828.9 ± 395.1 | 2375.5 ± 503.7 | 5228.0 ± 253.7 |

**Table S3.** Isotope effect on the kinetic rate constants of the back conversion processes. $k_{H2O}/k_{D2O}$

| Ni-SIr | Ni-SI$_{1961}$ | Ni-SL |
|:---:|:---:|:---:|
| $k_{H2O}/k_{D2O}$ | $k_{H2O}/k_{D2O}$ | $k_{H2O}/k_{D2O}$ |
| 0.75 ± 0.15 | 0.76 ± 0.17 | 0.74 ± 0.04 |
| 1.01 ±0.12 | 1.04 ± 0.16 | 0.92 ± 0.03 |
| 0.96 ±0.09 | 0.85 ± 0.10 | 1.02 ± 0.02 |
| 0.69 ± 0.06 | 0.60 ± 0.10 | 0.84 ±0.02 |
| 0.80 ± 0.05 | 0.76 ± 0.08 | 1.18 ± 0.04 |
| 0.84 ±0.07 | 0.78 ± 0.17 | 1.08 ± 0.03 |
| 1.28 ±  0.10 | 1.06 ± 0.17 | 1.40 ±0.04 |

*Appendix C*

# Appendix D

Supporting Information: Hydrogenase I from the hyperthermophilic bacterium *Aquifex aeolicus*: Activation process, redox intermediates and oxygen tolerance studied by FTIR spectroelectrochemistry and protein film voltammetry

**Table S1.** Comparison of the infrared frequencies ($cm^{-1}$) corresponding to the stretching vibrations of the CO and CN$^-$ ligands bound to Fe at 25 °C for the [NiFe] hydrogenases from: *Aquifex aeolicus* (Hase I), *D. vulgaris* Miyazaki F, *Allochromatium vinosum* and *Ralstonia eutropha* (MBH).

| redox state | *A. aeolicus* (Hase I) | | *D. vulgaris*[a] Miyazaki F | | *A. vinosum*[b] | | *R. eutropha*[c] (MBH) | |
| --- | --- | --- | --- | --- | --- | --- | --- | --- |
| | $\bar{v}$ (CO) | $\bar{v}$ (CN) | $\bar{v}$ (CO) | $\bar{v}$ (CN) | $\bar{v}$ (CO) | $\bar{v}$ (CN) | $\bar{v}$ (CO) | $\bar{v}$ (CN) |
| **Ni-A** | - | - | 1956 | 2085, 2094 | 1945 | 2082, 2093 | - | - |
| **Ni-B** | 1939 | 2081, 2092 | 1954 | 2081, 2090 | 1943 | 2079, 2090 | 1948 | 2081, 2098 |
| **Ni-SU** | - | - | 1958 | 2089, 2100 | 1948 | 2088, 2100 | 1942 | 2082, 2104 |
| **(Ni-SIr)I** | - | - | 1922 | 2061, 2070 | 1910 | 2052, 2067 | 1910 | 2055, 2063 |
| **(Ni-SIr)II** | - | - | 1943 | 2074, 2086 | 1931 | 2073, 2084 | 1936 | 2075, 2093 |
| **Ni-SIa** | 1927 | 2077, 2087 | 1943 | 2074, 2086 | 1931 | 2073, 2084 | 1936 | 2075, 2093 |
| **Ni-C** | 1949 | 2078, 2088 | 1961 | 2074, 2085 | 1951 | 2073, 2085 | 1957 | 2075, 2097 |
| **Ni-R1** | - | - | 1948 | 2061, 2074 | 1936 | 2059, 2072 | 1948 | 2068, 2087 |
| **Ni-R2** | 1910 | 2047, 2066 | 1932 | 2051, 2065 | 1921 | 2048, 2064 | 1930 | 2049, 2075 |
| **Ni-R3** | - | - | 1911 | 2045, 2061 | 1913 | 2043, 2058 | 1919 | 2046, 2071 |

[a] Taken from reference [1]

[b] Taken from reference [2]

[c] Taken from reference [3]

**Figure S2.** X-band cw EPR spectra of the as isolated Hase I-cyt*b* at 10 and 40 K. The principal values of the g-tensor of the Ni-B state are $g_x$ =2.30, $g_y$= 2.17 and $g_z$ = 2.01. Additional signals in the Ni region are present at g= 2.24, g =2.19. These can be better discerned by increasing the temperature from 10 to 40 K. Interestingly this signal disappears completely if the enzyme is heated to 80°C under aerobic conditions and the residual spectrum is a 'pure' Ni-B state. Experimental conditions: mw frequency 9.45567 GHz, modulation amplitude 1 mT, mw power 2 mW, sample concentration 120μM.
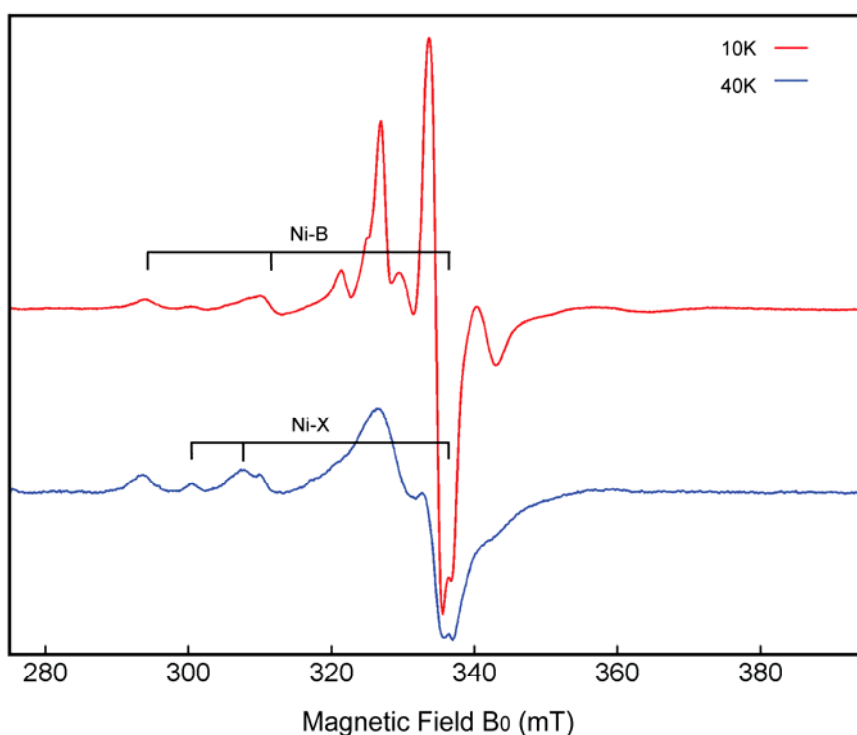
**Figure S3.** The additional signal present in the as isolated enzyme could be better separated in Q-band. The 2pulse-echo detected EPR spectra were recorded in the range of temperatures between 10 and 30 K. The NiFe centre is magnetically coupled to a proximal FeS cluster and the signals appear 'split'. However, at 30 K contributions from signals corresponding to Ni-B and the FeS centres have disappeared due to the different relaxation of this magnetically coupled system and the Ni-X state can be uniquely identified. The principal values of the g-tensor of this state are $g_x = 2.24$, $g_y = 2.19$ and $g_z = 2.01$ and are consistent with the signal in X-band. Most probably it is related to a [NiFe] state, conformationally different from Ni-B, which in addition does not magnetically interact with a FeS centre. Experimental conditions: $\pi/2 = 36$ ns, tau $= 330$ ns, mw frequency 33.97635 GHz, shot rep.time 0.6 ms, sample concentration 120 μM.

*Appendix D*
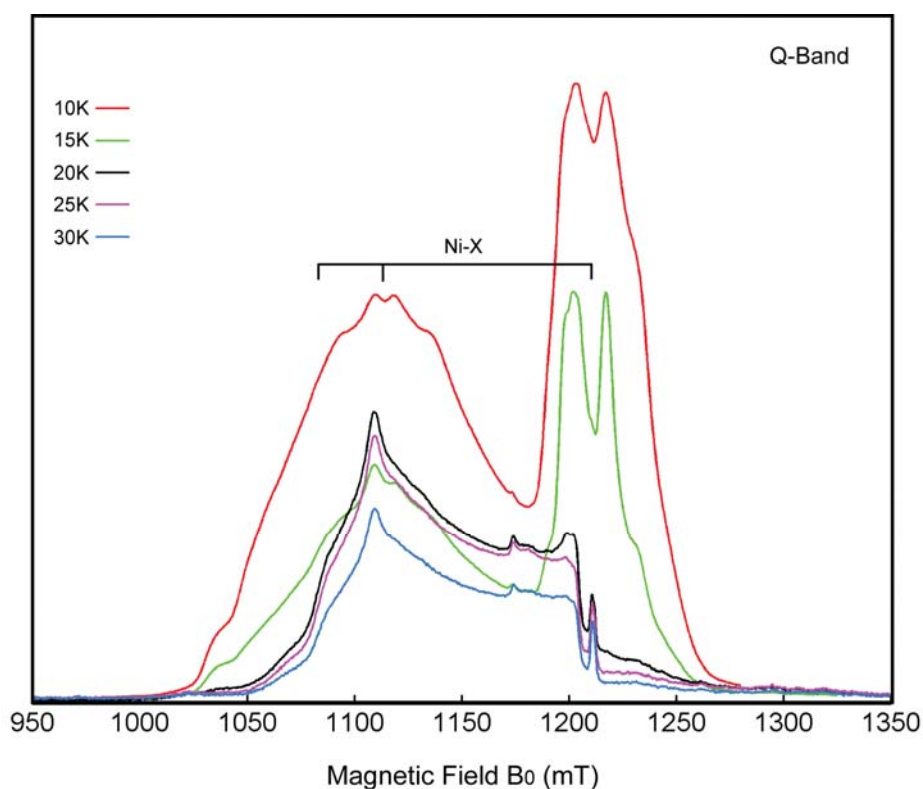
## References

1. Fichtner, C.; Laurich, C.; Bothe, E.; Lubitz, W. *Biochemistry* **2006,** *45* (32), 9706-9716.

2. Bleijlevens, B.; van Broekhuizen, F. A.; de Lacey, A. L.; Roseboom, W.; Fernandez, V. M.; Albracht, S. P. J. *J Biolog. Inorg. Chem.* **2004,** *9* (6), 743-752.

3. Saggu, M.; Zebger, I.; Ludwig, M.; Lenz, O.; Friedrich, B.; Hildebrandt, P.; Lendzian, F. *J Biolog. Chem.* **2009,** *8* (24), 16264-16276.

# Appendix E

Supporting Information: Hydrogenase I from the hyperthermophilic bacterium *Aquifex aeolicus*: CO inhibition studied by infrared spectroelectrochemistry and time-resolved FTIR at low temperatures

**Table S1:** Averaged lifetimes (inverse rate constants) obtained by analysing the back conversion kinetics corresponding to the disappearance of Ni-SI$_a$ and the recovery of Ni-SCO in *D. vulgaris*[1]. The experimental error is ± 8 %.

| Temperature (K) | bi-exponential time constants slow (s) | bi-exponential time constants fast (s) | mono-exponential time constants (s) |
|---|---|---|---|
| **76** | 1984 | 211 | 989 |
| **78** | 1098 | 99 | 570 |
| **80** | 847 | 80 | 471 |
| **85** | 419 | 48 | 249 |
| **90** | 216 | 27 | 133 |
| **92** | 172 | 18 | 567 |
| **95** | 157 | 16 | 45 |

Reference

1. Pandelia, M.E.; Ogata, H.; Currell, L.J.; Flores, M.; Lubitz, W. submitted in *Biochim. Biophys.a Acta, Bioenergetics* **2009**

*Appendix E*

# Appendix F

Supporting Information: Electron transfer and redox properties of the FeS clusters in the Hydrogenase I from the hyperthermophilic bacterium *Aquifex aeolicus*: A model for oxygen tolerance

**Figure S1.** Sequence alignment for the small subunit of *A. aeolicus* Hase I (mbhS1) and well-characterized hydrogenases.
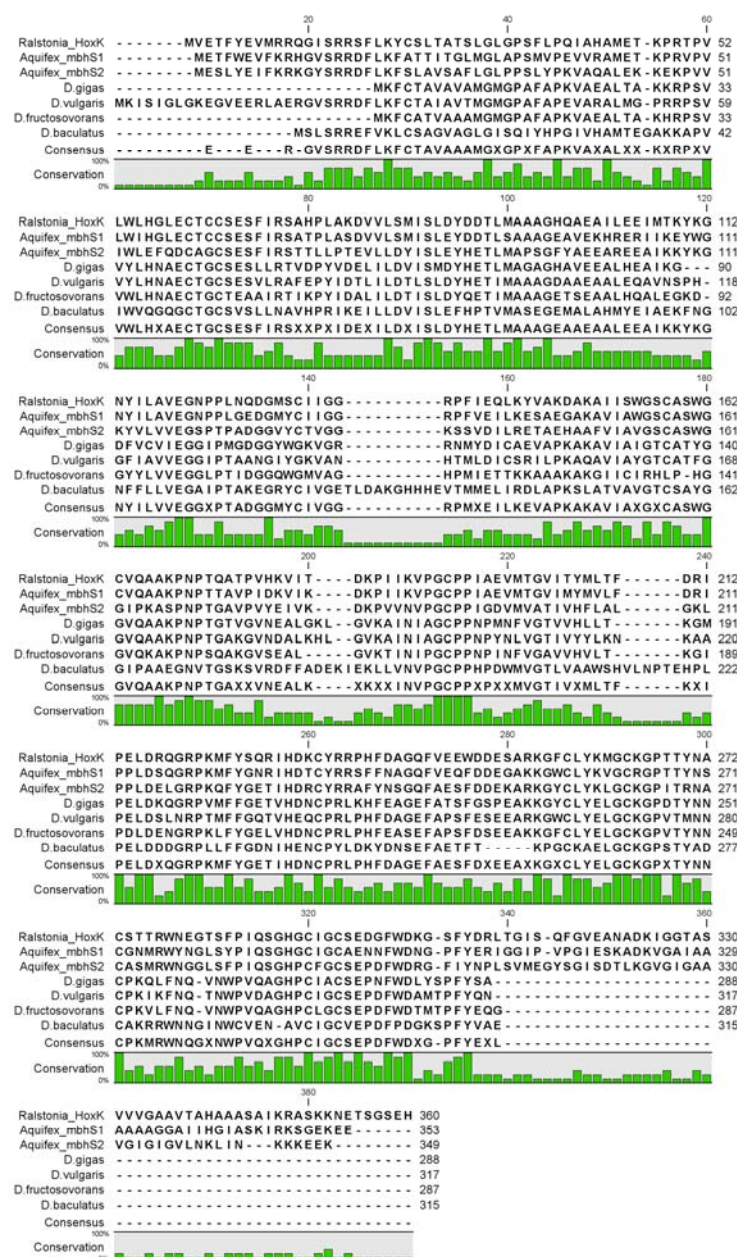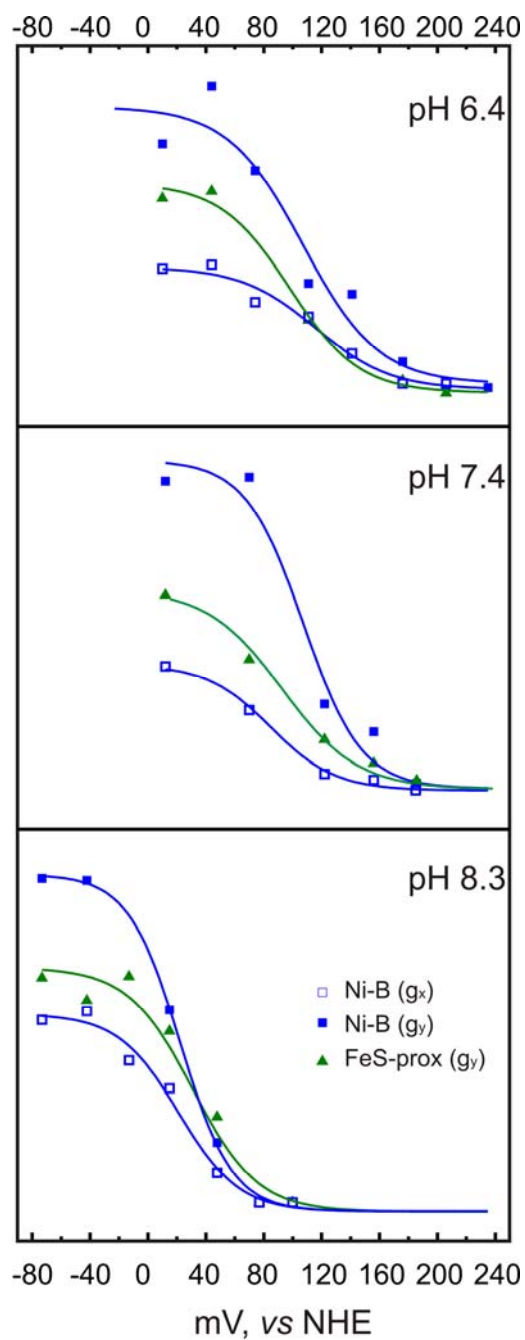
**Figure S2.** Potentiometric titrations corresponding to the proximal iron-sulphur cluster and the ‚split' Ni-B signal at three different pH values. The pH dependence of the midpoint potential becomes significant at the higher pH of 8.3.

# Appendix G

Supporting Information: Hydrogenase I from the hyperthermophilic bacterium *Aquifex aeolicus*: Detection of a loosely bound hydride ligand in the Ni-C state. A HYSCORE and ENDOR study at X- and Q-band frequencies

**Scheme S1.** Proposed mechanistic scheme for anaerobic hydrogenases. The intermediate states in red and blue denote the paramagnetic (S= 1/2) and EPR- silent species, respectively (adapted from[1]).
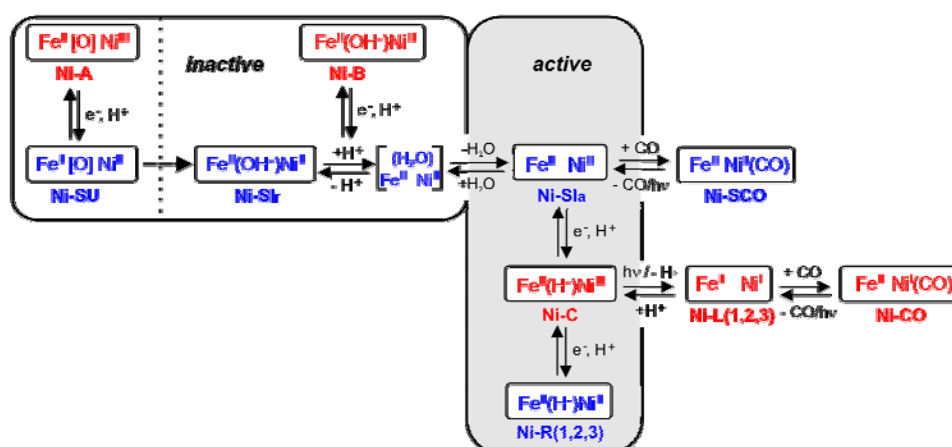
**Table S2.** Principal g-tensor values for the Ni-C and Ni-L states in *A. aeolicus, R. eutropha* (RH) and *D. vulgaris* Miyazaki F. The values for *A. aeolicus* were obtained by simulating the cw EPR spectra of the Hase I-cyt*b* complex presented in this work. The values for *R. eutropha* were taken from reference 2 and for *D. vulgaris* from reference 3.

| | *A. aeolicus* (Hase I) g | | *R. eutropha* (RH) g | | *D.vulgaris* g | |
|---|---|---|---|---|---|---|
| | Ni-C | Ni-L1 / Ni-L2 | Ni-C | Ni-L1 / Ni-L2 | Ni-C | Ni-L2 |
| x | 2.211 | 2.337 / 2.281 | 2.197 | 2.251 / 2.305 | 2.198 | 2.298 |
| y | 2.149 | 2.152 / 2.121 | 2.139 | 2.094 / 2.077 | 2.142 | 2.116 |
| z | 2.013 | 2.049 / 2.050 | 2.015 | 2.046 / 2.054 | 2.012 | 2.045 |

**Figure S3.** Light-minus-dark FTIR spectra of the $H_2$ reduced Hydrogenase I from *Aquifex aeolicus* a) at 200 K and b) at 130 K. The negative bands correspond to the Ni-C state (educt), which has a CO stretching vibration at 1952 $cm^{-1}$ and two coupled $CN^-$ stretching vibrations at 2080 and 2092 $cm^{-1}$, respectively. The positive bands correspond to the light-induced state Ni-L1 [$\bar{v}$ (CO) = 1862, $\bar{v}$ (CN)= 2024, 2045 $cm^{-1}$] and Ni-L2 [$\bar{v}$ (CO) = 1900, $\bar{v}$ (CN)= 2049, 2068 $cm^{-1}$]. Experimental: resolution 2 $cm^{-1}$, number of scans 2000.

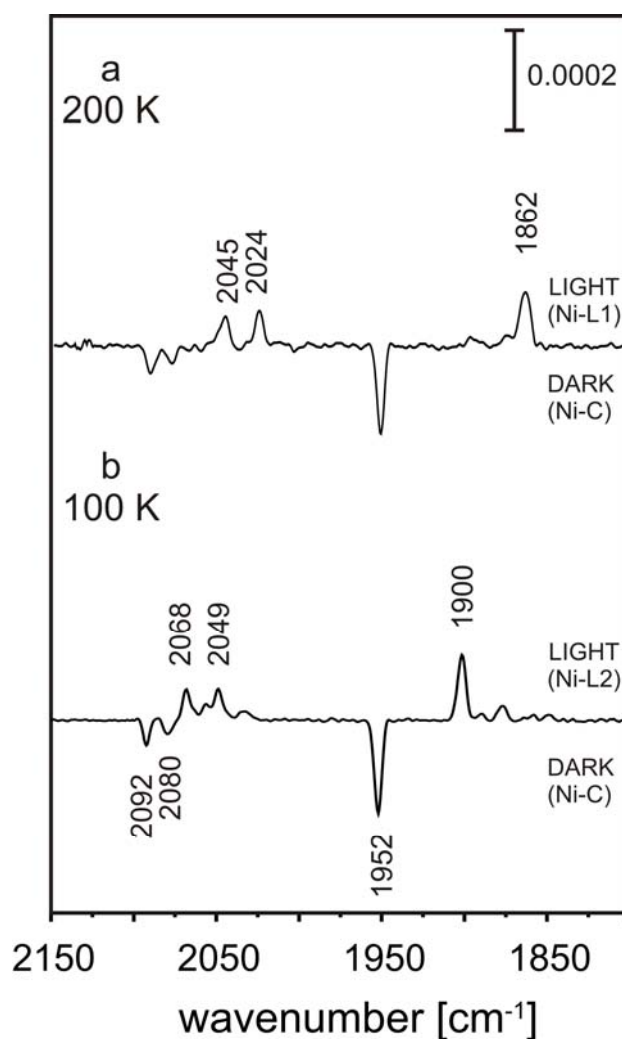**Figure S4.** CW EPR spectrum of the $H_2$ reduced Hase I-cyt*b* complex from *A. aeolicus* in the dark. Lowering the temperature to 70 K yields a significant fraction of the Ni-L1 state. Ni-L1 is already detectable at 100 K, as shown in Figure 2 of Chapter 10. Experimental conditions: mw frequency 9.4273 GHz, modulation amplitude 1 mT, microwave power 20.00 mW, temperature 70 K. Undefined signals are marked with an asterisk.
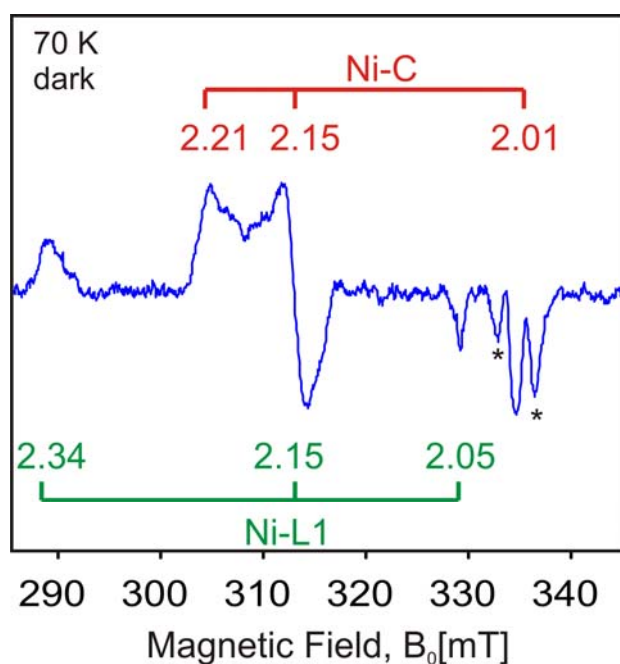
**Figure S5.** X-band 3pulse ESEEM spectra of the Ni-C state of Hase I-cyt*b* from *A. aeolicus* prepared in $H_2O(H_2)$. When the effective hyperfine coupling A of a $^{14}N$ nucleus is equal to twice the nuclear Zeeman frequency $v_n$, the condition of the so-called exact-cancellation is fulfilled; the hyperfine and nuclear Zeeman interactions cancel out in one $m_s$ manifold and the 'pure' quadrupole frequencies ($v_0$, $v_-$, $v_+$) are observed. From these frequencies the quadrupole coupling constant $K = (e^2qQ)/4h$ and the asymmetry parameter $\eta$ can be determined; $v_\pm = K(3 \pm \eta)$ and $v_0 = 2K\eta$. No differences in the $^{14}N$ quadrupolar values were detected between Ni-C samples prepared either with $H_2$ ($H_2O$) or $D_2$ ($D_2O$). Experimental conditions: $\pi/2 = 8ns$, $\tau = 140$ ns, mw frequency 9.7266 GHz, data points 512 x 16, temperature 7 K.

*Appendix G*

**Figure S6.** 2-pulse ESE-detected EPR spectrum of the Ni-C state prepared with D$_2$(D$_2$O) at Q-band. The area with a major contribution from the FeS centers in *A. aeolicus* is shaded in green. The asterisk denotes the cavity background signal. In addition, manganese impurity contributions are superimposed on the shape of the iron-sulphur clusters signals. The amount of the hydrogenase molecules in the Ni-C state with the proximal cluster magnetically coupled to the [NiFe] site was small and no splitting of the Ni-C signal was observed. The arrows indicate the magnetic field orientations for which the $M_I$s $^2$H ENDOR spectra were recorded (Figure 4 in the Chapter 10).



# References

1. Lubitz, W.; Reijerse, E.; van Gastel, M. *Chem. Rev.,* **2007**, *107,* 4331.
2. Brecht, M.; van Gastel, M.; Buhrke, T.; Friedrich, B.; Lubitz, W. *J. Am. Chem. Soc,* **2003**, *125 (43),* 13075.
3. Foerster, S.; van Gastel, M.; Brecht, M.; Lubitz, W. *J. Biolog. Inorg. Chem.* **2005**, *10 (1),* 51.

# Maria-Eirini Pandelia

Max-Planck-Institut für Bioanorganische Chemie
Stiftstr. 34-36, D-45470 Mülheim an der Ruhr
Phone: +49 02083063845, E-mail: pandelia@mpi-muelheim.mpg.de
Url: www.mpi-muelheim.mpg.de

**PERSONAL INFORMATION**

Name: Maria-Eirini Pandelia
Birth place/date: Athens 09.07.1981
Marital Status: Single
Current address (Private): Bachstr. 12, D-45468 Mülheim a.d. Ruhr

**EDUCATION**

1999-2003 - Bachelor Studies
University of Patra, Department of Physics, Greece
Degree: Very good (graduated in the top 5% of my year).
Diploma thesis subject: Bose- Einstein Condensation
Diploma thesis grade: Excellent

Summer 2003 - Specific oriented studies
University of Physics in Heraclion, Crete, Greece.
Course: School of advanced physics
Grade: Excellent

2003-2005 - Master Studies
National Technical University of Athens (NTUA)
Master diploma of Science on Advanced Applied Physics
Grade: Very Good

September 2005 to February 2006
Institute of Material Science in NSCR Demokritos
(National Research Centre)
Discipline: Polymer Science
'Chemical and electrochemical synthesis of conducting
polymers. Application of continuous wave EPR to examine
doping effects and relationship between measured conductivity
and EPR spectra'.

May 2006 to October 2009 - Doctoral studies
Max-Planck-Institut für Bioanorganische Chemie in association
with the Technical University of Berlin,
Supervisor: Prof. Dr. Wolfgang Lubitz
Title of the Dissertation: *'[NiFe] hydrogenases from Desulfovibrio
vulgaris Miyazaki F and Aquifex aeolicus studied by FTIR, EPR
and electrochemical techniques: Redox intermediates, $O_2$/CO
sensitivity and light-induced effects'*
Grade: Excellent (Summa cum laude)

November 2009 until present
Postdoctoral researcher in the Max-Planck-Institut für
Bioanorganische Chemie

**TEACHING EXPERIENCE**

<u>2002-2003</u>
Laboratory of Atomic and Nuclear Physics, Patra
Demonstration and explanatory support to the 3$^{rd}$ year students of experiments (Rb laser, Zeeman Effect).

**LANGUAGES**

Greek (mother tongue)
English (proficient)
German (advanced)
Language for the hearing impaired

**HONORS & PRIZES**

1. Promotion (doctoral degree) TU Berlin 2009
   summa cum laude
2. 1$^{st}$ poster prize, FEBS Combined practical and lecture course, 'Chemistry of Metals in Biological Systems'
   Universite Catholique de Louvain, Louvain-La –Neuve
   14-21 September 2009
3. Selected participant of the 58$^{th}$ Nobel Laureate Meeting in Lindau (Physics)
   29$^{th}$ June- 04$^{th}$ July 2008

**TRAINING-COURSES PARTICIPATION**

1. <u>Easyspin and Introduction to pulsed EPR spectroscopy</u>
   ETH Zürich
   1-29 September 2005
2. <u>Easyspin training school</u>
   ETH Zürich
   3-5 March 2006
3. <u>DFT school on computational and theoretical EPR spectroscopy</u>
   University of Bonn
   10-13 October 2007
4. <u>4$^{th}$ EFEPR Summer school</u>
   University of St.Andrews, Scotland
   22 August - 01 September 2008
5. <u>COST P15 Spin echo workshop (EPR)</u>
   Bruker Biospin, Karlsruhe
   10-13 March 2009
6. <u>FEBS Combined practical and lecture course</u>
   'Chemistry of metals in Biological systems'
   Universite Catholique de Louvain, Louvain-La -Neuve
   14-21 September 2009

**LIST OF ORAL PRESENTATIONS**

1. Seminar at Max-Planck-Institute for Bioinorganic Chemistry
15 March 2006
Maria Eirini Pandelia, Penelope Liatsi, Ioannis Daniilidis, Athanasios Tsirimpis
'EPR in the Examination of the Environment as seen from the Charge Carriers in the conducting Polymers: Polyaniline.'

2. Humbolt University Berlin
Workshop, News and Views on Membrane-bound NiFe hydrogenases
25 April 2008
M.E. Pandelia, P. Tron-Infossi, M.T. Giudici-Orticoni, W.Lubitz
'Preliminary FTIR and EPR investigation of the HaseI-cytb complex from Aquifex aeolicus'

3. Institute (BIP) Bioenergetique et Ingenierie des Proteines [IBSM-CNRS]
Marseille, France, 23 September 2008
M.E. Pandelia, P.Tron-Infossi, M.T. Giudici-Orticoni, W.Lubitz
'EPR and FTIR spectroscopic characterization of the [NiFe] hydrogenase from the extreme hyperthermophile Aquifex aeolicus.'

4. Solar H2 Meeting
Tarragona, Spain
April 2009
M.E. Pandelia, P. Tron, M.T. Giudici-Orticoni, W.Lubitz
'Investigation of the NiFe hydrogenase from the extreme hyperthermophilic bacterium Aquifex aeolicus.'

5. Institute (BIP) Bioenergetique et Ingenierie des Proteines [IBSM-CNRS],
Marseille, France
9 June 2009
M.E. Pandelia, W. Nitschke , P.Tron-Infossi, M.T. Giudici-Orticoni, W.Lubitz
'The [NiFe] hydrogenase I from the hyperthermophile Aquifex aeolicus. An EPR and FTIR spectroscopic characterization integrated with electrochemistry.'

**POSTER PRESENTATIONS**

1. The 8$^{th}$ International Hydrogenase Conference
5-10 August 2007, Breckenridge, Colorado, USA
Title:' FTIR and EPR Studies on the Light Sensitive Catalytic Intermediates and the CO/NO Inhibited States of [NiFe] Hydrogenase from D. vulgaris Miyazaki F.'
Maria-Eirini Pandelia, Hideaki Ogata, Marco Flores, Leslie Currell, Wolfgang Lubitz.

2. Solar H2 Meeting
May 2008, Bochum, Germany.
Title: 'Catalytic intermediates of the [Ni-Fe] hydrogenase from the hyperthermophilic bacterium *Aquifex aeolicus*. An EPR and FTIR study.'
Maria-Eirini Pandelia, PascaleTron-Infossi , Marie-Thérèse Giudici-Orticoni , Wolfgang Lubitz.

3. 5$^{th}$ International conference on Nitroxide Radicals**,**
7-11 September 2008, Ancona, Italy.
Title: 'NO inhibition of the [NiFe] hydrogenase from *Desulfovibrio vulgaris* Miyazaki F studied by EPR and FTIR spectroscopy.'
Maria-Eirini Pandelia, Hideaki Ogata, Wolfgang Lubitz.

4. 38$^{th}$ Meeting of the RSC Inorganic Reaction Mechanisms Group in conjunction with RSC Inorganic Biochemistry Discussion Group
4-6 January 2009, Oxford University, England
Title: 'Spectroelectrochemical study of [NiFe] hydrogenase of Desulfovibrio vulgaris Miyazaki F immobilized on biocompatible gold surfaces'
D. Millo, N. Wisitruangsakul, M. E. Pandelia, T. Utesch, M. A. Mroginski, W. Lubitz, P. Hildebrandt, I. Zebger

5. 7$^{th}$ EFEPR meeting and closing meeting of COST P15
6-11 September, Antwerp, Belgium
Title: 'A weakly bound hydride in the catalytic Ni-C state of the oxygen tolerant [NiFe] Hydrogenase I from *Aquifex aeolicus*'
M. E. Pandelia, P.Tron-Infossi , M.T. Giudici-Orticoni, W. Lubitz

6. FEBS Combined practical and lecture course
'Chemistry of metals in Biological systems'
Universite Catholique de Louvain, Louvain-La -Neuve
14-21 September 2009
Title: 'A weakly bound hydride in the catalytic Ni-C state of the oxygen tolerant [NiFe] Hydrogenase I from *Aquifex aeolicus*'
M. E. Pandelia, P. Tron-Infossi, M.T. Giudici-Orticoni, W. Lubitz

**PUBLICATIONS**

1. M.E. Pandelia, H.Ogata, L.J. Currell, M. Flores, W.Lubitz
   'Probing Intermediates in the Activation Cycle of [NiFe] Hydrogenase by Infrared Spectroscopy: The Ni-SIr state and its light sensitivity.'
   *J. Biolog. Inorg. Chem.* **2009**, 14, 1227-1241

2. P. Kellers$^{\S}$, M.E. Pandelia$^{\S}$, L.J. Currell, H. Görner, W. Lubitz
   'FTIR study on the light sensitivity of the [NiFe] hydrogenase from *Desulfovibrio vulgaris* Miyazaki F: Ni-C to Ni-L photoconversion, kinetics of proton rebinding and H/D isotope effect.'
   *Phys. Chem. Chem. Phys.*, **2009**, 11, 8680 – 8683
   $^{\S}$ *Equal contribution*

3. D. Millo, M.E. Pandelia, T.Utesch, N. Wisitruangsakul, M. A. Mroginski, W. Lubitz, P.Hildebrandt, I. Zebger
   'Spectroelectrochemical study of the [NiFe] hydrogenase from *Desulfovibrio vulgaris* Miyazaki F in solution and immobilized on biocompatible gold surfaces'
   *J. Phys. Chem. B*, in press (**2009**), DOI 10.1021/jp906575r

4. Jens Niklas, Boris Epel, Mikhail Antonkine, Sebastian Sinnecker, Maria-Eirini Pandelia, Wolfgang Lubitz
   'The Electronic Structure of the Quinone Radical Anion A1$^{\bullet-}$ of Photosystem I Investigated by Advanced Pulse EPR and ENDOR Techniques.'
   *J. Phys. Chem.* B **2009**, *113* (30), 10367-10379

5. M.E. Pandelia, H .Ogata, L.J. Currell, M. Flores, W.Lubitz
   'Inhibition of the [NiFe] Hydrogenase from *Desulfovibrio vulgaris* Miyazaki F by Carbon Monoxide: An FTIR and EPR Spectroscopic Study'
   *Biochim. Biophys. Acta, Bioenergetics* accepted for publication November **2009**

**PUBLISHED PROCEEDINGS & ABSTRACTS**

1. Jens Niklas, Boris Epel, Mikhail Antonkine, Sebastian Sinnecker, Maria-Eirini Pandelia, Wolfgang Lubitz
   'The electron acceptor quinone A(1) of photosystem I Investigated by pulse EPR and ENDOR spectroscopy.'
   *Photosynthesis Research,* **2007**, 91(2-3), 146

**PUBLICATIONS (SUBMITTED)**

1. Miguel Saggu, Christian Teutloff, Marcus Ludwig, Marc Brecht, Maria-Eirini Pandelia, Oliver Lenz, Bärbel Friedrich, Wolfgang Lubitz, Peter Hildebrandt, Friedhelm Lendzian, Robert Bittl
   'Comparative investigation of the oxidized ready state of the membrane-bound [NiFe] hydrogenases from *R. eutropha* H16 and *D. vulgaris* Miyazaki F with pulsed EPR spectroscopy'
   *Phys. Chem. Chem. Phys.*, submitted October **2009**

**PUBLICATIONS (TO BE SUBMITTED)**

1 M.E. Pandelia, H .Ogata, W. Lubitz
Structure and Function of the [NiFe]hydrogenase from
*Desulfovibrio vulgaris* Miyazaki F′
*Chem. Phys. Chem.,* Invited minireview, November **2009**

2 M.E. Pandelia, P.Tron-Infossi, V. Fourmond, C. Leger, M.-T. Giudici-Orticoni, W. Lubitz
'Hydrogenase I from the hyperthermophilic bacterium *Aquifex aeolicus*; Activation process, redox intermediates and oxygen tolerance studied by FTIR spectroelectrochemistry and protein film voltammetry.'
*To be submitted* **2009**[†]

3. M.E. Pandelia, P. Tron-Infossi, M.T. Giudici-Orticoni, W. Lubitz
'Hydrogenase I from the hyperthermophilic bacterium *Aquifex aeolicus*; Study of the CO inhibition by FTIR spectroelectrochemistry and time-resolved FTIR at low temperatures.'
*To be submitted* **2009**[†]

4. M.E. Pandelia, W. Nitschke, P. Tron-Infossi, M.T. Giudici-Orticoni, W. Lubitz
'Electron transfer in the Hydrogenase I from the hyperthermophilic bacterium *Aquifex aeolicus*; type and redox properties of the iron-sulphur clusters.'
*To be submitted* **2009**[†]

5 M.E. Pandelia, P. Tron-Infossi, M.T. Giudici-Orticoni, W. Lubitz
'Hydrogenase I from the hyperthermophilic bacterium *Aquifex aeolicus*; Detection of a loosely bound hydride ligand in the Ni-C state. A HYSCORE and ENDOR study at X-and Q-band freqencies.'
*To be submitted* **2009**[†]

[†] Part of the Doctoral Thesis